Investigating the effects of inflammation on resident peritoneal macrophage autonomy

Pieter Adriaan Louwe

Submitted for the degree of Doctor of Philosophy

The University of Edinburgh

2020

Acknowledgements

First off, I would like to thank my supervisor, Steve Jenkins. Throughout my PhD he has provided much needed guidance and encouragement and being in his lab has taught me so much. More importantly, I want to thank him for his continuous enthusiasm for anything macrophage-related, which inspired me throughout my PhD and reminds me to always enjoy science. Also, I would like to thank my second supervisor, Stuart Forbes, for his feedback and which helped steer my PhD in the right direction.

I would like to thank the past members of the Jenkins lab for their help and feedback, especially during the early stages of my PhD. A special thanks to Calum Bain, for helping me get started in the lab and teaching me how to organise and carry out a proper flow experiment.

I would also like to express my gratitude to the directors of the Tissue Repair programme, for giving me this amazing opportunity and Marieke and Kelly for coordinating everything programme-related. Also, a big thanks to all of the other Tissue Repair students, especially the 2016 cohort, for making the PhD a great and sociable experience.

I would like to thank all the people in the CIR who have made it such a great place to work. Also, a special thanks to the staff of the BVS facilities and the QMRI flow-cytometry facility, without whom my experiments would not have been possible.

Finally, I would like to thank my family who inspired me to pursue my dreams and whose endless support steered me through university and now a PhD. I also want to thank my partner, Martina, for her loving support through the many highs and lows of the PhD and reminding me to take a break every now and then.

Table of Contents

Acknowledgements **2**

Figures and tables **9**

Declaration **12**

Lay Summary **13**

List of abbreviations **14**

List of publications **18**

Abstract **19**

Chapter 1 ..... **22**

General Introduction **22**

1.1 From frog to tissue-resident macrophage 23

1.2 The shared immunological function of tissue-resident macrophages 23

1.3 Origin of tissue-resident macrophages 25

1.4 Tissue-specific identity and functionality of tissue-resident macrophages 31

1.5 Plasticity of the tissue-resident macrophage identity. 33

1.6 The niche hypothesis as a model of tissue-resident identity 35

1.7 The effect of inflammation on the origin of resident macrophages 37

1.8 The peritoneal macrophage niche 38

1.9 The function of resident peritoneal macrophages 43

1.10 Dynamics of acute peritoneal inflammation 44

1.11 Monocyte-derived cells may persist after peritoneal inflammation 49

1.12 Are monocyte-derived cells capable of reconstituting the macrophage niche. 52

1.13 Immune memory could affect resident or monocyte-derived macrophages following inflammation 54

1.14 Project aims 54

Chapter 2 ..... **57**

Materials & Methods **57**

2.1 Animals 58

2.2 Tissue-protected bone marrow chimeras 59

2.2.1 Preparation of donor bone marrow cells 59

2.3 Peritoneal inflammation models 60

2.3.1 Zymosan model of sterile peritonitis 60

2.3.2 LPS model of peritonitis. 60

2.4 Other substances administered 61

2.4.1 Clodronate liposomes 61

2.4.2 PKH26-PCL red fluorescent cell linker 61

2.4.3 All trans retinoic-acid 61

2.5 Cell isolation protocols 62

2.5.1 Isolation of peritoneal exudate cells 62

2.5.2 Isolation of omental leukocytes. 62

2.5.2 Isolation of liver leukocytes. 63

2.6 Sample preparation for Flow cytometry 63

2.6.1 Surface antibody staining 64

2.6.2 Intracellular staining 64

2.6.3 Acquisition and analysis 65

2.7 Adoptive transfer of macrophage subsets 66

2.8 *In vitro* studies 66

2.8.1 Production of omentum factors 66

2.8.2 *In vitro* culture of peritoneal macrophages post-zymosan. 67

2.8.3 *In vitro* LPS stimulation of purified macrophage populations 67

2.8.4 Phrodo-labelled *E.coli* phagocytosis assay 68

2.9 Transcriptional analysis 68

2.9.1 Nanostring mRNA analysis 69

2.9.1 Gene expression ranking and scoring 69

2.9.2 Gene set enrichment analysis (GSEA) 70

2.10 Assessment of peritoneal and serum levels of LPS-driven cytokines. 70

2.11 Assessment of serum levels of natural antibodies. 71

2.12 Statistical analysis 71

Chapter 3 74

Developing a 'toolbox' to investigate inflammatory macrophage survival and phenotype 74

3.1 Introduction 75

3.2 Dose responsiveness of the zymosan sterile peritonitis model. 78

3.3 PKH26-PCL labelling delineates macrophage subsets during mild peritonitis short-term. 80

3.3.1 Tissue protected BM chimeras corroborate PKH26-PCL labelling of resident macrophages during mild peritonitis. 83

3.3.2 Macrophage dynamics during in mild peritonitis following PKH26-PCL labeling of resident macrophages. 85

3.3.3 Excluded samples and exclusion criteria 85

3.4 Developing an assay to test the fate potential of inflammatory macrophages 86

3.5 Discussion 89

Chapter 4 105

Investigating inflammatory macrophage survival and identity following resolution of zymosan-induced peritonitis 105

4.1 Introduction 106

4.2 The post resolution environment allows inflammatory macrophage survival but inhibits phenotypic conversion. 107

4.3 The post resolution environment does not dictate inflammatory macrophage survival and phenotype. 109

4.4 Competition with incumbent resident macrophages inhibits proliferation of inflammatory macrophage and conversion. 110

4.5 PKH26-PCL dye labelling does not inhibit resident macrophage proliferation. 112

4.6 Transferred cells migrate into the omentum of clodronate pre-treated recipients. 114

4.7 Inflammatory macrophage phenotype is responsive to retinoic-acid and omentum factors *in vitro.* 117

4.8 Retinoic-acid drives expression of GATA6 and F4/80 by monocyte-derived macrophages *in vivo* 119

4.9 Inflammatory macrophages expand following transfer into FIRE$^{-/-}$ mice devoid of peritoneal resident macrophages. 120

4.9.1 Inflammatory macrophages migrate into the omentum of FIRE$^{-/-}$ recipient mice 121

4.10 Discussion 122

Chapter 5..... 141

Examining long-term survival and identity of inflammatory macrophages after mild peritonitis. 141

5.1 Introduction..... 142

5.2 Inflammatory macrophages persist long-term and remain phenotypically distinct. 143

5.3 Persistent inflammatory macrophages remain transcriptionally distinct..... 144

5.3.1 Transcriptional identity of inflammatory macrophages is partially due to impaired capacity to acquire retinoic acid. 144

5.3.2 Transcriptional profile of inflammatory macrophages resembles that of steady state monocyte-derived macrophages..... 146

5.4 Long-term competition with incumbent resident macrophage inhibits inflammatory macrophage conversion. 148

5.5 Inflammatory macrophages adopt a resident transcriptional identity following transfer into clodronate-depleted recipients. 149

5.6 Inflammatory macrophages remain phenotypically distinct following transfer into native or depleted recipients. 151

5.7 Inflammatory macrophages are long-lived and gradually acquire the resident identity. 152

5.8 Discussion 153

Chapter 6 170

Investigating the long-term consequences of inflammatory macrophage integration 170

6.1 Introduction 171

6.2 Developing a marker-based gating strategy to identity inflammatory macrophages long-term. 174

6.3 Heightened proliferation is a feature of monocyte-derived macrophages per se. 175

6.4 Monocyte-derived macrophages are characterized by low granularity and phagocytic capacity. 176

6.5 Altered cytokine production by monocyte-derived macrophages in response to LPS *in vitro*. 177

6.6 Investigating monocyte-derived macrophage responsiveness *in vivo* 180

6.6.1 Impaired TNFα production by monocyte-derived macrophages *in vivo* 181

6.6.2 Dampened transcriptional response by monocyte-derived macrophages 181

6.7 Discussion 184

Chapter 7 203

Assessing the survival and phenotype of inflammatory macrophages following severe peritonitis 203

7.1 Introduction 204

7.2 Severe peritonitis leads to an influx of monocytes and neutrophils. 205

7.3 Inflammatory macrophages persist after severe peritonitis and adopt a unique phenotype. 207

7.4 Following severe peritonitis the peritoneal environment drives expression of MHCII and Tim4. 209

7.5 Sterile peritonitis leads to impaired B1 cell expansion. 210

7.6 Discussion 211

Chapter 8 225

Discussion and perspective 225

8.1 Introduction 226

8.2 A niche that determines peritoneal macrophage survival and proliferation 226

8.3 The omentum as a short-term niche for inflammatory macrophage conversion 230

8.4 A niche that determines peritoneal macrophage identity. 232

8.4.1 The influence of time and origin on peritoneal macrophage identity and functionality 236

8.5 The functional effects of historic peritoneal inflammation 238

8.6 A severity-dependent state of altered homeostasis following peritoneal inflammation 239

8.7 Evidence for a peritoneal immune-cell niche. 242

8.8 The type of inflammatory stimuli likely dictates monocyte integration 244

8.9 Inflammation-driven integration of monocytes into the macrophage compartment likely occurs in humans 245

8.10 Conclusion 247

References 249

Figures and tables

Figure 1.1 Origin of tissue-resident macrophages. 30
Figure 1.2 The peritoneal niche. 42
Figure 1.3 Dynamics of zymosan induced peritonitis 48
Table 1 List of reagents used in this thesis 72
Table 2 list of antibodies used in this thesis 73
Figure 3.1 Zymosan induces resident macrophage disappearance in male and female mice. 92
Figure 3.2 PKH26-PCL labels peritoneal phagocytes. 94
Figure 3.3 By 24 hours, marginal free-floating PKH26-PCL remains. 96
Figure 3.4 PKH26-PCL-labelling discriminates resident macrophages from infiltrating cells following zymosan treatment. 97
Figure 3.5 PKH26-PCL delineates low-chimerism resident macrophages from high-chimerism monocyte-derived macrophages. 98
Figure 3.6 PKH26-PCL discriminates resident macrophages at different stages of zymosan-induced peritonitis. 100
Figure 3.7 Clodronate liposomes deplete peritoneal macrophages. 103
Figure 3.8 Peritoneal macrophages persist following transfer into clodronate-depleted recipients. 104
Figure 4.1 Inflammatory macrophages survive after resolution. 126
Figure 4.2 Inflammatory macrophages survive following transfer into 128
naïve recipients. 128
Figure 4.3 Inflammatory macrophages expand and undergo phenotypic conversion following transfer into clodronate-depleted recipients. 130
Figure 4.4 PKH26-PCL labelling does not impair proliferation. 132
Figure 4.5 Inflammatory macrophages infiltrate the clodronate-depleted Omentum. 134
Figure 4.6 Inflammatory macrophages are retinoic-acid and omentum factor responsive. 136
Figure 4.7 Oil-elicited inflammatory macrophages are retinoic-acid responsive. 137

Figure 4.8 Inflammatory appear to expand and downregulate MHCII, following transfer into FIRE$^{-/-}$ recipients. 139
Figure 4.9 Macrophage subsets migrate into the omentum following transfer into FIRE$^{-/-}$ recipients..... 140
Figure 5.1 Inflammatory macrophages persist long-term following zymosan-induced peritonitis. 157
Figure 5.2 Inflammatory macrophages remain transcriptionally distinct. 159
Figure 5.3 The inflammatory macrophage gene-signature suggests impaired retinoic-acid signalling..... 160
Figure 5.4 The monocyte-derived macrophage gene signature suggests impaired retinoic-acid signalling. 162
Figure 5.5 Inflammatory macrophages transferred into macrophage-deplete recipients adopt a resident phenotype. 163
Figure 5.6 Inflammatory macrophages adopt a resident identity following transfer into clodronate-depleted recipients. 165
Figure 5.7 Inflammatory macrophages adopt a resident phenotype following transfer into clodronate-depleted recipients. 166
Figure 5.8 Inflammatory macrophages persist until 5 months after inflammation and adopt a more resident-like phenotype. 168
Figure 6.1 Identification of RM-LPM and Mo-LPM on the basis of Tim4 and Sema4a expression. 189
Figure 6.2 Monocyte-derived macrophages exhibit heightened baseline proliferation. 191
Figure 6.3 Monocyte-derived macrophages are less granular and phagocytic than embryonically-seeded macrophages. 192
Figure 6.4 Monocyte-derived macrophages are differentially responsive to LPS *in vitro.* 195
Figure 6.5 Zymosan-induced inflammation does not alter LPS-responsiveness of peritoneal macrophage subsets. 196
Figure 6.6 Monocyte-derived macrophages are differentially responsive to LPS *in vivo.* 198
Figure 6.7 Transferred cells do not affect the systemic response to LPS… 200

Figure 6.8 Monocyte-derived macrophages exhibit dampened transcriptional responsive to LPS. 201
Figure 7.1 Macrophage and neutrophil dynamics after zymosan-induced peritonitis 215
Figure 7.2 High dose zymosan leads to replacement of peritoneal macrophages by monocyte-derived macrophages. 217
Figure 7.3 Inflammatory macrophages persist after severe peritonitis. 218
Figure 7.4 Persistent inflammatory macrophages after severe peritonitis are phenotypically unique. 220
Figure 7.5 Following severe peritonitis the peritoneal microenvironment is altered. 222
Figure 7.6 Severe peritonitis leads to impaired recruitment of B1 cells. 223
Figure 8.1 Long-term effects of zymosan-induced peritonitis 246

Declaration

I declare that this thesis has been composed by myself and that the work has not been submitted for any other degree or qualification. I confirm that the work presented in this thesis is my own, except where stated/acknowledged in the manuscript.

The majority of the work presented in this thesis has been submitted for publication and has been accepted at Nature Communications as " *Recruited macrophages that colonise the post-inflammatory peritoneal niche convert into functionally divergent resident cells*" by **P. A. Louwe**, L. Badiola Gomez, H. Webster, G. Perona-Wright, C. C. Bain, S. J. Forbes and S. J. Jenkins. I designed, performed and analysed all experiments for this manuscript, except the antibody-ELISA. I wrote the manuscript with S.J. Jenkins.

Pieter Adriaan Louwe

Lay Summary

Macrophages are part of the immune system and these cells are present in virtually every tissue of the body. Macrophages are sometimes referred to as ‘guardians of the tissue’ since they are vital for keeping the tissue healthy by clearing dead and dying cells. When infection or injury occurs, the macrophages recruit other immune cells to help clear the infectious agent. In addition, macrophages also carry out unique functions depending on the tissue which they inhabit. Using new technologies, we are trying to understand exactly how a macrophage is ‘trained’ to carry out these functions. Incomplete macrophage ‘training’ could allow disease to occur which would have been prevented by fully ‘trained’ macrophages.

I aimed to understand how this macrophage ‘training’ is occurring in the space between the abdominal organs. This space is called the peritoneal cavity, and the unique population of tissue macrophages that inhabit this cavity are referred to as peritoneal macrophages. When the peritoneal cavity is infected, cells are recruited from the blood into the cavity. These blood cells give rise to a new set of recruited macrophages that are needed to clear the infection. I found that these recruited macrophages persist long after the infection has been resolved and that they did not become true peritoneal macrophages. An important reason why these cells stayed different was because the original population of peritoneal macrophages prevented them from ‘training’. Consequently, the recruited macrophages did not receive training and they remained untrained recruited macrophages. Importantly, these untrained recruited macrophages are not as good at clearing bacteria, and are not carrying out the specific functions of peritoneal macrophages.

Hence, my work indicates that after a mild peritoneal infection the cavity is colonized by these recruited macrophages that don’t carry out macrophage functions as efficiently as true peritoneal macrophages. Consequently, the presence of these recruited cells likely alters the response of the cavity to subsequent infections.

List of abbreviations

ANOVA	Analysis of variance
ATRA	All trans retinoic acid
BHLHE40	Basic Helix-Loop-Helix Family Member E40
BHLHE41	Basic Helix-Loop-Helix Family Member E41
BM	Bone marrow
BSA	Bovine serum Albumin
C1q	Complement component 1q
CCL24	C-C Motif Chemokine Ligand 24
CCL5	C-C Motif Chemokine Ligand 5
CCR2	C-C Motif Chemokine Receptor 2
CCR5	C-C Motif Chemokine Receptor 5
CD	Cluster of differentiation (usually with number i.e. CD45)
CD206	Cluster of differentiation 206 (mannose receptor)
CD45.1	Cluster of differentiation 45α
CD45.2	Cluster of differentiation 45β
CEBP/β	CCAAT/enhancer binding protein
CREB	cyclic AMP-response element binding protein
CSF2r	Colony stimulating factor 2 receptor.
CSFr1	Colony stimulating factor 1 receptor (CD115)
Ctrl	Control
CX3CR1	fractalkine receptor
CXCL13	C-X-C Motif Chemokine Ligand 13
DNA	Deoxyribonucleic acid
dPBS	Dulbecco's Phosphate-Buffered Saline
EMP	Erythro-myeloid precursors
F4/80	EGF-like module-containing mucin-like hormone
receptor-like 1	
FCGR1	Fc Fragment Of IgG Receptor Ia
FCGR3	Fc Fragment Of IgG Receptor IIIa
FCS	Fetal calf serum

FIRE	Fms-intronic regulatory element
FOXP3	Forkhead box P3
FSC	Forward scatter
GATA6	GATA binding protein 6
GFP	Green Fluorescent protein
GM-CSF	Granulocyte-macrophage colony-stimulating factor
GO term	Gene ontology term
GSEA	Gene set enrichment analysis
ID3	Inhibitor Of DNA Binding 3, HLH Protein
DTR	Diphteria toxin
IFN	Interferon
Il	Interleukin
$IMac^{Z10}$	Inflammatory macrophage elicited using 10μg zymosan
$IMac^{Z1000}$	Inflammatory macrophage elicited using 1000μg zymosan
IP	Intraperitoneal
IRF4	Interferon Regulatory Factor 4
IV	Intravenous
KO	Knock out
LoxP	Locus of X-over P1
LPM	Large peritoneal macrophage
LPS	Lipopolysaccharides
LXRα	Liver X receptor α
Ly6b	Lymphocyte antigen 6b
Ly6c	Lymphocyte antigen 6c
Lysm	Lysin motif
MertK	c-mer proto-oncogene tyrosine kinase
MFI	Mean fluorescence intensity
MHCII	Major histocompatibility complex 2
Mo-LPM	Monocyte-derived LPM
Mo^{Z10}-LPM	Monocyte-derived LPM, elicited using 10μ zymosan
mRNA	Messenger ribonucleic acid

Ms4a3	Membrane Spanning 4-Domains A3
NK cells	Natural Killer cells
Om factors	Omentum Factors
PGSE2	Prostaglandin E2
PKH26-PCL	Paul Karl Horan 26 cell linker kit
PPARγ	Peroxisome proliferator-activated receptor γ
RAG	recombination activating gene 1
Relmα	Resistin like molecule α
Rfp	Red fluorescent protein
RFP	Red fluorescent protein
RM-LPM	Resident macrophage-derived LPM
RMac	Resident peritoneal macrophages
$RMac^{Z10}$	Resident peritoneal macrophages elicited using 10μg zymosan
RM^{Z10}-LPM	Resident macrophage-derived LPM, elicited using 10μg zymosan
Runx1	Runt-related transcription factor 1
RXRα	Retinoic X receptor α
RXRβ	Retinoic X receptor β
S.Aureus	Streptococcus Aureus
S.Pneumomoniae	Streptococcus pneumoniae
S100A4	S100 calcium-binding protein A
Flt3	Fms Related Receptor Tyrosine Kinase 3
SerpinB2	Serpin Family B Member 2
SPM	Small peritoneal macrophage
SSC	Side scatter
Tim4	T Cell Immunoglobulin And Mucin Domain Containing 4
TLR4	Toll Like Receptor 4
TNFα	Tumor Necrosis Factor α
CXCL1	C-X-C Motif Chemokine Ligand 1
CXCL10	C-X-C Motif Chemokine Ligand 10
CCL2	C-C Motif Chemokine Ligand 2

VSIG4	V-Set And Immunoglobulin Domain Containing 4
WT	Wild type
YFP	Yellow Fluorescent protein
Zeb2	Zinc finger E-box-binding homebox 2
FACS	Fluorescence-activated cell sorting
FMO	Fluorescence minus one
FRβ	Folate receptor β

List of publications

Bain, C. C., D. A. Gibson, N. J. Steers, K. Boufea, **P. A. Louwe**, C. Doherty, V. Gonzalez-Huici, R. Gentek, M. Magalhaes-Pinto, T. Shaw, M. Bajénoff, C. Bénézech, S. R. Walmsley, D. H. Dockrell, P. T. K. Saunders, N. N. Batada and S. J. Jenkins (2020). "*Rate of replenishment and microenvironment contribute to the sexually dimorphic phenotype and function of peritoneal macrophages.*" Sci Immunol 5.

Hawley, C. A., R. Rojo, A. Raper, K. A. Sauter, Z. M. Lisowski, K. Grabert, C. C. Bain, G. M. Davis, **P. A. Louwe**, M. C. Ostrowski, D. A. Hume, C. Pridans and S. J. Jenkins (2018). "*Csf1r-mApple Transgene Expression and Ligand Binding In Vivo Reveal Dynamics of CSF1R Expression within the Mononuclear Phagocyte System*." J Immunol 200(6): 2209-2223.

Li, Z., E. G. Solomonidis, M. Meloni, R. S. Taylor, R. Duffin, R. Dobie, M. S. Magalhaes, B. E. P. Henderson, **P. A. Louwe**, G. D'Amico, K. M. Hodivala-Dilke, A. M. Shah, N. L. Mills, B. D. Simons, G. A. Gray, N. C. Henderson, A. H. Baker and M. Brittan (2019). "*Single-cell transcriptome analyses reveal novel targets modulating cardiac neovascularization by resident endothelial cells following myocardial infarction*." Eur Heart J 40(30): 2507-2520.

Abstract

Inflammation is known to lead to long-term changes in the responsiveness to subsequent inflammatory challenges but the mechanism driving this alteration is poorly understood. In the peritoneal cavity a similar phenomenon has been described and historic peritoneal inflammation is thought to lead to dampened neutrophil recruitment in response to a subsequent insult. Acute peritoneal inflammation is characterized by the transient loss of embryonically-seeded resident macrophages and infiltration by large numbers of monocyte-derived inflammatory macrophages. The long-term fate of inflammatory macrophages post-inflammation has remained controversial. Hence, I hypothesized that inflammatory macrophages persist long-term but could remain functionally distinct. In addition, I aimed to explore what regulates the survival and identity of these cells by examining how severity of the initial inflammatory insult changes the post inflammation micro-environment. Furthermore, a combination of cell-intrinsic regulation and environmental signals limits inflammatory macrophages from converting into resident macrophages.

To investigate these questions, I developed a flow-cytometric method based on dye-labelling of resident macrophages in conjunction with conventional antibody staining to unequivocally delineate resident from inflammatory macrophages during resolution of a well characterised model of sterile peritoneal inflammation induced by injection of zymosan A. Following a low dose of zymosan, both resident and inflammatory macrophages persisted in the peritoneal cavity by day 3 whereas severe inflammation resulting from injection of a high dose of zymosan led to complete loss of resident macrophages. I then used adoptive transfer of purified resident or inflammatory macrophages present during resolution of mild peritonitis into congenic recipient mice that harboured an equivalent inflammatory response to investigate their long-term survival and identity. To investigate if the post resolution environment dictates these features, cells were transferred into naïve recipient mice. To ascertain if competition with incumbent resident macrophages for niche signals alters this fate and phenotype, donor cells were

transferred into recipient mice transiently-depleted of endogenous resident macrophages. Combined these data allowed me to ascertain to what degree survival and identity of inflammatory macrophages is dictated by environmental niche cues, competition with incumbent resident macrophages and to what degree these features are pre-determined.

These adoptive transfer experiments revealed that following mild peritonitis both resident and inflammatory macrophages persist through inflammation resolution, when the macrophage compartment contracts to pre-inflammation size. Long-term fate mapping indicated that transferred cells survived to an equivalent degree up to 8 weeks. This suggests that cells that persisted shortly after resolution become long-lived. However, Nanostring mRNA analysis at 8 weeks demonstrated that inflammatory macrophages acquired some resident features such as CD102 expression but remained transcriptionally distinct. Importantly, inflammatory macrophages failed to acquire equivalent levels of the peritoneal identity transcription factor GATA6 whilst maintaining high expression of inflammatory macrophage markers, most notably MHCII and Sema4a. Critically, inflammatory macrophages transferred into macrophage-deplete recipients adopted a more complete resident macrophage identity, including equivalent expression of GATA6 and MHCII to their resident counterparts, whilst retaining differential expression of few genes, including the embryonic macrophage marker Tim4. Combined these data indicate that the failure of inflammatory macrophages to adopt a resident identity is largely environment and competition dictated. However, over time more complete conversion occurs, as fate mapping until 5 months after mild peritonitis indicated that inflammatory macrophages gradually reprogram both environment dependent and independent features.

In contrast, after severe peritoneal inflammation resident macrophages were completely and irrevocably lost, which was confirmed using tissue-protected bone marrow chimeric mice. Inflammatory macrophages recruited during severe inflammation adopted a somewhat ‘resident like’ identity including high

levels of GATA6, equivalent to resident macrophages. However, after severe peritonitis, and complete loss of resident macrophages, inflammatory macrophages retained high levels of MHCII. As MHCII was rapidly downregulated by low dose inflammatory macrophages after transfer into macrophage-deplete recipients but not after transfer into naïve or equivalently inflamed recipients these data indicate that signals unique to the severely inflamed cavity drive expression of MHCII. Consistently, naïve resident macrophages expressing low levels of MHCII transferred into high dose zymosan treated recipients rapidly upregulated MHCII.

Finally, I showed that inflammatory macrophages that persisted 8 weeks after mild peritonitis were more proliferative, less phagocytic and produced less TNFα in response to LPS stimulation both *in vitro* and *in vivo.* One feature of inflammatory macrophages, irrespective of the severity of peritonitis was an inability to produce the B1 cell chemokine CXCL13 and as a likely consequence peritoneal B1 cells failed to accumulate post inflammation.

Hence, these data support a model where inflammation drives the integration of functionally divergent monocyte-derived inflammatory macrophages into the peritoneal cavity. Moreover, during mild inflammation competitive pressure from incumbent resident macrophages for environmental signals largely dictates the extent to which inflammatory macrophages adopt a more resident-like identity. Conversely, after severe peritonitis no competing resident macrophages persist but environmental signals are altered and consequently inflammatory macrophages adopt a unique identity.

Chapter 1

General Introduction

1.1 From frog to tissue-resident macrophage

The first in-depth characterization of phagocytes was carried out by Elie Metchnikoff in starfish and frogs[1-3]. He described a population of 'eating cells' involved in host defence as well as removal of the dying cells during development from tadpole into mature frog[1,2]. He named these cells 'phagocytes' and described distinct roles for circulating 'microphages' and tissue-resident 'macrophages' in the control of invading pathogens[1]. His work was expanded upon by numerous research groups which, in 1972, culminated in the definition of the mononuclear phagocyte system by van Furth et al to classify highly phagocytic cells and their precursors on the basis of morphology, function and origin[4].

Metchnikoff's initial description of tissue-resident macrophages as key players in immunological processes, including bactericidal control, as well as maintenance of tissue homeostasis and development, through phagocytosis of debris and dying cells, has been the cornerstone of contemporary macrophage research. With the advent of high-throughput sequencing technologies it has become clear that vast populations of transcriptionally distinct tissue-resident macrophages, uniquely adapted to the tissue they inhabit, are present in virtually every organ[5,6] across species, including humans. Reflecting this common functionality, tissue-resident macrophages share a core panel of genes and functions upon which a tissue-specific transcriptional and functional identity is over-laid[7-9]. Tissue-resident macrophages have proved vital in maintaining health through clearance of debris and immunological protection through phagocytosis of infectious agents regulation of initiation and resolution of inflammatory response [5,10].

1.2 The shared immunological function of tissue-resident macrophages

Tissue-resident macrophages have long been postulated to act as sentinels that survey the tissue. With advances in live imaging technologies this process has been visualized in great detail and tissue-resident macrophages have been shown to continuously survey the surrounding tissue using filopodia-like

protrusion in, for example, the brain[11] , the liver[12] and the lung[13]. Through a variety of pattern recognition receptors expressed on their surface, most notably: toll-like receptors, scavenger receptors and C-type lectins, tissue-resident macrophages detect a variety of pathogenic motifs and proceed to phagocytose invading microorganisms[10]. Phagocytosed particulates are encapsulated in phagosomes which subsequently acidify and fuse with lysosomes, forming highly acidic phagolysosomes that ultimately degrade engulfed particulates[14]. In response to encountering and engulfing pathogens tissue-resident macrophages produce a cocktail of inflammatory mediators dictated by the nature and severity of the encountered stimuli. In addition, tissue-resident macrophages influence adaptive immune response either via secreted mediators or through antigen presentation via class II MHC[10].

A key function of tissue-resident macrophages is the clearance of debris and dying cells via phagocytosis. Under homeostatic conditions, cell-death occurs predominantly through a regulated series of processes known as phagocytosis. As part of this apoptotic process, dying cells express various cellular components on their surface, including phosphatidylserine and calreticulin, that are normally sequestered inside the cell[15,16]. Exposed phosphatidylserine serves as ligands for soluble factors that are secreted by macrophages and dendritic cells. These soluble factors include milk-fat globule epidermal growth factor (MFG-E8), growth arrest-specific gene 6 and complement component 1q (C1q). Once bound, these mediators serve as bridging molecules and allow binding and engulfment by phagocytes via vitronectin receptor, c-mer proto-oncogene tyrosine kinase (MerTk) and C1q-receptors respectively. In addition, macrophages express numerous receptors that directly recognize phosphatidylserine including, T-cell immunoglobulin and mucin domain containing 1 and 4 (Tim1/4) and Stabilin-1[15-17]. Some of these surface receptors, such as MertK, are highly expressed by macrophages across tissues whereas others, such as Tim4, are more unique to tissue-macrophage subsets[18]. Pan-macrophage deletion of some of these receptors or soluble factors involved in apoptotic cell clearance, such as the bridging molecule MFGE8, leads to impaired apoptotic cell clearance across tissues[18].

In contrast, pan-macrophage deletion of Tim4, highly expressed by macrophages in the liver and the peritoneal cavity, does not affect apoptotic cell clearance in most tissues but does affect efferocytosis by Kupffer cells[19] and greatly affects homeostasis of the peritoneal cavity and clearance of apoptotic cells by peritoneal macrophages[19-21]. Hence, some mediators of apoptotic cell clearance are shared by macrophages across tissues[18] whereas others are specific to macrophages inhabiting distinct sites[19-21] suggesting tissue-specific types of apoptotic cell clearance.

1.3 Origin of tissue-resident macrophages

In 1972 van Furth et al proposed the mononuclear phagocyte system to group phagocytes[4,22] (recently review in[23]) in the body. He established a number of criteria for cells to be included in the mononuclear phagocyte system. Cells had to have high phagocytic capacity, a criterion which excluded less phagocytic endothelial cells. Moreover, van Furth et al argued that in order for a group of cells to constitute a system these cells had to have a shared origin. A number of studies indicated that following lethal irradiation macrophages, including those in the liver and the lung, were derived from circulating monocytes that in turn originated from the bone marrow[4,22]. To generate chimeric mice, animals where lethally irradiated to destroy bone marrow hematopoietic stem cells and reconstituted using congenic donor bone marrow, usually sourced from congenic CD45.1 mice, thus allowing long-term tracking of donor CD45.1$^+$ bone marrow-derived cells to CD45.2$^+$ immune cell populations. However, lethal irradiation also depletes various tissue-resident macrophage populations thus confounding these observations. Largely on the basis of these irradiation experiments van Furth suggested that the most immature cell of the mononuclear phagocyte system was the promonocyte, present in the bone marrow. Promonocytes gave rise to a more mature monocytes that circulated in the blood and infiltrated tissues where they gave rise to highly phagocytic macrophages. Interestingly, van Furth et al remarked on the existence of ‘fixed’ tissue macrophages of which the monocytic origin was yet to be established but that these cells should be included in

mononuclear phagocyte system based on their morphology and phagocytic capacity. Despite the inclusion of these fixed cells, of which the origin was ambiguous, the mononuclear phagocyte system and the bone marrow origin of tissue macrophages became established dogma until recently.

A major break from this idea that macrophages originated from monocytes came from studies using a model of murine parabiosis, a methodology that does not rely on irradiation. Using this methodology, it was found that circulating monocytes did not contribute over a 5 month period to Microglia[24] ,the resident macrophages in the brain, or over a period of 12 months to Langerhans cells[25], the resident macrophages in the skin. Hence, it was suggested that these cells were likely self-maintaining throughout life. Merad and colleagues observed that Langerhans cells self-maintenance was established directly following birth. Hence, they postulated that hematopoietic precursors infiltrated the skin during embryonic life and gave rise to Langerhans cells that self-maintained for at least 12 months and likely throughout life[25].

With the development of new fate-mapping tools the questions concerning the origin of tissue-resident macrophages have been investigated in more detail. The most important of these tool is the inducible gene-specific fate-mapping tools utilizing the Cre-loxP methodology. Briefly, this two-part system consists of a Cre recombinase that recognizes specific DNA sequences, known as LoxP sites, and mediates depletion of the DNA sequence between the two LoxP sites. Commonly, a transgenic Cre-driver mouse line is generated by placing expression of the Cre recombinase under control the promoter of a gene of interest. Usually, this gene is selected to be specific to a tissue or cell type of interest. Secondly, a transgenic mouse is generated where LoxP sites flank a gene of interest to generate a conditional knockout. Alternatively, LoxP sites can be placed around a stop codon placed prior to the DNA sequence encoding for a fluorescent protein. The Cre-recombinase will remove the stop codon and the fluorescent protein will be expressed allowing tracking of cells of interest. This methodology has been expanded upon with the generation of

an inducible system, referred to as CreERT or later generation versions as CreERT2, generated by fusing the Cre-recombinase with an estrogen receptor. This CreERT protein is normally sequestered in the cytoplasm but after administration of tamoxifen translocate to the nucleus and mediates depletion of the DNA sequence in-between LoxP sites similar to the original Cre-recombinase (reviewed in[26,27]).

Yona and colleagues placed cre-recombinase under the promoter of *CX3CR1* gene, widely expressed in the mononuclear phagocyte system[28]. Utilizing CX3Cr1^{gfp}, CX3Cr1^{cre}-R26^{yfp} and CX3Cr1^{CreER}- R26^{yfp} transgenic mouse lines allowed them to investigate historic and temporal expression of CX3CR1 by circulating monocytes and different tissue-resident macrophages. They found that, for example, Kupffer cells, alveolar macrophage and peritoneal macrophages did not express CX3Cr1^{gfp} after they had adopted the resident identity. However, using CX3Cr1^{cre}-R26^{yfp} tracking studies indicated that Kupffer cells, alveolar macrophage and peritoneal macrophages originated from precursor cells that had expressed CX3CR1. Finally, using the inducible CX3Cr1^{CreER}- R26^{yfp} it became clear that Kupffer cells, alveolar macrophage and peritoneal macrophages did not originate from CX3CR1-expressing monocytes. Consequently, they concluded that these populations of resident macrophages are self-maintaining and do not rely on circulating monocytes for replenishment[28] but do originate from a CXC3CR1-expressing progenitor. These findings were mirrored by work of Schultz et al[29], using a similar CX3CR1 based fate-mapping methodology. Utilizing S100a4^{Cre}- R26^{Tomato} and Flt3^{Cre}-R26$^{Tomato/GFP}$ transgenic monocyte-tracking mice, Hashimoto and colleagues concluded that resident macrophages in, for example, the brain, lung and peritoneal cavity did not rely on circulating monocytes for replenishment[30]. Parabiosis experiments carried out in the same study further supported this conclusion[30] . Combined, these data supported the hypothesis that precursors seeded tissue during embryonic life and subsequent gave rise to self-maintaining tissue-resident macrophage subsets. However, the identity of this precursor and the dynamics of embryonic seeding remained unclear.

The developmental origin of tissue-resident macrophages has been investigated by numerous groups. I will briefly touch on some of the key findings in this topic and highlight how embryonic precursors give rise to distinct tissue-resident macrophages population persisting throughout life.

A better understanding of the embryonic origin of tissue-resident macrophages came from studies that utilized Runt-related transcription factor 1 (Runx1- mer-cre-mer) transgenic mice. Runx1 is required for the development of erythro-myeloid precursors (EMPs) and primitive hematopoietic stem cells (HSCs)[31]. It should be noted that the terminology for macrophage precursors is not well established yet and early-EMPs have been referred to as yolk sac precursors[32]. For this introduction I will using the EMP-nomenclature as recently reviewed by Ginhoux and colleagues[33]

Importantly, expression of Runx1 is temporarily restricted to discrete stages of development. Consequently, tamoxifen treatment of inducible Runx1$^{MercreMer/EYFP}$ reporter mice at gestational day E7.0-E7.5 labelled Runx1-expressing early EMPs in the yolk sac that seed various tissues as embryonic macrophages but ultimately only persist as microglia in the brain following birth[31,34]. In contrast, later tamoxifen labelling at E8.5, marks a discrete population of Runx1-expressing late EMPs that infiltrate the fetal-liver and give rise to fetal-liver monocytes which seed various tissue sites as embryonic macrophages and persist as resident macrophages post birth[34,35]. Similar dynamics were observed using inducible CSF1R transgenic mice (CSF1R$^{MercreMer/EYFP}$). Early EMPs express high levels of CSF1R whereas late EMPs express low levels. Consequently, tamoxifen induction at E8.5 of inducible CSF1R$^{MercreMer/EYFP}$ mice, labels early EMPs but not late EMPs and similarly shows that early EMP-derived cells seed various sites but only persist as microglia in the brain[29,34,36]. These findings have been elaborated upon by utilizing inducible S100 calcium-binding protein A4 (S100a4^{Cre}-Rosa^{EYFP}) transgenic mice. S100a4 is largely absent in early and late EMPs but highly expressed by fetal-liver monocytes. Consistent with findings utilizing other fate-mapping methodologies, S100a4-expressing fetal liver monocytes were

found to give rise to various issue resident macrophage populations but not microglia[34].

It remained unclear to what degree fetal hematopoietic stem cells (HSCs) contributed to adult tissue-resident macrophage populations. Fetal-HSCs were initially thought to contribute based on studies utilizing inducible m-cell- factor receptor c-Kit ($Kit^{MercreMer}R26^{eYFP}$) transgenic mice. In these mice tamoxifen administration at E8.5 labelled all hematopoietic cells and resulted in labelling of most adult tissue-resident macrophage populations[37], leading the hypothesis that fetal c-Kit-expressing HSCs may be the source of tissue-resident macrophages. Utilizing HSCs-specific $FLT3^{Cre}$-$ROSA26^{YFP}$ reporter mice it was found that HSCs only marginally contributed to tissue-resident macrophages in the liver and the brain, whereas macrophages in the dermis and the gut had much higher contribution of HSCs. These findings were elaborated upon by utilizing inducible Tek-Mer-cre-Mer transgenic mice ($Tie2^{MeriCreMer}Rosa26^{YFP}$) which label both populations of EMPs and by fetal-HSCs[36]. Importantly, following tamoxifen administration, adult leukocytes (T-cells, B-cells and granulocytes) in the spleen were equivalently labelled as bone marrow-HSCs, indicative of their HSC origin. Labelling of Tie2-expressing cells at different stages of embryonic development indicated that labelling at E7.5 resulted in higher labelling of post birth of tissue-resident macrophages than leukocytes, labelling at E8.5 in comparable labelling between these populations whereas labelling at E.9.5 results in more frequent labelling of leukocytes than tissue-resident macrophages[36]. Hence, they concluded that tissue-resident macrophages originated largely independent of the HSC lineage and originated from yolk sac EMPs that express Tie2 at E7.5 but not at E9.5[36].

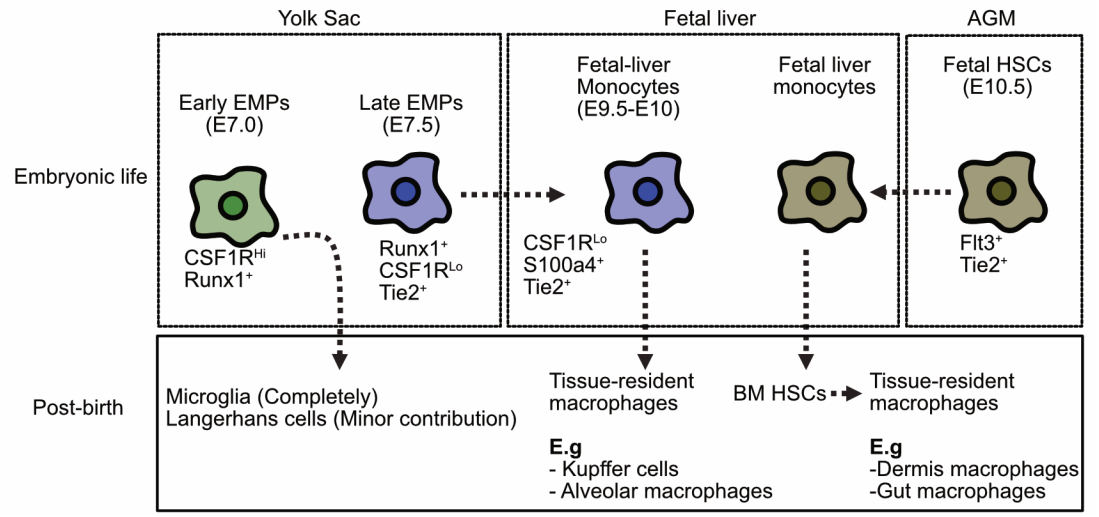

Figure 1.1 Origin of tissue-resident macrophages.

Developmental relationship between macrophage precursor populations, present at distinct times during embryonic development and tissue-resident macrophage populations present post-birth. At E7.0 yolk sac CSF1r^{Hi} Runx1^{+} early EMPs infiltrate various tissues, giving rise to macrophages. With the exception of Microglia in the brain and a small subset of Langerhans cells in the skin the majority of early EMP-derived macrophages are replaced by CSF1r^{Lo} S100a4^{+} Tie2 fetal-liver monocytes macrophages between E9.5 and E10. These fetal-liver monocytes are derived from yolk sac Runx1^{+} CSF1r^{Lo} Tie2^{+} late EMPs around E7.5. During embryogenesis fetal monocytes give rise to self-maintaining tissue-resident populations including Kupffer cells in the liver and alveolar macrophages in the lungs. Around E10.5 Flt3^{+} Tie2^{+} fetal HSCs from the Aorta-gonad-mesonephros (AGM) give rise to fetal liver monocytes that in turn give rise to bone-marrow HSCs which seed other tissue resident populations including those in the dermis and the gut during, a process which occurs continuously throughout life. This is a graphical summary of paragraph 1.3 which contains a more detailed description and the relevant references.

Since, it has become apparent that the origin of macrophages inhabiting different tissues is highly variable. Some tissue-resident macrophage populations, such as Kupffer cells[38], Langerhans Cells[25] and microglia[24,39] are

embryonically-seeded and completely self-maintaining. Others, such as the majority of tissue-resident macrophages in the gut wall[40], rely on continuous replenishment from circulating monocytes. Finally, some tissues, such as the heart[41], the peritoneal cavity[42] ,the lung[43] and intestine[44] are inhabited by phenotypically and functionally distinct subsets of embryonically-seeded and monocyte-derived macrophages. To what degree these dynamics take place in human macrophage populations has remained unclear. However, investigation of skin macrophages in sex-mismatched bone marrow transplant patients suggested that even 1 year after transplantation approximately a quarter of skin macrophages were not replaced[45],suggesting these cells are self-maintaining.

Although a full understanding of these dynamics is still lacking, taken together these data support a model whereby tissue-resident macrophages are seeded during embryogenesis. Depending on the tissue and potentially their anatomical location within the tissue, tissue-resident macrophages are reliant on infiltrating monocytes for replenishment throughout life in varying degrees.

1.4 Tissue-specific identity and functionality of tissue-resident macrophages

With the advent of next-generation sequencing technologies it has become apparent that different tissue-resident macrophage subsets share a core panel of genes, reflective of their shared functionality, but also contain a gene signature uniquely adapting them to carry out tissue-specific functions required to maintain homeostasis[7-9,46]. Some of these tissue-specific functions have been characterized and linked to human pathologies. A good example of this is the clearance of surfactant by alveolar macrophages and consequently the development of proteinosis in lungs devoid of alveolar macrophages. Proteinosis develops in the lungs of transgenic CSF2Rb$^{-/-}$ [47] mice and patients with mutations in the CSF2R[48,49], both of whom lack alveolar macrophages. Other tissue-resident macrophages that have been functionally characterized are Kupffer cells in the liver that are required for effective erythrocyte-derived

iron recycling[50] and microglia in the brain, implicated in synaptic pruning[51,52](reviewed in[10]). This raises the question of how this unique tissue-resident identity and functionality is imprinted and develops. As mentioned, different tissue-resident macrophages across tissues share a core program of genes related to shared functions. This core program is driven by a group of lineage-determining transcription factors[6]. The most well characterized of these lineage-determining transcription factors are Pu1[53,54], MafB[55] and the more recently discovered, Zeb2[56]. These core-program transcription factors drive expression of various pattern recognition receptors, Fc-receptors and phagocytic receptors required for core macrophage functionality described in section 1.2. Critically, Pu1 drives expression of CSF1R the receptor for CSF1 and Il34 which is vital for the survival and proliferation of most tissue-resident macrophage populations[54].

Upon this shared signature a tissue-specific gene identity is overlaid by tissue-identity imprinting transcription factors. A number of these tissue-identity imprinting transcription factors have been identified[6,57]. Recent findings have indicated that identity-imprinting transcription factors are not necessarily tissue-specific but can even be specific to one region within a tissue. For example, splenic red pulp macrophages rely on the transcription factor Spi-C[58] whereas splenic marginal zone macrophages rely on LXRα[59]. In addition, some tissue-identity driving transcription factors are seemingly shared between tissue-resident macrophages in different sites. A striking example of this overlay is the shared dependency of peritoneal and alveolar macrophages on C/EBPβ[60] and BHLHE40[61,62]. This overlap may indicate some degree of functional similarity. However, peritoneal macrophages are also uniquely dependent on the transcription factor GATA6[63-65] whereas alveolar macrophages are uniquely dependent on the nuclear receptor PPARγ[66] and the transcription factor BHLHE41[61]. Hence, the unique identity of tissue-resident macrophages is not necessarily dictated by unique tissue-identity imprinting transcription factors but rather a distinctive combination of transcription factors.

1.5 Plasticity of the tissue-resident macrophage identity.

It remained unclear how the tissue-resident identity is imparted on macrophages. Work by Lavin et al[7] and Gosselin et al found[9] an important role for the microenvironment in shaping tissue-resident identity via chromatin accessibility. Tissue-specific signals shape the chromatin landscape of resident macrophages thus impacting genome accessibility. Specifically, tissue signals were found to alter the chromatin landscape to allow binding of the core macrophage transcription factor Pu1 to common genomic locations, shared across tissue-resident macrophage subsets, but also to unique tissue-resident specific genomic locations[9]. Moreover, tissue signals altered the chromatin landscape to allow binding of tissue-resident specific transcription factors such as LXRα and GATA6[9]. After lethal irradiation tissue-resident macrophages in the liver, lung, spleen and liver were replaced by bone marrow-derived cells that adopted a complete resident-like epigenetic enhancer landscape[7]. Moreover, mature peritoneal macrophages transferred into the lung adopted an alveolar-like transcriptional identity, suggesting a high degree of plasticity[7]. Hence, monocytes and macrophages are highly plastic cells, reliant on environmental cues to imprint the resident identity and likely functionality.

Since, a number of these of environmental signals have been identified. For example, PPARγ, driving the alveolar macrophage signature, is regulated by GM-CSF abundant in the alveoli[66]. Conversely, expression of GATA6, the transcription factor that dictates the peritoneal macrophage identity, is driven by retinoic-acid, abundant in the peritoneal cavity micro-environment[63]. At present, little is known about the factors that drive CEBP/β, the transcription factor required for both peritoneal and alveolar macrophages[60], but it possible that expression of this transcription factor is driven by environmental cues shared between the alveolar space and the peritoneal cavity.

Based on these findings a number of studies set out to ascertain whether monocytes could give rise to bona-fide resident macrophages that are normally of embryonic origin, such as alveolar macrophages in the lung and Kupffer cells in the liver.

Utilizing $Csf2Rb^{-/-}$ mice devoid of alveolar macrophages it was found that transferred yolk-sac macrophages, fetal-liver monocytes and bone marrow-derived monocytes give rise to alveolar macrophages that are transcriptionally equivalent to embryonically seeded alveolar macrophages and clear surfactant. Importantly, all three transferred precursor populations expanded and fully reconstituted the alveolar macrophage niche. In contrast, transferred mature tissue-resident macrophage populations, including Kupffer cells and colonic macrophages did not persist. Unlike the study by Lavin et al, this study found that while transferred peritoneal macrophages persisted, these cells did not expand and only partially adopted an alveolar phenotype[67].

Subsequent studies in the liver found that following artificial depletion of embryonically-seeded Kupffer cells the liver macrophage compartment is reconstituted monocyte-derived Kupffer cells[38]. However, to what degree these cells were equivalent to bona-fide Kupffer cells varied depending on study. One study utilized a Clec4f-DTR mice to deplete embryonically-seeded Kupffer cells. Monocytes infiltrated the liver following Kupffer cell depletion and by day 15 had partially adopted a Kupffer cell transcriptome and by 30 almost completely adopted a Kupffer cell transcriptome. Moreover, these monocyte-derived Kupffer cells had similar self-renewal capacity and similar capacity to phagocytose *Escherichia coli* particles *ex vivo*[38]. In contrast, Beatie et al. found monocyte-derived Kupffer cell remained more transcriptionally distinct from their embryonically seeded counterparts than suggested by Scott et al. and had enhanced capacity to phagocytose *Neisseria meningitidis* and *Listeria monocytogenes in vivo* but responded similarly *to Leishmania donovani* infection[68]. One further study by David et al. indicated that monocyte derived Kupffer cells have impaired capacity to phagocytose E coli *in vivo* until 17 days after repopulating the depleted liver[69]. Furthermore, chemical injury of liver

was worse for at least 1 month in after Kupffer cell-depletion but had returned to normal by 2 months following depletion. Importantly, these studies utilized different tools to deplete Kupffer cells. Whereas Scott et al. and David et al. specifically depleted embryonically-seeded Kupffer cells using transgenic Clec4f-DTR mice[38] or clodronate liposomes[69], Beattie et al. lethally irradiated mice to deplete Kupffer cells[68]. Consistent with less targeted methodology Beattie et al found evidence of transient inflammation in the liver shortly after depletion[68] whereas the other studies did not. Similar studies depleting microglia using transgenic CX3CR1^{CreER} R26^{DTA} [70] mice or using lethal-irradiation[71] found that infiltrating monocytes give rise to monocyte-derived microglia that remain transcriptionally and phenotypically distinct from their embryonically seeded counterparts. Combined these studies suggest that monocyte derived cells can give rise to bona-fide tissue-resident macrophages but that the context under which they infiltrate the tissue may be altering their capacity do so.

1.6 The niche hypothesis as a model of tissue-resident identity

The observation that monocytes are capable of reconstituting an artificially depleted macrophage compartment and adopt a tissue-resident identity led to the formulation of the niche hypothesis by Guilliams et al. in 2017[72]. In short, they postulated that all macrophage precursors have the capacity to reconstitute a macrophage compartment but cells compete for a limited number of 'niches'. If the niche is available, a precursor-cells can take up residence in the niche which provides signals to adopt the unique tissue-resident identity. In some tissues, such as the liver, resident macrophages repopulate the niche when it becomes available as low numbers of resident macrophages die under homeostatic or mildly inflamed conditions. Under these conditions resident macrophages have a repopulation advantage and prevent monocytes from repopulating the available niche space. If more catastrophic loss of resident macrophages occurs resident monocyte repopulation does occur in these tissues.

This model was largely based on liver studies and indeed the first detailed description of the cellular composition of the macrophage niche was found in the liver. Using a combination of live imaging techniques and transgenic mouse lines Bonnardael et al[73] observed that monocyte that infiltrate the liver after depletion of Kupffer cells migrated to distinct areas in the perisinusoidal space and interacted with endothelial cells and stellate cells to acquire the Kupffer cell-identity determining transcription factor LXRα, and with hepatocytes to acquire expression of the ID3, another Kupffer cell-identity determining transcription factor. Work by Sakai et al published around the same time corroborated these findings and indicated that Notch signaling activated enhancers to drive LXRα and establish the Kupffer cell-identity[74].

Moreover, the niche concepts includes a role for niche cells in providing factors required for macrophage survival as well as imprinting. It has long been known that most tissue-resident macrophages rely on CSF1 for survival and proliferation and hence production of is likely to form a core part of any niche[75]. It has been postulated that for tissue-resident macrophages to acquire sufficient levels of CSF1 to undergo the proliferation required to self-maintain, a local source of CSF1 is required[76,77]. In various tissues where tissue-resident macrophages rely on CSF1[78], CSF1 producing stromal cells have been identified including the spleen[79], the liver[73] and the peritoneal cavity[80]. This exchange of growth factors between macrophages and stromal cells is similar to the two-cell systems proposed by Zhou et and colleagues which was based on their studies were macrophages and fibroblasts that were co-cultured and found to provide one another with survival factors. Macrophages provided PDGFB to fibroblasts whilst fibroblasts provide CSF1 indicating a symbiotic relationship[81].

Hence the tissue niche provides both identity and survival factors to the macrophages that inhabit the nice.

1.7 The effect of inflammation on the origin of resident macrophages.

It is poorly understood how the niche may be altered following an inflammatory insult, and how monocytes are programmed into resident macrophages after taking up residence in the niche under steady state conditions or following inflammation or artificially-driven depletion of resident macrophages. This question concerning the niche hypothesis in the context of inflammation is highly relevant as the biological process where a high degree of tissue-resident replacement is likely to occur is following inflammation. Indeed, inflammation induced loss of tissue-resident macrophages and a concurrent influx of monocytes has been observed in numerous tissues including the liver[69,82,83] the brain[84,85] and the peritoneal cavity[86,87]. Some studies indicated that monocytes only transiently inhabited the tissue in mouse models of acetaminophen induced liver injury[83] and encephalitis[85]. In contrast, it has been found that monocytes integrate into the resident macrophage compartment following autoimmune hepatitis-induced loss of Kupffer cells in the liver although it is unclear whether these cells persist long-term[88].

During the last year of my PhD there has been a number of studies that have shown that tissue inflammation can drive monocyte integration into the macrophage compartment in various tissues. In the skin, monocytes were found to give rise to Langerhans cells that transcriptionally resembled their embryonically seeded counterparts in a model of graft versus host disease [89]. Meningeal infection with lymphocytic choriomeningitis virus induced loss of resident macrophages and long-term integration of monocyte-derived macrophages but these cells remained transcriptionally and functionally discrete [90]. Monocytes were shown to give rise to long-lived Kupffer cells in the liver following loss of embryonically seeded pro-inflammatory Kupffer cells in a model of non-alcoholic steatohepatitis [91]. Similar integration occurs in metabolic-associated fatty liver disease[92] after which monocyte-derived Kupffer cells were found to inhabit discrete anatomical zones in the liver, compared to embryonically-seeded Kupffer cells. In the lungs, following bleomycin treatment, monocytes integrate into the alveolar macrophage

compartment and have a pro-fibrotic effect but also retain significant transcriptional differences, even by 10 months post injury[93]. Influenza drives integration of monocytes into the alveolar macrophage compartment that confer protection to subsequent *Streptococcus pneumonia* infection[94] but this effect was found not to last beyond 1-month post-viral infection.

These data emphasize that the degree and type of inflammation and also potentially the tissue site are likely determinants of monocyte fate following resolution of an inflammatory event. Moreover, these studies highlight the importance of understanding to what degree monocyte integration into the resident-macrophage compartment occurs, the potential impact of this phenomenon and the factors that dictate this integration following inflammation.

1.8 The peritoneal macrophage niche

Peritoneal cavity macrophages are arguably one of the most studied populations of tissue-resident macrophages. As the peritoneal cavity is a fluidic environment and peritoneal macrophages are easily collected by lavage as a single cell suspension, this site has often been used to model inflammation and these cells used to model and investigate macrophage functions. The peritoneal macrophage compartment is thought to consist of two subsets of peritoneal macrophages[95] By far the most predominant population of these cells have historically been characterized by high levels of the macrophage marker F4/80 and variable levels of MHCII and are often referred to as large peritoneal macrophages (LPM)[42,96] on the count of having a mean diameter of approximately 11μm. On the basis of surface markers, a second rarer population of peritoneal macrophages characterized by low levels of F4/80 and high levels of MHCII has been identified, referred to as small peritoneal macrophages as these cells have are smaller than their LPM counterparts with a mean diameter of approximately 8μm [42,95,96].

The origin of these macrophage subsets remained unclear until relatively recent. In CCR2$^{-/-}$ mice, in which monocytes are unable to egress from the bone marrow, it was found that the number of LPM was unaltered whereas numbers of SPM were strongly reduced suggesting that LPM self-maintain independent of circulating monocytes[42]. Moreover, LPM did not label in studies by Yona et al utilizing inducible CX3Cr1^{creER}-R26^{yfp} reporter mice, again indicating these cells do not rely on circulating monocytes for replenishment[28]. The most detailed description on the origin of peritoneal LPM and SPM came from Bain et al[42]. Utilizing a partial bone marrow chimera methodology, they irradiated the hindlegs of mice whilst protecting the peritoneal cavity resident macrophage pool. Hence, tissue-protected bone marrow chimeric mice, allowed them to ascertain contribution of bone marrow-derived cells to the peritoneal macrophage compartment without the confounding effects of full body irradiation. These studies indicated a low degree of chimerism 8-12 weeks following reconstitution but increasing chimerism 36 weeks after reconstitution. Hence, these data supported the notion that LPM were long-lived cells but that with time these cells were replaced by monocyte-derived macrophages. Moreover, monocyte integration into the LPM compartment occurred much more rapidly in males than in females, a phenomenon which was later found to be mediated by the local microenvironment following sexual maturation[97]. Moreover, found a high degree of chimerism of the SPM population indicating that these cells rely on continuous replenishment by circulating monocytes for their maintenance and are likely short-lived[42]. Because of their longer lifespan and their abundance, LPM are generally considered the resident macrophages of the peritoneal cavity.

The finding that circulating monocytes contribute to both the LPM and SPM in the peritoneal cavity suggests that the cavity microenvironment may contain factors that imprint the LPM or SPM identity on infiltrating monocytes. The identity of resident-LPM appears to be driven predominantly by environmental signals via tissue-resident identity imparting transcription factors. In the peritoneal cavity the CCAAT/enhancer binding protein (CEBP/β)[60] and GATA binding protein 6 (GATA6)[63-65] have been identified as tissue-resident identity

driving transcription factors. Loss of either one of these transcription factors leads to almost complete loss of peritoneal resident-LPM. Moreover, the small population of GATA6-deficient LPM lacks expression of a large set of genes expressed specifically by peritoneal LPM[63-65]. The number of SPM are unaffected in these mice, indicating that LPM and SPM, whilst inhabiting the same cavity, are regulated independently of one another.

Recent work has indicated that smaller subsets of tissue-resident identity genes are lost in peritoneal resident-macrophages deficient in the transcriptional factor BHLHE40[62] and the ligand-dependent transcription factors Retinoid X receptor alpha (RXRα) and beta (RXRβ)[98]. Both GATA6[63] and RXR signalling[98] are responsive to the active metabolite of vitamin A, retinoic-acid. In the peritoneal cavity the predominant source of retinoic-acid is thought to be mesothelial and fibroblastic stromal cells in the omentum[63,99]. At present little is known about how GATA6, RXRs or CEBP/β affect the lifespan of LPM.

In addition to serving as a source of retinoic-acid the omentum, a sheet of intra-abdominal adipose tissue directly adjacent to the peritoneal cavity[100], is thought to be important for the identity of resident-LPM in the peritoneal cavity[101]. It has been postulated that monocytes traverse through the neighbouring omentum and require GATA6 to exit the omentum and take up residence in the peritoneal cavity. However, this hypothesis is largely based on the accumulation of macrophages in the omentum of macrophage-specific GATA6-deficient mice, but no direct evidence of migration from omentum into the cavity has been shown[63]. The omentum is also thought to produce a variety of other, poorly defined, factors that drive expression of a set of peritoneal tissue-resident identity genes[63,99]. In addition, the omentum[102] and peritoneal mesothelium[80] are thought to be the predominant source of CSF1 in the cavity, vital for peritoneal macrophage survival. As the peritoneal cavity is a fluidic environment in which peritoneal cavity macrophages 'float'[103], most environmental cues are thought to be secreted factors. However, it has been postulated that peritoneal macrophages intermittently interact with cells that

line the peritoneal cavity. Indeed, peritoneal mesothelium has been shown to produce secreted and membrane bound CSF1 both of which can drive peritoneal macrophage proliferation *in vitro*[80] but that membrane bound CSF1 signalling requires direct interaction with peritoneal macrophages to do so. Similarly, omentum factors are thought to be secreted into the cavity and drive peritoneal macrophage identity[99]. However, a small subset of peritoneal identity genes are only induced by direct interaction between omentum cells and peritoneal macrophages *in vitro*[99], suggesting that interaction, likely intermittent, between peritoneal macrophages and omentum cells is required for peritoneal macrophages to completely adopt a resident identity.

At noted before, in contrast to their resident counterparts, the SPM in the peritoneal cavity do not rely on GATA6 for their development. Instead, SPM development relies on the transcription factor IRF4 and signals arising from the microbiota[104]. Interestingly, studies in macrophages deficient in GATA6 or CEBP/β observed a striking reduction in the overall numbers of peritoneal macrophages suggesting there was no compensatory increase in the number of SPM[60,63] to replace lost LPM. Loss of RXRαβ signalling in macrophages similarly depleted LPM but did lead to a concurrent increase in F4/80^{Lo}MHCII^{Hi} cells which transcriptionally resembled SPM, and expressed high levels of IRF4. Hence, these data suggest that RXRαβ signalling limits the SPM niche[98]. Indeed, SPM express both RXRα and RXRβ but less than their resident counterparts[98]. Finally, both resident-macrophages and SPM express CSF1R[105] and rely on CSF1 for their survival[106] and would appear to share a survival niche, as they are likely competing for secreted and membrane bound CSF1. Taken together, these data suggest that, except for CSF1, the environmental cues that dictate the number and identity of resident-LPM are largely discrete from those that drive the number and identity of SPM. This difference is surprising as both cells seemingly inhabit the same micro-environment unlike in, for example, the spleen and gut, where tissue-resident identity is imprinted by distinct anatomical regions[58,59,107].

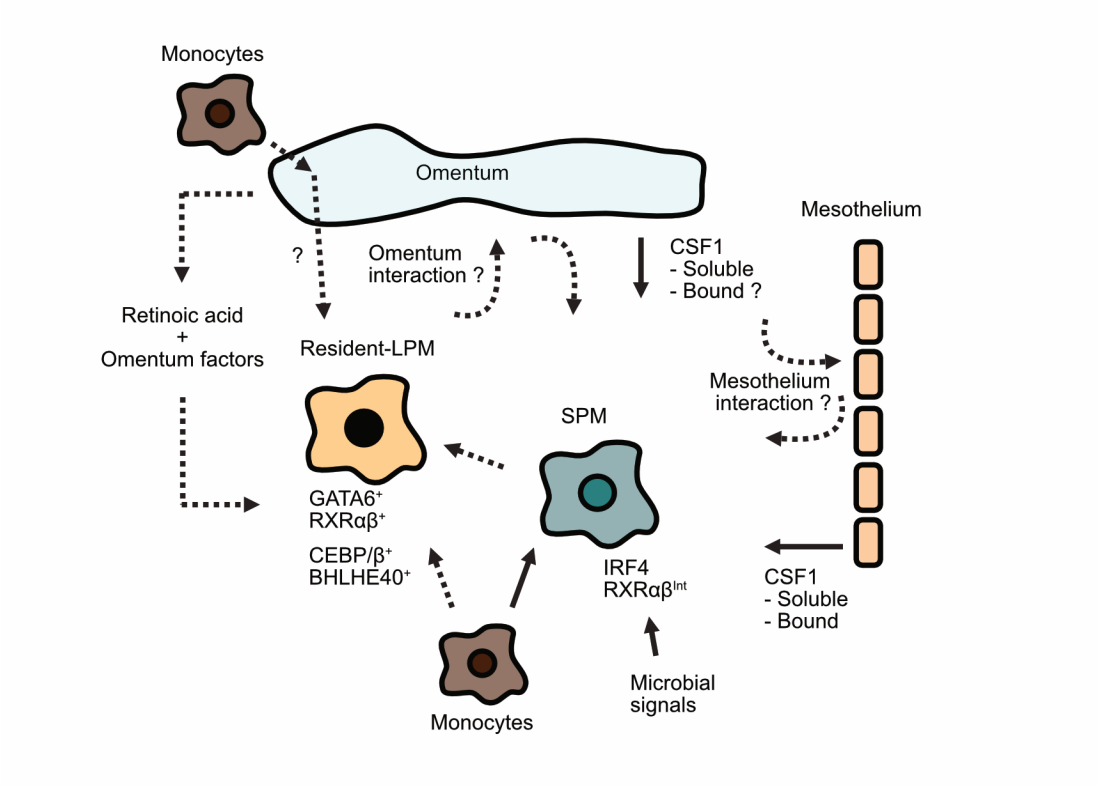

Figure 1.2 The peritoneal niche.

Overview macrophage subsets present in the steady-state peritoneal cavity with known identity-determining transcription factors and environmental signals. Interactions definitively shown to occur in vivo are depicted using solid lines. Interactions that are postulated to occur, or have been shown in vitro are in depicted using dashed lines. Resident-LPM account for the majority of macrophages in the peritoneal cavity and rely on a number of transcription factors (listed below the cell) to drive their peritoneal macrophage identity. The main transcription factor GATA6 is driven by retinoic acid, thought to predominantly originate from the omentum. The omentum also produces omentum factors that drive part of the resident LPM identity although the extent to which this occurs in vivo is unclear. Resident LPM are replaced by monocyte-derived cells over time but it is unknown whether infiltrating monocytes can give rise resident-LPM directly have to develop into SPM before giving rise to resident-LPM. Moreover, it is unclear if monocytes infiltrate the cavity directly or traverse the omentum before entering the peritoneal cavity. The smaller population of SPM in the cavity are derived from

circulating monocytes and rely on IRF4/microbial signals to establish their identity. Both peritoneal macrophage populations rely on CSF1 for survival and proliferation. The predominant source of CSF1 in the cavity are the omentum and the surrounding mesothelium both of which secrete CSF1 into the peritoneal cavity microenvironment but also produce membrane bound CSF1. The importance of the latter for peritoneal macrophage survival and proliferation is unclear. This is a graphical summary of paragraph 1.8 which contains a more detailed description and the relevant references.

Recently our lab has utilized single cell sequencing and found that the cells initially considered LPM actually comprise 3 transcriptionally distinct populations of cells. The predominant population of these cells consists of long-lived LPM whereas two smaller subsets of LPM are monocyte-derived[97] as determined by analysis of their replenishment by monocytes using tissue-protected bone marrow chimeras. Similar LPM heterogeneity was found using single cell sequencing by Wang et al[108] but contrasted by Lantz et al[109] who identified a cluster of Il1β producing LPM, not observed in our studies or by Wang et al. The developmental relationship between these resident-LPM clusters and if these cells share the same niche is unclear.

1.9 The function of resident peritoneal macrophages

Our overall understanding of the function of peritoneal macrophage is incomplete. It has been found that the phosphatidylserine receptor Tim4[110], a marker for the embryonically seeded subset of peritoneal resident-macrophages[42] is vital for peritoneal cavity homeostasis[20] and is required for the immunologically silent clearing of apoptotic cells[21]. As Tim4 expression is limited to the embryonically seeded cluster of resident-macrophages these cells may be uniquely adapted for apoptotic cell clearance. In addition to clearing apoptotic cells peritoneal macrophages have been found to carry out immunological functions, including the clearance of *Streptococcus pneumoniae(S.Pneumoniae)*[97,111] and *Escherichia coli* (*E.coli)*[103,112] and limiting dissemination of bacteria from the peritoneal cavity to the blood[103]. In

addition, a surprising function of peritoneal cavity macrophages is their ability to infiltrate the liver following a burn injury[12]. More recently, resident macrophages that reside in the pericardium, a physiologically-related serous cavity that surrounds the heart, that also depend on GATA6 expression have been shown to migrate into the heart following ischemic injury. This gives confidence that this migratory capacity of GATA6-expressing serous macrophages, including peritoneal LPM, might extend into many organs[113]. Moreover, peritoneal macrophages have been implicated in a number of peritoneal pathologies including endometriosis [114,115]and development of post-surgical adhesions[116,117] although their role in these diseases is not clear. Finally, peritoneal resident-macrophages are one of the main sources of peritoneal CXCL13, a chemokine required for the maintenance of peritoneal B1 cells in the cavity[118].

1.10 Dynamics of acute peritoneal inflammation

Various irritants have been utilized to induce acute peritoneal inflammation. Some infectious models including the cecal ligation and puncture model or direct injection of cecal contents into the cavity have been used to model polymicrobial sepsis[119]. A drawback of infectious models is that the pathogenicity and growth rate of pathogens and the dynamics of peritoneal inflammation vary greatly. Injection pure bacteria or fungi including *Staphylococcus Pneumoniae*[120] or *Candida Albicans*[121] suffers less from the drawbacks of polymicrobial models[119,122]. In recent years, sterile models of peritoneal inflammation have been used extensively. The main strength of these models is their convenience and reproducibility in comparison to infectious peritonitis models. To induce sterile peritonitis various substances have been used most notably injection of thioglycolate broth[86], zymosan[122] or LPS[123]. For this introduction I will discuss acute phases of the zymosan model of peritonitis in more depth and highlight similarities and differences with other commonly used models of sterile peritonitis. I am focussing on the zymosan model of peritonitis as it has been used in a number of recent studies that my project is based on and it is the model that I have used in this thesis.

Zymosan is a preparation of yeast cell wall and is commonly used as a model of sterile peritonitis. Zymosan is rich in β-glucan, the most abundant fungal cell wall polysaccharide[121], which is recognized by predominantly by the pattern recognition receptor Dectin1[124] but also by heterodimeric complexes of toll-like receptor 2 and 6[125]. Dectin1 is highly expressed by peritoneal macrophages[126]. Loss of Dectin1 abrogates zymosan recognition and phagocytosis by macrophages[127] and inhibits production of pro-inflammatory cytokines such as CCL2 and Il6 in response to zymosan treatment *in vitro*[124]. Critically, loss of Dectin1 results in impaired recruitment of monocytes and neutrophils into the cavity following zymosan treatment[124], emphasizing the importance of this receptor as a mediator of fungal responsiveness. During zymosan-induced peritonitis the peritoneal cavity is infiltrated by high numbers of monocytes and neutrophils[122]. Infiltrating monocytes rely on a CCR2-dependent precursor and are thought to originate from Ly6c^{Hi} circulating monocytes[111]. During the early stages of peritoneal inflammation monocytes are characterized by high expression of the monocyte marker Ly6c, reaffirming their likely origin from Ly6c^{Hi} circulating monocytes[111]. Monocyte recruitment into the cavity relies on CCL2[128,129] and can be inhibited using anti CCL2 blocking antibody or induced by injection of recombinant CCL2[130]. Following zymosan treatment, levels of peritoneal fluid CCL2 increase and peak approximately 4 hours later before reducing in the succeeding days[128,129]. Both LPM and SPM produce high levels of CCL2, 4 hours following zymosan treatment and then produce progressively less in the succeeding 72 hours[131], suggesting these cells are an important source of CCL2 in the cavity.

Depletion of peritoneal macrophages or mast-cells suggests that neutrophil recruitment into the cavity, following zymosan treatment, is mediated by mast-cells[132]. Indeed, mast cells have been shown to express Dectin1[133] which may explain the altered neutrophil recruitment followings zymosan treatment in Dectin1$^{-/-}$ mice[124]. Although peritoneal macrophages appear to be dispensable for the recruitment of neutrophils, depletion leads to heightened neutrophil

recruitment following zymosan treatment[132]. It has been proposed that peritoneal macrophages serve as a source of anti-inflammatory Il10 which inhibits the release of inflammatory cytokines and neutrophil recruitment[132]. As inflammation resolves the number of neutrophils in the cavity rapidly declines, through neutrophil apoptosis[134,135] and potentially migration of neutrophils into the omentum[136]

A key feature of most models of peritoneal inflammation, including zymosan-induced peritonitis is the loss of resident macrophages[5,137,138]. This phenomenon has been referred to as the macrophage disappearance reaction[138] and until recently was poorly understood. It has become clear that the macrophage disappearance reaction, at least following zymosan treatment, is due to LPM forming clots that serve to entrap microorganisms[103]. This clotting reaction would appear to occur independently of Dectin1 as macrophage disappearance occurs in mice deficient in Dectin1[124]. In addition, macrophages exhibit elevated levels of apoptosis, 6 hours following zymosan treatment[134], suggesting macrophage apoptosis likely contributes to the macrophage disappearance reaction.

As described monocytes infiltrate the cavity and their influx coincides with the loss of resident macrophages. Infiltrating monocytes differentiate into a subset of phagocytes referred to as inflammatory macrophages. Inflammatory macrophages are characterized by intermediate levels of the macrophage marker F4/80 and high levels of MHCII[87,139]. In various models of peritoneal inflammation resident-LPM and monocyte-derived inflammatory macrophages have been shown to inhabit the cavity over the course of inflammation[86,87,95].

All these inflammatory phenomena are highly dependent on the degree of peritoneal inflammation. Zymosan treatment seemingly induces a dose-dependent degree of peritoneal inflammation with, as indicated by neutrophil recruitment. Low dose zymosan treatment (10μg ~$2*10^6$ particles) is used to model localized mild peritonitis ,higher doses (100/1000μg ~$2*10^{7/8}$ particles)

are used to induce more severe localized peritonitis[87,122,139] and very high dose of zymosan is used to induce chronic systemic inflammation[120] (10,000μg~2*10^9 particles). Few studies have directly contrasted changes to the peritoneal cavity following different doses of zymosan. However, zymosan treatment leads to a dose-dependent influx of monocytes and neutrophils. High dose zymosan treatment is also characterized by high levels of CLL5 in the cavity, which is largely absent following low dose zymosan treatment[122], indicating that the peritoneal micro-environment is distinctly different following high dose zymosan compared to lower doses.

Thioglycolate injection, another commonly used model of peritoneal inflammation, induces more severe localized peritonitis and is characterized by almost complete loss of resident macrophages and influx of high numbers of monocytes[86,87]. These monocytes seemingly give rise to distinct subsets of inflammatory macrophages characterized by variable levels of MHCII[86]. Nguyen et al[140] suggested that these subsets may be programmed by cavity levels of Il10, transiently increased during the acute phases of peritoneal inflammation. Monocytes that infiltrate during this acute phase adopt an $MHCII^{Lo}$ phenotype whereas monocytes that infiltrate later, when Il10 levels have decreased, adopt an $MHCII^{Hi}$ phenotype. Critically, Nguyen et al injected cecal contents to induce peritoneal inflammation and it is not clear whether similar Il10 programming may occur following thioglycolate or zymosan-induced peritonitis. In the thioglycolate model, both subsets of inflammatory macrophages have been shown to undergo high levels of apoptosis during resolution of inflammation[86] whilst a small number migrate into draining lymph nodes[141,142] although the latter has been contested[86]. Similarly, high levels of apoptosis have been observed following resolution of zymosan-induced peritonitis[134]. At the same time resident macrophages exhibit high levels of proliferation whereas only a minor subset of inflammatory macrophages exhibits comparable levels of proliferation[87,143,144]. Combined, these studies have supported the notion that inflammatory macrophages present during resolution are largely lost due to apoptosis whilst resident macrophages

undergo elevated levels of proliferation to reconstitute the macrophage compartment.

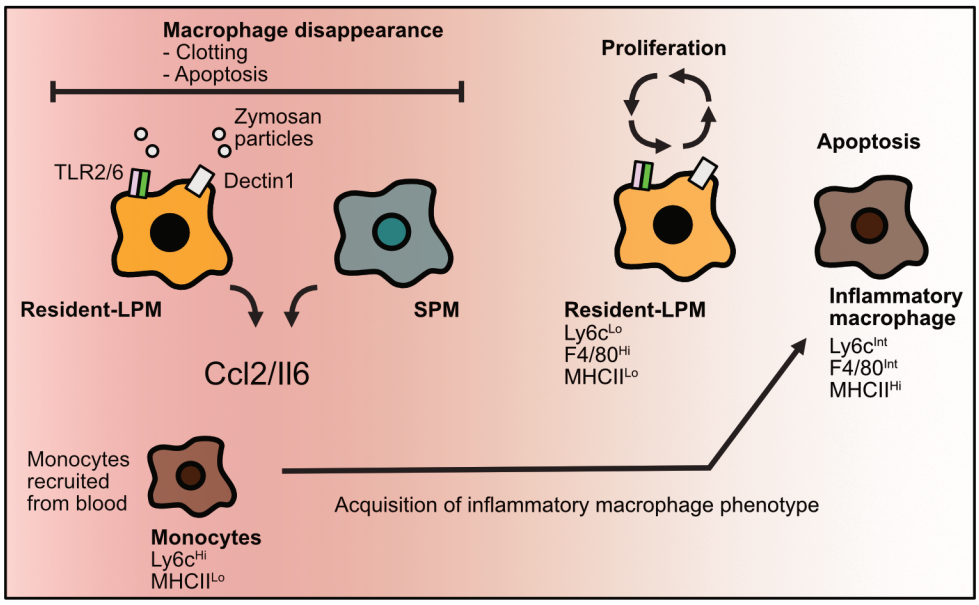

Figure 1.3 Dynamics of zymosan induced peritonitis

Overview myeloid dynamics at different stages of mild zymosan-induced peritonitis. Background colour denotes the degree of inflammation ranging from acute (red background on the left) to resolved (white on the right). Resident-LPM and SPM recognize zymosan particulates via Dectin1 and TLR2/6 heterodimers. In response to zymosan exposure both macrophage subsets produce high amounts of CCL2 and Il6. Consequently, Ly6c^{Hi} monocytes infiltrate the cavity from the blood and give rise to phenotypically distinct inflammatory macrophages over the course of the inflammatory event. Shortly following onset of inflammation resident-LPM are lost through the formation of clots and apoptosis. During resolution of inflammation (right) the remaining resident-LPM exhibit heightened proliferation whilst inflammatory macrophages seemingly undergo apoptosis and exhibit limited proliferation. This is a graphical summary of paragraph 1.10 which contains a more detailed description and the relevant references.

1.11 Monocyte-derived cells may persist after peritoneal inflammation

Because it has been assumed that resident macrophages reconstituted the macrophage compartment following peritoneal inflammation only few studies have attempted to investigate the long-term fate of monocytes. Studies utilizing CX3CR1^{CreErt2} transgenic mice to track infiltrating monocytes found evidence for some integration of monocyte-derived macrophages into the resident macrophage compartment following thioglycolate induced peritonitis[28,145]. However, interpretation of these studies is challenging as labelling efficiency of CX3Cr1^{creER}-R26^{yfp} in circulating and cavity-infiltrating monocytes was very inefficient[28]. Consequently, the number of labelled cells was quantitively minor in both studies and no definitive conclusions can be drawn regarding the survival of resident or monocyte-derived inflammatory macrophages. In later studies Gundra et al utilized CX3CR1$^{CreERT2\text{-}IRES\text{-}EYFP}$ transgenic mice to investigate monocyte integration following thioglycolate induced peritonitis. However, as the labelling efficiency of infiltrating monocytes was poor they opted to expand the entire macrophage compartment using Il4-treatment[146,147] to source sufficient labelled monocyte-derived cells for further transcriptional analysis[145]. Consequently, no definitive conclusions can be drawn about the degree to which monocytes persist following thioglycolate treatment. In addition, by pre-treating with Il4 they imprinted an Il4 gene-signature monocyte-derived macrophages making it challenging to asses to what degree these cells transcriptionally resemble bona-fide resident macrophages. Near the end of my PhD two new transgenic mouse models were developed: the Ms4a3^{Cre} -Rosa^{TdT} to track constitutive monocyte infiltration and the Ms4a3^{CreERT2} -Rosa^{TdT} to track temporal monocyte infiltration[123]. Importantly, following tamoxifen administration to Ms4a3^{CreERT2} -Rosa^{TdT} mice both circulating and cavity-infiltrating monocytes are efficiently labelled[123] unlike following tamoxifen administration to CX3Cr1^{creER}-R26^{yfp} transgenic mouse[28,145], utilized in previous studies. Using the Ms4a3^{CreERT2} -Rosa^{TdT} model, Liu and colleagues found that following thioglycolate-induced peritonitis monocyte-derived cells infiltrated the cavity that persisted up to 20 weeks following the inflammatory event[123]. However, they did not carry out in depth

analysis to the identity and functionality of these cells. The Ms4a3^{CreERT2} - Rosa^{TdT} could have been a very powerful tool for my PhD but became available too late for me to utilize.

Using a dye-labelling methodology Newson et al[111] labelled resident and inflammatory using discrete PKH-labelling reagents to track both populations long-term following zymosan-induced (100μg) peritonitis. They presented evidence that approximately half of inflammatory macrophages present 3 days after zymosan treatment persisted up until 17 days. In later experiments, survival of inflammatory macrophages up until 60 days following the inflammatory event was suggested, but the degree of integration was not quantified. As PKH-dyes are not degraded upon internalization, cells undergoing apoptosis transfer PKH-dye to engulfing phagocytes, thus confounding results when exclusively relying on dye-labelling as lineage-tracing tool. Hence, these data should be interpreted with caution. Intriguingly, 60 days following the zymosan-induced peritonitis insult neutrophil recruitment in response to *s.pneumoniae* infection was inhibited, compared to control mice that had not undergone a historic inflammatory event[111]. Although this effect could not be attributed to the integration of inflammatory macrophages it provides the evidence that the responsiveness of the peritoneal cavity on the whole is altered following a historic inflammatory event. Hence, it remains unclear to what degree monocytes integrate into peritoneal macrophage compartment following inflammation, to what degree they adopt the identity and functionality of the original tissue-resident macrophages, and what factors may regulate their integration.

It should be noted that the presence monocyte-derived cells in the resident macrophage compartment and the presence of SPM in the peritoneal cavity[42,104] provides proof-of-concept that the cavity is amenable to monocyte integration under steady-state conditions. Intriguingly, studies using the thioglycolate model of peritonitis found that following thioglycolate induced peritonitis there was small population of infiltrating macrophages that was transcriptionally distinct from inflammatory macrophages and identical to SPM

[86]. Similarly, following zymosan treatment it was found that although SPM were lost shortly after injection, a small fraction of infiltrating monocytes adopted an SPM identity whilst the majority adopted an inflammatory macrophage phenotype[139]. Hence, the inflamed peritoneal cavity is temporarily inhabited by three distinct subsets of macrophages. A relatively small population of resident LPM macrophages, a large population of inflammatory macrophages and a small population of SPM. Interestingly, these cells remain transcriptionally distinct despite seemingly being exposed to the same fluidic micro-environment[86].

These findings indicate that during peritoneal inflammation both the resident and the much smaller SPM niche are depleted and raises the question whether inflammatory macrophages are capable of colonizing either of these niches. As monocytes are known to contribute to the SPM population, differentiation of monocyte-derived inflammatory macrophages into SPM would not be surprising. If indeed this occurs, inflammatory macrophages that differentiate into SPM would likely persist relatively briefly as SPM are thought to be short-lived[42]. In contrast, if inflammatory macrophages take up residence in the resident niche, they will likely become long-lived self-maintaining cells[42].

It is challenging to extrapolate between datasets from different tissues, but there appears to be some indication that competition between infiltrating monocytes and resident-macrophages dictates the survival of the former. Following hepatic injury with acetaminophen, resident Kupffer cells are largely lost but a small persistent population undergoes high levels of proliferation to reconstitute the liver despite presence of large numbers of monocytes[83]. Similarly, following zymosan induced peritonitis resident-macrophages undergo high levels of proliferation despite the presence of high numbers of monocyte-derived inflammatory macrophages[87,143,144]. However, in the liver complete loss of Kupffer cells following viral infection[88] or bacterial infection[148] does result in monocyte integration. Although the data is incomplete, it would appear that resident-macrophages in the peritoneal cavity are lost following thioglycolate treatment and that monocytes, at least partially, reconstitute the

macrophage compartment long-term[28,123]. Hence, these data would support a key role for resident macrophage proliferation as a mechanism to inhibit integration of monocytes into the macrophage compartment.

1.12 Are monocyte-derived cells capable of reconstituting the macrophage niche.

These findings raise the question whether inflammatory macrophages have the capacity to persist and give rise to resident macrophages, irrespective of whether they are doing so following an inflammatory event. Similarly, monocyte-derived cells are capable of giving rise to Kupffer cells in the liver and alveolar macrophages in the lung but only do so in the absence of a competing population of resident macrophages. To investigate this question in the peritoneal cavity adoptive transfer of resident of monocyte-derived inflammatory macrophages into recipient mice that are deplete of peritoneal resident macrophages is the most viable option. Pan macrophage GATA6$^{KO63-65}$ and CEBPβ^{KO60} transgenic mice are largely devoid of resident peritoneal macrophages and hence could be amenable for such adoptive transfer studies without competition by incumbent resident macrophages. However, in the cavity of GATA6$^{KO\ 63-65}$ and CEBP$\beta^{KO\ 60}$ mice, a compensatory population of resident-like peritoneal macrophages has been found which are likely to compete with transferred cells. In addition, the CEBPβ^{KO60} mice suffer from peritoneal eosinophilia, suggesting profound changes to the peritoneal cavity immune compartment. Another possibility is the use of clodronate liposomes to temporarily deplete peritoneal macrophages[132]. The major advantage of this methodology is that clodronate liposomes are readily available and do not require the breeding of transgenic mouse lines. However, intraperitoneal delivery of clodronate liposomes depletes various other tissue resident macrophage populations, potentially inducing off target effects[149]. Moreover, clodronate-liposome depletion result in high numbers of apoptotic cells in the cavity[49] without the phagocytes required for immunologically silent clearing of these cells[21]. Hence, a major drawback of clodronate liposomes, and other temporary depletion methods, is the high numbers of death cells and

consequent inflammation that is induced following the depletion. Moreover, following clodronate depletion monocytes are likely to infiltrate the depleted tissue and thus only provide a limited window of time during which cells could be adoptively transferred. Finally, it is essential to validate that clodronate liposomes are effectively cleared at the time of transfer to prevent depletion of transferred phagocyte populations.

Recently a novel transgenic mouse model has been developed that is deficient in the fms-intronic regulatory element region of the CSF1r (FIRE$^{-/-}$) and consequently lacks various tissue-resident macrophage populations including peritoneal macrophages[106].Unlike GATA6^{KO} [63-65] and CEBPβ^{KO} [60] mice FIRE$^{-/-}$ mice do not have a compensatory population of resident-like macrophages in the peritoneal cavity[106]. Hence, this model would be a very powerful tool to use as it allows investigation of the fate potential of inflammatory macrophages without the confounding effects of resident-like macrophages or infiltrating monocytes. Although these mice are seemingly healthy it is important to note that the lack of peritoneal macrophages is potentially altering cavity homeostasis, which in turn may alter the fate of transferred cells. Moreover, it is unknown whether peritoneal macrophage produce factors required for the survival of other (immune) cells that are in, or adjacent to, the peritoneal cavity[150] and that consequently these cells could also be altered in FIRE$^{-/-}$ mice. This could in turn alter the cavity microenvironment and affect the fate of transferred cell populations. These phenomena have not been characterized in depth and could greatly affect the findings from adoptive transfer studies utilizing FIRE$^{-/-}$ recipient mice.

Hence, no perfect model exists to investigate the capacity of monocyte-derived inflammatory macrophages to persist in the cavity in the absence of competition. Instead, adoptive transfer of purified macrophage populations into clodronate-depleted or FIRE$^{-/-}$ recipient mice would be preferable as these methodologies complement one another.

1.13 Immune memory could affect resident or monocyte-derived macrophages following inflammation

An increasing number of studies have indicated that exposure of innate immune cells to inflammatory stimuli can 'train' these cells so upon re-exposure to inflammatory stimuli their response is altered. Epigenetic changes were found to underlie this innate immune memory[151,152]. Critically, exposure of monocytes to *Candida Albicans* or β-Glucan has been found to induce Dectin1-mediated epigenetic changes and leads to enhanced cytokine production *in vitro* and *in vivo*[153]. Little is known about epigenetic memory that may be acquired by monocytes that infiltrate the peritoneal cavity during peritonitis. However, *In vitro* studies have found heightened TNFα production by thioglycolate-elicited inflammatory macrophages in response to LPS treatment after pre-treatment with β-Glucan[154]. Hence, monocytes infiltrating the cavity during an inflammatory event could be imprinted to give rise to macrophages that are phenotypically and functionally distinct from resident-LPM but also differ from monocyte-derived macrophages that have differentiated under steady-state conditions.

1.14 Project aims

It is clear that monocyte integration into the resident-macrophage compartment occurs following inflammation in a number of tissues and that these cells can impact on tissue health and ability to respond to subsequent inflammatory insults. What underlies the divergent functions of such cells remains unclear but may be related to monocytic origin or related to the conditions under which these cells have differentiated or inhabit the cavity following resolution of inflammation.

It has remained unclear recruited monocytes integrate into the resident population following peritoneal inflammation. Due to the use of different models of peritoneal inflammation in combination with imperfect lineage-

tracing methodologies incomplete and contrasting datasets have been generated. Although the transcriptional identity of peritoneal macrophages has been shown to largely depend on environmental cues such as retinoic acid, it has remained unclear whether the niche hypothesis, based on phenomena observed in solid tissues, is applicable to tissue-resident macrophages in fluidic environments such as the peritoneal cavity. Moreover, it is unclear how inflammation alters the peritoneal micro-environment which may impact on the identity and functionality of both resident and inflammatory macrophages that inhabit the cavity.

Hence, I hypothesized that monocyte-derived inflammatory macrophages have the capacity to survive long-term and integrate into the peritoneal macrophage compartment. Following mild peritoneal inflammation, monocyte-derived inflammatory may not persist as resident LPM undergo proliferation to prevent integration of these cells into the macrophage compartment. However, following more complete loss of resident macrophages that may accompany severe peritonitis, monocyte-derived inflammatory macrophages will persist more readily. Moreover, I hypothesized that monocyte-derived inflammatory macrophages may be relying on environmental niche signals present in the peritoneal microenvironment to undergo conversion into resident peritoneal macrophages. Consequently, failure of monocyte-derived inflammatory macrophages to obtain these signals may prevent them from adopting a resident phenotype and functionality.

To investigate these hypotheses, I aimed to:

- Develop an adoptive transfer methodology to investigate long-term fate of inflammatory macrophages following resolution of peritonitis.
- Determine if inflammatory macrophages persist following resolution of mild peritonitis, and adopt a resident phenotype.
- Examine whether inflammatory macrophages persist long-term following mild peritonitis and adopt a transcriptional and phenotypic resident identity.

- Ascertain whether the post-inflammatory micro-environment, and particularly competition with resident macrophages, regulates inflammatory macrophages survival to and phenotypic conversion.
- Determine whether inflammatory macrophages that persist following peritoneal inflammation are functionally equivalent to resident macrophages.
- Investigate whether severe peritoneal inflammation leads to greater disappearance of resident macrophages and if this is associated with greater integration of inflammatory macrophages.

Chapter 2

Materials & Methods

2.1 Animals

Mice were bred and maintained in specific pathogen-free facilities at the University of Edinburgh. Unless indicated, all mice used were female and age-matched at 6-10 weeks of age at onset of the experiment. Work was carried out in various University of Edinburgh animal facilities. Early experiments, presented in chapter 3, were largely carried out at the Ann Walker facility and the March animal facility at King's Buildings campus. Later work was carried out at the Scottish Centre for Regenerative Medicine animal facility and Little France Phase 2 both at Little France campus. All experiments were permitted under project license (PP0860257) granted by the UK Home Office and approved by the University of Edinburgh Animal Welfare and Ethical Review Body.

C57BL/6-CD45.2$^+$ mice used during early studies were originally purchased from Charles River and bred in-house at the Ann Walker facility. To generate congenic C57BL/6 CD45.1$^+$CD45.2$^+$ mice, C57BL/6 CD45.2$^+$ were crossed with C57BL/6 CD45.1$^+$ mice in-house. During later studies C57BL/6 CD45.2$^+$ mice were obtained from the in-house colony of the Scottish Centre for Regenerative Medicine animal facility. To generate C57BL/6 CD45.1$^+$CD45.2$^+$ mice, C57BL/6 CD45.2$^+$ were crossed with C57BL/6 CD45.1$^+$ mice. FIRE$^{-/-}$ mice were a gift from Dr.Clare Pridans. FIRE$^{-/-}$ mice were generated on a B6CBAF1/J background[106] and crossed to C57BL/6. Offspring were interbred to establish the transgenic line. Mice used for experimental work were on a mixed background as the phenotype had proved to be lethal on a pure C57bl/6 background (personal communication C. Pridans and D. Hume). FIRE$^{-/-}$ mice were bred by in the Little France phase 1 animal facility. Mice were culled using increasing exposure to CO_2.

2.2 Tissue-protected bone marrow chimeras

Eight week-old female C57BL/6 CD45.1$^+$CD45.2$^+$ or CD45.2$^+$ C57BL/6 mice received subcutaneous injection of 8µl/g anaesthetic reagent, detailed below.

Reagent	Dose	Manufacturer
Medetomidin	500µl	Sold as Domitor by Vetoquinol
Ketamine	380µl	Boehringer Ingelheim
Sterile PBS	+4.12ml	Gibco

The hind-legs were exposed to a single dose of 9.5 Gy γ-irradiation for 19 minutes and 30 seconds. The rest of the body was protected by a 2-inch lead shield. Following irradiation mice were kept at 37°C to aid recovery. By 24 hours later animals were given 2-5×10^6 Bone marrow cells IV. Bone marrow cells were sourced from sex-matched congenic CD45.2$^+$ C57BL/6J or C57BL/6J CD45.1$^+$CD45.2$^+$. This protocol to generate tissue-protected bone marrow chimaeras is similar to the published protocol from the Jenkins laboratory[42]. Following reconstitution mice were kept for 8 weeks or 26 weeks due to COVID19 restrictions prior to zymosan treatment.

2.2.1 Preparation of donor bone marrow cells

To collect bone-marrow cells CD45.2$^+$ C57BL/6J or C57BL/6J CD45.1$^+$CD45.2$^+$ mice were culled as described. The tibia and femurs were collected and placed in ice-cold 70% ethanol. The bones were briefly washed using PBS and, using sterilized scissors and forceps, both ends of each bone were removed. Using a 23-gauge needle (BD) and a 10ml syringe, bone marrow was flushed from each bone with approximately 10ml of RPMI 1640 (Gibco). By repeatedly aspirating the cell mixture with a syringe, the bone marrow was broken up and a single cell suspension was prepared. The solution was filtered through a 40µm filter (VWR) into a 50ml falcon tube. Samples were centrifuged (300g at 4°C for 5 minutes) followed by red blood

cell lysis for 5 minutes using 5ml of red blood cell lysis buffer (Sigma). Cells were washed and resuspended in RPMI 1640 and counted using a haemocytometer. Cells were resuspended at $2.5x10^7$ cells/ml in dPBS (Gibco). For reconstitution mice received 200µl of bone-marrow mixture via intravenous tail vein injection.

2.3 Peritoneal inflammation models

All reagents that have been used in this thesis are detailed in **Table 1.**

2.3.1 Zymosan model of sterile peritonitis

A stock of zymosan was prepared by diluting 0.01g of Zymosan A (Sigma-Aldrich) in 1ml of sterile Dulbecco's PBS (dPBS; Invitrogen). The mixture was incubated at 95°C for 10 minutes and intermittently vortexed. The mixture was further broken up aspirating the mixture repeatedly using a 1ml syringe with a 23g needle (BD) followed by repeated aspiration using a 27g needle (BD). The resulting mixture was checked under a light microscope to verify no clear 'clumps' of zymosan were present. Stock was stored at 4°C for up to 2 weeks prior to use. On the day of injection stock solution was briefly vortexed and a working solution was prepared in sterile dPBS (Invitrogen). The working solution equilibrated to room temperature prior to use. To elicit sterile peritoneal inflammation, mice were injected IP with 10µg,100µg or 1000µg of zymosan A (Sigma-Aldrich) suspended in 200µl dPBS (Invitrogen). All steps, except zymosan weighing, were carried out in a laminar flow hood.

2.3.2 LPS model of peritonitis.

A stock solution of 1mg/ml of LPS (O111:B4; Sigma-Aldrich) in sterile dPBS (Invitrogen) was prepared and stored at -80°C in 50µL aliquots. On the day of injection, a working solution was prepared by diluting stock LPS in sterile dPBS (Invitrogen). To elicit inflammation, mice were injected IP with 5µg of LPS suspended in 200µl dPBS (Invitrogen). The injection solution was equilibrated to room temperature prior to injection. All steps were carried out in a laminar flow hood.

2.4 Other substances administered

All substances were equilibrated to room temperature prior to injection and administered IP using insulin syringes (BD)

2.4.1 Clodronate liposomes

Clodronate liposome stock (Liposoma) was stored at 4°C according to the manufacturer's instructions. On the day of injection, the appropriate amount of clodronate liposomes stock (5mg/ml) was diluted in sterile dPBS (Invitrogen). For earlier titration studies the indicated dose of clodronate liposomes was diluted in a total volume of 250ul sterile dPBS (Invitrogen) and administered IP. For subsequent studies 0.0625mg clodronate liposomes (Liposoma) diluted in a total volume of 250ul dPBS (Invitrogen) was administered IP to deplete peritoneal phagocytes. The injection solution was equilibrated to room temperature prior to injection. All steps were carried out in a laminar flow hood.

2.4.2 PKH26-PCL red fluorescent cell linker

Components were stored at 4°C according to the manufacturer's instructions. On the day of injection, a working solution of 700nm was prepared by diluting stock PKH26 cell linker (1000μM) in Diluent B (Sigma-Aldrich) to a working solution of 700nM. Mice were injected IP with 250μl of working solution equivalent to the dose used by Newson et al[120]. The injection solution was equilibrated to room temperature prior to injection. All steps were carried out in a laminar flow hood.

2.4.3 All trans retinoic-acid

A stock solution of all-trans-retinoic acid (ATRA) was prepared by dissolving ATRA in Dimethyl Sulfoxide (both Sigma-Aldrich) to a final concentration of 40mg/ml which was stored in aliquots at -80°C. On the day of injection stock ATRA was diluted 5 times in corn oil (Sigma-Aldrich) to a working solution of 8.33μg/μl ATRA. Mice received IP injections with 30μl working solution at the indicated times, equating to 250μg ATRA per IP injection as described[145]. All steps were carried out in a laminar flow hood and in the dark.

2.5 Cell isolation protocols

When collecting multiple tissues from one mouse, tissue collection was carried out in the order isolation protocols are described in this section. Unless stated otherwise centrifugation steps were carried out at 300g at 4°C for 5 minutes and all steps were carried out on ice using pre-cooled reagents.

2.5.1 Isolation of peritoneal exudate cells

The abdominal skin was carefully removed leaving the peritoneal wall intact. Using a 5ml syringes with 23g (BD) needle, 3ml of wash solution (dPBS containing 2mM EDTA (Invitrogen),1mM HEPES (Fisher Scientific)) or culture solution (RPMI 1640 containing 1mM HEPES (Fisher Scientific)) with approximately 1ml of air was injected into the peritoneal cavity. The needle was withdrawn and the body was shaken gently. The lavage fluid was withdrawn using the same needle and, when possible, the same entry-point in order to limit damage to the peritoneal wall. The collected fluid was immediately placed on ice in a 15ml falcon tube. This lavage procedure was repeated two more times without air. Cells were centrifuged and resuspended in 1ml of FACS-buffer (2mM EDTA(Invitrogen), 0.5%BSA (Sigma-Aldrich) in PBS) for quantification using CASY counter (Roche).

2.5.2 Isolation of omental leukocytes.

After collection of peritoneal cells, the peritoneal wall was cut open and the intestine were gently pushed to the left, exposing the omentum. The omentum was identified based its comparatively white colour relative to the surrounding fat[136]. The omentum was excised and immediately placed on ice in 0.5ml of RPMI in a 1.5ml Eppendorf tube. The omentum was then removed from the RPMI 1640 (Gibco) and finely cut using scissors and digested in 0.5ml pre-warmed enzyme mix. Enzyme mix was prepared fresh on the day and contained RPMI 1640 with 1% FCS (both Gibco) and 1mg/ml Collagenase D (Roche). The mixture was incubated for 15 minutes in an orbital shaker (37°C, 4Hz), briefly agitated using a P1000 Gilson pipette and incubated for an

additional 20 minutes (37°C, 4Hz). After incubation, samples were immediately placed on ice and 2.5µl of 0.5M EDTA (Invitrogen) was added followed by 0.5ml ice cold FACS buffer. The resulting mixture was strained though a 100µm strainer (VWR) and centrifuged (400g for 10 minutes at 4°C). The supernatant was discarded and the pellet resuspended in 0.5ml FACS-buffer for quantification using CASY counter (Roche).

2.5.2 Isolation of liver leukocytes.

The liver was perfused with approximately 10ml ice-cold dPBS (Gibco) via the inferior vena cava. The complete liver was collected and weighed. The left lobe was separated and 0.5g of the lobe was placed into RPMI 1640 (Gibco) and placed on ice. If required additional tissue from the right lobe was collected to achieve a final weight of 0.5g. The liver was finely cut, using a razor blade, and digested in 5ml of pre-warmed enzyme mix. Enzyme mix was prepared fresh on the day and contained RPMI 1640 (Gibco) with 0.625mg/ml collagenase D (Sigma-Aldrich), 30µg/ml DNase (Roche), 0.8mg/ml collagenase-V (Sigma), and 1mg/ml dispase (Invitrogen). The mixture was incubated for 22 minutes in an orbital shaker (37°C, 240rpm) and shaken vigorously every 5 minutes by hand. The mixture was strained through a 100µm filter (VWR) and washed using 50ml RPMI 1640 followed by a second 30ml RPMI 1640 wash. Red blood cells were lysed using 3ml of RBC lysis buffer (Sigma) for 3 minutes at room temperature after which the mixture was placed back on ice, and 3 ml of ice cold FACS-buffer was added. Cells were washed and strained through a 40µm strainer (VWR) and resuspended in 2ml of FACS buffer for quantification using CASY counter (Roche).

2.6 Sample preparation for Flow cytometry

All antibodies used in this thesis are detailed in Table 2.

Following preparation cells were resuspended using a CASY TT cell-counter (Roche) according to the manufacturer's instructions. Based on established protocols in the laboratory, events within 5.0µm and 15.30µm were considered

as cells and quantified. Following quantification, $1*10^6$ peritoneal lavage cells were stained in a total staining volume of 50μl. For omentum cells, absolute counts were low and variable. Hence, all omentum cells were stained and considered as $0.5*10^5$ cells for purposes of antibody staining and were stained in a staining volume of 50μl. For the liver, $2*10^6$ cells were stained in a total staining volume of 50μl

For adoptive transfer studies, all peritoneal cells were prepared and the staining volume was adapted accordingly.

2.6.1 Surface antibody staining

For samples that were used for analysis only viability staining was performed using Zombie Aqua (Biolegend). For samples that were used to sort cell populations viability was assessed by using DAPI, added prior to cell-sorting.

For zombie aqua staining 10μl of zombie aqua working solution (1:100 in PBS) was added to cells followed by a 10 minute incubation at room temperature in the dark. Cells were then placed on ice and incubated for 10 minutes with 10ul of blocking solution containing CD16/CD32 (1:200 Biolegend) with 10% mouse serum (Life Technologies). Cells were then incubated for 30 minutes on ice using a combination of the antibodies detailed in **Table 2**.

Following staining, cells were washed using FACS buffer. If needed cells were incubated on ice with fluorescently-labelled streptavidin (Biolegend) for 20-30 minutes and washed using FACS buffer. Cells were analyzed on the day of collection or fixed for analysis of intracellular proteins and later analysis

2.6.2 Intracellular staining

For intracellular protein staining, cells were fixed immediately after surface staining using 50μl of fixation reagent, prepared according to the manufacturer's instructions (eBioscience). Samples were stored at 4°C

overnight or 30 minutes at room temperature and washed with permeabilization buffer, prepared according to the manufacturer's instructions (eBioscience). Intracellular antibody staining was carried out using indicated antibodies in a total volume of 50μl of permeabilization buffer. After staining cells were washed once using permeabilization buffer and resuspended in FACS buffer for analysis. For GATA6 staining an additional staining step was carried out for 20 minutes on ice, using Zenon anti-rabbit reagent (ThermoFisher) in volume of 50μ permeabilization buffer. Next, cells were washed once using FACS buffer and resuspended in FACS buffer for analysis

For intracellular cytokine staining $1*10^6$ cells/sample were incubated for 4.5 hours at 37°C in 200μl RPMI 1640, supplemented with Brefeldin A and Monensin (Both Biolegend; 1:1000) in cell-repellent 96 well plates (Greiner Bio-One). After, cells were washed once with RPMI1640 and stained on ice for extracellular antigens as described in the previous section and intracellular antigens following fixation as described above with one additional Fc blocking step directly after fixation (10 minutes on ice).

2.6.3 Acquisition and analysis

Samples were acquired using an LSR Fortessa (BD). Cells used for adoptive transfer experiments were sorted using a FACS Fusion (BD). Cells purified for *in vitro* LPS stimulation were sorted using a FACS Fusion (BD) or FACSAriaII (BD) depending on equipment availability. Flow cytometry acquisition and purification was carried out at the QMRI flow cytometry facility. Due to COVID19 restrictions one later experiment was acquired using an LSR Fortessa (BD) at the SCRM flow cytometry facility. For each experiment a compensation matrix was calculated using the FACS Diva software using compensation beads (eBioscience) diluted 1:10 in FACS-buffer and stained with relevant antibodies. Flow cytometry data was analysed using FlowJo 10.4.1software (Tree Star)

2.7 Adoptive transfer of macrophage subsets

For adoptive transfer peritoneal cells were collected and stained as described in the previous section. All steps were carried out on ice, using sterile reagents and in a laminar flow hood. Due to unavailability of a laminar flow hood the necropsy for early experiments carried out at the Ann Walker animal facility was carried out on the bench.

Cells were sorted using a 100μm nozzle into sterile 1.5ml Eppendorf tubes that contained 100μl of buffer (10% FCS in sterile dPBS (both Gibco)) kept at 4°C during the sort and placed on ice immediately after. After the sort cells were pelleted by centrifugation (300g, 5 min at 4°C) and resuspended in 200ul of dPBS (Gibco). The sample was gently pipetted to bring cells into solution and counted using CASY Counter (Roche). The number of cells required were collected and transferred into new 1.5ml Eppendorf tube and supplemented with dPBS (Gibco) to a total volume of 200μl for IP injection. $1x10^5$ and $2x10^5$ cells of the indicated populations were transferred for short and long-term lineage tracing studies respectively. For high-dose zymosan rescue, $4x10^5$ of RMac were transferred. For LPS responsiveness studies *in vivo,* $2.5x10^5$ of the indicated cell populations was transferred. Purified populations were injected IP using BD insulin syringe (BD).

2.8 *In vitro* studies

For all *in vitro* studies peritoneal cells were collected in a laminar flow hood using sterile reagents.

2.8.1 Production of omentum factors

Omentum factor cocktail was generated using the protocol described by Okabe et al[63]. The authors kindly provided additional details required to repeat the procedure. The omentum was collected, as described in the previous

section, from naive mice and cultured in 1ml of macrophage serum free media (Gibco) at 37°C for 5 days. After 5 days the medium was collected and centrifuged (300g, 5 min at 4°C) and collected 1:2 in serum free media (Gibco) for use.

2.8.2 *In vitro* culture of peritoneal macrophages post-zymosan.

11 Days following low dose zymosan treatment(10μg/mouse), peritoneal exudate cells were collected as described in the previous section. Cells were counted and $5x10^5$ peritoneal cells were plated at 37°C for 2 hours in culture medium (RPMI 1640, 10%FCS, 1% L-Glutamine and 1% Pen/strep (all Gibco) supplemented with 20ng/ml CSF1(Peprotech). After 2 hours the media was aspirated and cells were incubated for 24 hours in 250μl culture medium supplemented with 250μl Omentum factors or an equivalent volume of macrophage-serum free media (Gibco) with or without ATRA (Sigma-Aldrich, 1μm) hours. After 24 hours the medium was aspirated and adherent cells were incubated with ice-cold 5mM EDTA (Invitrogen) in dPBS (Gibco) for 10 minutes on ice to release cells. Using a microscope wells were inspected confirm only few adherent cells remained. Cells were counted and prepared for analysis using flow-cytometry as described.

2.8.3 *In vitro* LPS stimulation of purified macrophage populations

Using sterile reagent peritoneal exudate cells were collected in a laminar flow hood using the protocol described in the previous sections. For each of the indicated populations of interest $1x10^3$ cells were sorted into a sterile 1.5ml Eppendorf tube containing 75μl sort medium (Folic acid deficient RPMI containing 20% FCS (confirmed low endotoxin, Ge-Healthcare), 2% L-Glutamine and 2% Pen/strep (both Gibco). Sorted cells were centrifuged (100g, 5 min at 4°C) to make sure all cells were in the fluid. The cell-mixture was transferred into a 96-well plate and incubated for 2 hours at 37°C. Media was gently aspirated and cells were resuspended in 75μl cell culture medium

(Folic acid deficient RPMI supplemented with 1μg/ml Folic Acid (Sigma-Aldrich), 10% FCS (Ge-Healthcare), 1% L-glutamine and 1% Pen/Strep (both Gibco). In later studies ready-made complete RPMI 1640 (containing 1μg/ml Folic Acid) was used as base medium. As indicated, culture medium was supplemented with LPS of 1ng/ml (O11:B4, Sigma-Aldrich) or equivalent amount of dPBS (Gibco). After incubation for 14 hours, medium was collected and analysed for cytokine release using Legendplex Mouse Anti-Virus or Mouse-Inflammation panels (Biolegend) according to the manufacturer's instructions. All samples were measured in duplicate and samples with high degree of variability between duplicates were excluded. Data was acquired on an Attune flow cytometer and analysis was carried out using the Legendplex analysis software (Biolegend).

2.8.4 Phrodo-labelled *E.coli* phagocytosis assay

Peritoneal exudate cells were collected and prepared as described. For each sample $2x10^6$ cells were washed twice using ice-cold RPMI 1640. Cells were split equally between two polypropylene FACS tubes and incubated on ice for 10 minutes. To each tube 10μl of Phrodo *E.Coli* reagent (ThermoFisher) was added and for each sample one tube was incubated at 37°C and one at 4°C for 1 hour. Immediately following incubation cells were placed on ice, washed using 300μl Buffer C (ThermoFisher) and resuspended in 300μl Buffer C. Cells were analysed using an LSR Fortessa (BD) immediately after.

2.9 Transcriptional analysis

All transcriptional analysis was carried out by me utilizing datasets generated by me or that have been made publicly available. When using public datasets, the original publication and the relevant database identifier have been indicated.

2.9.1 Nanostring mRNA analysis

For indicated populations 5000 cells were sorted into sterile 1.5ml Eppendorf tubes containing 2µl of RLT (Qiagen) using a FACSFusion with a 70µm nozzle (BD). Immediately after collection the cell-RLT mixture was centrifuged at maximum speed for 15 seconds followed by 10 seconds of vertexing. This step was repeated once and cells were stored at -80°C until analysis using the nCounter Myeloid innate immunity panel or a mouse Immunology panel (Nanostring) according to the manufacturer's instructions. The Nanostring assay was carried out by Alison Munro at the the MRC Institute of Genetics and Molecular Medicine in Edinburgh. Quality control and data analysis was carried out using the nSolver advanced analysis software package (Nanostring). To calculate differential gene expression pairwise comparison was carried out between IMac^{Z10} and RMac ^{Z10} to RMac for the first set of experiments. Following LPS stimulation pairwise comparison was carried out between RM^{Z10}-LPM and Mo^{Z1}-LPM. Nominal P-values were adjusted using Benjamini Hochberg method and genes with adjusted p-value <0.05 were considered differentially expressed. Figures were generated using R with the following packages: Pheatmap, EnhancedVolcano, GGplot2 and GOplot. Similar Nanostring analysis was carried out on dataset deposited NCBI's Gene Expression Omnibus under accession number GSE102735 to identify LPS-driven genes (P<0.05).

2.9.1 Gene expression ranking and scoring

Following mRNA analysis using Nanostring advanced analysis package normalized mRNA values were obtained. For all detected genes normalized mRNA transcripts were ordered based on expression level and each gene was assigned a percentile score based on the rank in the gene list. For each gene a delta gene rank percentile was calculated (Percentile rank in native environment – Percentile rank in depleted environment). This analysis methodology was adapted from work by Galatro et al[155].

2.9.2 Gene set enrichment analysis (GSEA)

A list of GATA6-regulated genes was generated by analysis of published datasets deposited on NCBI's Gene Expression Omnibus under accession numbers: GSE56711, GSE37448 and GSE47049. All of these datasets assessed the transcriptome of $GATA6^{KO}$ LPM. Datasets were analyzed using the GEO2R web tool. Genes that were differentially expressed in 2 out of the 3 published datasets (adjusted $p<0.05$) were considered GATA6-regulated, similar to earlier analysis by Shroder et al[156]. Genes were then split into those upregulated in $GATA6^{KO}$ LPM and downregulated in $GATA6^{KO}$ LPM. GSEA analysis was performed using GSEA software package version 4.1 (Broad institute) using default settings and 10.000 gene-set permutations. For RXR$\alpha\beta$ analysis, the dataset GSE129095 was analyzed using the GEO2R web tool and differentially expressed genes (adjusted p value <0.05) were split into genes upregulated in RXR$\alpha\beta$ ^{KO} LPM and downregulated in RXR$\alpha\beta$ ^{KO} LPM. GSEA analysis was performed using GSEA software package version 4.1 (Broad institute) using default settings and 10.000 gene-set permutations. Figures were generated using the GSEA software package version 4.1 and simplified using affinity designer for inclusion in the thesis.

2.10 Assessment of peritoneal and serum levels of LPS-driven cytokines.

To collect concentrated peritoneal lavage, the peritoneal-cell collection protocol was altered. The first wash was carried out using 1ml of altered lavage buffer (RPMI 1640 (Gibco) 1:100 HEPES (Fisher Scientific)). The remainder of the lavage washed was carried out according to the normal protocol, but were kept separate. Following collection, the first wash was centrifuged and the lavage fluid was collected and stored at -80°C. To collect serum, the carotid artery was cut using a scalpel and blood was collected into BD Microtainer SST tubes (BD). If insufficient amount of blood was obtained using this methodology more blood was collected from the inferior vena cava after

peritoneal wash. Serum was collected by centrifugation according to the manufactures instructions and stored at -80°C.

Measurement of serum and lavage cytokines was carried out by Ms. Holly Webster and Dr. Georgia Perona-Wright. As I was not directly involved in this analysis, the methods for this assay are not included here.

2.11 Assessment of serum levels of natural antibodies.

Serum collected as described in the previous section and stored at -80°C. Measurement of natural antibodies was carried out by Ms. Lucia Badiola Gomez and Dr. Steve Jenkins. As I was not directly involved in this analysis, the methods for this assay are not included here.

2.12 Statistical analysis

Data were analysed and visualized using Prism version 7 (GraphPad). For each experiment the statistical test is detailed in the figure legend.

Reagent	Manufacturer	Catalogue NO
Brefeldin A	Biolegend	420601
BSA	Sigma-Aldrich	A7906-100g
Casein	VWR	22544.292
Clodronate Liposomes	Liposoma	n/a
dPBS	Gibco/ThermoFisher	14190-094
EDTA 0.5M	Invitrogen	15574020
FCS	Gibco/ThermoFisher	10500-064
Folic Acid	Sigma-Aldrich	F8758-5G
FoxP3 Transcription factor staining set	ThermoFisher	00-5523-00
FSC (LE confirmed in house)	GE-Healthcare	n/a
HEPES 1M	Fisher Scientific	10041703
Intracellular Fixation and	ThermoFisher	889-8824-00
L-Glutamine 200mM	Gibco/ThermoFisher	25030024
LEGENDplex mouse anti-virus	Biolegend	740622
LEGENDplex mouse inflammation	Biolegend	740446
LPS (O111:B4)	Sigma-Aldrich	L2630-10MG
Macrophage SFM	Gibco/ThermoFisher	12065074
Monensin	Biolegend	420701
PC-BSA	2B Scientific	PC-1011-10
Pen/Strep	Gibco/ThermoFisher	15140122
Phrodo E.coli phagocytosis kit	Invitrogen/ThermoFisher	A10025
PKH26-PCL Cell Linker kit	Sigma-Aldrich	PKH26PCL-1KT
Recombinant murine CSF1	Peprotech	315-02
Red blood cell lysis buffer	Sigma-Aldrich	R7757
Retinoic Acid	Sigma-Aldrich	R2625-50MG
RPMI 1640	Gibco/ThermoFisher	21870076
RPMI 1640 no folic acid	Gibco/ThermoFisher	27016021
Zombie Aqua	Biolegend	423102
Zymosan A	Sigma-Aldrich	01-1111-42

Table 1 List of reagents used in this thesis

Target	Manufacturer	Clone	Fluorochrome	Catalogue NO
CD3	Biolegend	17A2	Biotin	100244
			PB	100214
CD11b	Biolegend	M1/70	PE-Dazzle	101256
CD11c	Biolegend	N418	APC-Cy7	117324
CD16/32	Biolegend	2.4G2	Purified	101320
CD19	Biolegend	6D5	Biotin	115504
			PB	115523
CD45.1	Biolegend	A20	FITC	110706
			AF700	110724
CD45.2	Biolegend	104	AF700	109822
CD102	Biolegend	3C4	FITC	105606
			AF647	105612
			Biotin	105604
CD209b	eBioscience/ThermoFisher	22D1	APC	17-2093-82
GATA6	Cell Signalling Technologies	D61E4	Purified	5851S
F4/80	Biolegend	BM8	PE-Cy7	123114
			APC-Cy7	123118
FRβ	Biolegend	10/FR2	APC	153306
			PE	153303
Sema4a	Biolegend	5E3/SEMA4a	APC	148406
			PE	148404
CCR5	Biolegend	HM-CCR5	AF488	107008
CD62L	Invitrogen	MEL-14	SuperBright 702	67-0621-82
			FITC	11-0621-82
MHC II (IA-IE)	Biolegend	M5/114.15.2	AF700	107622
			PB	107620
			APC-Cy7	107628
Ly6C	Biolegend	HK1.4	BV711	128037
SiglecF	Miltenyi Biotec	ES22-10D8	Biotin	130-101-861
VSIG4	eBioscience/ThermoFisher	NLA14	PE-Cy7	25-5752-82
Ly6G	Biolegend	1A8	Biotin	127604
			PB	127612
Tim4	Biolegend	RMT4-54	PE	130006
			PE-Cy7	130010
			AF647	130008
Streptavidin	Biolegend		BV650	405232
Zenon anti-rabbit reagent	Molecular Probes		AF647	Z25308
Siglec F	BD	E50-2440	BV421	562681
Ki67	Miltenyi	REA183	FITC	130-117-803
CXCL13	Invitrogen	M1/70	APC	17-7981-82
CD11c	Biolegend	N418	APC-Cy7	117324
TNFα	Biolegend	MP6-XT22	BV421	506328
Rat IgG1,lso	Biolegend	RTK2071	BV421	400439

Table 2 list of antibodies used in this thesis

Chapter 3

Developing a ‘toolbox’ to investigate inflammatory macrophage survival and phenotype

3.1 Introduction

As discussed in the general introduction, numerous studies have investigated monocyte fate and phenotype at various stages of peritoneal inflammation. However, due to the use of different peritonitis models in conjunction with various lineage tracing tools a comprehensive understanding of monocyte fate post peritonitis is lacking with some datasets contrasting one another. In the two most commonly used models of peritonitis, thioglycolate or zymosan injection, it has been suggested that monocyte derived macrophages do not persist and the majority undergo apoptosis[86] or emigrate into draining lymphatics[141]. However, these conclusions were drawn on the basis of surface markers[86] or short-term monitoring in partial BM chimeras[87] or following in vivo dye labelling methodology[111,120]. Conversely, experiments using transgenic Cx3cr1^{creER}R26-rfp[28] and more recently Ms4a3^{Cre}-Rosa^{TdT}[123] mice to track infiltrating monocytes or using dye labelling to distinguish resident and inflammation-elicited macrophages over a longer time frame suggested that monocyte-derived macrophages do persist after thioglycolate or zymosan induced peritonitis[28,111,145]. Moreover, the irritant used to induce peritoneal inflammation appears to affect the progression of inflammation and consequently the fate of inflammation-elicited macrophages. Whereas thioglycolate induced peritonitis is characterized by the complete loss of resident macrophages during early inflammation and prolonged monocyte infiltration[86,123], in zymosan-induced peritonitis the extend of these phenomena varies greatly depending on the dose[87,122,139]. Is it likely that these differences account for some of the contrasting results between work by Newson et al[111,120] using a relatively high dose of zymosan and Davies et al[87,144] using a lower dose of zymosan . Hence, the extent of resident macrophage disappearance and the concurrent monocyte influx would appear to be the two processes that determine the constitution of the peritoneal macrophage compartment during resolution and consequently are likely to shape the fate and relative contribution of monocyte derived macrophages thereafter.

To definitively ascertain the fate of monocyte-derived macrophages post-resolution requires a robust lineage tracing method. Studies, carried out by the Jenkins laboratory prior to my PhD used partial bone marrow chimeras to investigate the contribution of monocyte derived cells to the resident macrophage pool[42]. Although this is a very powerful tool that I could have used to investigate integration of monocyte-derived cells post resolution it lacks the capacity to differentiate monocytes infiltrating during inflammation from those that infiltrate the cavity in preceding and succeeding weeks. Studies at the time when I started my PhD had used a transgenic Cx3cr1^{creER} driver line to show contribution of monocyte derived cells to the macrophage compartment after thioglycolate induced peritonitis[28]. However, no recombination was detectable in classical blood monocytes and as a likely consequence the authors found that only 0.3% of peritoneal macrophages were of monocyte origin[28]. This contrasts with earlier work, using CCR2$^{-/-}$ mice indicated that the majority of the macrophage compartment are monocyte derived following thioglycolate treatment[157]. Near the end of my studies, a transgenic Ms4a3^{CreERT2} mouse line with more effective recombination (over 90%) in circulating blood monocytes was generated[123] which could have been a powerful lineage tracing tool. Indeed, using this transgenic line it was confirmed that following thioglycolate treatment large numbers of monocytes infiltrate the cavity and persist long-term[123].

Critically, all these tools lack the capacity to investigate the role of the resolution environment, and competition with incumbent resident macrophages and their effect on inflammatory macrophage fate and conversion potential. Hence, I took advantage of the fluidic nature and easy access to the peritoneal cavity to develop an adoptive transfer system whereby purified resident and monocyte-derived macrophages present during resolution could be transferred into congenic CD45.1/2^{+} mice that were either at an equivalent stage of inflammation, naïve or depleted of macrophages recipients to investigate: 1) their actual fate and phenotype post inflammation resolution, 2) to what degree the resolution environment is a determinant of

these features and 3) whether competition with incumbent resident macrophages influences these phenomena.

To investigate these questions, I sought to induce a degree of peritoneal inflammation where both resident and monocyte derived macrophages could be sourced from the same resolved cavity, thus allowing me to contrast the phenotype and survival potential of these populations after adoptive transfer into mirroring inflamed or naïve recipients. Importantly, a potential drawback of an adoptive transfer methodology is that purified donor cells will be coated with antibodies which are likely to affect their functionality and survival. Hence, I set out to limit the number of antibodies required by validating a dye labelling methodology as described by Newson et al[111,120].

Finally, to investigate the role of competitive pressure in shaping survival and phenotype of transferred cells I sought to transfer purified populations into recipient mice devoid of competing macrophages. This approach was similar to studies by van der Laar et al in which purified macrophage or monocyte populations where adoptively transferred into the lungs of $CSF2Rb^{-/-}$ mice, deficient of alveolar macrophages[67]. However, whereas $CSF2Rb^{-/-}$ mice are relatively healthy $CSF1R^{-/-}$ mice, the equivalent peritoneal macrophage survival factor receptor, are in poor health and even lethal of a C56bl/6 background (personal communication from Dr. Clare Pridans). Alternatively, macrophage deficiency of GATA6 or CEBP/β has been shown to result in a peritoneal cavity largely devoid of resident macrophages[60,63]. However, in both mouse lines a compensatory population of macrophages is present. The effect these cells might have on adoptively transferred cells is unclear. Moreover, we did not have direct access to either of these mouse lines. Hence, I set out to use clodronate liposomes to deplete resident peritoneal macrophages as described[12]. Transfer into this temporarily deplete cavity would allow me to investigate whether the absence of resident macrophages alters survival and phenotype of transferred populations. Towards the end of my PhD an alternative transgenic line deficient in an enhancer domain of the CSF1R was

developed (FIRE-/-), largely devoid of peritoneal macrophages[106] which I utilized to verify some of my findings in Chapter 4.

Hence, in this first result chapter I set out to

- Use zymosan to induce varying degrees of peritoneal inflammation and affect the balance between resident macrophage disappearance and monocyte influx and consequently the constitution of the resolution phase macrophage compartment. Importantly, I aimed to find a dose of zymosan where both resident and monocyte derived cells were present during resolution.
- Optimize a dye labelling system to better delineate resident macrophages already present prior to inflammation from monocyte derived macrophages during inflammation with minimal antibody labelling as to prevent confounding effects of transferring antibody coated cells.
- Finally, I set out to artificially deplete the peritoneal macrophage compartment using clodronate liposomes and carry out a proof of principle study to verify that donor macrophages could be transferred into this artificially depleted environment.

Combined, these tools will serve as a 'toolbox' to investigate the determinants of monocyte derived macrophage fate and phenotype throughout this thesis.

3.2 Dose responsiveness of the zymosan sterile peritonitis model.

In order to effectively asses phenotypic conversion of inflammatory macrophages using an adoptive transfer methodology it was important that I could purify and transfer both resident and inflammatory macrophages from the same resolution phase donor mice to allow me to reference the fate and

phenotype of transferred monocyte-derived macrophages with that of transferred resident macrophages. As different doses of zymosan have been used to induce varying degrees of sterile peritoneal inflammation I first set out to investigate if I could find a dose where a clear population of resident macrophages persisted whilst monocytes infiltrated the inflamed cavity, as reported by Davies et al[87]. To this end, I treated mice with three commonly used doses of zymosan (10μg,100μg or 1000μg) and investigated to what extent these altered the peritoneal macrophage compartment by driving disappearance of resident peritoneal macrophages and recruitment of monocytes, 24 hours after administration. Since recent work from the Jenkins laboratory had indicated a sexual dimorphism in turnover and function of peritoneal macrophages[42] I verified sex did not alter the parameters of peritoneal inflammation as has described by Davies et al[87].These experiments were carried out in age matched male and female mice. **(Figure 3.1a)**

To identify peritoneal macrophages within the peritoneal exudate cells I excluded doublets and dead cells on the basis of their FSC profile and zombie aqua labelling respectively. I then gated on cells expressing high levels of CD11b and low levels of lineage antibodies (CD3,CD19,Ly6G, SiglecF) to exclude T cells, B cells, neutrophils, and eosinophils and identify peritoneal phagocytes[42] **(Figure 3.1b,c)** as previously published by the Jenkins laboratory[42]. Injection of zymosan caused a loss in frequency of F4/80^{Hi} resident macrophages **(Figure3.1c,d)** in both male and female mice irrespective of dose. The frequency of infiltrating F4/80$^{Lo/Int}$ cells with variable levels of the monocyte marker Ly6C expanded considerably **(Figure3.1c,e)**. However, the absolute numbers of both F4/80^{Hi} and F4/88$^{Lo/Int}$ macrophages were highly variable (**Figure 3.1d,e**). Although absolute numbers are the only definitive indication of macrophage disappearance, it is likely that in these experiments the absolute numbers are not reliable as these experiments were the first peritoneal washes, I carried out independently and the quality of the washes was highly variable. There was also considerable variability in the PBS treated group indicating that this was likely due to inexperience rather than

treatment **(Figure 3.1d, left).** Importantly, after 10μg a sizeable and defined population of F4/80^{Hi} macrophages persisted but also a clear population of F4/80$^{Lo/Int}$ Ly6C$^{Int/Hi}$ cells that phenotypically resembled described inflammatory macrophages[87,139] **(Figure 3.1c)** was present.

On the face of it, these data indicate that zymosan does not induce a dose-dependent loss of resident macrophages and concurrent monocyte influx. However, as 10μg induced mild peritoneal inflammation with a quantifiable population of both resident macrophages and infiltrating monocyte derived macrophages I opted to use this dose for the majority of my subsequent experiments as it allows me to source both resident and monocyte-derived macrophages from the same resolution cavity.

3.3 PKH26-PCL labelling delineates macrophage subsets during mild peritonitis short-term.

During the previous experiment I had found that marker expression was variable even within the same treatment group. Consequently, finding a consistent gating strategy was challenging and at times gates fitted poorly across samples and groups. I considered using a more extensive flow cytometry panel using more novel markers such as the phosphatidylserine marker Tim4 and CD102 both of which label resident peritoneal macrophages[42,63,97] or Ly6B shown to label a subset of monocyte-derived macrophages[87,144]. However, I was keen to optimise a flow cytometry panel using minimal antibody to circumvent potential confounding effects of adoptive transfer of antibody-coated cells. Hence, to help delineate myeloid subsets post zymosan using a limited antibody panel I adapted a labelling system as utilized by Newson et al[111,120] that employs a particulate dye to label all phagocytes in the peritoneal cavity prior to inflammation. Although Newson et a[111] had confirmed that after injection PKH26-PCL followed 24 hours later by 0.1mg of zymosan A, cell-labelling was limited to Cx3cr1-GFP^{Neg} F4/80^{Hi} , CCR2 independent resident macrophages I wanted to confirm the specificity

of dye-labelling. Importantly, I wanted to confirm that 24 hours after PKH26-PCL injection no free dye particulates remained that could be subsequently taken up by monocytes recruited upon zymosan injection.

Indeed, 24 hours after injection of PKH26-PCL fluorescent dye practically all F4/80^{Hi} resident macrophages and the majority of F4/80^{Lo} CD226^{+} small peritoneal macrophages were labelled **(Figure 3.2a,b).** Of the numerically negligible population of F4/80^{Lo} CD226^{-} cells that consists predominantly of CD11c^{+} dendritic cells and immature macrophages[42,95,104,139], approximately 30% was labelled **(Figure 3.2a,b)**. Importantly, F4/80^{Hi} resident macrophages remained almost completely labelled until 5 days after dye injection whereas F4/80^{Lo} MHCII^{Hi} CD226 appeared to lose dye-labelling **(Figure 3.2c)**, possibly due to higher levels of monocyte integration into this population.

As PKH26-PCL forms dye aggregates dye labelling is thought to be largely restricted to phagocytes. In line with this, there was only minor PKH26-PCL labelling in Lineage^{+} non-macrophages **(Figure 3.2a)**. However, using CD11B,MHCII,Ly6C in combination with the side scatter characteristics of these cells I was able to identify peritoneal B1 cells (Lineage^{+}, CD11B^{+},MHCII^{+}), B cells (Lineage^{+},CD11B^{-},MHCII^{+}),eosinophils (Lineage^{+}, MHCII^{Lo}, SSC-A^{Hi}), neutrophils (Lineage^{+}, MHCII^{Lo}, SSC-A^{Int}, Ly6C^{Int}) and T cells (Lineage^{+}, MHCII^{Lo}, SSC-A^{Lo}) within the lineage^{-} gate, and using this strategy revealed that only peritoneal B1 cells appeared to have some labelling **(Figure 3.2d,e),** consistent with phagocytic and antigen presenting capacity[158]. It should be noted that the amount of PKH26-PCL labelling was considerably lower than that of macrophages.

Next, I set out to confirm that 24 hours after injection of PKH26-PCL there were no longer free dye particulates which could be taken up by infiltrating cells. To investigate this recipient CD45.2^{+} were injected with PKH26-PCL and 24 hours later unlabelled PEC from CD45.1/2^{+} mice was transferred into these recipients **(Figure 3.3a)**. I postulated that 2 hours would give sufficient time for

transferred cells to take up free floating dye particulates whilst limiting the uptake of dye released by dying resident macrophages. By 2 hours post transfer donor cells did appear to take up some residual dye but the proportion that had done so was relatively small **(Figure 3.3b)** indicating few free-floating dye particulates were present at the time of transfer i.e. 24 hours post PKH26-PCL injection.

I then combined the dye labelling system with the low dose zymosan model of peritonitis described in section 3.1 and postulated that a clearly labelled population of F4/80^{Hi} resident macrophages would be present concurrent with an unlabelled population of F4/80$^{Int/Lo}$ infiltrating monocyte derived macrophages. To confirm this, mice were injected with PKH26-PCL and 24 hours later received an IP injection of 10μg zymosan. By 24 hours post zymosan injection, F4/80^{Hi} PKH26-PCL^{Hi} resident macrophages could be clearly differentiated from F4/80^{Int} PKH26-PCL^{Lo} infiltrating cells. **(Figure 3.4a)** After 5 days F4/80^{HI} PKH26-PCL^{HI} could still be delineated from F4/80^{Int} PKh26-PCL^{Lo} infiltrating cells with relative ease. **(Figure 3.4a,b)**

The phosphatidylserine receptor Tim4 has been used as an alternative marker expressed by the majority of peritoneal resident macrophages and largely absent from infiltrating cells[64,87]. Hence to further validate the dye labelling methodology I confirmed that F4/80^{Hi} PKH26-PCL^{Hi} cells I had identified as resident macrophages almost exclusively expressed high levels of Tim4 at both timepoints. Importantly, resident macrophages identified this way 5 days post zymosan expressed similar levels as PBS controls indicating no off target labelling of Tim4^{-} infiltrating cells **(Figure 3.4c)**. In contrast, F4/80^{Int} PKH26-PCL^{Lo} infiltrating cells expressed high levels of the monocyte marker Ly6C 24 hours after zymosan which was largely lost after 24 hours as cells acquired the F4/80^{Int} inflammatory macrophage phenotype. **(Figure 3.4a)**. Importantly, only a very minor population of F4/80^{Int} PKH26-PCL^{Lo} cells expressed Tim4, possibly indicative of minor contamination by Tim4^{+} resident macrophages. Moreover, whereas after 24 hours post zymosan there was a very striking

difference between labelled and non-labelled populations with a clear distinction between the two subsets, the difference was less apparent by day 5 which might be due to gain of PKH26-PCL fluorescence by the infiltrating cells **(Compare Figure 3.4b 24h vs 5d)**.

Hence, dye labelling proved to be a powerful tool to help delineate resident from infiltrating macrophages but by day 5 monocyte-derived macrophages acquire low levels of labelling, likely released from resident macrophages that have died.

3.3.1 Tissue protected BM chimeras corroborate PKH26-PCL labelling of resident macrophages during mild peritonitis.

Although my previous study had used the peritoneal cavity 5 days post zymosan as the latest timepoint, work by Davies et al[87] indicated that after low dose zymosan neutrophilia was already resolved by day 3. As this is defined as the resolution of inflammation, I focused my subsequent experiments on the day 3 timepoint.

To further validate that I correctly identified resident and infiltrating cells at this stage of peritonitis I proceeded to generate partial bone marrow chimeras with the help of my supervisor, Dr. Steve Jenkins. Briefly, the hindlegs of $CD45.2^{+}$ recipient mice were irradiated with lead shielding used to protect the upper body and, importantly, the peritoneal cavity. Mice were reconstituted with $CD45.1/2^{+}$ bone marrow and left for 8 weeks. After 8 weeks they received a single injection of PKH26-PCL followed 24 hours later by 10μg of zymosan or PBS. By 3 days post zymosan mice were sacrificed and the peritoneal exudate cells investigated using flow cytometry **(Figure 3.5a)**. The chimerism of circulating $Ly6c^{Hi}$ monocytes was approximately 20% and was unaltered by zymosan treatment **(Figure 3.5b)**. The chimerism observed in peritoneal subsets was normalized to the chimerism of circulating $Ly6C^{Hi}$ monocytes (referred to as normalized chimerism) as described[42].

Using a similar gating strategy as described in 3.3 I found that by day 3 there was very low levels of chimerism in the population of F4/80^{Hi} PKH26-PCL^{Hi} macrophages I postulated to be resident macrophages **(Figure 3.5c,d)**. Importantly the level of chimerism was equal to that of F4/80^{Hi} PKH26^{Hi} macrophages in PBS treated mice indicative of no or negligible contribution of monocyte derived cells to this population. **(Figure 3.5d)**. In line with published work I divided the infiltrating PKH26-PCL$^{Lo/Int}$ cells into F4/80^{Int} cells with variable levels of Ly6C, most likely inflammatory macrophages and a minor fraction of cells with the classic Ly6C^{Hi} monocyte phenotype **(Figure 3.5c)**. Both of the populations identified had approximately 100% chimerism indicative of their monocytic origin **(Figure 3.5d)**. Similar to the day 5 data presented earlier I found that approximately 80% of resident F4/80^{Hi} PKH26-PCL^{Hi} cells expressed Tim4 and that this proportion was not altered after zymosan treatment **(Figure 3.5e)**. Moreover, the minor fraction PKH26-PCL$^{Lo/Int}$ cells that expressed Tim4, I postulated to be contaminating resident cells in the previous section were highly chimeric suggesting these cells were also predominantly of monocyte origin **(Figure 3.5f,right)**.

Taken together, these data indicate that by using a gating strategy based on PKH26-PCL, F4/80 and Ly6C I can delineate macrophage subsets 3 days post 10μg zymosan with a high degree of certainty and using minimal number of antibodies. For the remainder of the text PKH26-PCL^{+} F4/80^{Hi} resident macrophages will be referred to as RMac^{Z10} and PKH26-PCL^{Lo} F4/80^{Int} inflammatory macrophages as IMac^{Z10}.

In these experiments I had noticed that in some PBS injected control samples there appeared to be some MHCII upregulation by resident macrophages indicating of some degree of inflammation. Similarly, the resident macrophage chimerism of approximately 20% in partial BM chimeras **(Figure 3.5d)** slightly higher as we would have expected based on earlier work by our lab[42]. Moreover, previous work by Jenkins et al found indication that IP injection with PBS alone already caused minute inflammation and small loss of resident

macrophages[146]. Hence, for the remainder of the text I will be using complete naïve mice as control group to source naïve resident macrophages unless otherwise indicated.

3.3.2 Macrophage dynamics during in mild peritonitis following PKH26-PCL labeling of resident macrophages.

Next, I set out to replicate some of the dynamics of early peritoneal inflammation described[122,139] using the dye labelling methodology. Mice received a single injection of PKH26-PCL followed 24 hours later by IP injection of 10μg zymosan. In these experiments, the population of RMac had reduced considerably in number by 4 hours post zymosan while an almost equivalent number of Ly6C^{+} monocytes had infiltrated the cavity **(Figure 3.6a,b)**. By day 3 the population of RMac had partly recovered but was still reduced compared to its homeostatic level and the number of these cells was roughly equivalent to that of IMac^{Z10} that inhabited the cavity at this time **(Figure 3.6a,b)**. As described by Davies et al[87] neutrophils had largely disappeared indicating inflammation had resolved whereas monocytes had largely adopted the F4/80^{Int} inflammatory macrophage phenotype **(Figure 3.6c)**

In summary, I have established a dye labelling strategy which can be utilized in conjunction with a minimal number of surface markers to definitively delineate incumbent resident macrophages and infiltrating monocyte-derived cells during the earlier phases of low dose zymosan induced peritonitis until resolution.

3.3.3 Excluded samples and exclusion criteria

A drawback of using IP injections to deliver substances is that it is not possible to visually confirm that the injection was carried out successfully. As the failure rate of IP injections is thought to be 10-20%[159,160] and has been shown to directly affect experimental variability and experimental results[161] this is likely

to influence my experiments as well. In line with the described failure rate, in the dataset presented in Figure 3.6 one out of the 9 samples (11%) in the naïve group had no PKH26-PCL dye labelling clearly indicative of failed IP injection. Moreover, one sample out of 10 (10%) in both the 4 hour and 3 days post zymosan treatment group showed no signs of monocyte infiltration. Hence, I excluded these samples from experimental analysis and for subsequent studies defined the absence of dye labelling or the absence of infiltrating monocytes shortly after zymosan treatment as valid exclusion criteria.

3.4 Developing an assay to test the fate potential of inflammatory macrophages

A number of papers investigating the earlier phases of zymosan induced peritonitis suggested that long-term contribution of monocyte derived cells was unlikely to occur. Most notably, at the onset of resolution they observed high levels of proliferation by resident macrophages whereas inflammatory macrophages appeared to undergo little proliferation[87,144]. These observations are consistent with a model in which resident macrophages proliferate to reconstitute the peritoneal macrophage compartment and in doing so inhibit inflammatory macrophage survival, similar to what occurs in the liver after acetaminophen overdose[83]. However, in the liver it had been found that although monocyte-derived macrophages are normally outcompeted by Kupffer cells following inflammation, monocytes are able to reconstitute the macrophage niche and completely adopt a Kupffer cell identity after artificial depletion of incumbent Kupffer cells[38,68]. Hence, I set out to develop an assay that would allow me to investigate if monocytes infiltrating the peritoneal cavity have the capacity to repopulate a cavity devoid of resident macrophages and give rise to bona fide resident macrophages irrespective of whether they do so during normal resolution.

At the time of the start of my PhD two transgenic mouse lines were available that lacked peritoneal macrophages. Both lines used the macrophage/neutrophil specific Lysm-cre crossed to floxed lineage

determining transcription factors mouse lines, the CEBP/$\beta^{fl/fl}$ [60] or $GATA^{fl/fl}$ [63-65]. It should be noted that in both these models peritoneal macrophages are not completely absent, but instead the peritoneal cavity is inhabited by a smaller population of F4/80 intermediate resident-like macrophages. This compensatory population in combination with the fact that we did not have the opportunity to rapidly acquire either one of these lines led me to investigate the use of clodronate liposomes to deplete peritoneal macrophages instead. Clodronate liposomes have been used extensively for the targeted depletion of phagocytes in various tissues including the peritoneal cavity[12,132].

To generate an artificially depleted peritoneal cavity which would be amenable to adoptive transfer experiments there where two key criteria:

1) The dose had to be sufficient to completely deplete resident peritoneal macrophages.
2) At the time of transfer, no or negligible amounts of free-floating liposomes should be present in the cavity.

I first set out to trial the dose used by Wang et al[12] and if, similar to their study, I could effectively deplete peritoneal macrophages 7 days post administration. As I was aiming to use the minimal concentration of clodronate liposomes required I trialled several lower doses as well. Indeed, I found that injection of 0.5mg as used by Wang et al[12] effectively depleted all $F4/80^{Hi}$ resident peritoneal macrophages but appeared to lead to an influx of neutrophils **(Figure 3.7a,b)**. Moreover, 0.5mg appeared to be excessive as 0.125mg of clodronate liposomes, the lowest dose trialed, also completely depleted peritoneal macrophages but without the associated neutrophil influx **(Figure 3.7b)**.

Hence, I repeated the experiment using 0.125mg as the highest dose and further titrating down the concentration of clodronate liposomes required. Doing this I found that the lowest doses of 0.0156 mg and 0.03125mg decreased the number of $F4/80^{Hi}$ resident macrophages but that the depletion

was not as complete as the depletion induced by 0.0625mg and 0.125mg of clodronate liposomes **(Figure 3.7c)**. Hence, I decided to proceed using the dose of 0.0625mg as this was the lowest dose where complete depletion occurred and with which the fewest free-floating liposomes should theoretically be present by day 7. In subsequent validation experiments I found that already 24 hours after injection with 0.0625mg clodronate liposomes virtually all F4/80^{Hi} RMac were depleted and remained so until day 7 **(Figure 3.7d)**. Notably, whereas by 24 hours a population of Ly6c^{+} monocytes was present, suggesting a degree of repopulation, these were largely absent by day 7 and the majority of CD11b^{+} myeloid cells were F4/80^{Lo} CD226^{+} cells that resemble SPM **(Figure 3.7d)**.

As IP delivery of Clodronate liposomes has been used to deplete Kupffer cells in the liver[12], I investigated if using the treatment protocol, I optimized for peritoneal phagocyte depletion also depleted Kupffer cells. Indeed, whereas after PBS treatment Tim4^{+} Kupffer cells were clearly discernible and accounted for approximately 20% of all live cells, these cells were largely lost, 24 hours after treatment with clodronate liposomes, suggesting that clodronate liposomes are rapidly drained form the peritoneal cavity after administration. Critically, the one sample where peritoneal cavity macrophages were depleted incompletely **(Figure 3.7d datapoint in red)** was also poorly depleted in the liver **(Figure 3.7e, datapoint in red).** As repopulating monocytes that infiltrate the liver after Kupffer cell depletion are exclusively Tim4^{-}[38] I interpreted the presence of Tim4+ Kupffer cells in the liver as indicative of a failed IP injection in this mouse. Moreover, since the inability of monocyte-derived Kupffer cells to acquire Tim4 persists for many weeks[38] I postulated that the absence of Tim4^{+} Kupffer cells in the liver could be used as a readout to confirm successful IP injection of clodronate liposomes long-term.

Next, as proof of principle I depleted the peritoneal cavity of CD45.1/2^{+} mice using 0.0625mg of clodronate liposomes and 7 days later adoptively transferred 100.000 purified PKH26-PCL labelled RMac sourced from naïve

mice or equivalent numbers of Ly6C^{Hi} monocytes sourced 4 hours post zymosan. By 8 days post transfer both transferred cell populations had persisted and contributed to the CD11B^{+} Lineage^{-} macrophage compartment with donor RMac seemingly contributing more than transferred monocytes **(Figure 3.8a)**. Clodronate depletion only temporarily depleted peritoneal macrophages and consistent with repopulation by host monocytes (**Figure 3.7d**) the absolute number of CD11B^{+} myeloid cells was equivalent between depleted and non-depleted mice at this stage, irrespective of the transferred population (**Figure 3.8b**). Whereas in non-depleted mice the majority of F4/80^{Hi} macrophages expressed Tim4, after clodronate treatment F4/80^{Hi} macrophages largely lacked Tim4 (**Figure 3.8c,d**), consistent with their monocytic origin[42]. This loss of peritoneal macrophages expressing Tim4 corresponded to loss of Tim4^{+} Kupffer cells in the liver **(Figure 3.8e)** indicative of successful depletion in all samples. Combined, these data show that levels of Tim4 on host peritoneal macrophages can be utilized as surrogate readout of successful clodronate depletion. Hence, for studies where cells will be adoptively transferred into clodronate depleted recipients the absence of host Tim4^{+} macrophages will be considered indicative of successful depletion and will be further analyzed.

In summary, I have established a method to artificially deplete the peritoneal macrophage compartment and found that using a dose of 0.0625mg of clodronate liposomes leads to effective depletion of peritoneal cavity resident F4/80^{Hi} macrophages with sufficiently few liposomes remaining by day 7 to allow adoptive transfer of peritoneal macrophages.

3.5 Discussion

Here I set out to optimize a ‘toolbox’ which would allow me to investigate determinants of fate and phenotype of inflammatory macrophages following resolution of inflammation. By using a combination of PKH26-PCL dye labeling

of resident phagocytes in combination with traditional macrophage and monocyte markers F4/80 and Ly6C I was able to identify labelled F4/80^{Hi} resident macrophages and unlabeled F4/80^{Int} inflammatory macrophages during resolution low dose zymosan induced peritonitis. The identity of resident and inflammatory macrophages identified this way was confirmed by expression of Tim4, a marker largely restricted to embryonically seeded resident macrophages[42], and using partial bone marrow chimeras to confirm that inflammatory macrophages exhibited a high degree of chimerism and hence were exclusively of BM origin, while dye-positive resident macrophages exhibited low chimerism. It should be noted that by using the PKH26-PCL dye labelling the number of antibodies required to identify macrophage subsets was minimized, thus limiting confounding results of transferring antibody coated cells. However, PKH26-PCL dye particulates are sequestered in the phagolysosome of macrophages and are retained for long periods of time[111]. Little is known about how this dye persistence may potentially affect the functionality or activation state of labelled phagocytes. This is especially important as the PKH26-PCL labelling might affect the comparison between PKH26-PCL labelled resident macrophages and PKH26-PCL negative inflammatory macrophages in my experimental system.

In order to investigate the potential of inflammatory macrophages to persist long-term in the absence of competing incumbent resident macrophages I optimized a clodronate liposomes treatment protocol to deplete host F4/80^{Hi} resident macrophages. To this end, I titrated down clodronate liposomes to the lowest dose where complete depletion takes place and found that this depleted cavity is indeed amenable to adoptive transfer of macrophages. This methodology has two potential drawbacks. First off, the cavity will likely contain large numbers of dying cells at the time of adoptive transfer which may affect the survival and phenotype of transferred cells. Secondly, immediately following depletion of peritoneal macrophages high numbers of monocytes will start infiltrating the cavity[112,132]. Consequently, transferred cells will be competing with infiltrating monocytes for residency in the peritoneal cavity.

Indeed, donor monocytes persisted relatively poor following transfer into clodronate-depleted recipients, which may be due to their impaired capacity of these cells to compete with infiltrating, developmentally equivalent, host monocytes. In contrast, transferred resident macrophages, which are more mature cells that are exquisitely suited to the peritoneal microenvironment, persisted better following transfer into clodronate-depleted recipients, possibly due to heightened capacity to compete with infiltrating monocytes.

In the next chapter I set out to assess whether purified monocyte derived inflammatory macrophages are capable of integrating into the peritoneal macrophage compartment and whether the post-resolution environment alters this capacity. Furthermore, using the depleted niche I have generated will allow me to investigate if competition with incumbent resident macrophages alters the fate potential of monocyte-derived inflammatory macrophages.

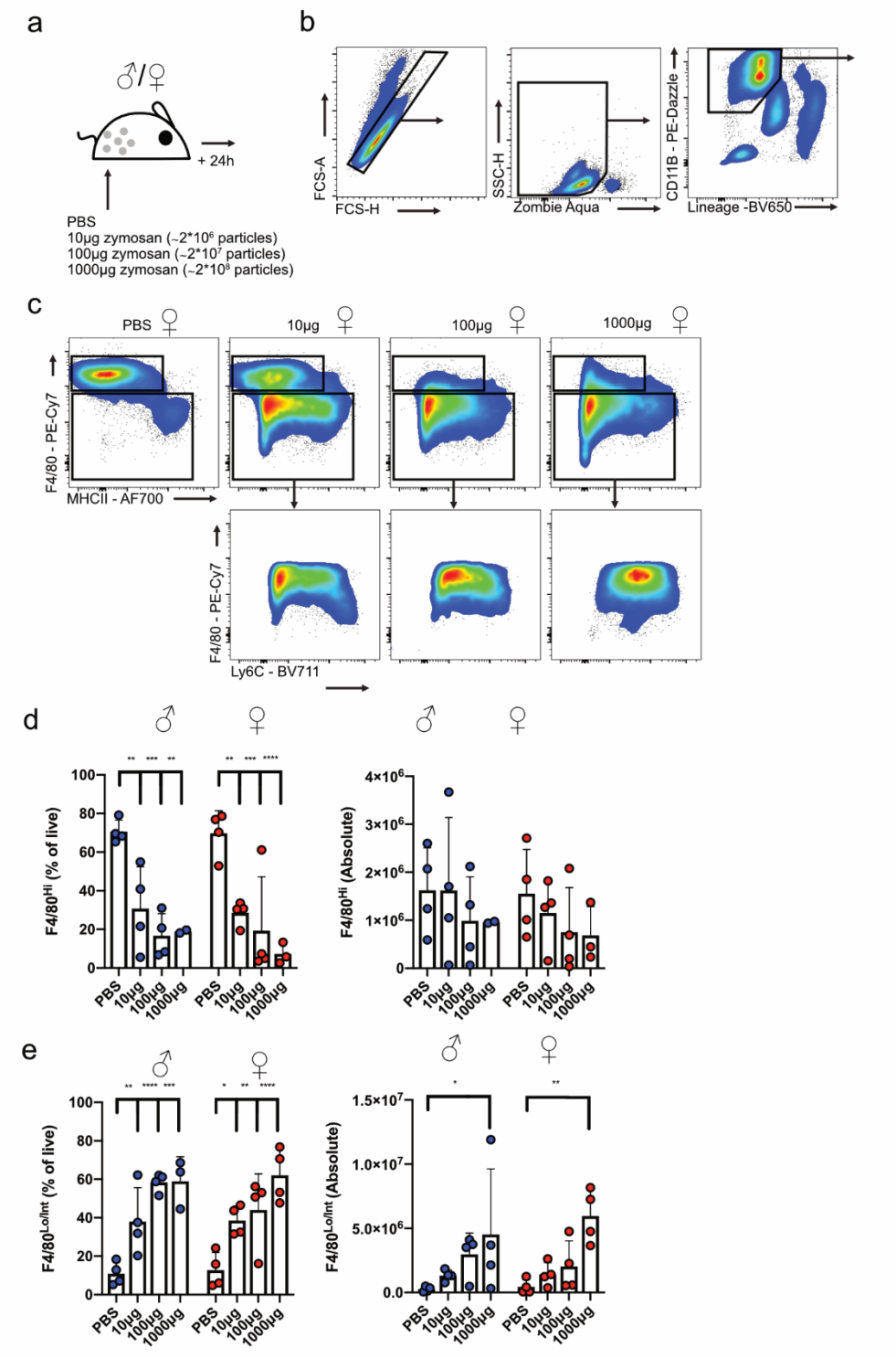

Figure 3.1 Zymosan induces resident macrophage disappearance in male and female mice.

(a) Experimental scheme for IP delivery of indicated doses of PBS or Zymosan A into male or female mice.**(b)** Representative gating strategy used to identity

single (FSC-A vs FSC-H), live (Zombie aqua^{-}) peritoneal macrophages (CD11B^{+} Lineage^{-}) **(c)** Representative expression of F4/80, MHCII and Ly6c on CD11B^{+}Lineage^{-}myeloid cells in the cavity, 24 hours post PBS administration or administration of the indicated dose of zymosan A. Myeloid cells are identified as shown in panel b. **(d).**Proportion of live cells and absolute number of F4/80^{Hi} macrophages in male (blue) and female (red) 24 hours post: PBS (male n=4, female n=4), 10μg zymosan (male n=4, female n=4),100μg zymosan (male n=4, female n=4),1000μg zymosan (male n=2, female n=3). **p<0.01 ***p<0.001 determined by two ANOVA with Sidak's multiple comparisons test. **(e)** Proportion of live cells and absolute number of F4/80$^{Lo/Int}$ macrophages in male (blue) and female (red) 24 hours post: PBS (male n=4, female n=4), 10μg zymosan (male n=4, female n=4),100μg zymosan (male n=4, female n=4),1000μg zymosan (male n=2, female n=3). **p<0.01 ***p<0.001 determined by two ANOVA with Sidak's multiple comparisons test. Data are presented as mean ± standard deviation with each symbol representing an individual animal. Data were pooled from 2 independent experiments,

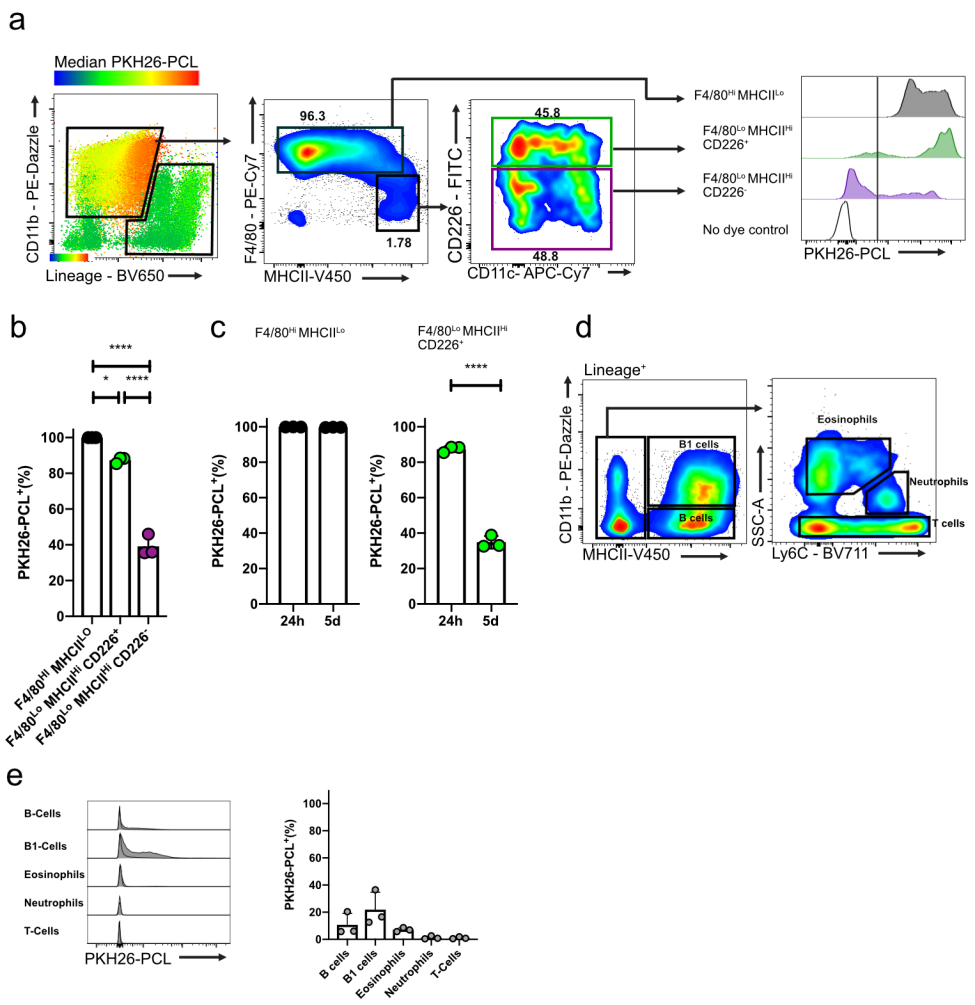

Figure 3.2 PKH26-PCL labels peritoneal phagocytes.

(a) Representative gating of F4/80^{HI} MHCII^{LO} resident peritoneal macrophages and F4/80^{LO} MHCII^{HI} CD226^{+} small peritoneal macrophage and CD226^{-} dendritic cel l(DC) / immature macrophage subsets. **(b)** PKH26-PCL-labelling of F4/80^{HI} MHCII^{LO} resident macrophages (black), F4/80^{LO}MHCII^{HI} CD226^{+} small peritoneal macrophages (green) or CD226^{-} DCs/immature macrophages (purple) 24 hours after IP injection of PKH26-PCL (n=3). **p<0.01 determined by one-way ANOVA with Tukey's multiple comparisons test. **(c)** Proportion of F4/80^{HI} MHCII^{LO} resident macrophages (black) and F4/80^{LO}MHCII^{HI} CD226^{+} small peritoneal macrophages (green) that are PKH26-PCL labelled, 24 hours and 5 days after IP administration of PKH26-PCL (n=3/timepoint). ****p<0.0001 determined by student's t test. **(d)** Representative gating strategy to identify non-myeloid Lineage^{+} cells in the cavity **(e)** Proportion of each of the

non-myeloid lineage_ cells in the cavity that are PKH26-PCL-labelled, 24 hours post PKH26-PCL administration (n=3). For each population the unlabelled, vehicle control injected, PKH26-PCL labelling intensity is shown as black line in the histogram. Data shown as mean ± standard deviation. Each symbol represents an individual animal.

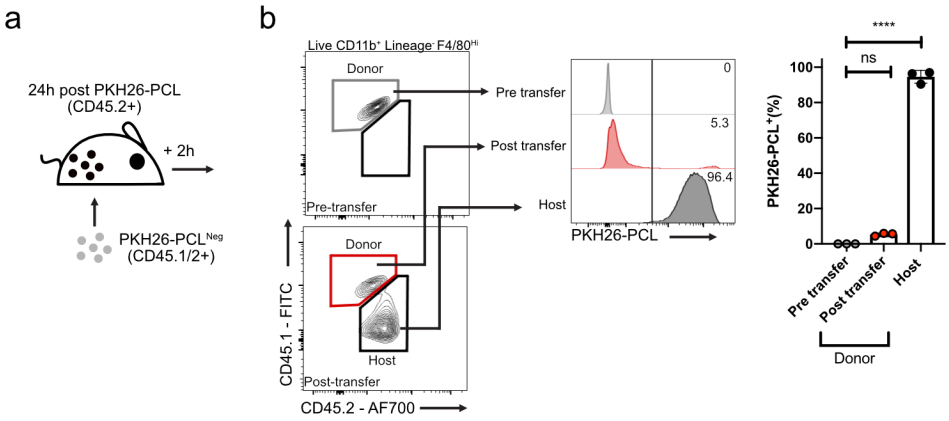

Figure 3.3 By 24 hours, marginal free-floating PKH26-PCL remains.

(a) Experimental outline for adoptive transfer of unlabelled CD45.1/2^{+} peritoneal exudate cells via IP injection into CD45.2^{+} mice that were IP injected with PKH26-PCL 24 hours prior. **(b)** Representative PKH26-PCL-labelling of donor F4/80^{hi} macrophages prior to transfer (grey; n=3) and 2 hours following transfer (red; n=3), compared to host F4/80^{Hi} macrophages (black; bottom). ****p<0.0001 determined by one-way ANOVA with Tukey's multiple comparisons test. Data shown as mean ± standard deviation. Each symbol represents an individual animal.

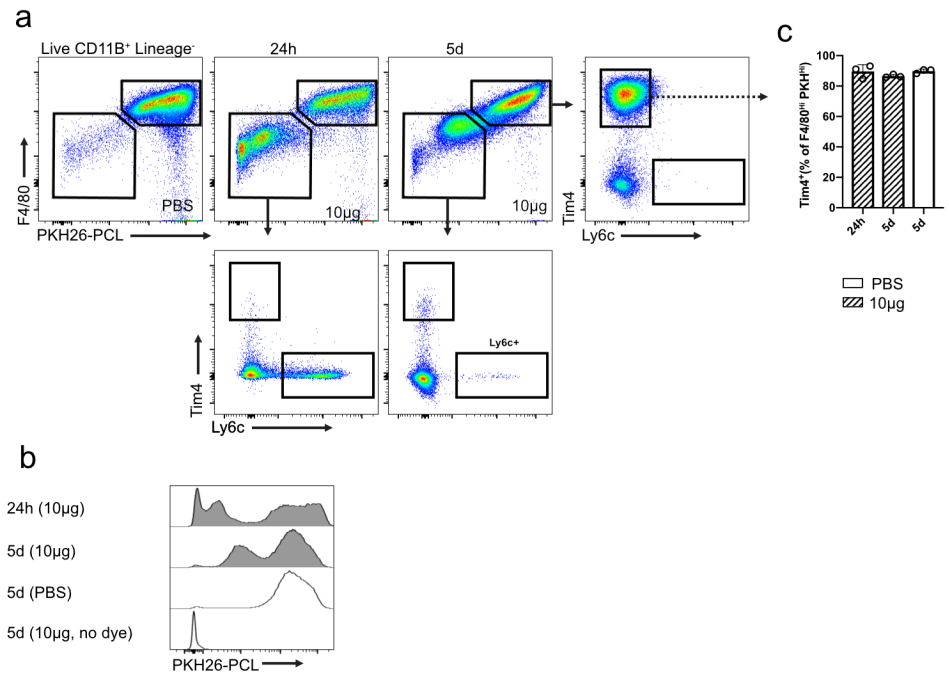

Figure 3.4 PKH26-PCL-labelling discriminates resident macrophages from infiltrating cells following zymosan treatment.

(a) Representative PKH26-PCL-labelling of peritoneal $CD11B^{+}Lineage^{-}$ myeloid cells in conjunction with macrophage markers F4/80, Tim4 and the monocyte marker Ly6c **(b)** PKH26-PCL labelling of $CD11B^{+}Lineage^{-}$ myeloid cells at indicated timepoints. Bottom histogram is representative PKH26-PCL labelling in a control mouse injected with vehicle alone. **(c)**Proportion of $F4/80^{HI}$ $PKH26\text{-}PCL^{Hi}$ resident macrophages that express the embryonic macrophage marker $Tim4^{+}$ (gated as shown in a) at indicated time-points after IP injection with zymosan (striped bar) or PBS (blank bar). Data shown as mean ± standard deviation. Each symbol represents an individual animal.

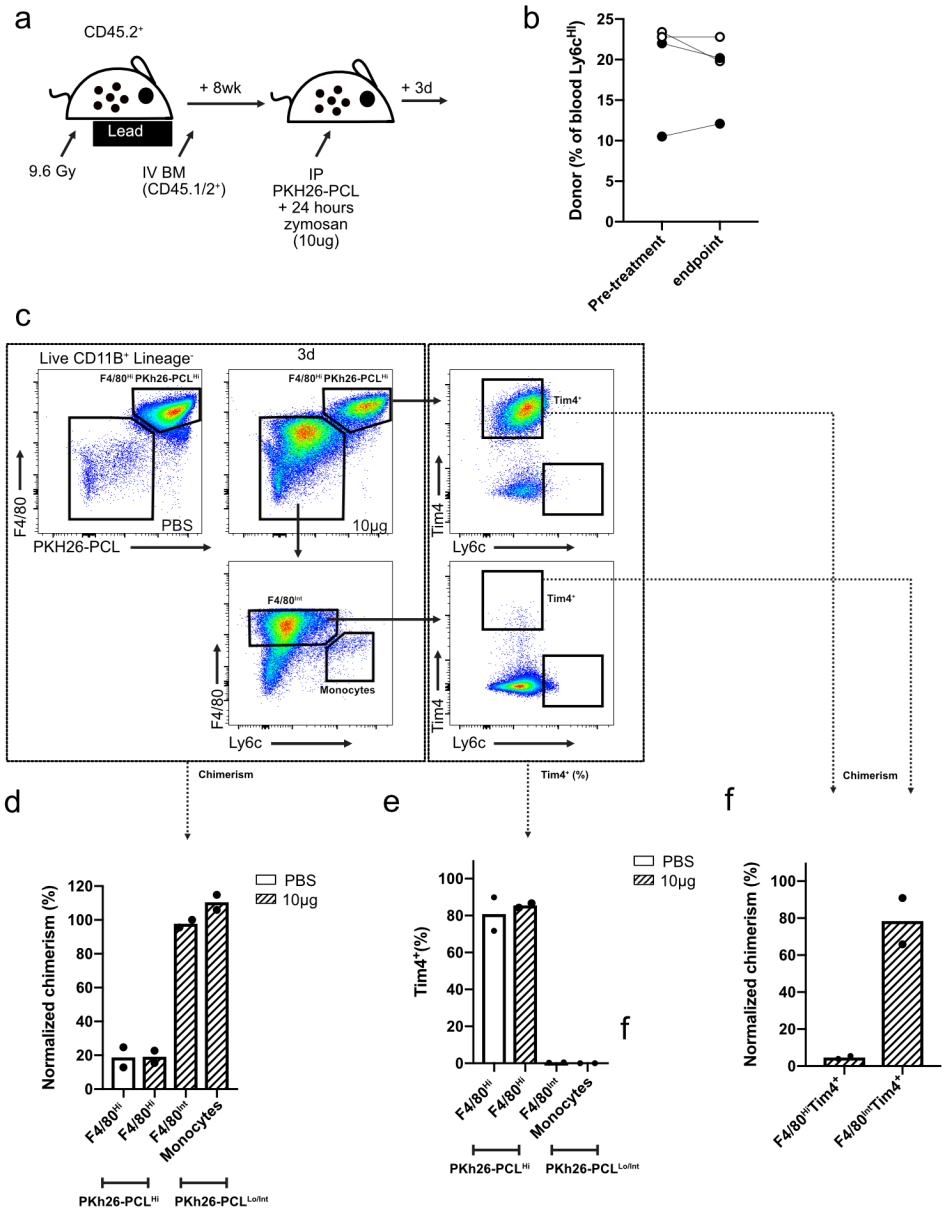

Figure 3.5 PKH26-PCL delineates low-chimerism resident macrophages from high-chimerism monocyte-derived macrophages.

(a) Experimental outline to generate tissue-protected bone marrow chimeras. The hindlegs of CD45.2^{+} mice were irradiated whilst the upper body was protected. Mice were reconstituted using CD45.1/2^{+} bone marrow for 8 weeks. Following reconstitution mice received IP injection of PKH26-PCL followed 24 hours later by treatment with the indicated dose of zymosan. **(b)** Proportion of circulating blood Lyc^{Hi} monocytes that are of donor origin (chimerism) prior to experimental intervention (pre-treatment; left side) and at the experimental endpoint (endpoint; right side). PBS treated mice in white, zymosan treated

mice in black. **(c)** Representative PKH26-PCL-labelling of peritoneal $CD11B^{+}Lineage^{-}$ myeloid cells in conjunction with macrophage markers F4/80, Tim4 and the monocyte marker Ly6c **(d)** Chimerism detected within the indicated peritoneal macrophage population as gated in (c) normalized to the chimerism in circulating blood Lyc^{Hi} monocytes (Normalized chimerism), 3 days following IP administration of PBS (white bar) or zymosan (striped bar) **(e)** Proportion of indicated populations, as gated in (c), that are $Tim4^{+}$, 3 days after IP administration of PBS (white bar) or zymosan (striped bar). **(f)** Normalized chimerism of $F4/80^{Hi}PKH26\text{-}PCL^{+}$ $Tim4^{+}$ macrophages and $F4/80^{Int}PKH26\text{-}PCL^{-}$ $Tim4^{+}$ macrophages, 3 days after IP administration of zymosan. Data shown as mean ± standard deviation. Each symbol represents an individual animal.

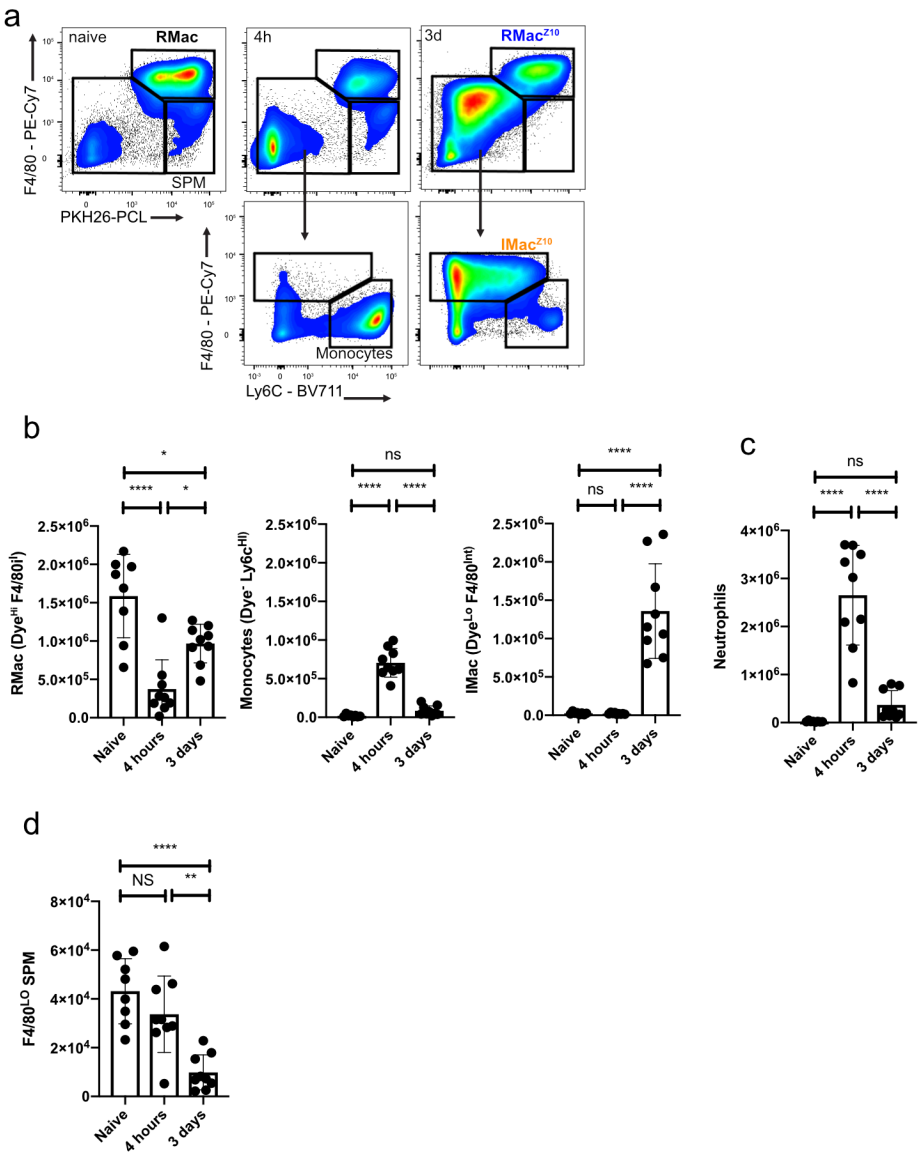

Figure 3.6 PKH26-PCL discriminates resident macrophages at different stages of zymosan-induced peritonitis.

(a) Representative expression of F4/80, Ly6C antibody staining of $CD11B^{+}Lineage^{-}$ myeloid cells in the cavity in conjunction with PKH26-PCL-labelling. Indicated gates identity $F4/80^{HI}$ $PKH26\text{-}PCL^{HI}$ resident macrophages, $PKH26\text{-}PCL^{LO}$ $Ly6c^{+}$ monocytes and $PKH26\text{-}PCL^{LO}$ $F4/80^{INT}$ inflammatory macrophages in naïve mice or mice IP treated with 10μg zymosan at indicated times. **(b)** Absolute number of RMac, Monocytes, IMac in the the naïve peritoneal cavity (n=8), 4 hours post zymosan (n=9) and 3 days post zymosan (n=9). *<0.05, ****p<0.0001 determined by one-way

ANOVA with Tukey's multiple comparisons test. **(c)** Number of neutrophils (gated as detailed in Figure 3.2d) in the naïve peritoneal cavity (n=8), 4 hours post zymosan (n=9) and 3 days post zymosan (n=9). ****p<0.0001 determined by one-way ANOVA with Tukey's multiple comparisons test. Data shown as mean ± standard deviation. Each symbol represents an individual animal. Data were pooled from 3 independent experiments

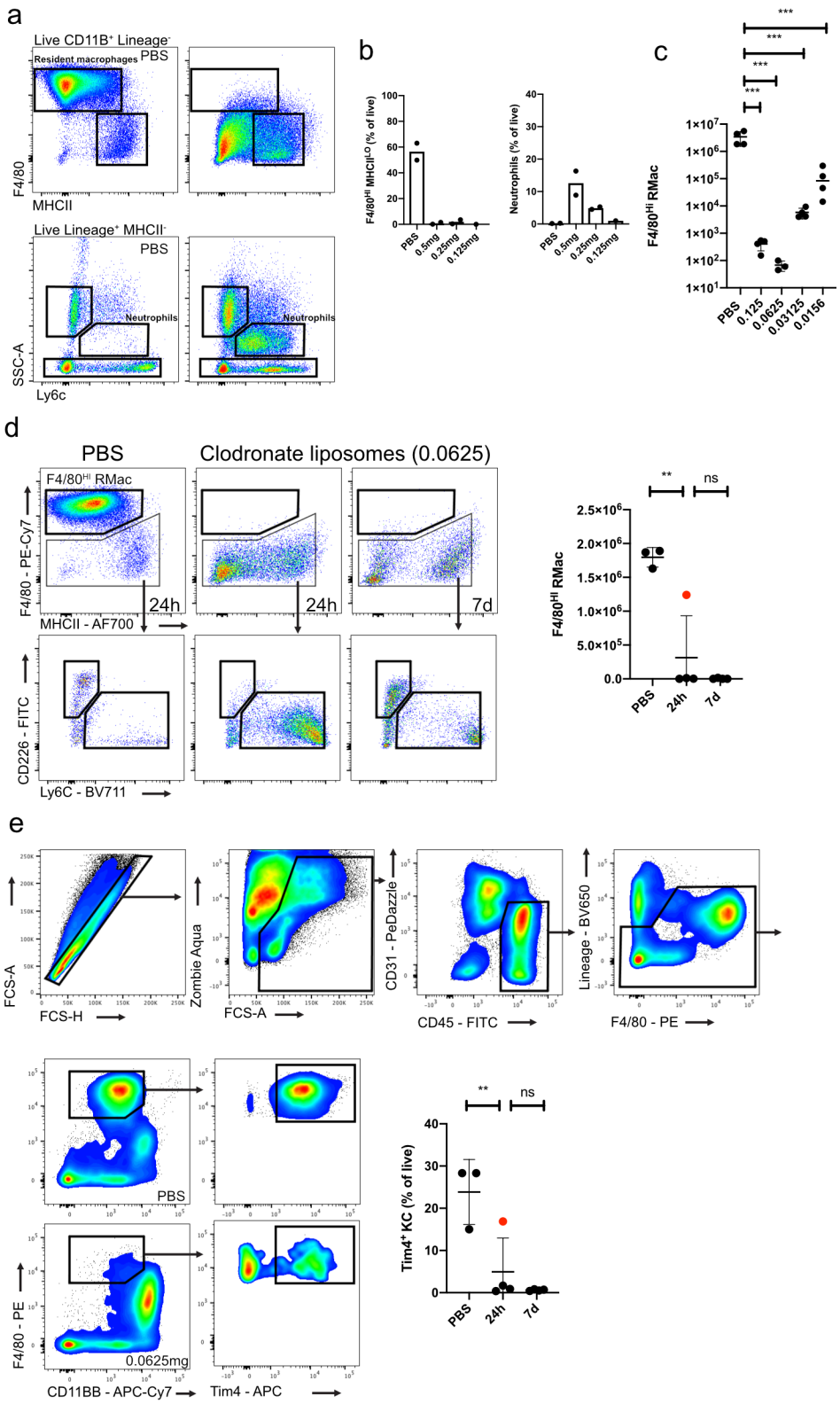
a
Live CD11B+ Lineage-
Resident macrophages
PBS
F4/80
MHCII
Live Lineage+ MHCII-
PBS
Neutrophils
Neutrophils
SSC-A
Ly6c
b
F4/80HI MHCIILO (% of live)
PBS
0.5mg
0.25mg
0.125mg
Neutrophils (% of live)
PBS
0.5mg
0.25mg
0.125mg
c
F4/80Hi RMac
PBS
0.125
0.0625
0.03125
0.0156
d
PBS
Clodronate liposomes (0.0625)
F4/80HI RMac
F4/80 - PE-Cy7
MHCII - AF700
24h
24h
7d
CD226 - FITC
Ly6C - BV711
F4/80HI RMac
PBS
24h
7d
ns
e
FCS-A
FCS-H
Zombie Aqua
FCS-A
CD31 - PeDazzle
CD45 - FITC
Lineage - BV650
F4/80 - PE
PBS
0.0625mg
F4/80 - PE
CD11BB - APC-Cy7
Tim4 - APC
Tim4+ KC (% of live)
PBS
24h
7d
ns

Figure 3.7 Clodronate liposomes deplete peritoneal macrophages.

(a) Representative Identification of peritoneal macrophages/monocytes on the basis of F4/80, MHCII and Ly6c (top) and neutrophils (bottom) (**b)** Proportion of live peritoneal cells that are $F4/80^{Hi}MHCII^{Lo}$ resident macrophages (left) and neutrophils (right) 7 days after IP administration of clodronate liposomes. **(c)** Absolute number of $F4/80^{Hi}$ $MHCII^{Lo}$ macrophages 7 days after IP injection with the indicated dose of clodronate liposomes. ***p<0.001 determined by one-way ANOVA with Sidak's multiple comparisons test. **(d)** Representative identification (left) and quantification (right) of $F4/80^{Hi}$ resident macrophages (black) 24 hours after IP injection of PBS (n=3) or 0.0625mg of clodronate liposomes (n=4) and 7 days post IP injection with 0.0625mg clodronate liposome (n=4). **p<0.01 determined by one-way ANOVA and Dunnet's multiple comparisons test. **(e)** Representative gating strategy to identify $F4/80^{Hi}CD11B^{Int}$ liver Kupffer. At the bottom, proportion of live cells that are $Tim4^{+}$ Kupffer cells, 24 hours after IP delivery of PBS (n=3) or clodronate liposomes (n=4) and 7 days after IP delivery of clodronate liposomes (n=4). **p<0.01 determined by one-way ANOVA and Dunnet's multiple comparisons test. Data shown as mean ± standard deviation except for (b) which is presented without standard deviation. Each symbol represents an individual animal. Data were pooled from 2 independent experiments, except (a,b) which are from a single experiment.

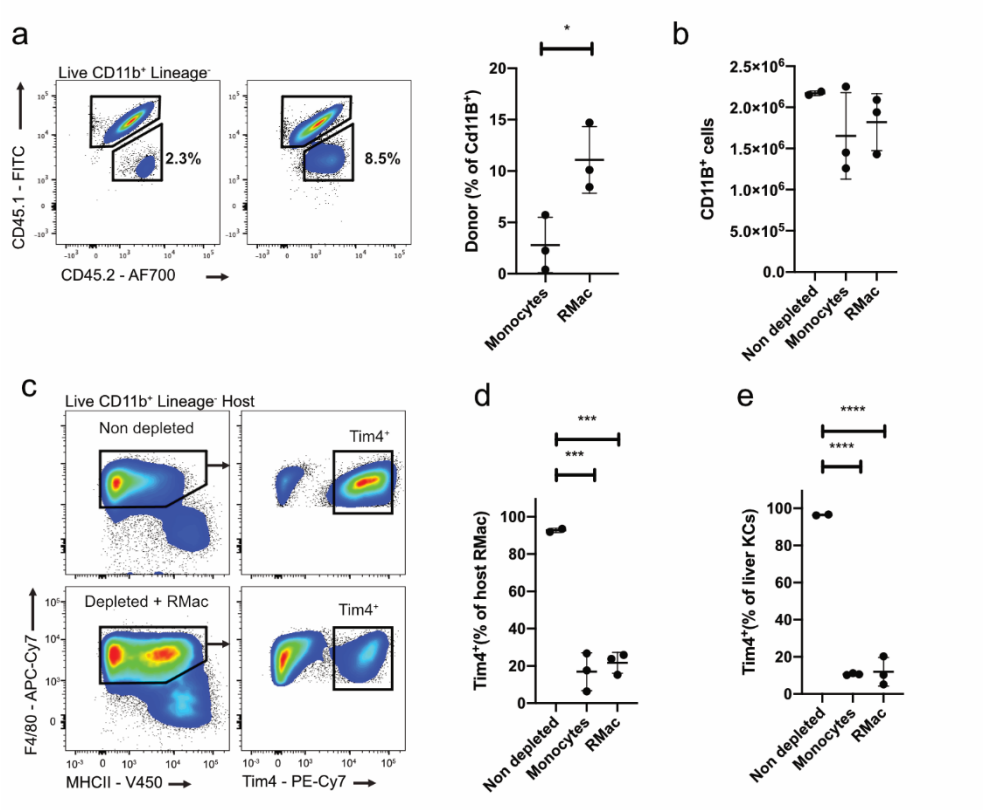

Figure 3.8 Peritoneal macrophages persist following transfer into clodronate-depleted recipients.

(a) Representative identification of proportion of $CD11B^{+}Lineage^{-}$ cells that are of donor origin 8 day after transfer of monocytes (left) or RMac (right). *p<0.05 determined by student's t test. **(b)** Absolute number of total (donor+host) $CD11B^{+}Lineage^{-}$ myeloid cells 8 days after transfer. **(c)** Representative expression of F4/80, MHCII and Tim4 by host cells in non-depleted (top) and depleted (bottom) mice 8 days after transfer. **(d)** Proportion of host peritoneal $F4/80^{Hi}$ macrophages that express Tim4, 8 days following adoptive transfer. ***p<0.001 determined by one way ANOVA with Dunnett's multiple comparisons test. **(e)** Proportion of Kupffer cells that express Tim4, 8 days following adoptive transfer of indicated populations. ****p<0.0001 determined by one way ANOVA with Dunnett's multiple comparisons test. Data shown as mean ± standard deviation. Each symbol represents an individual animal.

Chapter 4

Investigating inflammatory macrophage survival and identity following resolution of zymosan-induced peritonitis.

4.1 Introduction

In the previous chapter, I optimized a 'toolbox' to investigate the survival and identity of inflammatory macrophages after zymosan induced peritonitis. Moreover, the low dose zymosan model of peritonitis allowed purification of resident and inflammatory macrophages 3 days post zymosan from the resolved cavity and subsequent transfer into various recipient mice.

Importantly, the overall size of the peritoneal macrophage compartment, including both resident and inflammatory macrophages combined, is enlarged at this timepoint compared to pre-inflammation[139], yet this inflammation driven expansion is temporary as the peritoneal compartment contracts back to pre-inflammation size over the succeeding week[162]. Moreover, during contraction resident macrophages undergo high levels of proliferation, whereas only a minor subset of inflammatory macrophages proliferates[87,144]. The combination of these two phenomena is likely to dictate the survival and conversion potential of inflammatory macrophages over this period. Hence, for my first studies I decided to focus on the survival and phenotype of inflammatory macrophages shortly following resolution.

The rate at which inflammatory macrophages can undergo phenotypic conversion and consequently the extent to which this occurs during this post resolution contraction period is unknown. The only published study that gives an estimate of the rate at which conversion into resident macrophages can occur are SPM transfer studies, carried out by Cain et al. Briefly, under naïve conditions small peritoneal macrophages are largely monocyte-derived cells, that are thought to give rise to resident peritoneal F4/80^{Hi} macrophages[42]. Using C/EBP$\beta^{-/-}$ mice that are deplete of resident F4/80^{Hi} macrophages, Cain et al show that transferred F4/80^{Lo} SPM largely acquire a resident like F4/80^{Hi} MHCII^{Lo} phenotype within an 8-day period after transfer[60]. Inflammatory macrophages present during resolution of zymosan induced peritonitis by day 3 are characterized by an F4/80^{Int} MHCII^{Hi} phenotype[139] , somewhat similar to

SPM. Hence, I postulated that conversion into an F4/80^{Hi} MHCII^{Lo} phenotype should be possible over an 8-day period. As this 8-day period post-resolution coincides with the period during which the cavity macrophage compartment contracts back to steady-state levels I decided to focus my studies on this specific time-point.

In this chapter I sought to investigate if inflammatory macrophages present during resolution of inflammation, persist following the contraction of the macrophage compartment that occurs in the succeeding 8 days and if so, whether they convert into a resident like phenotype. Moreover, I sought to ascertain whether the survival and fate of inflammatory macrophages are dictated by the post-inflammatory environment and, if so, whether competition with incumbent resident macrophages plays affects the phenotype of these cells. To assess the phenotypic conversion potential of inflammatory macrophages I focussed on the markers F4/80 and MHCII, as these markers are commonly used in the literature to identity inflammatory macrophages. In addition, I investigated levels of GATA6, as this is the key peritoneal macrophage identity determining transcription factor highly expressed by resident macrophages[63-65]. Moreover, I assessed expression of CD102, a GATA6 independent marker highly expressed by resident peritoneal macrophages[63] and Tim4, expression of which is thought to be largely limited to embryonically seeded resident macrophages[42].

4.2 The post resolution environment allows inflammatory macrophage survival but inhibits phenotypic conversion.

To investigate if inflammatory macrophages survive after resolution of inflammation and if they remained phenotypically distinct from resident macrophages, 100,000 CD45.2^{+} resident or inflammatory macrophages, present 3 days post-zymosan injection were purified, as described in chapter 2, and adoptively transferred into recipient CD45.1/2^{+} mice at the same stage of peritoneal inflammation **(Figure 4.1a).** Using this methodology allowed

identification of donor cells on the basis of their CD45.2^{+} mismatch. By day 8, transferred donor cells accounted for approximately 1.5% of the total CD11b^{+} Lineage^{-} myeloid cell compartment irrespective of type of macrophage transferred **(Figure 4.1B, left)**. To better describe their ability to survive I calculated the engraftment efficiency, defined as the percentage of transferred cells that were present at the experimental endpoint **(Figure 4.1B, bottom)**. Although variable, the engraftment efficiency of RMac^{Z10} was marginally higher than that of IMac^{Z10} (**Figure 4.1b, right**), indicating that RMac^{Z10} had a slight survival advantage following resolution. Moreover, IMac^{Z10} largely failed to acquire the F4/80^{Hi}MHCII^{Lo} phenotype that characterizes resident macrophages under steady-state conditions and donor RMac^{Z10} at this stage. Consequently, these markers could be used as a rudimentary method to discriminate between the two populations **(Figure 4.1c)**. Similar to work by Davies et al[87]. within the host macrophage compartment, two subsets of macrophages could be identified. These subsets aligned to donor RMac^{Z10} (F4/80^{Hi} MHCII^{Lo}) and IMac^{Z10} (F4/80^{Int} MHCII^{Hi}). In addition, a minor population of F4/80^{Lo} MHCII^{Hi} cells that phenotypically resembled F4/80^{Lo} MHCII^{Hi} SPM, present under steady-state conditions[42], was present but did not appear to originate from either donor population **(Figure 4.1c)**. Importantly, the balance between host F4/80^{Hi} MHCII^{Lo} and F4/80^{Int} MHCII^{Hi} macrophages was equivalent irrespective of the type of donor cell transferred. This suggests that transferred populations do not differentially affect the cavity into which they have been transferred **(Figure 4.1c)**.

As described, a large part of the peritoneal macrophage identity is driven by the transcription factor GATA6[63-65]. By day 8, both donor RMac^{Z10} and IMac^{Z10} were almost universally positive for GATA6, although the level of expression was significantly lower in IMac^{Z10} **(Figure 4.1d,e),** as determined by the mfi of expression in each population. Moreover, the subsets of host macrophages showed a similar pattern with resident-like F4/80^{Hi} MHCII^{Lo} cells expressing higher levels of GATA-6 than inflammatory-like F4/80^{Int} MHCII^{Hi} macrophages, whereas F4/80^{Lo}MHCII^{Hi} cells largely lacked GATA6 consistent with an SPM

identity **(Figure 4.1d,f)**. I also investigated the expression of two additional markers expressed by resident peritoneal macrophage markers, CD102[63,97] and Tim4[42,97]. RMac^{Z10} expressed high levels of both markers, whereas IMac^{Z10} expressed equivalently high levels of CD102, but largely lacked Tim4 **(Figure 4.1g)**.

In summary, using the adoptive transfer methodology I was able to ascertain that inflammatory macrophages persist short-term after resolution of inflammation, albeit somewhat less well than their resident counterparts. During this period, they maintain an inflammatory macrophage phenotype, characterized by intermediate levels of F4/80 and high levels of MHCII but also express resident markers GATA6 and CD102.

In these experiments 2 out of the 10 RMac^{Z10} samples and 1 out of the 9 IMac^{Z10} sample were excluded as no donor cells were present in these animals. In both RMac^{Z10} animals failure of cell transfer could be confirmed due to the complete absence of dye in any recipient cells.

4.3 The post resolution environment does not dictate inflammatory macrophage survival and phenotype.

As both monocytes and macrophages are thought to be highly responsive to environmental signals[7,9] I set out to investigate if the impaired survival and unique identity of inflammatory macrophages is determined by the post-resolution environment or if these phenomena are pre-determined features, imprinted on inflammatory macrophages earlier in their development. Hence, I used the same adoptive transfer methodology as described in 4.1, but transferred purified Imac^{Z10} and Rmac^{Z10} into naïve recipient mice thus removing the post-resolution environment as a possible factor in their survival and phenotype **(Figure 4.2a)**.

As naïve recipient mice have a completely intact macrophage compartment, it was surprising to find that IMac^{Z10} persisted similarly to transferred RMac^{Z10}**(Figure 4.2b)**. IMac^{Z10} remained phenotypically distinct and could largely be differentiated from RMac^{Z10} on the basis of their F4/80^{Int} MHCII^{Hi} phenotype following transfer into naïve recipients **(Figure 4.2c)**. However, unlike in recipient mice that had been pre-treated with zymosan, the host macrophage compartment of naïve recipient mice largely comprised an F4/80^{Hi} MHCII^{Lo} population comparable to RMac^{Z10}, but with no population corresponding to F4/80^{Int} MHCII^{Hi} IMac^{Z10} **(Figure 4.2c)**. Again, similar to their phenotype in the native environment IMac^{Z10} were also almost exclusively GATA6^{+}, although levels were lower than detected in RMac^{Z10}**(Figure 4.2d, e)**. Moreover, virtually all RMac^{Z10} expressed CD102 and Tim4, unlike IMac^{Z10} which were CD102^{+} but largely Tim4^{-} **(Figure 4.2f)**.

In conclusion, the post-resolution environment does not appear to greatly affect the survival and conversion potential of transferred inflammatory macrophages.

4.4 Competition with incumbent resident macrophages inhibits proliferation of inflammatory macrophage and conversion.

In the previous experiments transferred IMac^{Z10} were placed in environments in which they directly competed with incumbent resident macrophages. Considering competition for niche space is thought to be an important regulator of monocyte to macrophage conversion in solid organs, for example the liver[38,73] it is possible that the presence of competing resident macrophages affects the fate of IMac^{Z10}. Consistent with this hypothesis, SPM transferred into recipient mice, largely deplete of resident macrophages (C/EPB$\beta^{-/-}$ recipient mice), adopted a resident like F4/80^{Hi} MHCII^{Lo} phenotype, but failed to do so after transfer into mice with an intact resident compartment (C/EPB$\beta^{+/+}$ recipient mice)[60].

Hence, I postulated that competition with resident macrophages would not affect survival of IMac^{Z10} but could be inhibiting conversion of transferred IMac^{Z10}. To test this hypothesis, I adoptively transferred RMac^{Z10} or IMac^{Z10} into recipient mice pre-treated with clodronate 7 days prior to transfer **(Figure 4.3a)**. By day 8, IMac^{Z10} accounted for approximately 20% of the total CD11B^{+}Lineage^{-} macrophage compartment with an engraftment efficiency of approximately 250%, suggesting these cells had expanded considerably **(Figure 4.3b)**. Conversely, RMac^{Z10} appeared unable to undergo a similar expansion with an engraftment efficiency of approximately 90%, indicating that, although these cells persisted somewhat better than they did in the competitive settings of the inflamed or uninflamed cavities, they did not expand to the same degree as IMac^{Z10} **(Figure 4.3b)**. Critically, IMac^{Z10} more fully downregulated MHCII adopting a more resident like phenotype **(Figure 4.3c)**. Notably, the host macrophage compartment **(Figure 4.3c)** resembled the macrophage compartment post inflammation based on F4/80 and MHCII **(Figure 4.1c)**, suggesting that monocyte-derived macrophages had repopulated the cavity following depletion of the resident cells **(Figure 3.7d)**. Moreover, IMac^{Z10} almost exclusively expressed GATA6^{+}, but the level of expression remained lower than in RMac^{Z10}**(Figure 4.3d,e)**. Again, RMac^{Z10} almost exclusively expressed CD102 and Tim4, whereas IMac^{Z10} expressed equivalent levels of CD102, but did not express Tim4 **(Figure 4.3f)**. However, I did notice that the fraction of RMac^{Z10} that expressed Tim4 appeared more variable and on the whole lower than on RMac^{Z10} transferred into mirroring inflamed or naïve recipients **(Compare 4.1g to 4.2f to 4,3f).**

Hence, these data indicate that the presence of competing resident macrophages inhibits the ability of IMac^{Z10} to undergo conversion to an MHCII^{lo} phenotype and suppresses the proliferative capacity of IMac^{Z10}.

In these experiments 2 out of 10 RMac^{Z10} samples were excluded due to incomplete depletion and 2 out of the 8 IMac^{Z10} samples were excluded, one because of incomplete depletion and the other one because the gut was

severely inflamed, both indicative of failed IP injection.

4.5 PKH26-PCL dye labelling does not inhibit resident macrophage proliferation.

The ability of IMac^{Z10} to proliferate after transfer into depleted recipients and the apparent inability of RMac^{Z10} to do so was surprising. To interpret this data correctly I wanted to verify that PKH26-PCL labeling did not affect cell proliferation as transferred RMac^{Z10} were labelled and seemingly did not proliferate whereas transferred IMac^{Z10} were unlabeled and proliferated.

I was unable to find any published data that investigated or described an inhibitory effect of PKH26-PCL dye on cell proliferation. However, during my earliest trial experiments presented in **Figure 3.8**, during which I adoptively transferred dye labelled RMac sourced from naïve donor mice into depleted recipients I had stained purified RMac directly after sorting and prior to adoptive transfer for Tim4 to verify the purity on the day. As I had also included Tim4 in the panel at the experimental endpoint I was able to quantify if the fraction of RMac that expressed Tim4 was altered between the time of transfer and at the time of collection. If so, this could also help explain the variable and lower levels of Tim4 on RMac^{Z10} after transfer into depleted recipients discussed in the previous section. Critically, under naïve homeostatic conditions the absence of Tim4 has been shown to label a minor fraction of resident peritoneal macrophages that are of monocyte origin and that have higher levels of proliferation[42]. Hence, I postulated that after transfer into depleted recipients the Tim4^{-} fraction of RMac should proliferate more thus providing evidence that PKH26-PCL labelling does not inhibit the capacity of labelled cells to proliferate.

To investigate this, I pooled the data from the RMac transfer presented in **Figure 3.8.** with one additional repeat experiment where I transferred RMac into clodronate pre-treated recipients. **(Figure 4.4a)**. I confirmed that the

purified RMac population at the time of transfer largely consisted of Tim4^{+} macrophages **(Figure 4.4b,c)** and importantly that the Tim4^{+} and Tim4^{-} fraction were equivalently labelled with PKH26-PCL **(Figure 4.4b,c)**. By day 8 post transfer the Tim4^{-} fraction appeared to have become enriched within the transfer population (**Figure 4.4d)**

It has been described that Tim4 is slowly acquired by macrophages[42] and in my hands appears to be acquired minimally by IMac^{Z10} over an 8 day period even after transfer into depleted recipients **(Figure 4.3).** Hence, I made the assumption that over the 8 days proliferating Tim4^{-} RMac would largely give rise to Tim4^{-} offspring, whereas proliferating Tim4^{+} RMac would predominantly give rise to Tim4^{+} RMac. Hence, I quantified a separate engraftment efficiency for Tim4^{-} RMac and Tim4^{+} RMac. This analysis indicated that Tim4^{-} RMac had a proliferative capacity somewhat similar to that identified for IMac^{Z10}, with an engraftment efficiency of approximately 290%, whereas Tim4^{+}RMac appeared less able to proliferate, with an engraftment efficiency of approximately 150% **(Figure 4.4e)**.

There are currently no data available on how PKH26-PCL labelling dilutes after cell division. However, it has been shown that intracellular particles sequestered in macrophages are equally divided between daughter cells upon cell division, unless microbial or environmental factors promote unequal distribution[163]. Consistent with PKH26-PCL labelling being divided equally between daughter cells Tim4^{-} RMac had lost more PKH26-PCL labelling compared to the Tim4^{+} RMac fraction **(Figure 4.4f)** likely as a result of higher levels of proliferation in the former population.

Moreover, work by Cain et al carried out experiments where they transferred 80.000 purified F4/80^{Hi}LPM into macrophage deplete C/EPB$\beta^{-/-}$ recipient mice or C/EPB$\beta^{+/+}$ recipient mice and quantified the number of donor cells retrieved up until 30 days post transfer[60]. The authors kindly provided me with the published dataset and have given me permission to include these data in my

thesis. In the publication they presented the absolute number of donor cells which were hard to compare directly to my results. Hence, I calculated an engraftment efficiency based on their absolute cell counts, allowing easy comparison between my adoptive transfer studies and the ones published by Cain et al. The overall engraftment efficiency in their experiment was approximately 12%, somewhat lower than in the experiments I carried out. Importantly, there did not appear to be a great difference in the number of donor LPM retrieved after transfer into C/EPBβ$^{-/-}$ or C/EPBβ$^{+/+}$ mice **(Figure 4.4g).** These data suggest that, similar to my findings, transferred LPM were unable to expand considerably after transfer into macrophage deplete recipients. Critically, in their study they did not use a dye labelling methodology suggesting that the apparent inability to expand in my hands is unlikely to be due to confounding effects of PKH26-PCL labelling.

4.6 Transferred cells migrate into the omentum of clodronate pre-treated recipients.

The omentum is thought to be an important source of CSF1, vital for the survival and proliferation of peritoneal macrophages. Moreover, the omentum is thought to be the predominant source of retinoic acid in the peritoneal cavity, which has been shown to drive expression of the peritoneal identity determining transcription factor GATA6[63]. In addition, the omentum is thought to produce additional, poorly defined, factors that are required for maintenance of the peritoneal macrophage identity. *In vitro* studies indicate that secreted omentum factors drive part of the peritoneal macrophage identity, but also that a small proportion of peritoneal macrophage identity genes requires the direct interaction between peritoneal macrophages and the omentum[99]. The importance and extent of interplay between the omentum and peritoneal macrophages *in vivo* is poorly understood. Peritoneal cells have been shown to interact with the omentum *in vivo* during homeostasis[164]. Moreover, GATA6 signalling, predominantly driven by omental retinoic acid, has been suggested to be required for macrophages to exit the omentum and enter the peritoneal

cavity. It has been postulated that migration through the omentum is required for maintenance of the GATA6^{+} peritoneal macrophage population[63]. However, no migration of macrophages from the peritoneal cavity into the omentum or vice versa has been definitively shown to occur under steady state conditions. In the context of peritoneal inflammation it has been suggested that inflammatory monocytes/macrophages could be migrating from the omentum into the peritoneal cavity and vice versa after LPS treatment[63] zymosan treatment [165] or *S.Typhi* immunization[166]. However, these datasets draw this conclusion largely on the basis of markers[63], or indirectly from the observation that monocyte derived cells accumulate in the omentum[165] prior to accumulation peritoneal cavity[166]. Critically, none of these datasets directly shows migration from macrophages or monocytes present

As the adoptive methodology I developed was exquisitely adapted to investigate migration from the peritoneal cavity into the omentum I set out to determine if in the experiments presented in the previous sections RMac^{Z10} or IMac^{Z10} had indeed migrated into the omentum. I postulated that post resolution IMac^{Z10} would not migrate and consequently why they failed to acquire a F4/80^{Hi}MHCII^{Lo} resident phenotype whereas after clodronate pre-treatment IMac^{Z10} could migrate into the depleted omentum and acquire proliferation and differentiation factors.

The omental CD11B^{+} Lineage^{-} myeloid compartment can divided into CD102^{+} GATA6^{+} 'peritoneal like' macrophages, CD102^{-} F4/80^{+} omental macrophages and F4/80^{-} CD102^{-} monocytes and cDCs[42]. As there was no indication to which population transferred cells might contribute, the myeloid compartment was rudimentary split into two populations namely: macrophages (F4/80^{+} and/or CD102^{+}) and monocytes (F4/80^{-}/CD102^{-}) **(Figure 4.5a)**. The population of macrophages can be divided into CD102^{+} MHCII^{Lo} 'peritoneal like' macrophages and CD102- MHCII^{Hi} macrophages thought to be omental macrophages (**Figure 4.5a**)[97]. Of note, the cell counts obtained after omentum preparation using the CASY counter proved highly variable, partially because

of the debris present after preparation. Hence, the data presented here are quantified as proportions rather than absolute numbers. After transfer into mirroring inflamed or naive recipients neither donor RMac^{Z10} nor IMac^{Z10} were detectable within the omental macrophage or monocyte fraction **(Figure 4.5b,c)** suggesting that negligible migration from the peritoneal cavity occurs during homeostasis and shortly after resolution of inflammation.

Intraperitoneal injection with clodronate liposomes has been used to deplete omental phagocytes[102]. As I had not previously investigated the depletion of phagocytes in the omentum in my hands, I first verified that by D15 post-clodronate treatment the proportion of omentum macrophages that express Tim4 was reduced as a rudimentary readout of successful depletion. Indeed, by D15 the proportion of Tim4-expressing omental macrophages was reduced compared to control mice **(Figure 4.5d)** although the effect was less striking than observed in liver Kupffer cells **(Figure 3.7e)** or host peritoneal macrophages. Hence, it would appear that clodronate treatment, at least partially, depleted omentum macrophages.

After transfer into clodronate pre-treated recipients both donor RMac^{Z10} and IMac^{Z10} were detectable within the omentum macrophage compartment, but not the F4/80^{-}CD102^{-} monocyte/cDC 8 days post transfer. **(Figure 4.5f)**. Whereas RMac^{Z10} phenotypically resembled the CD102+ MHCII^{Lo} fraction of omental 'peritoneal like' macrophages, approximately half of IMac^{Z10} expressed this phenotype, while the remaining cells exhibited a CD102^{Lo}MHCII^{Hi} phenotype aligning with the remainder of omental macrophages **(Figure 4.5g)**. In earlier experiments I had collected the omentum after transfer of IMac^{Z10} or naïve RMac into clodronate depleted recipients. During the first rounds of experiments there were some issues with variability of the zymosan and I was unable to consistently source RMac^{Z10} for transfer during these experiments. Hence, only IMac^{Z10} and naïve RMac were transferred in these experiments. Surprisingly, in these earlier experiments IMac^{Z10} seemingly migrated into the omentum more efficiently than RMac

(**Figure 4.5h**). Indeed, when pooling these data (squares) with the dataset previously presented in Figure 4.5f (circles) it would appear that donor IMac^{Z10} might be migrating more readily into the omentum than RMac **(Figure 4.5h)** although there is a high degree of variability between the datasets

In summary, using the adoptive transfer methodology I was able to ascertain that after partial depletion of omentum macrophages both resident and inflammatory macrophages migrate into the omentum.

4.7 Inflammatory macrophage phenotype is responsive to retinoic-acid and omentum factors *in vitro.*

The data I generated suggested that by 8 days post transfer (11 days post zymosan) inflammatory macrophages were capable of adopting a more resident like MHCII^{Lo} phenotype, but only in the absence of competing resident macrophages. This ability to convert coincided with some degree of migration of inflammatory macrophages into the macrophage deplete omentum. However, the fraction of IMac^{Z10} that migrated into the omentum seemed minor compared to the expanded population of cells retained in the peritoneal cavity. Although IMac^{Z10} could be continuously migrating in and out of the omentum, another possibility is that the more complete conversion of IMac^{Z10} and possibly the proliferation occurs because of secreted omentum factors. This would be consistent with *in vitro* data indicating that the omentum predominantly affects peritoneal macrophage identity via secretion of retinoic acid and omentum factors, while direct interaction is only required to drive a relatively minor fraction of peritoneal identity genes[99].

Hence, I postulated that retinoic-acid and omentum factors secreted into the peritoneal cavity by the omentum drive inflammatory macrophage conversion through up and downregulation of F4/80 and MHCII respectively. To investigate this, I collected peritoneal exudate cells 11 days after injection of low dose zymosan. Importantly, at this timepoint transferred IMac^{Z10} were

characterized by an F4/80^{Int} MHCII^{Hi} phenotype in their native post resolution environment, but were capable of downregulating MHCII in the clodronate depleted environment. Macrophages were then adherence purified and treated for 24 hours with 250ul cell culture media containing all trans retinoic-acid (ATRA; 1μm), Omentum factors (Om factors), produced as described by Okabe et al[63], both ATRA and Om factors or neither (Ctrl) and investigated using flow cytometry **(Figure 4.6a)**.

During earlier adoptive transfer experiments I had found that CD102 and Tim4 expression delineated RMac from IMac^{Z10}irrespective of the recipient environment **(Figure 4.3f)**. Hence, I opted to use a combination of these markers as a surrogate method to identify resident (CD102^{+} Tim4^{+}) and inflammatory macrophages (CD102^{+} Tim4^{-}) after culture. Importantly, none of the treatments altered the proportion of CD102 and Tim defined macrophages based on these markers. **(Figure 4.6b)**. Culture with ATRA led to increased expression of the GATA6 responsive marker F4/80[63] by CD102^{+}/Tim4^{+} (resident) and CD102^{+}Tim4^{-} (inflammatory) macrophages, but not down-regulation of MHCII **(Figure 4.6c,d)**. Surprisingly, F4/80 was not upregulated in response to treatment with both ATRA and omentum supernatant. Culture with omental supernatant with or without ATRA led to downregulation of MHCII by CD102^{+}Tim4^{-} inflammatory macrophages **(Figure 4.6d)**

In summary, these data indicate that inflammatory macrophage F4/80 expression is responsive to retinoic acid, whereas MHCII expression is responsive to other omentum factors. Combined these data suggest that post-resolution inflammatory macrophages might be unable to compete for omentum derived factors and consequently fail to adopt a resident like F4/80^{Hi} MHCII^{Lo} phenotype.

4.8 Retinoic-acid drives expression of GATA6 and F4/80 by monocyte-derived macrophages *in vivo*

Combined the *in vivo* and *in vitro* experiments suggested that IMac^{Z10} might be failing to compete with resident macrophages for ATRA and/or omentum factors and consequently fail to adopt a resident like phenotype. To ascertain whether this competitive disadvantage was indeed limiting phenotypic conversion I attempted to adapt a protocol published by Gundra et al[145] to investigate whether treatment with excess ATRA would allow inflammatory macrophages to upregulate GATA6 to equivalent level as their resident counterparts. In their publication Gundra et al[145] injected ATRA IP to successfully induce expression of F4/80 on peritoneal macrophage after thioglycolate induced peritonitis. In their protocol ATRA was dissolved in DMSO and injected IP. However, during trial experiments I found that both injection of DMSO alone and ATRA in DMSO caused significant discomfort to the mice, as indicated by hunched posture and temporary paralysis of the hindlegs. In addition, the wash collected after either treatment regimen was consistently contaminated with blood irrespective of the treatment group, suggesting DMSO might be disrupting peritoneal vasculature. Hence, I altered the protocol and prepared a high concentration ATRA stock in DMSO which I then dissolved in corn oil to prepare a working solution for injection as suggested by the manufacturer and used previously[167,168]. I then proceeded to carry out an adoptive transfer protocol similar to that presented in Figure 4.1 transferring RMac^{Z10} or IMac^{Z10} into equivalently inflamed recipients that subsequently received 250μg ATRA or vehicle (20% DMSO/ 80% corn oil) every other day IP until harvest at day 8 **(Figure 4.7a)**.

Following collection of the samples the omentum was no longer discernible irrespective of the treatment group. Instead, it looked like the omentum had been encapsulated into one large clump of fat. Preparation of a single cell suspension from this apparent adipose tissue using the omentum preparation protocol yielded no viable cells. Furthermore, neither RMac^{Z10} nor IMac^{Z10}

were detectable in peritoneal lavage fluid, irrespective of the treatment group indicating that the peritoneal macrophage compartment per se had been replaced by monocyte derived cells due to the vehicle treatment **(Figure 4.7b)**. Consistent with an inflammatory event high numbers of neutrophils were present in cavity of vehicle treated mice, with approximately twice as many in the ATRA treated mice **(Figure 4.7c)**. Despite driving inflammation, ATRA treatment significantly expanded the number of $CD11B^{+}$ $Lineage^{-}$ host macrophages expressing high or intermediate levels of GATA6 but not GATA6 negative macrophages **(Figure 4.7e)** compared with treatment with oil vehicle alone. Moreover, ATRA treatment did not affect the levels of MHCII on these GATA6-defined subsets consistent with *in vitro* findings. **(Figure 4.7f)**

4.9 Inflammatory macrophages expand following transfer into $FIRE^{-/-}$ mice devoid of peritoneal resident macrophages.

A drawback of using clodronate liposomes as a depletion method is that host monocytes infiltrate the cavity and consequently transferred cells are repopulating the peritoneal cavity in parallel with infiltrating host monocytes. I was keen to validate the expansion of $IMac^{Z10}$ and migration into the omentum using $FIRE^{-/-}$ recipient mice, devoid of peritoneal and omental macrophages[106]. The $FIRE^{-/-}$mice were on a mixed C57BL/6-CBA background. Unfortunately, as we were backcrossing to C57BL/6 we discovered that deletion of the FIRE domain is lethal on a pure C57BL/6 background. Importantly, Dr. Clare Pridans confirmed that despite being on a mixed C57BL/6-CBA background $FIRE^{-/-}$ mice and littermate controls exclusively expressed the H-2Kk MHC class I alloantigen (personal communication) indicating that transfer of littermate cells into $FIRE^{-/-}$ recipients was possible. Hence, I set out to use the $FIRE^{-/-}$ mice on a mixed background to validate my earlier findings. Unfortunately, I was unable to use the tracking methodology utilized in the previous experiments. However, as $FIRE^{-/-}$ mice were almost completely devoid of peritoneal macrophages a method to track donor cells was not strictly necessary as any cells present

would originate predominantly from donor cells. In addition, expression of the CD115 (CSF1R) was largely absent FIRE$^{-/-}$ mice[106] whereas both RMac^{Z10} and IMac^{Z10} expressed high levels of CD115 **(Figure 4.8a)**.

Hence, I carried out an adoptive transfer experiment where I transferred RMac^{Z10} or IMac^{Z10} sourced from FIRE$^{+/+}$or FIRE$^{+/-}$ control mice and transferred these cells into FIRE$^{-/-}$ recipients **(Figure 4.8a).** By day 8, the small fraction of F4/80^{Hi} CD115^{-} macrophages present in PBS treated non-transferred FIRE$^{-/-}$ mice was complemented by a clear population of donor PKH26-PCL^{+} RMac^{Z10} or PKH26-PCL^{Lo} IMac^{Z10}, both of which expressed high levels of CD115 **(Figure 4.8b)**. However, as definitive discrimination between host and donor cells was not possible, the size of the whole myeloid compartment 8 days post transfer (CD11B^{+} Lineage^{-}) was quantified. This analysis suggested an expansion of the myeloid compartment after transfer RMac^{Z10} but more so after transfer of IMac^{Z10} **(Figure 4.8c)**, similar to IMac^{Z10} expansion observed after transfer into clodronate-depleted recipients (**Figure 4.3b**). However, the data was highly variable and although in each experiment IMac^{Z10} had expanded more than RMac^{Z10} the data indicated no significant differences. This experiment would have to be repeated to be sure. IMac^{Z10} appeared to have higher levels of proliferation as measured by Ki67 **(Figure 4.8d)**. Finally, after transfer into FIRE$^{-/-}$ recipient mice IMac^{Z10} downregulated MHCII **(Figure 4.5e)** consistent with earlier transfer studies into clodronate-depleted recipients (**Figure 4.3c**).

4.9.1 Inflammatory macrophages migrate into the omentum of FIRE$^{-/-}$ recipient mice

During preliminary experiments my supervisor Dr. Steve Jenkins found that the omentum of FIRE$^{-/-}$ mice is largely devoid of macrophages. As I had found earlier that RMac^{Z10} and IMac^{Z10} migrated into the partially-depleted omentum, I set out to investigate if migration occurred into the omentum of FIRE$^{-/-}$ recipient mice.

Indeed, upon investigation of the omentum I found that transferred cells appeared to have migrated into the omentum **(Figure 4.9a)**. In PBS injected mice FIRE$^{-/-}$ omental macrophages (F4/80^{+}/CD102^{+}) were virtually absent, but after transfer of RMac^{Z10} or IMac^{Z10} a clear population was detectable, likely derived from transferred cells **(Figure 4.9a)**. However, as donor cells could not be definitively identified, I quantified the size of the complete omental myeloid cell compartment. This analysis indicated that RMac^{Z10} and IMac^{Z10} both expanded the complete myeloid-cell compartment **(Figure 4.9b)**. Intriguingly, this myeloid expansion after RMac^{Z10} transfer did not appear to coincide with an increase in the proportion of cells with a macrophage F4/80^{+}/CD102^{+} phenotype, whereas transfer of IMac^{Z10} did lead to the presence of an expanded F4/80^{+}/CD102^{+} macrophage population **(Figure 4.9a,c)**. These data would suggest that transfer of RMac^{Z10} leads to expansion of the CD102^{-}/F4/80^{-} monocyte compartment. This is likely through increased infiltration of monocytes, as levels of Ki67 detectable in CD102^{-}/F4/80^{-} cells were equivalent after transfer of RMac^{Z10} and IMac^{Z10} (**Figure 4.9e**).

4.10 Discussion

In this chapter I sought to establish if inflammatory macrophages present during the resolution of inflammation persist through the succeeding period during which the overall size of the macrophage compartment contracts to pre-inflammation levels. By adoptively transferring RMac^{Z10} and IMac^{Z10} into mirroring inflamed recipients I found that IMac^{Z10} persist through this period, albeit less well than RMac^{Z10}, and that they are characterized by an F4/80^{Int}MHCII^{Hi} phenotype. Surprisingly after transfer into naïve recipient mice, IMac^{Z10} seemingly persisted equally well as RMac^{Z10} despite competing with a completely intact host macrophage compartment. This discrepancy could be due to the myeloid compartment expansion at the time of transfer, 3 days post zymosan, compared to naïve mice. However, it is likely that IP injection of donor cells itself induces loss of resident macrophages, thus allowing donor IMac^{Z10} and RMac^{Z10} to persist. Indeed, IP injection with PBS has been shown

to drive a minor loss of resident macrophages[146] (Personal communication Dr. Steve Jenkins). Over the succeeding 8 days post transfer the compartment contracted back to pre-inflammation levels. As IMac^{Z10} seemingly persisted less during this contraction period than their RMac^{Z10} counterparts this could indicate that competitive pressure from both resident and other inflammatory macrophages limits, but does not prevent IMac^{Z10} survival. Indeed, IMac^{Z10} transferred into recipient mice deplete of peritoneal macrophages expanded considerably and adopted a more resident like F4/80^{Hi} MHCII^{Lo} phenotype. When transferring RMac^{Z10} or IMac^{Z10} into clodronate-depleted recipient mice, donor cells were transferred into a cavity containing high numbers of death cells and placed in direct competition with infiltrating host monocytes for peritoneal cavity residency. However, these phenomena are unlikely to have affected the experimental readouts as adoptive transfer experiments into FIRE$^{-/-}$ recipients, devoid of resident macrophages and infiltrating monocytes, suggested a similar ability of IMac^{Z10} to expand and downregulate MHCII expression. Hence, competition with incumbent resident macrophages after resolution of inflammation does not prevent the survival of inflammatory macrophages, but seemingly inhibits the proliferation and phenotypic conversion of these cells.

The ability of inflammatory macrophages to undergo more complete conversion in the resident macrophage deplete environment could be related to their capacity to acquire omental differentiation factors in this environment. Indeed, *in vitro* the inflammatory macrophage phenotype is responsive to retinoic acid and other omentum factors, indicating that their impaired capacity to convert *in vivo* is not due to an inability to respond to these cues but likely due to an inability to acquire these factors whilst competing with incumbent resident macrophages. However, as both RMac^{Z10} and IMac^{Z10} were capable of migrating into the macrophage deplete omentum, the latter seemingly doing so more readily, it cannot be excluded that migration into, or interaction with, the omentum rather than uptake of secreted omentum factors from the cavity microenvironment, is underlying the inability of IMac^{Z10} to undergo phenotypic

conversion when competing with resident macrophages. Alternatively, the seemingly increased migration capacity of IMac^{Z10} might account for the striking expansion of these cells in the peritoneal cavity after transfer into mice deplete of resident macrophages. As little is known about the mechanisms regulating this migration it is challenging to design an experiment to test this hypothesis. In addition, it remains unclear whether donor cells found in the omentum subsequently migrate back into the peritoneal cavity or remain sequestered in the omentum. Combined these data indicate a potential role for the omentum in shaping the post resolution identity of inflammatory macrophages, but the exact mechanisms via which this may occur remain unclear.

By injecting retinoic-acid into the post zymosan cavity I attempted to investigate if excess retinoic acid would indeed drive GATA6 expression on IMac^{Z10} to levels equivalent to RMac^{Z10}. When I carried out this experiment there were no published data on the inflammatory effects of IP injection with corn oil. Hence, interpretation of these data was complex without additional experimentation. Due to time constraints I chose to focus on other parts of my project and did not repeat this experiment or carry out additional experiments to verify the inflammatory effects of oil. Recent work indicated that IP injection with oil causes chronic inflammation and monocyte infiltration[169]. Specifically, IP delivery of corn oil causes complete loss of Tim4^{+} resident macrophages. These findings support the idea that the corn oil vehicle used in this experiment led to complete replacement of macrophage compartment as indicated by the complete absence of transferred cells. Hence, these data would suggest that retinoic-acid *in vivo* drives expression of GATA6 by monocyte-derived inflammatory macrophages recruited during oil induced peritonitis. Hence, these data support the hypothesis that the inability of IMac^{Z10} to acquire equivalent levels of GATA6 as RMAc^{Z10} after zymosan induced peritonitis might be due to an impaired ability to compete for retinoic-acid.

To investigate the survival and conversion potential of inflammatory

macrophages I have chosen to use an adoptive transfer method. This method is powerful as it allows transfer into varying recipient environment. However, a potential drawback of the adoptive transfer methodology is that by transferring in donor cells the environment is altered, thus affecting experimental results. As donor cells accounted for a relatively small proportion of the macrophage compartment in all transfer experiments, they are unlikely to significantly affect the cavity as a whole. Moreover, the transfer of $RMac^{Z10}$ or $IMac^{Z10}$ did not differentially affect the host macrophage compartment indicating that if donor cells affected the cavity both donor populations did so similarly. During later studies I carried out a time-course experiment investigating the peritoneal cavity at different timepoints after zymosan induced peritonitis. These studies allowed me to verify that features found here using the adoptive transfer methodology are not affected by the transfer itself.

In summary, these data indicate that inflammatory macrophages present during resolution of peritonitis survive and remain phenotypically distinct. This is a direct result of competition with incumbent resident macrophages for differentiation factors, such as retinoic-acid, likely originating from the omentum.

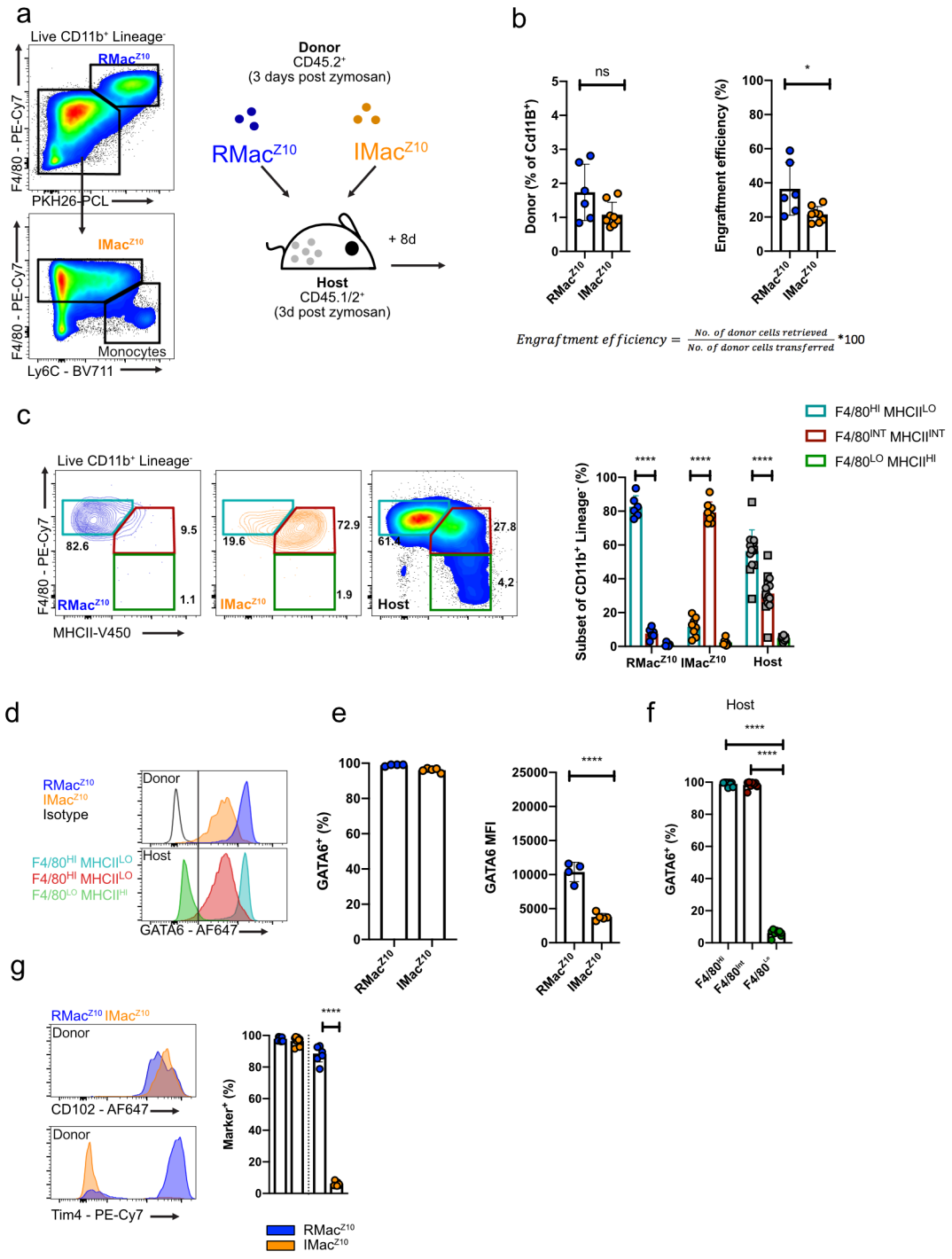

Figure 4.1 Inflammatory macrophages survive after resolution.

(a) Experimental outline for IP delivery of CD45.2⁺ RMac^{Z10} or IMac^{Z10} into inflamed CD45.1/2⁺ recipient mice. For a more detailed gating strategy see Figure 3.6a **(b)** Proportion of CD11B⁺ Lineage⁻ cells that are of donor origin (RMac^{Z10} in blue; IMac^{Z10} in orange) by 8 days after transfer. To the right,

engraftment efficiency of donor RMac^{Z10} (n=6) and IMac^{Z10} (n=8) 8 days after transfer. Engraftment efficiency was calculated based on absolute numbers as described in the M&M section. *p<0.05 determined by Mann-Whitney test. **(c)** Expression of F4/80 and MHCII on donor RMac^{Z10} (n=6), IMac^{Z10} (n=8) and host (n=14) myeloid cells 8 days after transfer. ****p<0.0001 determined by two-way ANOVA and post hoc Tukey test **(d)** GATA6 MFI on indicated donor populations 8 days after transfer. On the bottom, GATA6 MFI on equivalent host macrophage subsets identified on the basis of F4/80 and MHCII as indicated. **(e)** Proportion of donor RMac^{Z10}(n=4), IMac^{Z10} (n=5) that express GATA6 and normalized levels of GATA6 MFI. **(f)** Proportion of host macrophage subsets that express GATA6 11 days after zymosan treatment (8 days after cell transfer; n=9) ****p<0.0001 determined by one-way ANOVA with Tukey's multiple comparisons test. **(g)** Proportion of donor RMac^{Z10}(n=7) and IMac^{Z10}(n=8) that are CD102^{+}/Tim4^{+} 8 days after transfer. ****p<0.0001 determined by one-way ANOVA and Sidak's multiple comparisons test. Data shown as mean ± standard deviation. Each symbol represents an individual animal. Data were pooled from 3 independent experiments

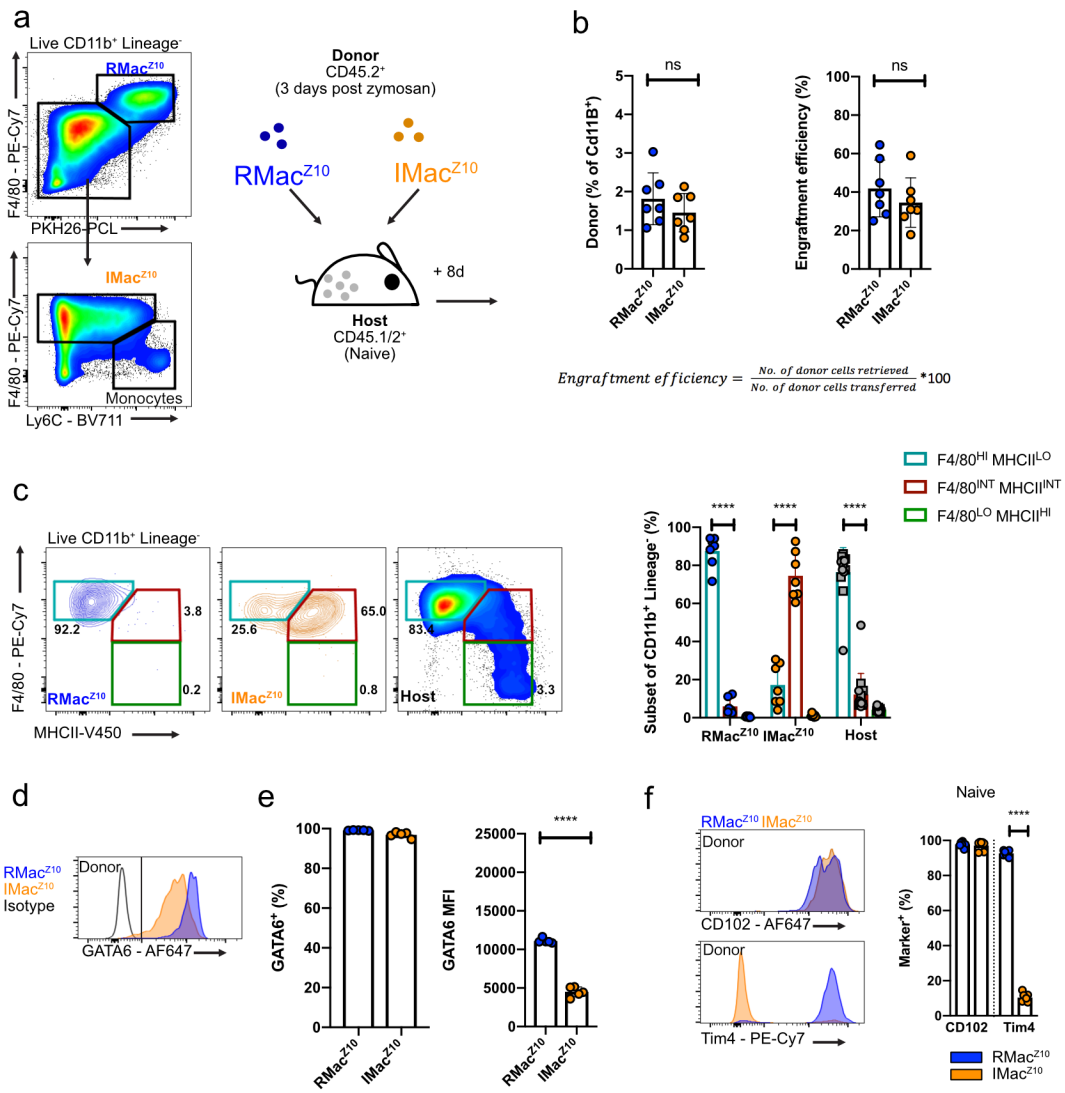

Figure 4.2 Inflammatory macrophages survive following transfer into naïve recipients.

(a) Experimental outline for IP delivery of CD45.2⁺ RMac^{Z10} or IMac^{Z10} into naive CD45.1/2⁺ recipient mice. **(b)** Proportion of CD11B⁺ Lineage⁻ cells that are donor (RMac^{Z10} in blue; IMac^{Z10} in orange) 8 days post transfer. To the right, engraftment efficiency of transferred RMac^{Z10} (n=7) and IMac^{Z10} (n=7) 8 days following transfer. **(c)** Expression of F4/80 and MHCII on donor RMac^{Z10} (n=7), IMac^{Z10} (n=7) or host (n=14) lineage⁻ cells 8 days following transfer. .****p<0.0001 determined by two-way ANOVA and post hoc Tukey test **(d)** GATA6 MFI on donor populations 8 days after transfer. **(e)** Proportion of donor

RMac^{Z10} (n=4) and IMac^{Z10} (n=5) that express GATA6 and GATA6 MFI 8 days post transfer. ****p<0.0001 determined by student's t test. **(f)** Donor RMac^{Z10}(n=7) and IMac^{Z10}(n=7) that express CD102/ Tim4^{+} 8 days after transfer. ****p<0.0001 determined by one-way ANOVA and Sidak's multiple comparisons test. Data shown as mean ± standard deviation. Each symbol represents an individual animal. Data were pooled from 3 independent experiments.

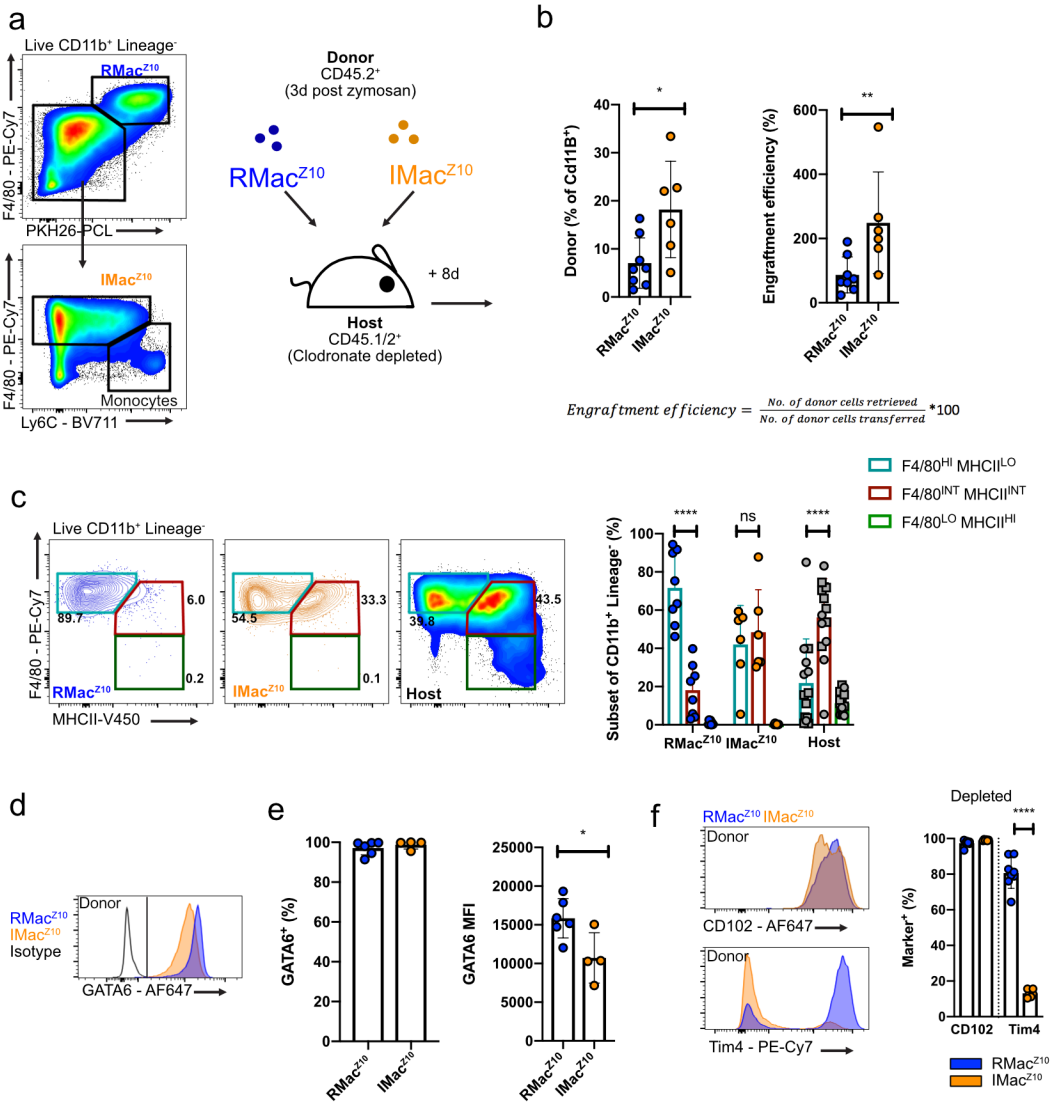

Figure 4.3 Inflammatory macrophages expand and undergo phenotypic conversion following transfer into clodronate-depleted recipients.

(a) Experimental outline for IP delivery of donor CD45.2^{+} RMac^{Z10} or IMac^{Z10} into clodronate liposomes pre-treated CD45.1/2^{+} recipient mice. **(b)** Proportion of CD11B^{+} Lineage^{-} cells that are of donor origin (RMac^{Z10} in blue; IMac^{Z10} in orange) 8 days after transfer. To the right, engraftment efficiency of donor RMac^{Z10} (n=8) and IMac^{Z10} (n=6) 8 days post-transfer. **(c)** F4/80 and MHCII expression on donor RMac^{Z10} (RMac^{Z10} n=8), IMac^{Z10} (n=6) or host (n=14) lineage^{-} cells 8 days after transfer. ****p<0.0001 determined by two-way ANOVA and post hoc Tukey test. **(d)** GATA6 expression levels on indicated

donor populations 8 days post transfer. **(e)** Donor RMac^{Z10} (n=6) and IMac^{Z10} (n=5) that express GATA6 and GATA6 MFI 8 days after transfer. ****p<0.0001 determined by student's t test. **(f)** Proportion of donor RMac^{Z10}(n=8) and IMac^{Z10}(n=6) that express CD102/Tim4 8 days after transfer. ****p<0.0001 determined by one-way ANOVA and Sidak's multiple comparisons test. Data shown as mean ± standard deviation. Each symbol represents an individual animal. Data were pooled from 3 independent experiments

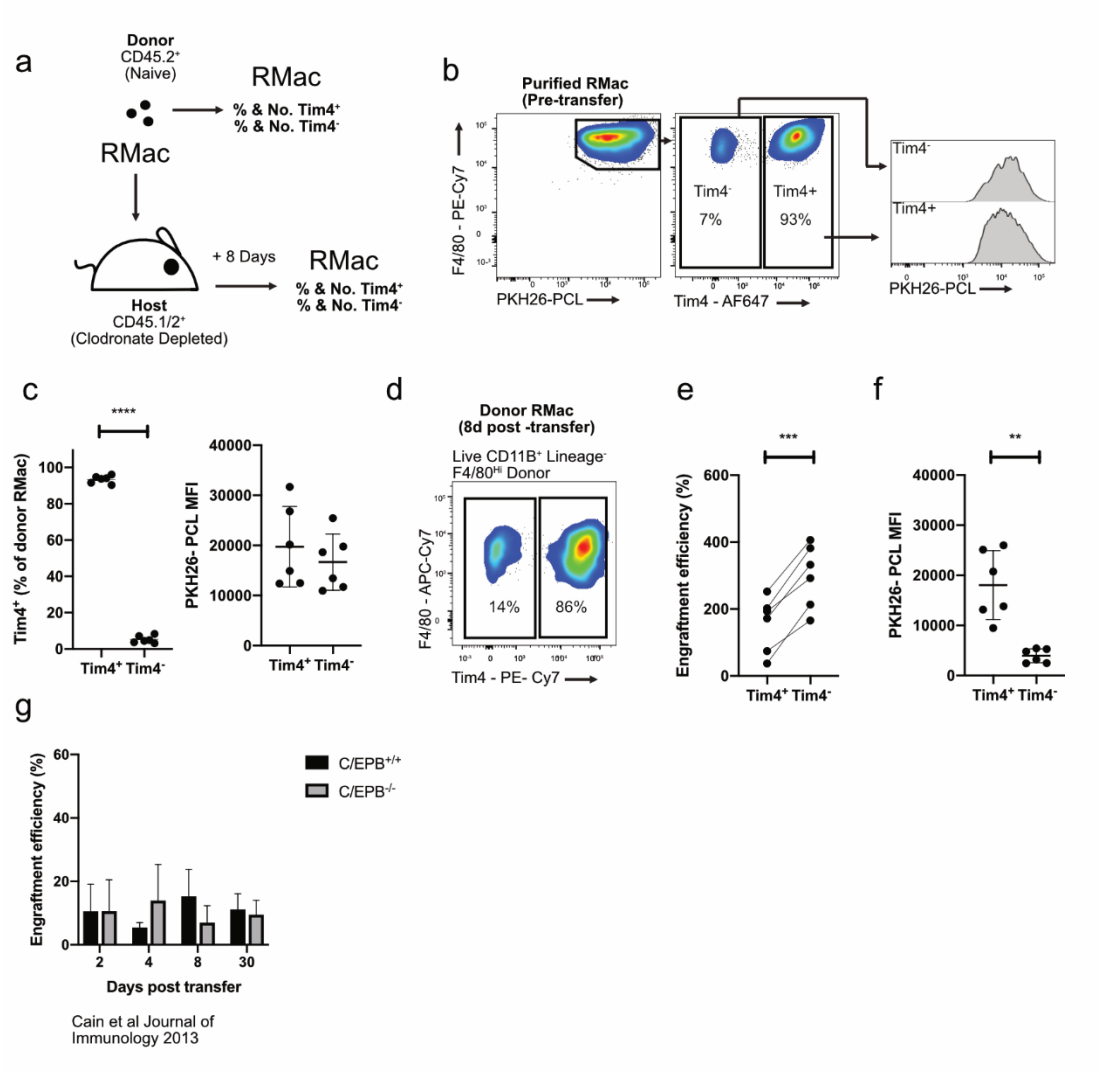

Figure 4.4 PKH26-PCL labelling does not impair proliferation.

(a) Experimental outline for IP transfer of CD45.2$^+$ RMac into clodronate pre-treated CD45.1/2$^+$ recipient mice. **(b)** Representative Tim4 antibody labelling and PKH26-PCL dye labelling on purified donor RMac prior to transfer. **(c)** Proportion of purified donor RMac (n=6) express Tim4$^+$ or do not. To the right, MFI of PKH26-PCL on purified Tim4$^+$ or Tim4$^-$ donor RMac (n=6) ****p<0.0001 determined by paired student's t test. **(d)** Representative Tim4 antibody staining on donor RMac 8 days after transfer into clodronate-depleted recipients. **(e)** Engraftment efficiency of transferred Tim4$^+$ RMac and Tim4$^-$ RMac 8 days post-transfer into clodronate-depleted recipients(n=6). ***p<0.001 determined by paired student's t test. **(f)** PKH26-PCL MFI on donor Tim4$^+$/Tim4$^-$ RMac (n=6), 8 days post transfer **p<0.01 determined by paired

student's t test.

(g) Engraftment efficiency of F4/80^{Hi}GFP^{+} LPM transferred into C/EPB$^{+/+}$ (n=4,2,3,2 for each timepoint respectively) or C/EPB$^{-/-}$ (n=4,2,2,2 for each timepoint respectively) recipient mice. Data adapted from Cain et al[60] with permission from the authors. Data shown as mean ± standard deviation. Each symbol represents an individual animal. Data were pooled from 2 independent experiments

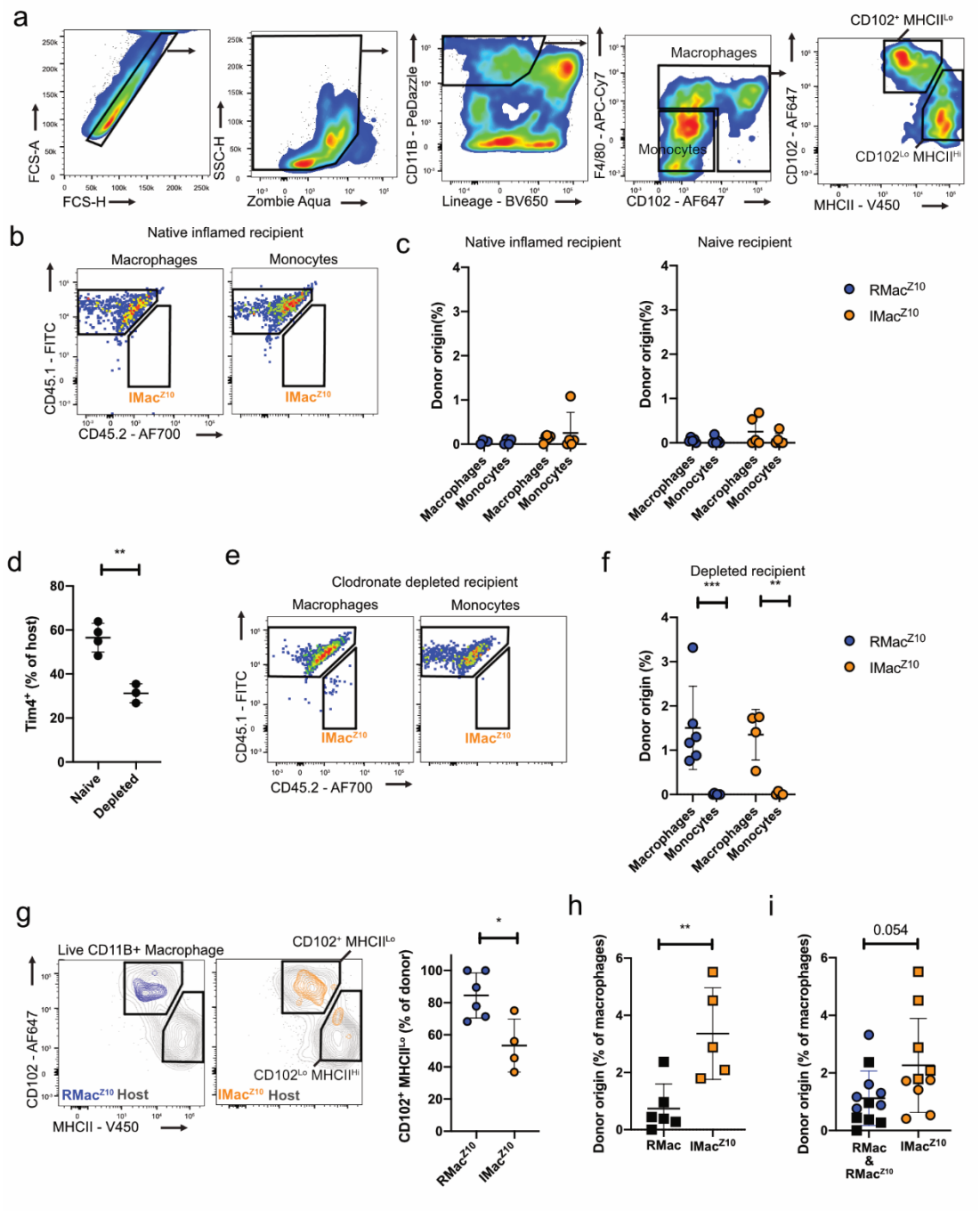

Figure 4.5 Inflammatory macrophages infiltrate the clodronate-depleted Omentum.

(a) Representative gating strategy to identify macrophages and monocytes in the omentum. **(b)** Identification of CD451^{-}CD45.2^{+}donor IMac^{Z10} within the indicated populations of omental myeloid cells. **(c)** Proportion of omentum macrophages or monocytes that are donor, 8 days after transfer of RMac^{Z10} or

IMac^{Z10} into inflamed (left, n= 4,5) or naïve recipients (right, n=5,5) 8 days prior. **(d)** Proportion of omentum macrophages that express Tim4, in naïve mice (n=4), or mice pre-treated with clodronate liposomes (n=3), 15 days prior. **p<0.01 determined by student's t test. **(e)** Identification of donor IMac^{Z10} within the indicated populations of omental myeloid cells. **(f)** Proportion of omentum macrophages or monocytes that are of donor origin 8 days after transfer of RMac^{Z10}(n=6) or IMac^{Z10}(n=4) into depleted recipients. **p<0.01 determined by two way ANOVA followed by Sidak's multiple comparisons test. **(g)** Proportion of RMac^{Z10} (n=6) or IMac^{Z10} (n=4) present in the omentum 8 days post transfer into depleted recipient that are CD102^{+} MHCII^{Int} . *p<0.05 determined by student's t test. **(h)** Proportion of omentum macrophages or monocytes that are of donor origin 8 days after transfer of naïve RMac (n=6) or IMac^{Z10}(n=5) **p<0.01 determined by student's t **(i)** Combined datasets presented in (f) and (h) indicating the proportion of omentum macrophages or monocytes that are of donor origin, 8 days after transfer of RMac (n=12, RMac in black, RMAc^{Z10} in blue) or IMac^{Z10}(n=10), into depleted recipients. Statistical significance determined by student's t test. Data shown as mean ± standard deviation. Each symbol represents an individual animal. Data were pooled from 2 independent experiments except (i) which is pooled from 3 independent experiments.

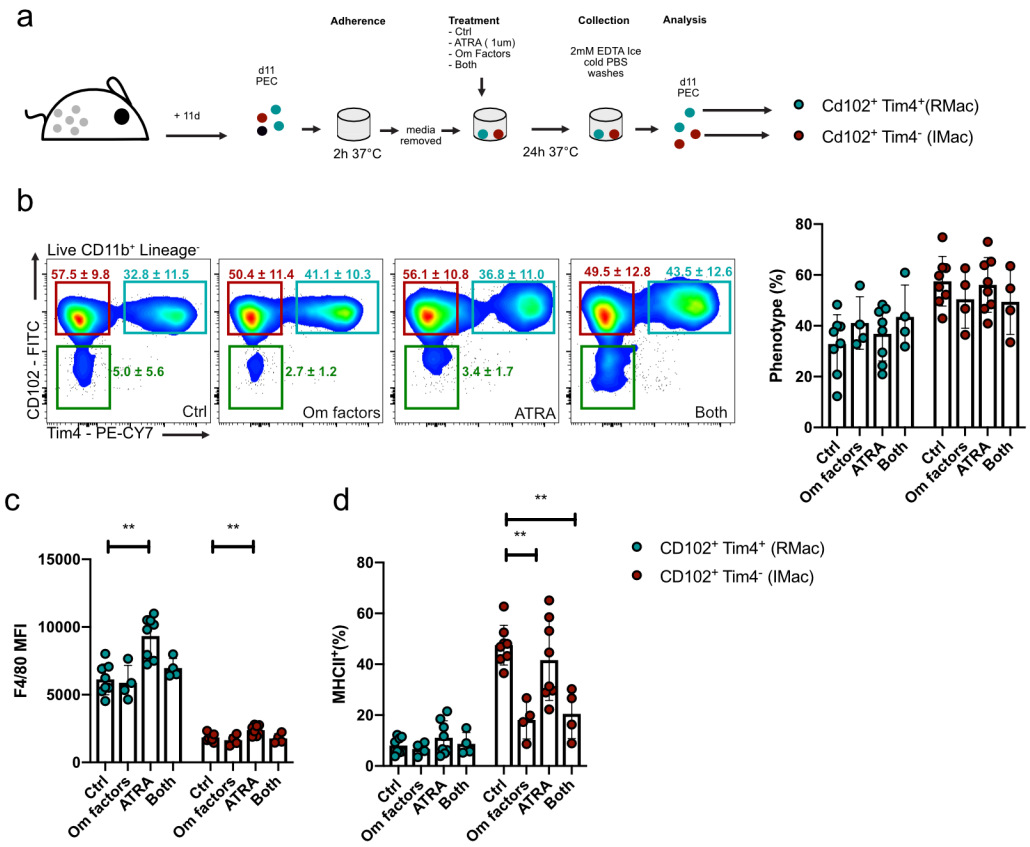

Figure 4.6 Inflammatory macrophages are retinoic-acid and omentum factor responsive.

(a) Experimental outline for isolation of complete peritoneal exudate cells 11 days after zymosan treatment, followed by adherence purification and treatment as indicated. **(b)** Proportion of adhered macrophages that express CD102 and Tim4 , 24 hours after culture in media supplemented with control-media (n=8), omentum factors (n=4), ATRA (n=8) or omentum factors and ATRA (n=4). **(c)** F4/80 MFI on indicated macrophage subsets after 24 hours culture in media supplemented with indicated treatment. **p<0.01 determined by one way ANOVA and Dunnet's multiple comparisons test for each subset individually, followed by Bonferroni adjustment. **(d)** Proportion of macrophage subsets that express MHCII after 24 hours of culture with indicated treatment. **p<0.01 determined by one way ANOVA and Dunnet's multiple comparisons test for each subset individually, followed by Bonferroni adjustment. Data shown as mean ± standard deviation. Each symbol represents an individual

animal per culture-condition. Data were pooled from 2 independent experiments except.

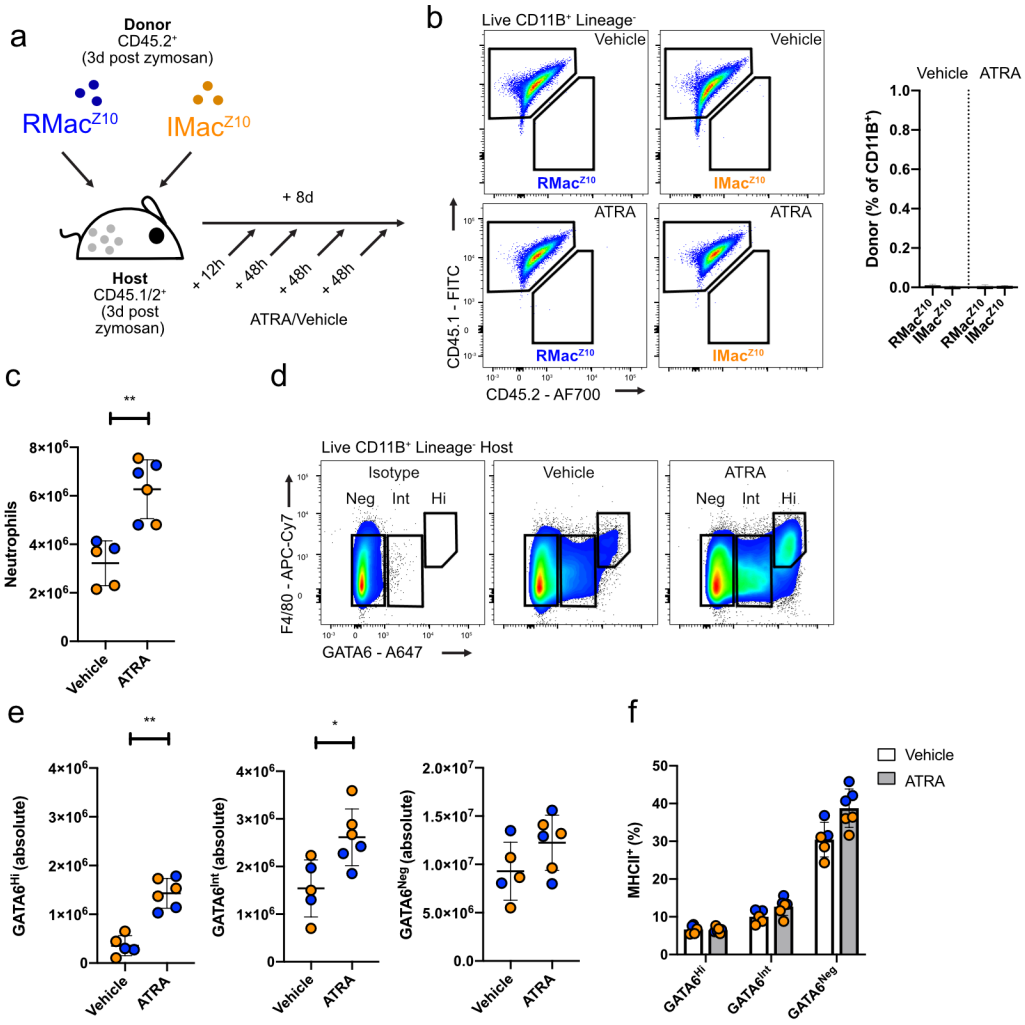

Figure 4.7 Oil-elicited inflammatory macrophages are retinoic-acid responsive.

(a) Experimental outline for IP delivery of purified (For gating see Figure 3.6a) CD45.2^{+} RMac^{Z10} or IMac^{Z10} into equivalent inflamed CD45.1/2^{+} recipient mice, followed by ATRA or vehicle treatment every other day, as indicated. **(b)** Proportion of myeloid CD11B^{+} Lineage^{-} cells that are donor, after transfer of RMac^{Z10} or IMac^{Z10} followed by indicated treatment. **(c)** Absolute number of neutrophils present after adoptive transfer followed by vehicle (n=5) or ATRA treatment (n=6). Datapoints in orange are IMac^{Z10} recipients, datapoints in blue are RMac^{Z10} recipient mice. **p<0.01 determined by student's t test.

(d) Representative expression of GATA6 and F4/80 by host $CD11B^{+}$ $Lineage^{-}$ cells after adoptive transfer followed by indicated treatment. **(e)** Absolute number of $GATA6^{Hi}$, $GATA6^{Int}$ and $GATA6^{Neg}$ macrophages after adoptive transfer followed by vehicle (n=5) or ATRA treatment (n=6). Datapoints in orange are $IMac^{Z10}$ recipients, datapoints in blue are $RMac^{Z10}$ recipient mice. *p<0.05 **p<0.01 determined by student's t test. **(f)** Proportion of host $GATA6^{Hi}$, $GATA6^{Int}$ and $GATA6^{Lo}$ macrophages that are $MHCII^{+}$ after adoptive transfer followed by vehicle (n=5) or ATRA treatment (n=6). Datapoints in orange are $IMac^{Z10}$ recipients, datapoints in blue are $RMac^{Z10}$. Data shown as mean ± standard deviation. Each symbol represents an individual animal.

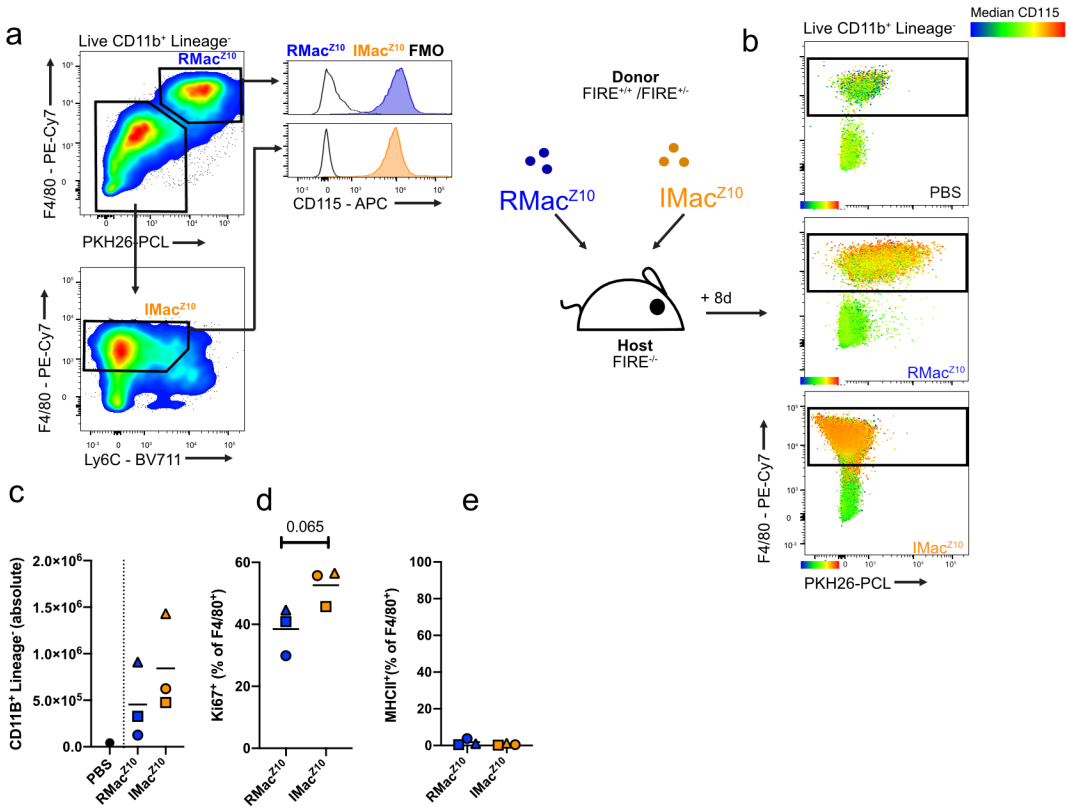

Figure 4.8 Inflammatory appear to expand and downregulate MHCII, following transfer into FIRE$^{-/-}$ recipients.

(a) Experimental outline for IP delivery of CD115^{+} RMac^{Z10} or CD115^{+} IMac^{Z10} sourced from FIRE$^{+/-}$ or FIRE$^{+/+}$ donors into macrophage deplete FIRE$^{-/-}$ recipient mice. **(b)** Representative expression of F4/80 and CD115 and PKH26-PCL labelling, 8 days post transfer of indicated populations. **(c)** Absolute number of CD11B^{+}Lineage^{-} myeloid cells 8 days post transfer of indicated cell populations. **(d)** Proportion of F4/80^{Hi} macrophages that are Ki67^{+} 8 days post transfer of the indicated cell populations. Statistical significance determined by student's t test. **(e)** Proportion of F4/80^{Hi} macrophages that are MHCII^{+} 8 days post transfer of the indicated cell populations. Each symbol represents an individual animal. Data were pooled from 3 independent experiments; each symbol denotes an experimental repeat.

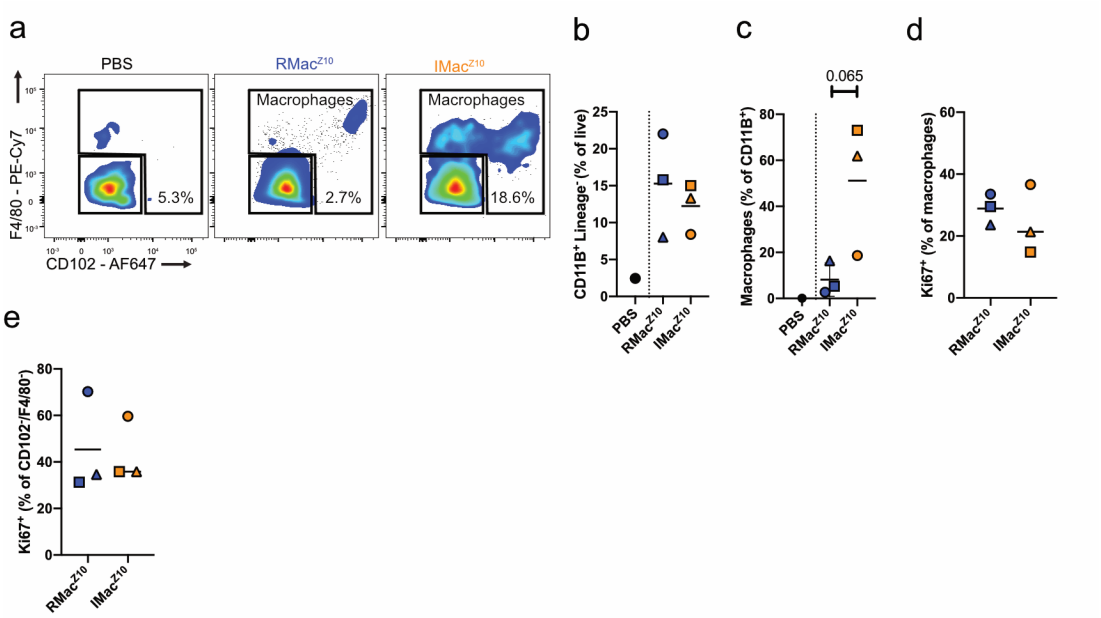

Figure 4.9 Macrophage subsets migrate into the omentum following transfer into FIRE$^{-/-}$ recipients.

(a) Representative gating strategy to identify macrophages and monocytes in the omentum. **(b)** Proportion of live cells that are omental CD11B^{+}Lineage^{-} myeloid cells, 8 days post transfer of indicated cell populations. **(c)** Proportion of omental CD11B^{+}Lineage^{-} myeloid cells that are macrophages (F4/80^{+} or CD102^{+}), 8 days post transfer of indicated cell populations.**(d)** Proportion of omental macrophages that are Ki67^{+},8 days post transfer of indicated cell populations. **(e)** Proportion of omental CD102^{-}F4/80^{-} myeloid cells that are Ki67^{+}, 8 days post transfer of indicated cell populations. Statistical significance determined by student's t test. Each symbol represents an individual animal. Data were pooled from 3 independent experiments; each symbol denotes an experimental repeat.

Chapter 5

Examining long-term survival and identity of inflammatory macrophages after mild peritonitis.

5.1 Introduction

Having found that inflammatory macrophages persisted immediately following resolution the question arose whether these cells were long-lived and would persist long-term. Observations published by Yona et et al suggest that after thioglycolate induced peritonitis the proportion of monocyte-derived macrophages in the cavity seemingly peaks 3 weeks after the inflammatory event[28]. Conversely, using a dye labeling methodology Newson et al indicated that monocyte derived cells present shortly after zymosan-induced peritonitis largely persisted up until 8 weeks[111]. Neither of these studies carried out an in-depth analysis to determine to what degree monocyte-derived macrophages recruited during the inflammatory event persisted long-term and to determine their phenotypic identity. The most detailed analysis of monocyte-derived macrophage phenotype post-inflammation comes from work by Gundra et al[145]. Using transgenic Cx3cr1$^{CreERT2\text{-}IRES\text{-}EYFP}$ mice to track infiltrating monocytes they showed that monocytes recruited after thioglycolate-induced peritonitis and treatment with IL-4 are characterized by an F4/80^{Int} CD206^{+}PD-L2^{+}MHCII^{Hi} phenotype 4 weeks after the inflammatory event. By week 8 these cells had upregulated F4/80 and downregulated the latter 3 markers, seemingly adopting a more resident like phenotype. However, due to the co-treatment with IL-4 it is hard to understand to what degree these findings are representative of 'normal' resolution of peritonitis without Il4 co-treatment.

Hence, in this chapter I set out to investigate if inflammatory macrophages present during resolution persist in the succeeding 8 weeks and whether they adopt a more resident F4/80^{Hi} MHCII^{Lo} phenotype in this time. If these cells did persist, I sought to ascertain whether this phenotypic conversion is indicative of a greater transcriptional integration into the resident macrophage population. Moreover, I set out to investigate if, similar to the short-term experiments in chapter 4, competition with incumbent resident macrophages inhibits inflammatory macrophage conversion.

5.2 Inflammatory macrophages persist long-term and remain phenotypically distinct.

I first set out to investigate if transferred IMac^{Z10} and RMac^{Z10} persisted until 8 weeks post-inflammation. However, I adapted the basic adoptive transfer methodology to include an additional group where I sourced RMac from naïve donor mice and transferred them into naïve recipient mice **(Figure 5.1a)** to ascertain if survival and phenotype of resident macrophages is altered after undergoing an inflammatory event. Moreover, to increase the chance of sourcing sufficient donor cells for more in depth transcriptional analysis I increased the number of transferred cells from 100,000, as used in the short-term experiments, to 200,000.

By 8 weeks post-transfer into equivalently inflamed recipients, all 3 donor populations had persisted with an engraftment efficiency of approximately 35% **(Figure 5.1b)**. However, retrospective pooling of all the datapoints I generated for this time-point indicated that RMac^{Z10} persisted marginally more readily than IMac^{Z10} **(Figure 5.1c)**, similar to the 8 day time-point **(Figure 4.1b)**. By week 8, IMac^{Z10} had seemingly adopted an F4/80^{Hi} MHICII^{Lo} phenotype and could not readily be distinguished on the basis of these markers from RMac^{Z10}(**Figure 5.1d**). However, IMac^{Z10} retained higher levels of MHCII and slightly lower levels of F4/80 even at this time point **(Figure 5.1e)**. Similar to the earlier time point, IMac^{Z10} expressed were almost universally CD102^{+} **(Figure 5.1f)**. Moreover, the expression of GATA6 was strikingly similar to that observed at the 8 day timepoint, in that Imac^{Z10} were almost exclusively positive for GATA6, but their overall expression level was lower than that of RMac^{Z10} **(Figure 5.1g)**.

During these experiments I found that, on average, only about 70% of the transferred RMac^{Z10} had retained PKH26-PCL labelling, while some host macrophages had acquired detectable levels of PKH26-PCL labelling **(Figure 5.1h)**. These findings emphasize that PKH26-PCL labelling should not be used

for long-term lineage tracing studies and that care should be taken when interpreting results from studies using this methodology for long-term studies.

In these experiments, 2 out of 11 RMac^{Z10} recipient samples had very few donor cells present. This is likely due to incomplete IP injection, but as some residual dye was present these samples were not excluded from analysis.

5.3 Persistent inflammatory macrophages remain transcriptionally distinct

To investigate if this apparent phenotypic conversion was indicative of a greater transcriptional conversion into a resident identity, I re-purified donor RMac, RMac^{Z10} and IMac^{Z10} after 8 weeks and investigated their transcriptome, using a Nanostring mouse myeloid panel. Using this analysis, I found that of the 372 genes that were detected, none were differentially expressed between RMac and RMac^{Z10}. However, approximately a fifth of all detected genes (78), were differentially expressed between RMac^{Z10} and IMac^{Z10} (adjusted p value <0.05) **(Figure 5.2a)**. Moreover, of the 13 genes included in the Nanostring panel considered unique to peritoneal tissue-resident macrophages 11 were differentially expressed (**Figure 5.2b)**. Although the Nanostring panel only assessed a relatively small set of genes, these data indicate that historic inflammation does not alter the transcriptional profile of enduring resident macrophages. Moreover, these data indicated that persistent inflammatory macrophages largely fail to adopt a resident macrophage transcriptional profile.

5.3.1 Transcriptional identity of inflammatory macrophages is partially due to impaired capacity to acquire retinoic acid.

Gene expression analysis using Nanostring indicated that *GATA6* was differentially expressed between IMac^{Z10} and RMac^{Z10} **(Figure 5.2b)**, but that the change was relatively small (Log2FC -0.7). This pattern resembled my earlier findings indicating that IMac^{Z10} were largely GATA6^{+}, but expression

was somewhat lower than on RMac^{Z10} **(Figure 5.1g)**. As GATA6 is thought to regulate a significant portion of peritoneal macrophage genes[63-65], I postulated that part of the altered gene signature of IMac^{Z10} could be due to lower expression levels of GATA6. Using the three published datasets that investigated transcriptional changes in GATA6^{KO} LPM compared to GATA6^{WT} LPM, I generated a gene list of GATA6 regulated genes. Genes were considered GATA6 regulated if they were differentially expressed (adj p value<0.05) in at least 2 of the published datasets. This list was split on genes upregulated and downregulated in GATA6^{KO} LPM. I then used GSEA analysis to investigate if GATA6-regulated genes were enriched within the Nanostring dataset. Indeed, genes upregulated in GATA6^{KO} LPM were positively enriched in IMac^{Z10}, whereas genes downregulated in GATA6^{KO} LPM were negatively enriched **(Figure 5.3a)**.

Retinoic-acid is thought to be an important driver of GATA6 expression. Indeed, in Chapter 4 I had found that retinoic-acid treatment appeared to drive expression of the GATA6 responsive gene F4/80 *in vitro* and GATA6 *in vivo*. Retinoic acid signaling is thought to take place, in part, via retinoic X receptor (RXRs)[98]. In the peritoneal cavity macrophages exclusively express RXRα and RXRβ. Indeed, in macrophage-specific RXRα^{KO}-RXRβ^{KO} (RXRAB$^{-/-}$) mice, the peritoneal macrophage compartment is radically altered[98]. Notably, there is a loss of LPM and a concurrent increase in SPM[98]. This contrasts with the phenotype of GATA6^{KO} mice, which have reduced number of 'LPM like' cells that exhibit altered expression of approximate 40% of LPM-specific genes, and normal numbers of SPM[63-65]. Hence, complete lack of GATA6 appears to affect LPM survival and phenotype more severely than a lack retinoic-acid signaling. Indeed, the transcriptional profile of the few LPM that remained in RXRAB^{KO} mice did not fully overlap with that of GATA6^{KO} LPM, suggesting that RXRα/RXRβ signaling affects gene expression independently of GATA6 as well as via GATA6[98]. Hence, to investigate if GATA6-independent RXR signaling could also be dictating part of the IMac^{Z10} gene signature, I re-analyzed the dataset published by Casanova-Acebes[98], comparing the

transcriptional profile of RXRAB^{WT} versus RXRAB^{KO} LPM. I then selected only differentially expressed genes that are not GATA6 regulated, using the gene list of GATA-6 dependent genes I had generated. This analysis generated a list of genes, expression of which, is RXRα/RXRβ-responsive, but independent of GATA6. I then used GSEA analysis to investigate if these RXRα/RXRβ-regulated genes were enriched in the Nanostring dataset. Indeed, genes upregulated in RXRAB^{KO} LPM were positively enriched in IMac^{Z10}, but genes that were downregulated RXRAB^{KO} were not negatively enriched **(Figure 5.3b)**.

By combining the analysis of GATA6^{KO} and RXRAB^{KO} LPM it became apparent that of the 72 genes differentially expressed between RMac^{Z10} and IMac^{Z10,} almost half are thought to be regulated by retinoic-acid either via GATA6 (19 genes, 24%) or via RXRAB signaling independent of GATA6 (14 genes 18%) **(Figure 5.3c)**. Indeed, the expression pattern observed between RMac^{Z10} and IMac^{Z10} overlapped almost completely with the pattern between WT and GATA6^{KO} or RXRAB^{KO} LPM with the exception of *Marco*, *Serpinb6a* (GATA6-regulated) and *Ctsl* (RXRAB-regulated) **(Figure 5.3c)**.

5.3.2 Transcriptional profile of inflammatory macrophages resembles that of steady state monocyte-derived macrophages

Around this point in my PhD, I was involved in another research project in the laboratory, aiming to understand the sex dimorphism between male and female peritoneal macrophages. For this project I purified the complete CD11B^{+} Lineage^{-} myeloid compartment from the peritoneal cavity of male and female mice and these were analyzed using 10x single cell sequencing. These data have been published and I will be referring to the published dataset as I did not carry out this analysis myself.

Our single cell analysis indicated that in both male and females F4/80^{Hi} MHCII^{Lo} LPM comprised 3 distinct clusters[97]. The largest of these clusters

consisted predominantly of embryonically seeded resident macrophages, whereas the two remaining clusters comprised predominantly of monocyte-derived resident macrophages, as determined by subsequent fate-mapping experiments[97]. I postulated that the transcriptional profile of IMac^{Z10} might not be unique, but might overlap with the signature of monocyte-derived resident macrophages present under uninflamed steady state conditions. Hence, I investigated if the 78 genes that delineated IMac^{Z10} from RMac^{Z10} (**Figure 5.2a**) overlapped with cluster genes unique to each of the single cell clusters. This analysis indicated that the gene profile of IMac^{Z10} overlapped considerably with cluster 3, that comprised the most recently monocyte-derived LPM present in the naïve female cavity (most notably genes related to MHCII presentation) **(Figure 5.4a)**.

As the IMac^{Z10} signature appeared to be regulated by retinoic-acid (**Figure 5.3c**), I quantified what proportion of cluster markers from steady-state LPM overlapped with GATA6 or RXRAB-regulated genes. Indeed, the cluster genes that identified monocyte derived LPM (cluster 3) showed considerable overlap with genes upregulated in GATA6^{KO} LPM compared to GATA6^{WT} LPM (e.g. *Folr2, Mrc1*), but less with genes upregulated in RXRAB^{KO} LPM compared to RXRAB^{WT} **(Figure 5.4b)**. Conversely, the cluster genes that identified embryonically seeded LPM (Cluster 5) overlapped considerably with genes upregulated in GATA6^{WT} LPM compared to GATA6^{KO} LPM (e.g. *Serpinb2*, *ApoC1*) (**Figure 5.4b**). Similarly these cluster genes overlapped with genes upregulated in RXRAB^{WT} LPM compared to RXRAB^{KO} LPM (e.g. *Gata6* and *C4b)*(**Figure 5.4b**). Combined these analyses indicate that under homeostatic conditions approximately 65% of the genes that define embryonic LPM from recently recruited monocyte-derived LPM are responsive to retinoic-acid either via GATA6 or independently of GATA6 and their expression profile suggests effective uptake of retinoic-acid. Conversely, approximately 30% of the genes that define monocyte-derived LPM are retinoic acid responsive, almost exclusively via GATA6 and their profile would suggest less effective uptake of retinoic-acid by these cells.

In summary, persistent inflammatory macrophages retain a unique transcriptional profile, that delineates them from RMac^{Z10} and which resembles monocyte-derived LPM present under naïve homeostatic conditions. Furthermore, it would appear that lower expression levels of GATA6 significantly impact the transcriptional profile of both IMac^{Z10} and steady state monocyte-derived LPM.

5.4 Long-term competition with incumbent resident macrophage inhibits inflammatory macrophage conversion.

By day 8, the failure of inflammatory macrophages to downregulate MHCII and upregulate F4/80 was in part due to the presence of incumbent resident macrophages. Similarly, by week 8 IMac^{Z10} in their native competitive environment failed to completely adopt an F/80^{Hi} MHCII^{Lo} resident phenotype. This failure to undergo phenotypic conversion coincided with a failure to adopt a transcriptional resident profile. To investigate whether this long-term failure to convert was also due to the presence of competing resident macrophages RMac, RMac^{Z10} or IMac^{Z10} were adoptively transferred into clodronate-depleted recipients and investigated 8 weeks post-transfer (**Figure 5.5a**).

Similar to the 8-day time-point data, transferred IMac^{Z10} had expanded considerably with an engraftment efficiency of approximately 300% **(Figure 5.5b)**. Indeed, the similarity between the expansion after 8 days and 8 weeks suggests that the proliferative event occurred shortly after transfer and does not affect IMac^{Z10} survival long-term. Similar earlier experiments investigating the phenotype of IMac^{Z10} after 8 weeks in their native environment (**Figure 5.1d**) IMac^{Z10} could not readily distinguished on the basis of F4/80 and MHCII **(Figure 5.5c)**. However**,** contrary to their phenotype in the native environment at this time, IMac^{Z10} expressed similar levels of MHCII and F4/80 and as RMac^{Z10} **(Figure 5.5d)**. Similar to the native environment IMac^{Z10} were almost universally CD102+ **(Figure 5.5e)**. Moreover, GATA6, which, in the native

environment was responsible for part of the unique IMac^{Z10} signature, was expressed at equal levels by IMac^{Z10} to their resident macrophage counterparts **(Figure 5.5f)**. Hence, the impaired capacity of IMac^{Z10} to acquire GATA6 driving signals, like retinoic-acid, is likely due to the presence of competing resident macrophages.

In these experiments in 3 out of 11 IMac^{Z10} and 2 out of 12 for both RMac and RMac^{Z10} samples were excluded due to incomplete depletion or complete absence of donor cells.

5.5 Inflammatory macrophages adopt a resident transcriptional identity following transfer into clodronate-depleted recipients.

Using the same methodology as described in section 5.3, I re-purified donor RMac, RMac^{Z10} and IMac^{Z10} 8 weeks after transfer into depleted recipients and investigated their transcriptome using a Nanostring mouse myeloid panel. This analysis identified no transcriptional differences between RMac and RMac^{Z10}, but indicated that IMac^{Z10} adopted a more resident-like transcriptome, with expression of only 8 genes differentiating between RMac^{Z10} and IMac^{Z10}(adjusted p value <0.05) **(Figure 5.6a)**. By overlapping the IMac^{Z10} gene signature in their native environment (**Figure 5.2a**) and the depleted environment **(Figure 5.6a)** genes could be divided into:

1) Environment-regulated genes, some of which are responsive to competitive pressure. These are genes that were differentiated IMac^{Z10} in their native environment, but not in the depleted environment **(Figure 5.6b, blue)**.

2) Cell-intrinsically-regulated genes, that appear to be unresponsive to environmental cues and competitive pressure. These are genes that differentiated IMac^{Z10} in both their native and the depleted environments **(Figure 5.6b, red)**.

The majority of the IMac^{Z10} transcriptional signature (71) consisted of environment regulated genes including *Gata6,* the GATA6 and RXR-regulated genes, and genes related to *MHCII* function. However, a small part of the IMac^{Z10} signature consisted of genes that appear to be cell-intrinsically regulated, including *Timd4* (encoding for Tim4), *Sema4a* and *Marco.* Finally, *Ndufa7* was only differentially expressed between RMac^{Z10} and IMac^{Z10} in the depleted environment only. The change was relatively modest (log2FC -0.39) and likely an artefact of the artificially-depleted environment (**Figure 5.6b**).

Another explanation for the observed effect was that in the depleted environment resident macrophages adopted a more inflammatory-like transcriptional profile and as a consequence the RMac^{Z10} and IMac^{Z10} appeared more transcriptionally similar. This could be occurring as I previously found that the Tim4^{-} monocyte-derived LPM fraction of RMac expanded more than their Tim4^{+} embryonically-seeded LPM counterparts 8 days after transfer into depleted recipient **(Figure 4.4e)**. As the transfer experiments into native and depleted environment were not carried out at the same time, it was not possible to directly compare the transcriptional profile of RMac in their native and depleted environment. However, Galatro et al described a method to qualitatively asses transcriptional similarity between published datasets obtained at different times and using different techniques[155]. The corresponding author Prof. Eggen kindly provided me with additional details to replicate this methodology. Briefly, all the genes detected were ordered on mRNA expression level and each gene was assigned a percentile score based on their rank in the gene list. Then, for each gene a delta gene rank percentile was calculated (Percentile rank in native environment – Percentile rank in depleted environment). Hence, genes altered by the depleted environment would have a large delta gene rank percentile score indicating that their relative position in the native environment gene list differed from their relative position in the depleted environment gene list. Conversely, genes unaltered by the depleted environment would have a relatively small delta gene rank percentile score, indicating that their relative position in the genelist is similar

in the native environment and the depleted environment. This analysis indicated that transfer into depleted recipients had relatively little impact on the expression profile of either RMac or Rmac^{Z10} populations, with only few genes changing their relative percentile by more than 5% whereas the gene profile of IMac^{Z10} was more profoundly affected **(Figure 5.6c)**.

5.6 Inflammatory macrophages remain phenotypically distinct following transfer into native or depleted recipients.

At this stage, it had become apparent that by week 8, GATA6, F4/80 and MHCII protein expression by IMac^{Z10} was indeed dictated by environmental factors as suggested by the combined Nanostring and protein expression analysis. To validate additional genes that appeared environment-responsive and some that appeared to be cell-intrinsically regulated, I repeated the adoptive transfer of RMac, RMac^{Z10} and IMac^{Z10} into native or clodronate pre-treated recipients and investigated expression after 8 weeks using flow cytometry.

Consistent with divergent expression of *Timd4*, *Sema4a*, *Sell* and *Ccr5* identified using Nanostring, by week 8 IMac^{Z10} in their native environment expressed lower levels of Tim4 and higher levels of Sema4a, CD62L and CCR5 than either RMac population **(Figure 5.7a, b)**. Moreover, after transfer into depleted recipients IMac^{Z10} expressed lower levels of Tim4 and higher levels of Sema4a and CD62L **(Figure 5.7b)**, consistent with Nanostring findings indicating that expression is intrinsically regulated. Contrary, CCR5 expression on IMac^{Z10} was highly variable and on the whole lower in the depleted environment such that it did not differ compared to either RMac population, consistent with Nanostring findings indicating that expression is regulated by environmental cues **(Figure 5.7b)**.

As the purification protocol takes a significant amount of time, it was challenging to carry out the transfer into the native and the depleted

environment side by side. Therefore, only one of the two experimental repeats contains both native and depleted recipients side by side. To confirm that indeed gene expression of these markers was not altered on RMac by the environment post transfer, as indicated by the ranking analysis **(Figure 5.7c),** I plotted separately the experiment where both native and depleted transfers were carried out side by side. Indeed, there was no indication that either of the RMac populations altered the expression of Tim4, Sema4a, CD62L or CCR5 after transfer into depleted recipients **(Figure 5.7c)**. Expression Tim4, Sem4a, CD62L on IMac^{Z10} appeared unaltered, again consistent with cell intrinsic regulation, but the CCR5 expression was noticeably lower, although this was not statistically significant after p value adjustment **(Figure 5.7c)**.

Since IMac^{Z10} appeared to transcriptionally resemble monocyte derived LPM present under homeostatic conditions **(Figure 5.4),** I validated some additional surface markers, known to be highly expressed by monocyte-derived LPM (Folate receptor B (FRβ)) or embryonically-seeded LPM (CD209b and V-set immunoglobulin domain-containing 4 (VSIG4)) that were not included in the Nanostring panel[97,170]. The latter two of these are unlikely to be regulated by retinoic-acid as their expression was unaltered in GATA6^{KO} and RXRAB^{KO} LPM[63,98]. Indeed, CD209b and VSIG4 were expressed by a subset of both RMac populations, but were largely absent on IMac^{Z10} irrespective of the recipient environment **(Figure 5.7d)**. In contrast, IMac^{Z10} expressed high levels of FRβ in their native environment, but expression was largely lost after transfer into depleted recipients, suggesting down-regulation by environmental cues consistent with negative regulation of *Folr2* by GATA6[65].

5.7 Inflammatory macrophages are long-lived and gradually acquire the resident identity.

Next, to investigate if IMac^{Z10} persisted long-term and if more complete reprogramming might occur naturally over their lifespan, I tracked transferred RMac, RMac^{Z10} and IMac^{Z10} until 5 months post-inflammation in their native

environment. By 5 months IMac^{Z10} were still present in the peritoneal cavity, but their overall engraftment had decreased to approximately 20% down from 30% at the 8-week timepoint **(Figure 5.8a).** Surprisingly at this timepoint naïve RMac seemingly engrafted equivalent to the 8-week timepoint (± 35% at week 22 versus ±40% at week 8), whereas RMac^{Z10} also engrafted less well (±20% at week 22 versus ±40% at week 8) **(Figure 5.8b)**. Even at this stage IMac^{Z10} remained distinct with high expression of Sema4a and CCR5, although the latter had seemingly reduced compared to expression levels 8-week post transfer (±38% at week 22 versus ±70% at week 8) **(Figure 5.8b)**. Moreover, IMac^{Z10} still expressed lower levels of GATA6, but the difference appeared less apparent than after 8 weeks (**Figure 5.8c**). Similarly, IMac^{Z10} did not express equivalently high levels of Tim4 and CD209b as their RMac counterparts, but expression of Tim4 appeared to have increased compared to 8 weeks (±55% at week 22 versus ±30% at week 8) **(Figure 5.8)**. Moreover, after 5 months IMac^{Z10} expressed equivalent levels of MHCII, Frbβ and VSIG4 as their RMac counterparts **(Figure 5.8b,d)**.

Combined these data indicate that IMac^{Z10} persist long-term and with time adopt a more resident-like phenotype by altering expression of both environment-dependent and cell-intrinsically regulated features.

5.8 Discussion

In this chapter I set out to answer three key questions of my PhD: 1) Do inflammatory macrophages present during resolution of peritonitis persist long-term, despite the presence of competing resident macrophages and 2) to what extent can and do these cells adopt a resident identity and 3) which factors dictate inflammatory macrophage conversion into a resident identity.

Briefly, in chapter 4 I investigated the phase directly following resolution when the macrophage compartment contracts to pre-inflammation size. During this phase inflammatory macrophages persisted and retained a unique F4/80^{Int}

MHCII^{Hi} phenotype. This was largely due to competition with incumbent resident macrophages as inflammatory macrophages adopted a more resident-like phenotype after transfer into clodronate-depleted recipients.

In this chapter I expanded on these findings by investigating the long-term survival and phenotype of inflammatory macrophages. Here I found that IMac^{Z10} that had persisted through this initial contraction phase largely survived long-term. Even after 8 weeks IMac^{Z10} retained lower levels of F4/80 and GATA6 and relatively high levels of MHCII. This failure to adopt a resident phenotype proved indicative of a failure to adopt a resident transcriptional identity. Approximately 20% of the 372 genes detected by Nanostring transcriptional profiling differentiated IMac^{Z10} from their resident counterparts. Importantly, the number of genes investigated using Nanostring assay was relatively limited and hence this methodology is not detecting the full degree to which RMac^{Z10} and IMac^{Z10} are transcriptionally divergent. However, those genes that were included in the Nanostring panel are known regulators of myeloid biology and are likely to have a functional role. Hence, although the complete transcriptional divergence between RMac^{Z10} and IMac^{Z10} is unclear these data suggest these cells likely differ functionally from one another. *In silico* analysis indicated that approximately half of the differentially-expressed genes could be attributed to impaired retinoic-acid signalling either directly or indirectly via GATA6, suggesting that environmental retinoic acid strongly impacts IMac^{Z10} identity, consistent with my findings described in chapter 4. However, this *in silico* analysis compared the transcriptional profile of GATA6 intermediate IMac^{Z10} to that of transgenic GATA6^{KO} peritoneal macrophages. Although this analysis highlights a role for GATA6 in shaping the IMac^{Z10} gene signature it does not account for the possibility that part of the IMac^{Z10} gene signature could be driven by lower (but not absent) levels of transcription factors such as GATA6. Unfortunately, at present there are limited tools available to investigate how divergent levels of transcription factors, such as GATA6, affect gene expression.

Finally, the transcriptional profile of Mac^{Z10} largely overlapped with monocyte-derived LPM present under homeostatic conditions. Again, although the number of genes assessed was relatively limited, these data suggest that persistent inflammatory macrophages do not give rise to a wholly unique population of macrophages, but expands a numerically minor fraction of monocyte-derived LPM present under homeostatic conditions. Indeed, *in silico* analysis suggests that the identity of monocyte-derived LPM present under steady-state conditions appears to be largely due to impaired retinoic-acid signalling similar to the inflammatory macrophage signature.

Throughout the experiments presented in chapter 4 and 5 it has become apparent that a subset of IMac^{Z10} did adopt a more resident-like phenotype. As these converted cells only represent a relatively minor population, I have chosen not to focus on these IMac^{Z10} that had seemingly adopted a more resident phenotype. Single cell transcriptional analysis of all IMac^{Z10} would have been very valuable to ascertain the degree to which this more resident-like subset of IMac^{Z10} transcriptionally resembles resident macrophages and investigate which signals have established this resident-like identity.

Similar to my findings at 8 days, by 8 weeks post-transfer into a macrophage-depleted environment IMac^{Z10} had expanded considerably In this environment, IMac^{Z10} adopted a more F4/80^{Hi} GATA^{Hi} MHCII^{Lo} resident phenotype and transcriptional identity with only 8 genes differentiating IMac^{Z10} from their resident counterparts. Using flow cytometry, I found that consistent with the Nanostring findings that IMac^{Z10} retained high expression of Sema4a, CCR5 and Frβ, the latter two of which were downregulated after transfer into depleted recipients. In contrast, IMac^{Z10} expressed marginal levels of Tim4, CD209B and VSIG4 and were unable to acquire these features even after transfer into depleted recipients. However, after 5 months in their native environment, IMac^{Z10} adopted a more resident-like phenotype, as indicated by lower

expression of MHCII, Frβ and higher expression of VSIG4, indicating that gradual conversions occurs over time despite competitive pressure.

Combined these data indicate that inflammatory macrophages persist long-term and that their phenotype is a combination of: 1) Intrinsically regulated features retained over time and not reprogrammed by environmental signals (Sema4a), 2) Features that do not reprogram due to an inability to compete with $RMac^{Z10}$ for environmental cues but are reprogrammed with time (MHCII, GATA6, CCR5, FRβ) and 3) Features related to time-of-residency irrespective of competition (VSIG4, Tim4, CD209b).

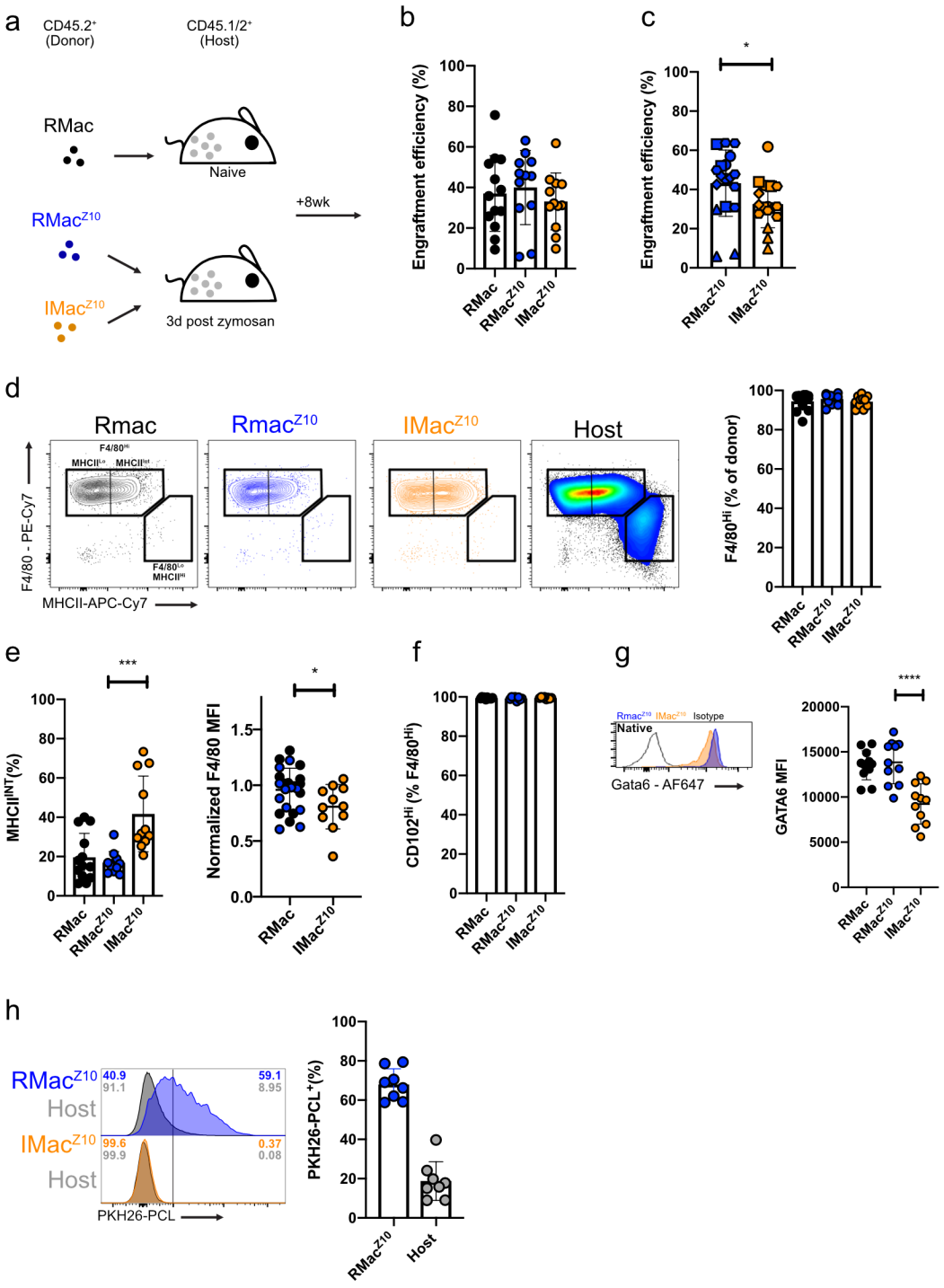

Figure 5.1 Inflammatory macrophages persist long-term following zymosan-induced peritonitis.

(a) Experimental outline for the transfer of donor RMac into naïve recipients or RMac^{Z10} and IMac^{Z10} into inflamed recipients. Populations gated as shown in Figure 3.6a **(b)** Engraftment efficiency of RMac, RMac^{Z10} and IMac^{Z10}, 8 weeks

following transfer into mirroring recipient mice (left; n=13, n=9, n=9) **(c)** Pooled engraftment efficiency of $RMac^{Z10}$ and $IMac^{Z10}$ 8 weeks following transfer inflamed recipients. Symbols denote independently carried out experiment. *p<0.05 determined by student's t test. **(d)** Proportion of RMac, $RMac^{Z10}$ and $IMac^{Z10}$ that are $F4/80^{Hi}$ $MHCII^{Lo}$, after transfer into mirroring (n= 12,11,11) recipients. **(e)** RMac (n=13), $RMac^{Z10}$ (n=11) and $IMac^{Z10}$ (n=11) that express MHCII, 8 weeks following transfer into mirroring recipients. ***p<0.001 determined by one-way ANOVA and Tukey's multiple comparisons test. To the right. Expression of F4/80 on RMac , $RMac^{Z10}$and $IMac^{Z10}$, 8 weeks following transfer into mirroring recipients(n=12,11,11). MFI is normalized to mean F4/80 MFI of RMac. *p<0.05 determined by student's t test. **(f)** Proportion of $F4/80^{Hi}$ $MHCII^{Lo}$: RMac, $RMac^{Z10}$ or $IMac^{Z10}$ that express CD102, 8 weeks following transfer into mirroring recipients (n= 12,11,11) **(g)** GATA6 MFI on donor RMac, $RMac^{Z10}$ or $IMac^{Z10}$ 8 weeks following transfer into mirroring recipients (n=12,11,11). ****p<0.0001 determined by one-way ANOVA and Tukey's multiple comparisons test.**(h)** Proportion of donor $CD45.2^{+}$ $F4/80^{Hi}$ $RMac^{Z10}$ and host $CD45.1/2^{+}$ $F4/80^{Hi}$ macrophages that have been PKH26-PCL labelled, 8 weeks after transfer into inflamed recipients (n=8). Data shown as mean ± standard deviation. Each symbol represents an individual animal. Data are pooled from at least 2 independent experiments.

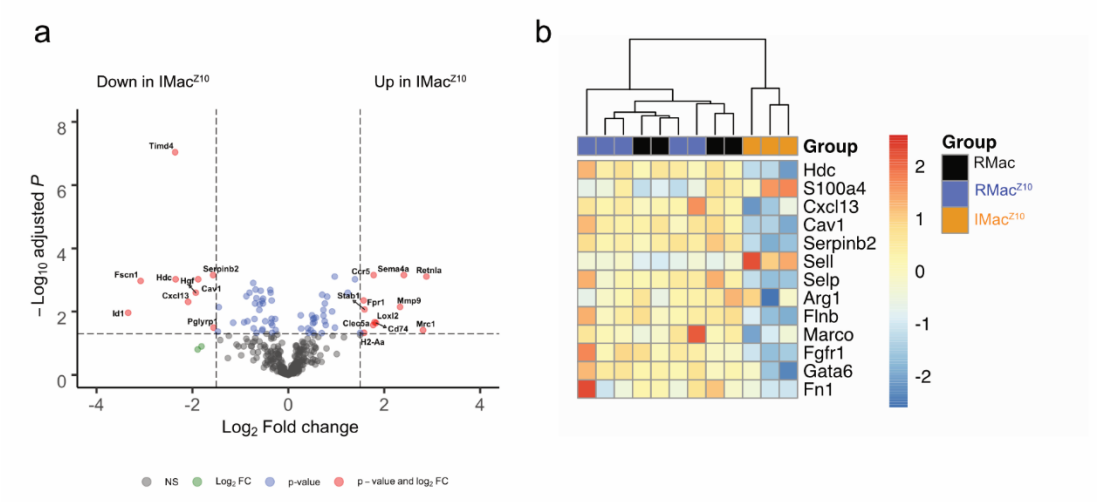

Figure 5.2 Inflammatory macrophages remain transcriptionally distinct. **(a)** Volcano plot indicating Log2Fold change (x-axis) and adjusted p-value (y-axis) of IMac^{Z10} in gene expression relative to expression levels exhibited by RMac^{Z10}, 8 weeks after transfer into inflamed recipients. **(b)** Heatmap indicating normalized gene expression of peritoneal macrophage specific genes included on the Nanostring panel on indicated donor populations (top) 8 weeks following transfer into inflamed recipients.

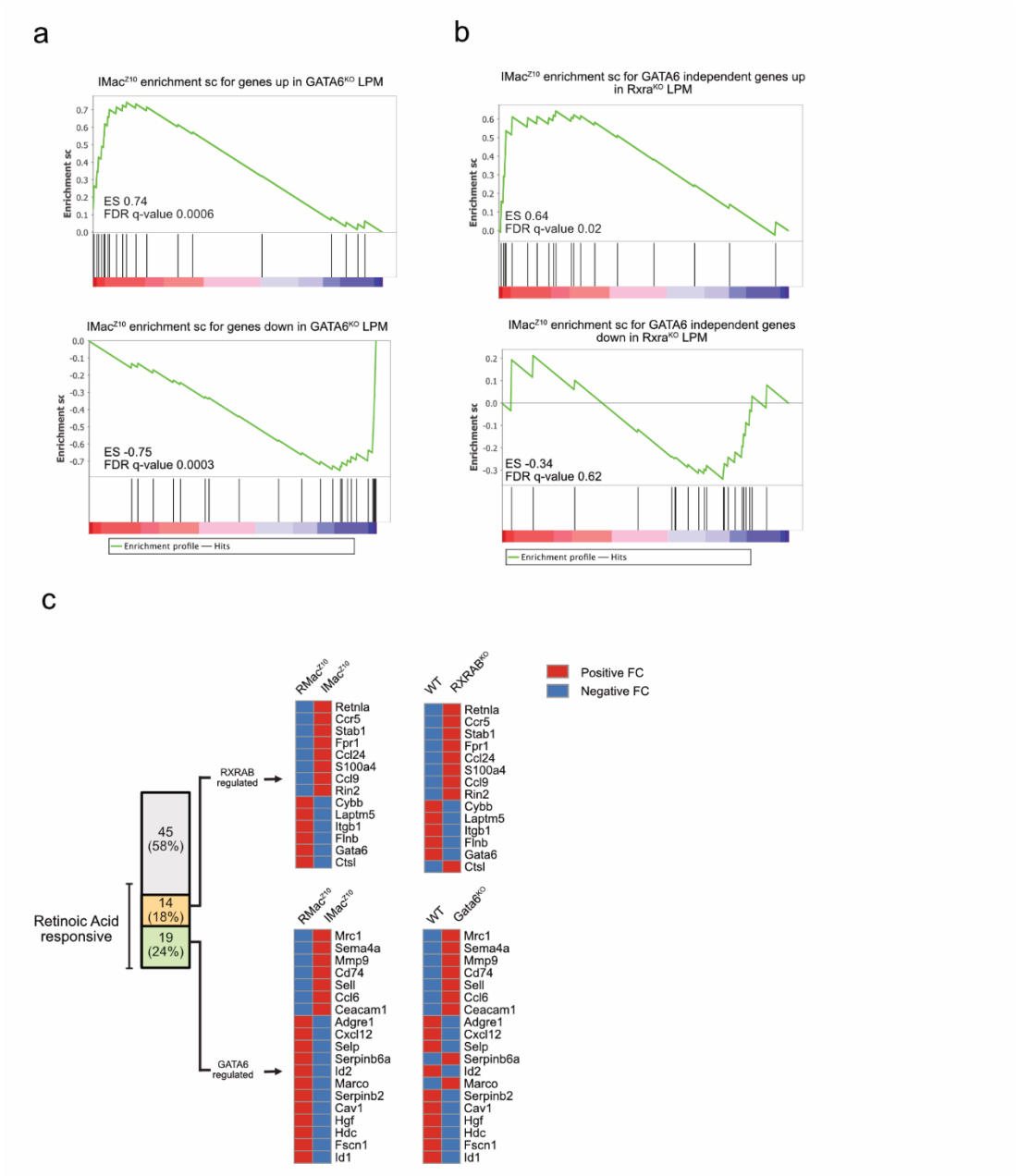

Figure 5.3 The inflammatory macrophage gene-signature suggests impaired retinoic-acid signalling.

(a) GSEA analysis of genes expressed by RMac^{Z10}and IMac^{Z10},8 weeks following transfer into inflamed recipients, relative to genes up or downregulated in GATA6^{KO} LPM (in reference to GATA6^{WT} LPM). **(b)** GSEA analysis of genes expressed by RMac^{Z10}and IMac^{Z10},8 weeks following transfer into inflamed recipients, relative to genes up or downregulated in RXRAB^{KO} LPM (in reference to RXRAB^{WT} LPM). **(c)** Proportion of differentially expressed genes between RMac^{Z10} and IMac^{Z10},8 weeks following transfer

into inflamed recipients, that are known to be regulated by GATA6 (green) or RXRAB (orange). The middle heatmaps denote the direction of gene-expression of GATA6 and RXRAB-regulated genes between $RMac^{Z10}$ and $IMac^{Z10}$. Heatmap to the right denotes the direction of gene-expression of $GATA6^{KO}$ and $RXRAB^{KO}$ LPM in reference to their WT counterparts. Transcriptional data for analysis of GATA6-regulated genes[63-65] and RXRAB-regulated genes[98] was sourced from published work and analysed as described in the M&M.

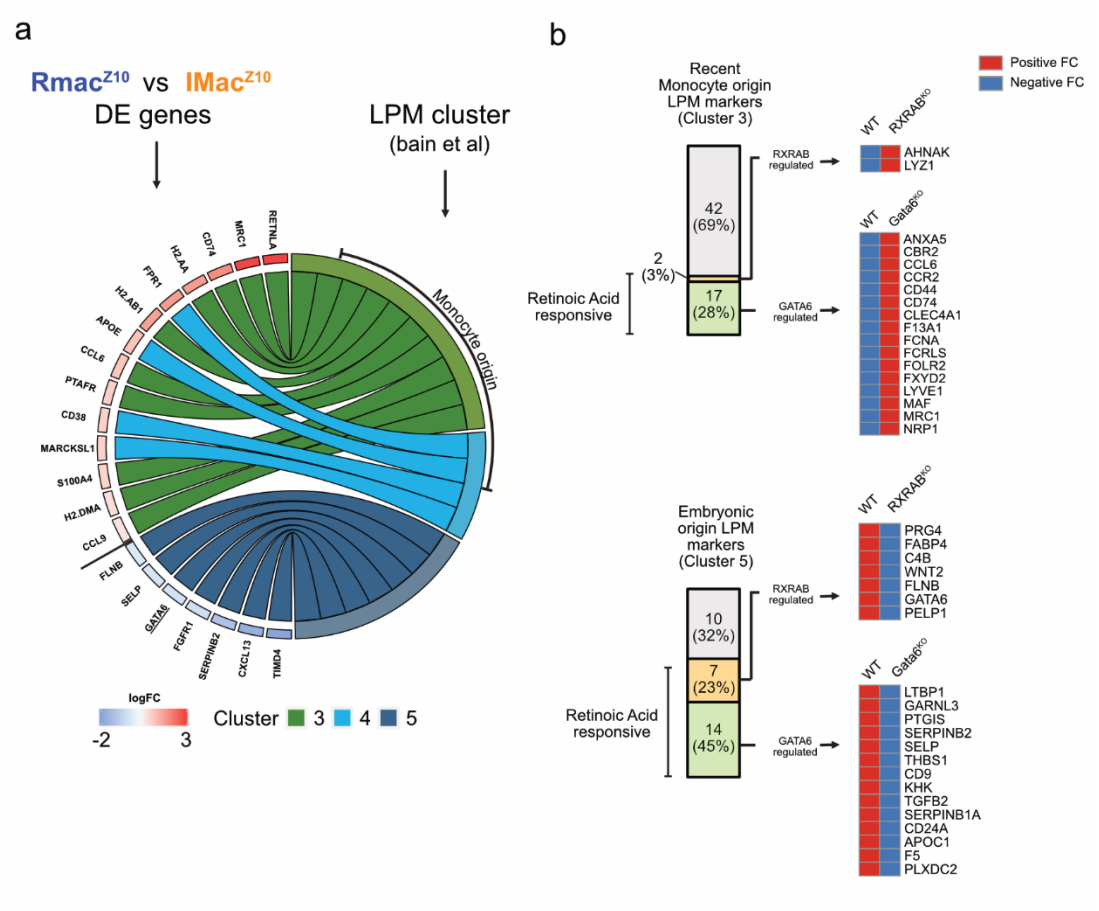

Figure 5.4 The monocyte-derived macrophage gene signature suggests impaired retinoic-acid signalling.

(a) Circus plot indicating genes that are differentially expressed between RMac^{Z10} and IMac^{Z10} (left side of the circus plot; genes more highly expressed by IMac^{Z10} in red, genes more highly expressed by RMac^{Z10} in blue) that are cluster-specific for subsets of peritoneal macrophages (right side of the circus plot), identified using single cell-sequencing. Single-cell data was sourced from published work by Bain et al[97]. **(b)** Cluster-genes that identify peritoneal macrophages of monocyte origin or embryonic origin which are regulated by GATA6 (green) or RXRAB (orange). To the right, direction of gene-expression for GATA6 and RXRAB regulated genes between GATA6^{KO} or RXRAB^{KO} LPM relative to WT LPM. Transcriptional data for analysis of GATA6-regulated genes[63-65] and RXRAB-regulated genes[98] was sourced from published work and analysed as described in the M&M.

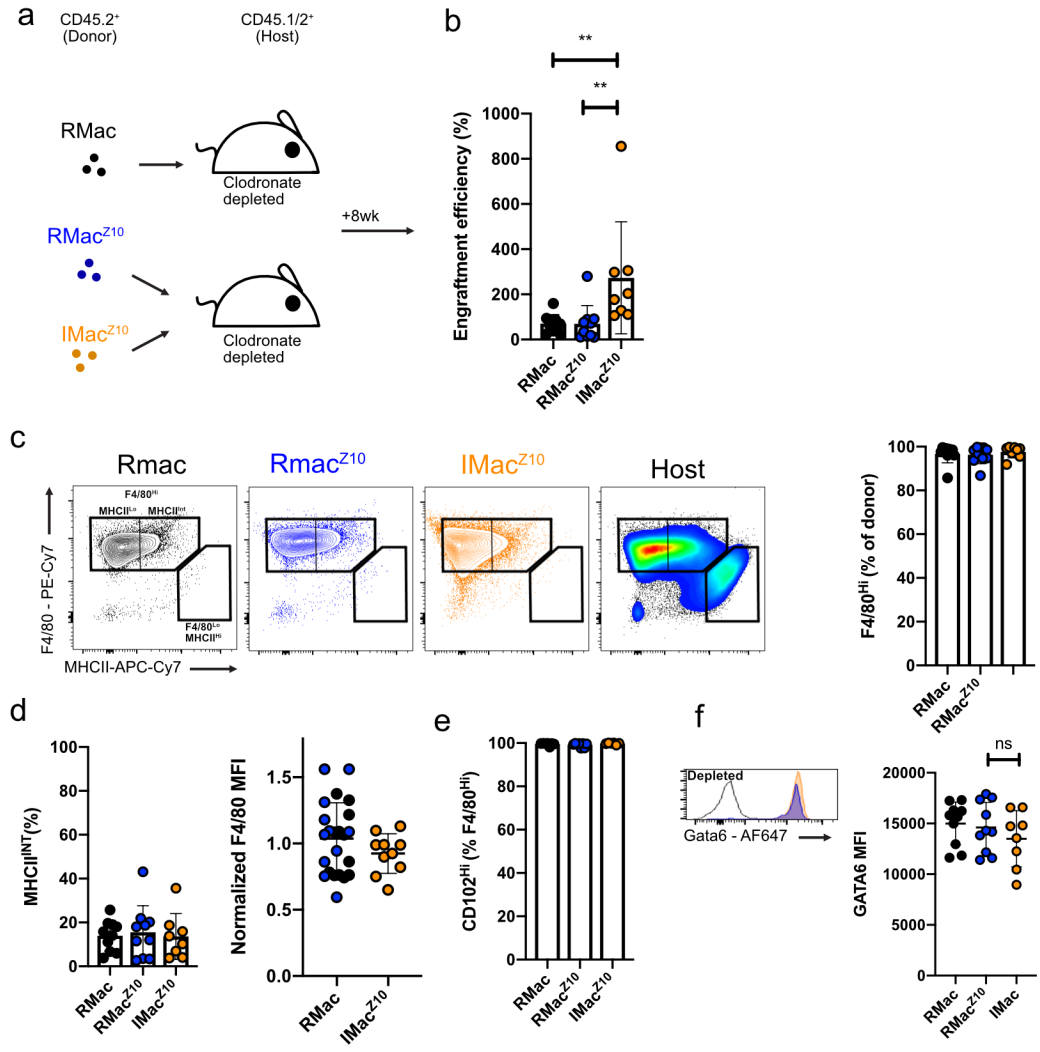

Figure 5.5 Inflammatory macrophages transferred into macrophage-deplete recipients adopt a resident phenotype.

(a) Experimental outline for transfer of RMac, RMac^{Z10} and IMac^{Z10} (gated as shown in Figure 3.6a) into clodronate-depleted recipients. **(b)** Engraftment efficiency of RMac, RMac^{Z10}and IMac^{Z10} 8 weeks following transfer clodronate-depleted recipients (left; n=10, n=10, n=8). **p<0.01 determined by one-way ANOVA and Tukey's multiple comparisons test **(c)** Proportion **of** RMac, RMac^{Z10} and IMac^{Z10} that are F4/80^{Hi} MHCII^{Lo}, 8 weeks after transfer into clodronate-depleted recipients (n= 12,11,11). **(d)** Proportion of RMac (n=10) , RMac^{Z10} (n=10) and IMac^{Z10} (n=8) that express MHCII, 8 weeks following transfer into clodronate-depleted recipients. To the right. normalized F4/80

MFI on donor RMac , RMac^{Z10}and IMac^{Z10}, 8 weeks following transfer into clodronate-depleted recipients (n=10,10,8). MFI is normalized to mean F4/80 MFI on RMac. **(e)** Proportion of F4/80^{Hi} MHCII^{Lo} RMac, RMac^{Z10} or IMac^{Z10} that express CD102, 8 weeks following transfer into clodronate-depleted recipients (n= 10,8,8). **(g)** GATA6 MFI on RMac, RMac^{Z10} or IMac^{Z10}, 8 weeks following transfer into clodronate-depleted recipients (n= 10,8,8). Data shown as mean ± standard deviation. Each symbol represents an individual animal. Data are pooled from at least 2 independent experiments.

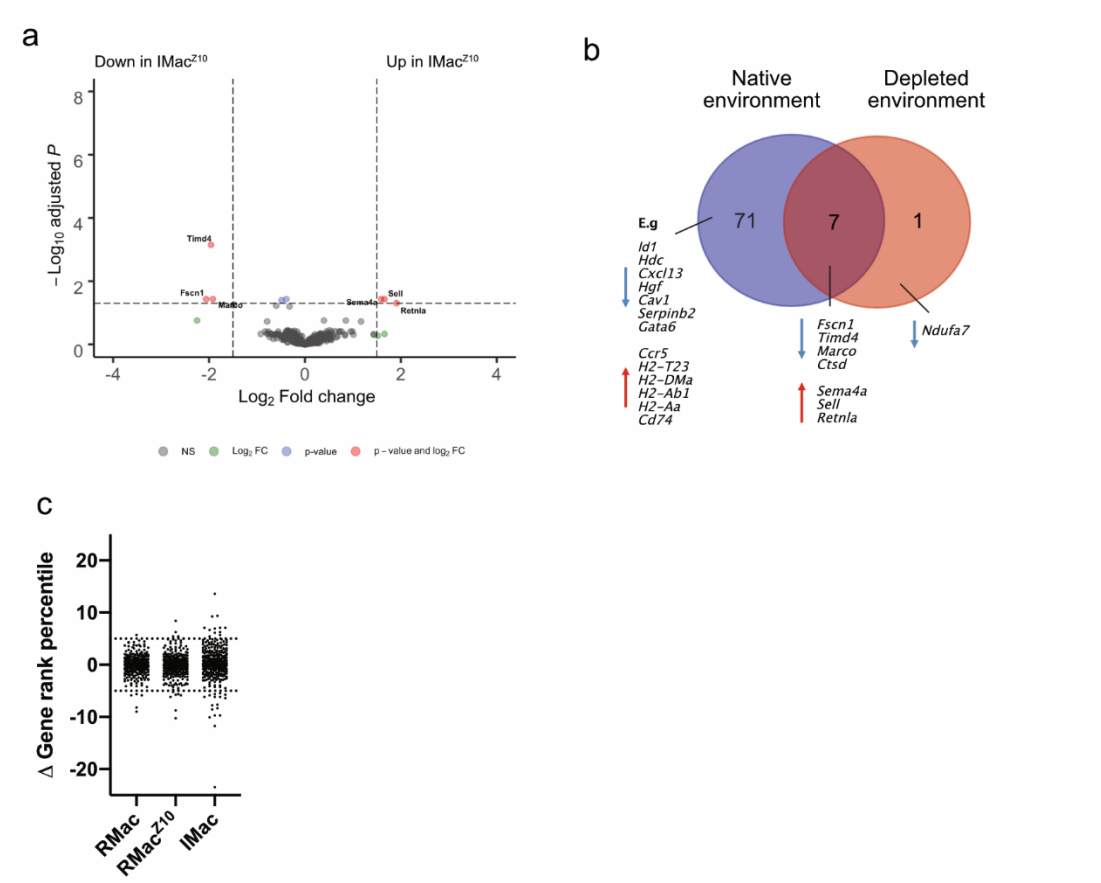

Figure 5.6 Inflammatory macrophages adopt a resident identity following transfer into clodronate-depleted recipients.

(a) Volcano plot indicating Log2Fold change (x-axis) and adjusted p-value (y-axis) of IMac^{Z10} in gene expression relative to expression levels exhibited by RMac^{Z10}, 8 weeks after transfer into clodronate-depleted recipients. **(b)** Number of genes that are differentially expressed between RMac^{Z10}and IMac^{Z10} (adj p value <0.05), 8 weeks following transfer into native (left, in blue) or clodronate-depleted recipients (right, in red). **(c)** Changes to percentile rank (ΔGene rank percentile = Percentile rank in native environment – Percentile rank in clodronate-depleted environment) for each detected genes. Dashed lines indicate a percentile change of 5%. This analysis was adapted from Galatro et al[155].

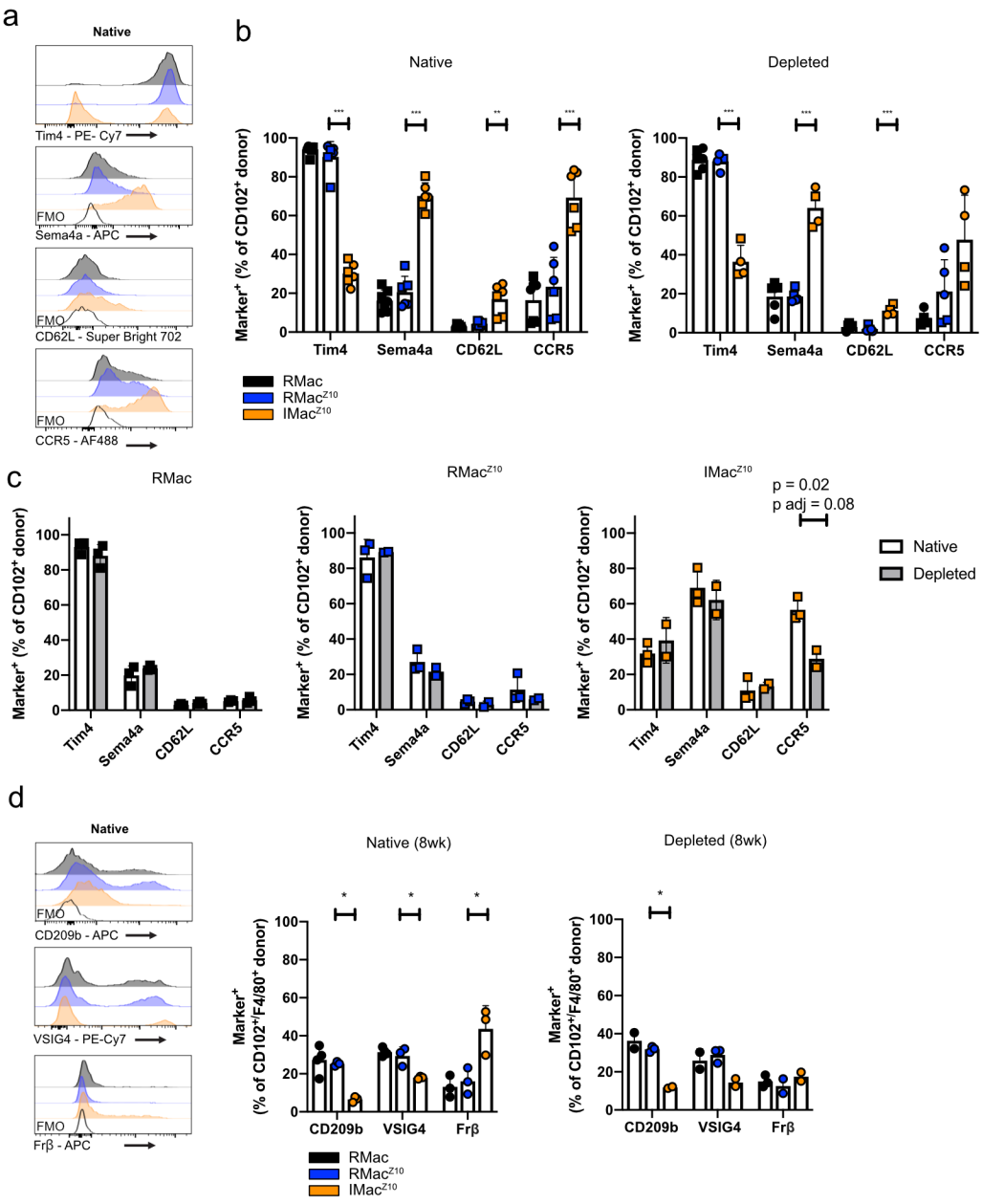

Figure 5.7 Inflammatory macrophages adopt a resident phenotype following transfer into clodronate-depleted recipients.

(a) Proportion of RMac (black), RMac^{Z10} or IMac^{Z10} that express Tim4, Sema4a, CD62L and CCR5, 8 weeks following transfer into native recipients. **(b)** Proportion of CD102^{+} RMac (black), RMac^{Z10} (blue) and IMac^{Z10} (orange) that express Tim4, Sema4a, CD62L and CCR5, 8 weeks following transfer into native (left; n=7,6,6) or clodronate-depleted recipients (right; n= 5, 5, 4). **p<0.01, **p<0.01 ***p<0.001 determined by one way ANOVA and Dunnet's

multiple comparisons test for each marker separately, followed by Bonferroni adjustment. **(c)** Proportion of $CD102^+$ or $F4/80^+$ RMac (black) $RMac^{Z10}$ (blue), $IMac^{Z10}$ (orange) that express Tim4, Sema4a, CD62L and CCR5, 8 weeks following transfer into native (n=4,3,3) or clodronate-depleted recipients (n=2,3,2). This dataset is a subset of the datasets presented in **(a)** and **(b)** in which datapoints were shown shown as square symbols. In this experiment the adoptive transfer of RMac (black) $RMac^{Z10}$ (blue), $IMac^{Z10}$ (orange) into native and into clodronate-depleted recipients was carried out in the same experiment and can therefore be directly compared. *p<0.05 determined by one way ANOVA and Dunnet's multiple comparisons test for each marker separately, followed by Bonferroni adjustment. **(d)** Proportion of $CD102^+$ or $F4/80^+$ donor RMac, $RMac^{Z10}$ or $IMac^{Z10}$ that express CD209b, VSIG4 and Frβ, 8 weeks following transfer into native (n=4,3,3) or clodronate-depleted recipients (n=2,3,2). **p<0.01 determined by one-way Anova and Dunnet's multiple comparisons test for each marker separately, followed by Bonferroni adjustment. Data shown as mean ± standard deviation. Each symbol represents an individual animal. Data were pooled from 2 independent experiments except (c,d) which are from a single experiments.

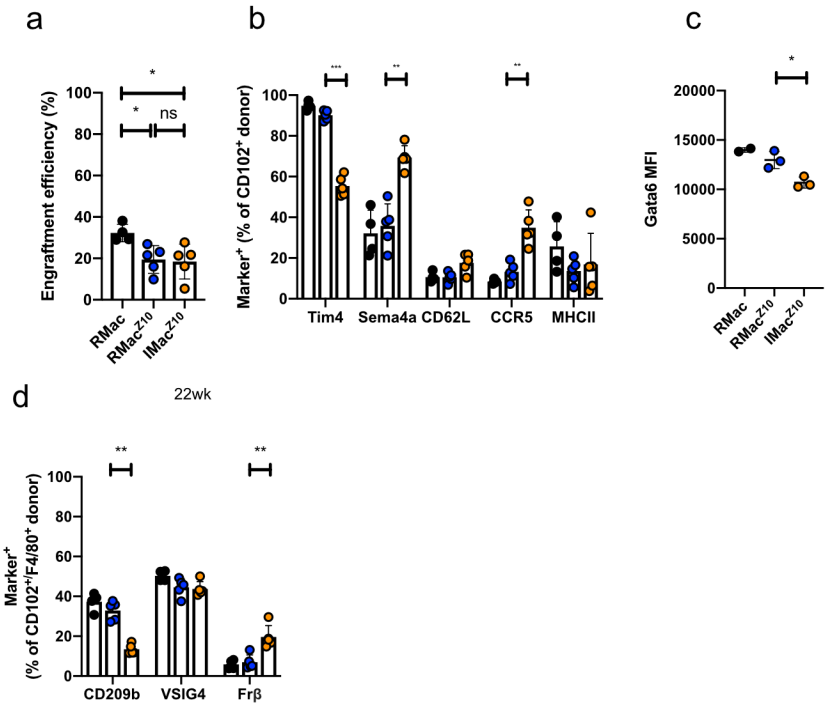

Figure 5.8 Inflammatory macrophages persist until 5 months after inflammation and adopt a more resident-like phenotype.

(a) Engraftment efficiency of RMac, RMac^{Z10} and IMac^{Z10}, 5 months following transfer into inflamed recipients (n=4, 5, 5). *p<0.05 determined by one-way ANOVA and Tukey's multiple comparisons test **(b)** Proportion of CD102^{+} RMac (black), RMac^{Z10} (blue) and IMac^{Z10} (orange) that express Tim4, Sema4, CD62L, CCR5 and MHCII, 5 months following transfer into inflamed (n=4, 5, 5) recipients. **p<0.01 ***p<0.001 determined by one way ANOVA and Dunnet's multiple comparisons test for each marker separately followed by Bonferroni adjustment. **(c)** GATA6 MFI on donor RMac, RMac^{Z10}or IMac^{Z10} 5 months following transfer into inflamed recipients (n=4, 5, 5). *p<0.05 determined by one-way ANOVA and Tukey's multiple comparisons test **(d)** Proportion of CD102^{+} or F4/80^{+} donor RMac (black; n=4) RMac^{Z10} (blue; n=5), IMac^{Z10} (orange; n=5) that express CD209b, VSIG4 and Frβ, 5 months following transfer into inflamed recipients. **p<0.01 determined by one-way Anova and Dunnet's multiple comparisons test for each marker separately, followed by Bonferroni adjustment. Data shown as mean ± standard deviation.

Each symbol represents an individual animal. Data were pooled from 2 independent experiments except (c) which was from a single experiment.

Chapter 6

Investigating the long-term consequences of inflammatory macrophage integration.

6.1 Introduction

In the previous chapter I found definitive evidence for long-term integration of phenotypically distinct inflammatory macrophages into the macrophage compartment after mild zymosan induced peritonitis. Persistent inflammatory macrophages largely lacked expression of numerous surface proteins important for internalization of pathogens, most notably the complement receptor VSIG4, shown to enhance internalization of complement-opsonized particles[170] and the pattern recognition receptor CD209B, shown to play a role in peritoneal clearance of *Streptococcus pneumoniae*[97,171]. Hence, their phenotype alone would indicate that persistent inflammatory macrophages are likely to be functionally divergent from their resident counterparts upon stimulation. The only published data investigating the responsiveness of the peritoneal cavity after historic zymosan-induced peritonitis is work by Newson et al[111]. They found that neutrophil recruitment in response to IP injection of *S. pneumoniae* is dampened in mice pre-treated with zymosan 8 weeks prior. However, in this study they did not attribute the altered response to changes in functionality of peritoneal macrophages.

These data raise the question whether the macrophages could be responsible for this dampened responsiveness, or if other peritoneal cells could be responsible for this phenomenon. In a subsequent study, Newson et al found that up to 21 days post-zymosan peritonitis infiltrating NK cells produce IFNγ resulting in prostaglandin E2 production by myeloid cells and a reduced mouse sickness score after subsequent *S. pneumoniae* treatment[120]. These data highlight that inflammation indeed alters the peritoneal cavity responsiveness long-term and that various cells in the cavity could be functionally altered after a historic inflammatory event which may impact the response of the cavity as a whole. However, whether changes to the macrophage compartment found in my studies alter the functional profile of the macrophage compartment remains unclear.

In patients with decompensated cirrhosis two populations of macrophages have been characterized in the peritoneal cavity[172,173]. One population resembles large peritoneal macrophages and is characterized by high levels of VSIG4 and GATA6, whereas the other population largely lacks VSIG4 and expresses lower levels of GATA6 and higher levels of CCR5[173] and seemingly resembles inflammatory macrophages found in my studies. This population of 'inflammatory-like' macrophages was found to have lower granularity and less or equal phagocytic capacity as their resident counterparts[172,173]. Moreover, in response to *in vitro* LPS treatment 'inflammatory-like' macrophages produced less TNFα than their resident counterparts[172] . Combined, these data not only suggest that inflammatory macrophage integration may be occurring in humans, but also that it is likely that inflammatory macrophage are indeed functionally distinct from their resident counterparts in response to inflammatory stimuli.

However, inflammatory macrophages are likely functionally divergent under unstimulated steady state conditions. Indeed, Bain et al show that there is a degree of ontogeny-related functional heterogeneity in the murine resting steady state cavity. Tim4$^-$ monocyte-derived LPM are undergoing high levels of proliferation whereas established Tim4$^+$ LPM proliferate less [42]. Moreover, I found that inflammatory macrophages had the capacity to expand considerably and repopulate a depleted cavity, indicating a high degree of proliferative capacity. Moreover, inflammatory macrophages appear to transcriptionally and phenotypically resemble the highly proliferative monocyte-derived LPM present under homeostatic conditions. Hence, it is likely that inflammatory macrophages could have similar heightened baseline proliferation compared to their resident counterparts. A key difference I found was that persistent inflammatory macrophages largely failed to acquire Tim4 expression. Tim4 is expressed by the majority of resident macrophages and has been found to mediate immunologically silent uptake of apoptotic cells by LPM[20,21], thus playing a key role in maintaining peritoneal homeostasis.

As discussed in the introduction, inflammation driven integration of monocytes into the macrophage compartment has been found to occur in various sites. The degree to which these integrated monocytes were able acquire a resident functionality appears to be tissue and stimulation dependent. In the majority of these studies monocyte integration occurred after almost complete loss of the resident macrophage populations. My studies indicated that competition with incumbent resident macrophages strongly inhibits the capacity of inflammatory macrophages to acquire a resident identity. Hence, I postulated that in this competitive context persistent inflammatory macrophages would remain functionally distinct.

Moreover, the transcriptional and phenotypic identity resembles that of monocyte-derived LPM present under homeostatic conditions. Hence, it is likely that under steady state conditions functionally distinct macrophage subsets inhabit the peritoneal cavity and that following inflammation this functional heterogeneity is enhanced due to inflammatory macrophage integration.

Hence in this chapter I set out to:

- Ascertain the baseline proliferation levels of persistent inflammatory macrophages and their monocyte counterparts in the naïve and post-zymosan cavity.
- Investigate whether, similar to human peritoneal phagocytes, persistent inflammatory macrophages are less granular and less phagocytic than their resident counterparts.
- Establish whether persistent inflammatory macrophages respond differently to resident macrophages to challenge with LPS, but similarly to monocyte-derived resident macrophages present in the naïve cavity.
- Explore whether persistent inflammatory macrophages respond transcriptionally and functionally similar to their resident counterparts to LPS *in vivo*. To exclude confounding effects of changes to the peritoneal cavity following historic zymosan induced peritonitis, which

could affect subsequent LPS responsiveness, purified resident or inflammatory macrophages were transferred into naïve recipients followed by LPS injection.

6.2 Developing a marker-based gating strategy to identity inflammatory macrophages long-term.

The most definitive method to identify persistent inflammatory macrophages was using the adoptive transfer methodology. However, a drawback of this method was that too few donor cells were present for functional studies *in vitro.* Hence, I first set out to develop a gating strategy to identify inflammatory macrophages long-term. As I had not found a marker unique to either resident or inflammatory macrophages, I opted to use the two most exclusive markers Tim4 and Sema4a I had identified after 8 weeks in prior experiments **(Figure 5.7b)**.

Combined analysis of these markers on $RMac^{Z10}$ and $IMac^{Z10}$ 8 weeks post-transfer into native recipients identified 4 distinct quadrants. Whereas $RMac^{Z10}$ almost exclusively contributed to the $Tim4^{+}$ $Sema4a^{Lo}$ quadrant, $IMac^{Z10}$ largely contributed to the $Tim4^{-}$ $Sema4a^{H}$ quadrant **(Figure 6.1a)**. Moreover within the host macrophage compartment there was a quantifiable loss of $Tim4^{+}$ $Sema4a^{Lo}$ macrophages, consistent with loss of resident macrophages and gain of $Tim4^{-}$ $Sema4a^{Hi}$ macrophages in line with inflammatory macrophage integration 8 and 22 weeks post zymosan **(Figure 6.1a,b)**. Importantly, in separate experiments performed without cell transfer or dye-labelling, a similar loss of $Tim4^{+}$ $Sema4a^{Lo}$ macrophages and gain of $Tim4^{-}$ $Sema4a^{Hi}$ inflammatory macrophages occurred following low-dose zymosan injection **(Figure 6.1a,b)** confirming that dye labelling nor adoptive cell transfers alter the composition of the macrophage compartment following zymosan-induced peritonitis. As inflammatory macrophage-derived macrophages resembled monocyte-derived macrophages present under homeostatic conditions I examined whether $Tim4^{-}$ $Sema4a^{Hi}$ macrophages expressed higher levels of MHCII, which demarks resident macrophages of

recent monocyte origin[42] . Indeed, in both naïve and zymosan-injected mice, the Tim4^{-} Sema4a^{Hi} quadrant R3 expressed high levels of MHCII **(Figure 6.1c)**. Hence, I concluded that using this combination of markers the majority of inflammatory macrophage derived large peritoneal macrophages could be identified on the basis of their Tim4^{-} Sema4a^{Hi} phenotype at least until 8 weeks post-zymosan injection (referred to as Mo^{Z10}-LPM) whereas in naïve mice Tim4^{-} Sema4a^{Hi} cells largely correspond to large peritoneal macrophages of recent monocyte origin (referred to as Mo-LPM). In contrast Tim4^{+} Sema4a^{Lo} cells corresponded to incumbent resident large peritoneal macrophages in naïve (referred to as RM-LPM) and zymosan-treated mice (referred to as RM^{Z10}-LPM) **(Figure 6.1d)**.

6.3 Heightened proliferation is a feature of monocyte-derived macrophages per se.

As Bain et al[42] previously described that Tim4^{-} monocyte-derived LPM present under steady state conditions exhibit heightened proliferation, and since this population largely overlaps in phenotype with persistent inflammatory macrophages, I first set out to investigate whether Mo-LPM and Mo^{Z10}-LPM identified based on Tim4^{-} Sema4a^{+} expression had higher baseline levels of proliferation as their resident counterparts. Indeed, in naïve mice Mo-LPM had significantly higher levels of proliferation than RM-LPM **(Figure 6.2a,b)** consistent with earlier work[42], based on the proliferation marker Ki67. Moreover Mo^{Z10}-LPM similarly exhibited higher levels of baseline proliferation than RM^{Z10}-LPM **(Figure 6.2a,b)** indicating that differentiation of monocytes under inflammatory conditions does not dictate their capacity to maintain heightened proliferation long-term.

6.4 Monocyte-derived macrophages are characterized by low granularity and phagocytic capacity.

Human studies indicated that a subset of peritoneal cavity macrophages that resembled resident macrophages had discrete granularity and phagocytic capacity[172]. Hence, I set out to investigate these features and ascertain whether murine resident and monocyte-derived macrophages present long-term following zymosan-induced peritonitis had similar heterogeneity.

To examine granularity, RM^{Z10}-LPM and Mo^{Z10}-LPM were purified 8 weeks post zymosan injection and stained using Haematoxylin and Eosin. Mo^{Z10}-LPM appeared to have less vacuoles and an overall less granular structure than RM^{Z10}-LPM **(Figure 6.3a),** possibly indicative of impaired phagocytic capacity. Using flow cytometry, I confirmed that Mo^{Z10}-LPM and Mo-LPM had significantly lower side-scatter characteristics than their resident counterparts consistent with lower granularity **(Figure 6.3b)**. To investigate if the contrasting morphology indeed reflected a difference in phagocytic capacity, peritoneal cells where cultured with pHrodo-labelled *Escherichia coli* particles. This analysis indicated that $Tim4^+$ LPM mice phagocytosed significantly more *Escherichia coli* particles than $Tim4^-$ LPM **(Figure 6.3c)**, irrespective of whether macrophages originated from naïve or 8-week post-zymosan treated mice. It should be noted that in these experiments incubating cells at 37^{o}C for 1 hour caused rapid acquisition of surface Sema4a by $Tim4^+$ macrophages rendering this marker unusable.

This difference in phagocytic potential prompted me to re-analyse my earlier short-term (8 day) adoptive transfer experiments, where naïve or inflamed recipient mice had received labelled $RMac^{Z10}$. In these experiments I found an $RMac^{Z10}$ engraftment efficiency of approximately 35%, indicating that approximately 65% of donor cells had disappeared and likely had died **(Figure 4.1b)**. As transferred $RMac^{Z10}$ were labelled with PKH26-PCL, any phagocytosis of these cells by host macrophages would consequently lead to

acquisition of PKH26-PCL labelling. Hence, PKH26-PCL dye uptake by host cells could be utilized as indicator of phagocytic capacity. Consistent with my *in vitro* findings, Tim4^{+} host macrophages efficiently acquired PKH26-PCL by 8 days following transfer of labelled RMac^{Z10} into naïve or zymosan-treated recipients, consistent with phagocytosis of dying donor cells, whereas Tim4^{-} host macrophages did not **(Figure 6.3d)**. Moreover, Tim4^{-} host macrophages also failed to phagocytose dying cells after inflammation when the number of Tim4^{+} macrophages was reduced ,suggesting that Tim4^{+} macrophages are more efficiently phagocytosing dying cells even when their number is decreased **(Figure 6.3e)**. Combined with my earlier findings indicating that free-floating PKH26-PCL dye particles were not phagocytosed more effectively by Tim4^{+} macrophages (**Figure 4.4)** these data indicate that under steady state conditions or between 3 to 11 days following zymosan injection, Tim4^{+} macrophages are more efficient at phagocytosing dying cells than their Tim4^{-} counterparts.

6.5 Altered cytokine production by monocyte-derived macrophages in response to LPS *in vitro*.

Published work using human peritoneal macrophages found evidence for divergent cytokine production, most notably TNFα[172], between those populations of human peritoneal macrophages that seemingly corresponded to resident and monocyte-derived LPM in my studies. To investigate this, I measured cytokine production by RM^{Z10}-LPM and Mo^{Z10}-LPM in response to LPS. Briefly, for this assay 10.000 cells of the indicated populations were sorted on the basis of Tim4 and Sema4a. Importantly, RM^{Z10}-LPM and Mo^{Z10}-LPM purified this way had equivalent post-sort viability **(Figure 6.4a)**. Cells were then allowed to adhere for 2 hours, after which the media was careful removed. Then, treatment medium containing LPS (1ng/ml) or vehicle control was added and cells were incubated for 14 hours. After, medium was collected and assessed for cytokine production using a LEGENDplex bead-based immunoassay **(Figure 6.4a)**.

During trial experiments I had found that by culturing 10,000 macrophages with LPS in a total of 75μl of medium resulted in detectable levels of most analytes within range of the LEGENDplex assay. Ideally, 10,000 cells would have been sorted and treated without the additional adherence step. However, when sorting cells every purified cell is contained in a droplet of flow cytometry fluid (PBS) which, when sorting 10,000 cells, equated to a total volume of 50μl of flow cytometry fluid. Direct treatment in a total volume of 75μl would have resulted in a very diluted medium and adversely affected cell viability. Hence, I opted to include a cell adherence step. After the adherence the sort-medium mixture was gently removed and replaced with treatment medium.

Purified RM^{Z10}-LPM secreted significantly more CXCL1, TNFα CCL2, CCL5, Il1β, CXCL10, GM-CSF, Il10 and Il6 after treatment with LPS than following culture with vehicle alone **(Figure 6.4b)**. Similarly, with the exception of CXCL10, Mo^{Z10}-LPM also secreted these cytokines and chemokines in response to LPS **(Figure 6.4b)**. Hence, I concluded that these LPS responsive cytokines/chemokines could be detected and measured after LPS treatment using this assay. It should be noted that both Il-12(p70)[174] and IFNα,β,y[175,176] are known to be secreted by LPS-treated peritoneal macrophages *in vitro* but, were not detectable in this assay. Of note, both RM^{Z10}-LPM and Mo^{Z10}-LPM produced high levels of Il6 in response to culture alone. After culture with LPS levels of this Il6 were above the detectable limit of the assay. Hence, Il6 was excluded from further analysis.

When directly comparing supernatant levels of these LPS-driven cytokines between RM^{Z10}-LPM and Mo^{Z10}-LPM, it became apparent that Mo^{Z10}-LPM produced significantly more Il10 and GM-CSF than RM^{Z10}-LPM **(Figure 6.4c,left)**. Conversely Mo^{Z10}-LPM produced less CCL5, TNFα and CXCL10. Purified Mo-LPM sourced from naïve mice similarly secreted higher levels of Il-10 than their RM counterparts, but also secreted higher levels of Il1β **(Figure 6.4c, right)**. It should be noted that in both the analyses shown in Figure 6.4c,

cytokine levels produced in response to LPS were not normalized to baseline levels produced in control PBS treated cells. This was because Mo-LPM in naïve mice are so rare **(Figure 6.1b)** that sufficient cells could not be obtained to treat with PBS and LPS and consequently only LPS treatment was carried out. However, as post-zymosan Mo^{Z10}-LPM were much more abundant **(Figure 6.1b)** sufficient cells could be sourced to carry out both PBS and LPS treatment. This analysis indicated that baseline production for most LPS-driven cytokines was equivalent between Mo^{Z10}-LPM and RM^{Z10}-LPM **(Figure 6.4d)**. However, Mo^{Z10}-LPM did produce less CCL5, TNFα and more CXCL1 than RM^{Z10}-LPM **(Figure 6.4d)**. For these 3 factors I confirmed that after normalization to PBS production levels Mo^{Z10}-LPM still produced less CCL5 and TNFα in response to LPS and that the difference observed was not because of baseline differences in secretion **(Figure 6.4e).**

Using a similar methodology, I then set out to investigate whether the response of resident or monocyte-derived macrophages to LPS was altered after historic zymosan-induced peritonitis. Of note, a different cytokine array was used because that included many analytes found to be differentially expressed between monocyte-derived and resident LPM, but also included some additional analytes not yet assessed. To source sufficient Mo-LPM from naïve mice for PBS and LPS treatment, Mo-LPM from different mice were purified for PBS and LPS treatment. Whereas RM-LPM and RM^{Z10}-LPM had equivalent baseline production of all analytes, Mo^{Z10}-LPM produced somewhat less IL1β, IL6 and GM-CSF than Mo-LPM **(Figure 6.5a)**. The decreased baseline production of IL1β might explain why previously I had found that Mo-LPM produced more IL1β than RM-LPM, but Mo^{Z10} -LPM did not appear to produce less than RM^{Z10}-LPM **(Figure 6.4c)**. For each analyte, levels detected in response to LPS were normalized to mean levels produced by corresponding populations in response to PBS to provide a measurement of LPS-induced cytokine production. In response to LPS, the cytokine profile of resident and monocyte-derived LPM sourced from the naïve or post-zymosan cavity was, except Il12, largely equivalent indicating that historic zymosan-

induced peritonitis does not significantly alter the LPS responsiveness of either population **(Figure 6.5b)**.

6.6 Investigating monocyte-derived macrophage responsiveness *in vivo*

Next, I wanted to investigate if the different responsiveness of Mo^{Z10}-LPM and RM^{Z10}-LPM to LPS also occurred *in vivo* and if the presence of Mo^{Z10}-LPM would alter the responsiveness of the cavity as a whole. To examine this I purified Tim4 and Sema4a-defined RM^{Z10}-LPM and Mo^{Z10} LPM from mice treated 8 weeks prior with zymosan and then adoptively transferred 250,000 of each population into naïve recipient mice **(Figure 6.6a)**. Mice were left to recuperate for 2 days after cell transfer before receiving IP injection with 5μg LPS, a dose which was relatively low compared to similar studies by Li et al that used a higher dose (approximately 40μg) of the same LPS serotype (O111:B4) to induce systemic inflammation[177]. However, during trial experiments I had found that 5μg LPS already induced discomfort to the animals as indicated by hunched posture and squinted eyes following injection. As 5μg LPS induced quantifiable neutrophil recruitment I opted to use this comparatively low dose **(Figure 6.6a)** as to limit discomfort for experimental animals.

2 Days post-LPS both donor populations were detectable, although Mo^{Z10} LPM appeared to persist somewhat less well than RM^{Z10}-LPM **(Figure 6.6b)**. Irrespective, both donor populations accounted for approximately 5% of the complete $F4/80^{Hi}$ macrophage compartment **(Figure 6.6b)**. Irrespective of cell transfer, injection of LPS caused rapid weight loss over the succeeding 8 hours **(Figure 6.6c)**, indicative of systemic inflammation. Surprisingly, mice that had received either donor population recruited fewer neutrophils into the peritoneal cavity than mice that received no donor cells (PBS) **(Figure 6.6d)**. This effect was surprising, given that donor populations accounted for only a minor

fraction of the macrophage compartment.

6.6.1 Impaired TNFα production by monocyte-derived macrophages *in vivo*

When performing this experiment, I carried out intracellular staining for TNFα and Il10, the production secretion of which, *in vitro,* differentiated Mo^{Z10}-LPM from their RM counterparts **(Figure 6.4c)**. Unfortunately, Il10 staining is notoriously hard and, in my hands, proved very variable and could not be trusted. Intracellular TNFα was readily detectable and analysis indicated that a smaller portion of Mo^{Z10}-LPM produced TNFα than RM^{Z10}-LPM **(Figure 6.6e,f)**, consistent with the lower overall production of TNFα by Mo^{Z10}-LPM detected *in vitro*. However, those Mo^{Z10}-LPM that produced TNFα appeared to produce more TNFα on a per cell basis than RM^{Z10}-LPM (**Figure 6.6e,f, right)**. Moreover, a smaller proportion of Mo^{Z10}-LPM produced TNFα than $F4/80^{Hi}$ host macrophages in the same cavity, comprising predominantly of RM-LPM, whereas the proportion of RM^{Z10}-LPM that produced TNFα was similar to the corresponding $F4/80^{Hi}$ host macrophage population **(Figure 6.6g)**.

During these experiments the peritoneal lavage fluid and serum were collected from treated mice. These samples were analysed for levels of Il1β, Il6, CCL2 and TNFα by Dr. Georgia Perona Wright and Ms. Holly Webster. This analysis indicated that cell-transfer had no effect on the lavage or serum levels of these analytes **(Figure 6.7a,b)**.

6.6.2 Dampened transcriptional response by monocyte-derived macrophages

To investigate whether the transcriptional signature of Mo^{Z10}-LPM was similar to RM^{Z10}-LPM in response to LPS, I re-purified the donor cells 8 hours post LPS injection and investigated their transcriptome using a Nanostring Mouse inflammation panel. This analysis indicated that 38 out of 269 detected genes

differentiated between RM^{Z10}-LPM and Mo^{Z10} LPS. Importantly, because of the long sorting times required for this experiment I had not included mice that received either donor population and PBS vehicle instead of LPS in this experiment. Hence, a control PBS treated group to directly identify LPS-driven genes was missing from this experimental analysis. Hence, for the interpretation of this Nanostring dataset I carried out the following steps. By overlapping this geneset with my previous Nanostring dataset (presented in section 5.3) I found that 8 out of the 38 differentially expressed genes were not differentially expressed between $RMac^{Z10}$ and $IMac^{Z10}$ at baseline in the original dataset, but were differentially expressed between RM^{Z10}-LPM and Mo^{Z10}-LPM post-stimulation with LPS (**Figure 6.8ai**). This indicates that differential expression of these genes was likely related to the LPS challenge. Conversely, 13 out of the 38 differentially expressed genes (e.g. genes related to MHCII presentation, *Ccr5* and *Marco*) were differentially expressed between $RMac^{Z10}$ and $IMac^{Z10}$ *ex vivo* as well as between post-LPS RM^{Z10}-LPM and Mo^{Z10}-LPM in this dataset (**Figure 6.8aii**) and consequently are likely related to baseline differences in gene expression in these cells rather than differences in response to the LPS challenge. Moreover, 5 out of the 38 differentially expressed genes have been shown to LPS-responsive in peritoneal macrophages[177] (**Figure 6.8aiii**) and expression differences are likely related to LPS treatment. For the remaining 12 differentially expressed genes it cannot be ascertained whether they differentially expressed between Mo^{Z10}-LPM and RM^{Z10}-LPM in response to LPS or at baseline (**Figure 6.8aiiii**).

For those differentially expressed genes likely to be driven by LPS stimulation (**Figure 6.8ai&iii**), expression by Mo^{Z10}-LPM was universally lower than RM^{Z10}-LPM, suggestive of a dampened ability to respond to LPS. Notably, although expression of TLR4, the main LPS receptor[178-180], was equivalent between the two populations, expression of *CD14* and *CD55* encoding accessory proteins was lower on Mo^{Z10}-LPM **(Figure 6.8ai&iii)**.

I then generated a gene list, excluding those genes that were differentially expressed at baseline between $RMac^{Z10}$ and $IMac^{Z10}$. It should be noted that although the resulting list will include a number of genes differentially expressed prior to the inflammatory insult that were not included in the original Nanostring panel. GSEA analysis of this gene list compared to the gene ontology gene-sets available at the Molecular Signatures Database indicated possible negative enrichment in Mo^{Z10}-LPM for genes positively regulated in humoral response (FDR<0.25) **(Figure 6.8b)**. Indeed Mo^{Z10}-LPM appeared to express lower levels of complement components *C2*,*C1ra*,*C1qbp,* but also low levels of *CD55*, thought to inhibit complement activation[181]. It should be noted that GSEA analysis includes all detected genes and identifies enriched genes on the basis of their relative difference in expression level between groups instead of based on a list of differentially- expressed gene. Consequently, GSEA identified some genes, potentially of interest (*C1ra*, *C1qbp)* that were not differentially expressed in the Nanostring analysis. With a Log2FC of -3.4 *CD55* was the most altered differentially expressed gene.

Although only a single gene-set was enriched with an FDR<0.25, 17 gene-sets were potentially enriched with nominal p<0.05. GSEA analysis can be expanded upon by investigating if certain genes are overrepresented in all the potentially enriched gene-sets using leading edge analysis. These genes are more likely to be of biological relevance as their expression impacts multiple known pathways. This analysis indicated that lower expression of *CD55* by Mo^{Z10}-LPM is likely to have biological implications as lower *CD55* affected 6 out of the 17 potentially differentially expressed gene-sets **(Figure 6.8c)**.

In summary, these data indicate that Mo^{Z10}-LPM are functionally distinct from RM^{Z10}-LPM, as they produce less TNFα and have a distinct, seemingly dampened, transcriptional response to LPS *in vivo*.

6.7 Discussion

In this chapter I set out to ascertain to what extent persistent inflammatory macrophages are functionally similar to their embryonically-seeded resident counterparts. Utilizing a combination of markers identified using the adoptive transfer methodology I developed a gating strategy to identify RM^{Z10}-LPM ($Tim4^{+}$ $Sema4a^{Lo}$) and Mo^{Z10}-LPM ($Tim4^{-}$ $Sema4a^{Hi}$) after 8 weeks post-injection of zymosan and the equivalent populations in naïve mice. Critically, this gating strategy allowed me to ascertain whether the functional profile of Mo^{Z10}-LPM resembles that of Mo-LPM, as their transcriptional and phenotypic identity overlaps, and how the functional profile of Mo-LPM and Mo^{Z10}-LPM differs from their established resident counterparts. As discussed in the previous chapter this gating strategy does exclude the, numerically minor, population of $IMac^{Z10}$ that did upregulate Tim4 and are more likely to have a resident-like functionality. Hence, in these studies the functional divergence between RM^{Z10}-LPM and Mo^{Z10}-LPM and their naïve counterparts is potentially overestimated.

Monocyte-derived LPM were more proliferative than their resident counterparts, irrespective of whether they had differentiated under steady-state or inflammatory conditions. This was somewhat surprising as Mo^{Z10}-LPM accounted for a considerably larger population than found under naïve homeostatic conditions. These findings are consistent with earlier work from our lab [42], indicating that the $Tim4^{-}$ fraction of resident macrophages present in the naïve cavity is characterized by high baseline levels of proliferation. Hence, heightened proliferation appears to be a characteristic shared between Mo^{Z10}-LPM and Mo-LPM.

In patients with decompensated cirrhosis two subsets of macrophages inhabit the peritoneal cavity[172,173]. These subsets appear to overlap with resident and monocyte-derived LPM in my experimental work. Consistent with the equivalent human population, Mo-LPM had less vacuoles and lower granularity indicative of lower phagocytic capacity. Moreover, Mo-LPM,

irrespective of their differentiation conditions, less readily phagocytosed *Escherichia coli* particles *ex vivo* similar to the equivalent human peritoneal macrophage subset[173]. Hence, murine monocyte-derived LPM appear to functionally mirror a subset of human peritoneal macrophages that after LPS stimulation *in vitro* produce a unique cocktail of cytokines. The decreased and increased secretion of TNFα and Il10 respectively by Mo^{Z10}-LPM compared to their resident counterparts seemingly indicates a more anti-inflammatory profile.

Notably, *in vitro* assessment of cytokine production also revealed that Mo-LPM produced more Il1β than their RM-LPM counterparts, whilst the difference in Il1β secretion was only marginal between post-zymosan Mo^{Z10}-LPM and RM^{Z10}-LPM. However, no difference in Il1β secretion could be detected when Mo^{Z10}-LPM and Mo-LPM, or RM^{Z10}-LPM and RM-LPM were directly compared, in response to LPS. These finding questions the robustness of Il1β measurements or suggests any difference in production of this cytokine must be minor. Surprisingly, baseline production of Il1β, Il6 and GM-CSF was elevated in Mo-LPM compared to Mo^{Z10}-LPM although the difference was relatively small. Moreover, baseline cytokine production between RM-LPM and RM^{Z10}-LPM was equivalent, although after LPS stimulation RM^{Z10}-LPM seemingly produced more Il12-(p70). A possibly explanation for divergent cytokine production between monocyte-derived and resident macrophages sourced from naïve mice and their counterparts sourced from zymosan treated mice could be generation of innate immune memory in macrophages post-zymosan. Indeed, *in vitro* studies indicated that, predominantly monocyte-derived, macrophages present after thioglycolate-induced peritonitis are able to establish immune memory and can be sensitized to subsequent LPS stimulation *in vitro* by pre-treatment with purified β-glucan components but, surprisingly not by pre-treatment with zymosan A, despite consisting largely of β-glucans[154]. *In vivo* it has been found that microglia are able to establish immune memory after peripheral LPS challenge which is retained up to 6 months, modulating responsiveness to neurophatologies[182]. Little is known

about how trained immunity may be influencing baseline production levels of inflammatory mediators. Further studies to what degree this may be occurring after peritonitis are needed.

It should be noted that although my findings suggest that RM-LPM and RM^{Z10}-LPM and Mo-LPM and Mo^{Z10}-LPM resemble one another transcriptionally and functionally my studies are insufficient to definitively draw this conclusion. Future studies should investigate the complete transcriptional and epigenetic profile of these populations to definitively ascertain that these populations are indeed equivalent or if there are (subtle) differences between them. Indeed, it is possible that, having differentiated under inflammatory conditions, Mo^{Z10}-LPM may carry epigenetic memory[183] that differentiates them from their naïve Mo-LPM counterparts.

Consistent with lower TNFα secretion by Mo^{Z10}-LPM *in vitro* they also appeared to produce less TNFα *in vivo* in response to LPS stimulation. However, those cells that did produce TNFα appeared to produce higher levels than RM^{Z10}-LPM. This discrepancy might explain why in Nanostring analysis of Mo^{Z10}-LPM and RM^{Z10}-LPM stimulated *in vivo* with LPS, expression of *Tnf* was seemingly unaltered between these populations. Genes encoding for cytokines differentially secreted *in vitro* by Mo^{Z10}-LPM and RM^{Z10}-LPM in response to LPS were either not differentially expressed (*Il1b*, *Tnf*, *Ccl5*, *Cxcl10*) or below the detection limit (*Il10*, *Csf2*) when examined by Nanostring in purified populations stimulated *in vivo*. However, Mo^{Z10}-LPM did appear to express less *Il6* in response to LPS stimulation consistent with a less inflammatory role, but this did not correspond with changes in peritoneal lavage or serum levels of Il6. Indeed, none of the cytokines assessed in the peritoneal lavage or the serum of treated mice (Il6, Il1β,Ccl2, TNFα) appeared to be altered, despite donor cells seemingly inhibiting neutrophil recruitment. A possible explanation for this phenomenon could be that by artificially increasing the number of phagocytes in the cavity LPS was more cleared and consequently, less neutrophils were recruited. Alternatively, dying transferred

cells could be altering the responsiveness of host macrophages to LPS stimulation. Due to time constraints, I did not carry out additional studies to exclude these possibilities. A potential follow-up experiment would be to adoptively transfer equivalent numbers of non-phagocytic peritoneal cells, such as T cells, into naïve mice followed by LPS stimulation to ascertain whether adoptive transfer of cells, irrespective of cell type, modulates LPS responsiveness If no changes are found, this would indicate that the altered neutrophil recruitment observed is due to an expanded phagocyte population.

In summary, the data presented here indicate discrete LPS responsiveness of Mo^{Z10}-LPM compared to RM^{Z10}-LPM *in vitro* and *in vivo*. These findings highlight that the impact Mo^{Z10}-LPM may have on the cavity as a whole during subsequent inflammatory stimuli remains unclear.

On the whole the post-LPS transcriptional profile of Mo^{Z10}-LPM seemingly indicated an impaired ability to respond to LPS, as all LPS-driven gene differences were due to impaired expression by Mo^{Z10}-LPM. This was surprising as expression of TLR4 was equivalent between RM^{Z10}-LPM and Mo^{Z10}-LP, although the latter did express lower levels of genes encoding for TLR4 accessory proteins (e.g *CD14*, *CD55*). Moreover, Mo^{Z10}-LPM expressed lower levels of *Fcgr1* and *Fcgr3.* Complete Fcgr ligation has been shown to promote an anti-inflammatory profile in macrophages and increase Il10 production [184] whereas loss Fcgr3 is thought to inhibit the responsiveness of peritoneal macrophages to LPS *in vitro*[185].

One key shortcoming of both the *in vitro* and *the vivo* experiments presented in this chapter is that the antibodies for Tim4 and Sema4a that were used to purify RM^{Z10}-LPM and Mo^{Z10}-LPM, or their naïve counterparts, are blocking antibodies[110,186]. When carrying out these experiments I thought this to be of little importance as Tim4 and Sema4a are involved in clearance of apoptotic cells and T cell activation respectively[110,186] and are unlikely to affect the early responsiveness to LPS *in vitro* or *in vivo.* However, with recent work identifying

Tim4 as a scavenger receptor, involved in the clearance of LPS[187], the results from my experiments should be interpreted with care as the response of $Tim4^+$ RM-LPM and RM^{Z10}-LPM could be altered and ideally should be repeated utilizing alternative antibodies to purify the cell populations of interest.

Combined the data presented in this chapter indicate that monocyte-derived LPM are functionally distinct from their resident counterparts, irrespective of whether they have differentiated under naïve or inflammatory conditions. Consequently, zymosan-induced peritonitis exacerbates the degree of functional heterogeneity of the steady-state cavity by driving integration of large numbers of monocyte-derived macrophages. The altered functionality of monocyte-derived LPM is apparent under steady-state conditions with high levels of baseline proliferation by monocyte-derived LPM, but becomes more apparent during subsequent stimulation when monocyte-derived LPM are on the whole less phagocytic and seemingly more anti-inflammatory than their resident counterparts. However, exactly how the expanded monocyte-derived LPM population affects the response of the peritoneal cavity to subsequent inflammatory insults remains unclear.

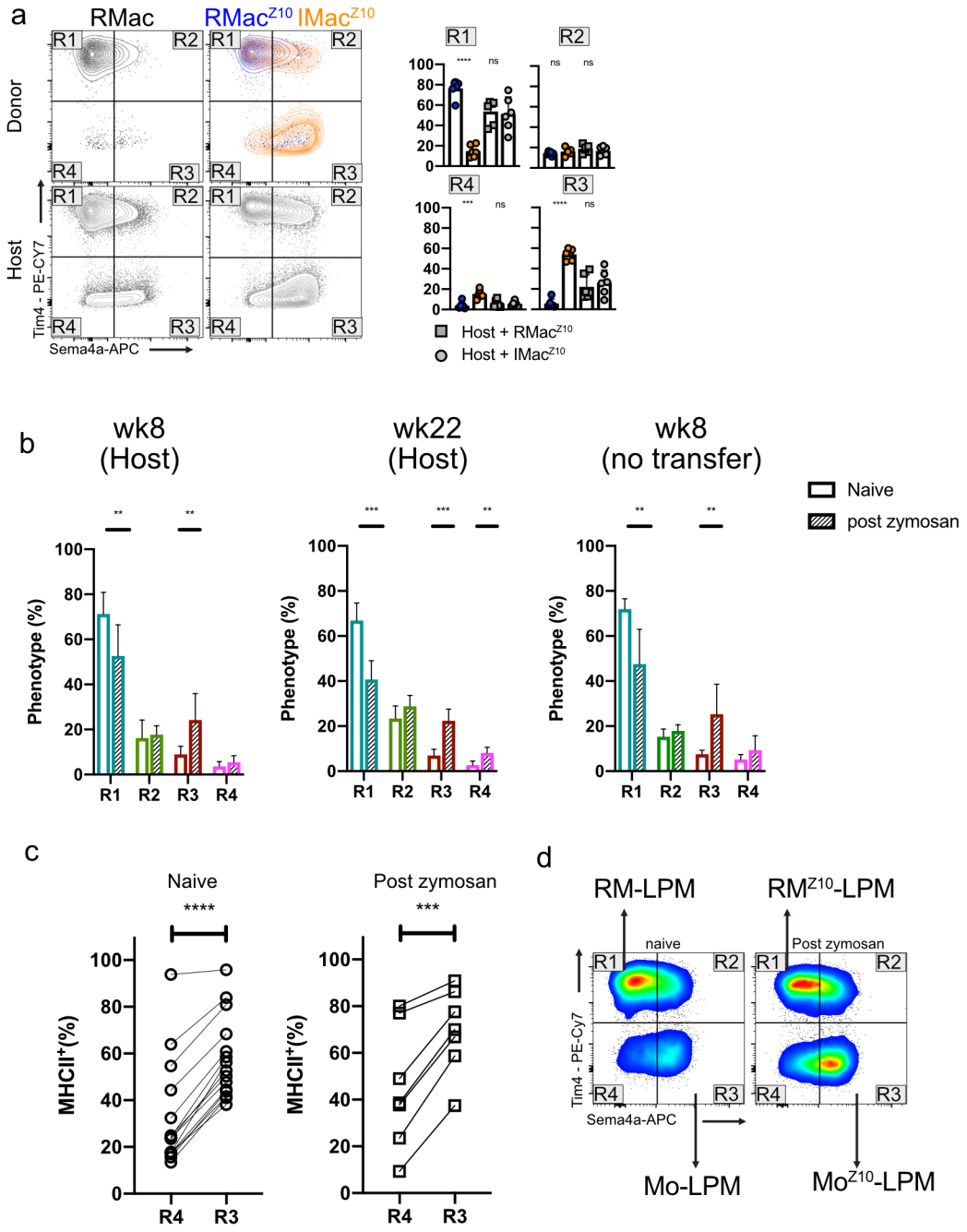

Figure 6.1 Identification of RM-LPM and Mo-LPM on the basis of Tim4 and Sema4a expression.

(a) Proportion of donor RMac^{Z10} (blue, n=6) and IMac^{Z10} (orange, n=6) with an (R1) Sema4a^{LO}Tim4, (R2) Sema4a^{HI}Tim4^{+}, (R3) Sema4a^{Hi}Tim4^{-} or (R4) Sema4a^{Lo}Tim4^{-} expression profile, 8 weeks after transfer into native recipients. Below host F4/80^{Hi} MHCII^{Lo} macrophages split into the same quadrants are shown in grey.***p<0.001, ****p<0.0001 determined by one-way

ANOVA followed by Tukey's multiple comparisons test **(b)** Proportion of host macrophages (as shown in a) with an (R1) Sema4a^{LO}Tim4, (R2) Sema4a^{HI}Tim4^{+}, (R3) Sema4a^{Hi}Tim4^{-} or (R4) Sema4a^{Lo}Tim4^{-} expression profile, 8 weeks after low-dose zymosan treatment (naïve =6, zymosan treated =12) or 22 weeks after low-dose zymosan treatment (graph in the middle; naïve = 4, zymosan treated 10). Graph to the right, host macrophages with an (R1) Sema4a^{LO}Tim4, (R2) Sema4a^{HI}Tim4^{+}, (R3) Sema4a^{Hi}Tim4^{-} or (R4) Sema4a^{Lo}Tim4^{-} expression profile, 8 weeks after low-dose zymosan treatment, without adoptive transfer (naïve=15, zymosan treated = 8). ***p<0.001**p<0.01 determined by repeated student's t test followed by Holm-Sidak correction. **(c)** Proportion of Sema4a^{Lo}Tim4^{-} (R4) and Sema4a^{Hi}Tim4^{-} (R3) that express MHCII, in naïve mice (n=15) or mice treated with zymosan 8 weeks earlier (n=7). ***p<0.001****p<0.0001, paired student's t test. **(d)** Representative gating strategy and expression of Tim4 and Sema4a on LPM sourced from naïve or mice treated with zymosan 8 weeks earlier. Data shown as mean ± standard deviation. Each symbol represents an individual animal. Data were pooled from at least 2 independent experiments.

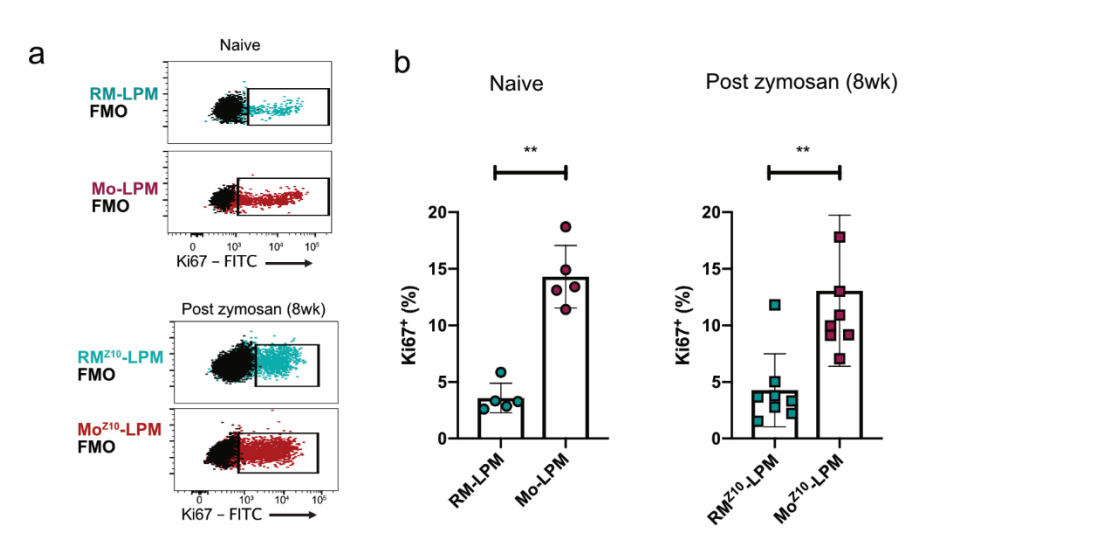

Figure 6.2 Monocyte-derived macrophages exhibit heightened baseline proliferation.

(a) Representative Ki76 antibody staining on on RM-LPM (teal)/Mo-LPM(red) sourced from naïve mice (top) or RM^{Z10}-LPM(teal)/Mo^{Z10}-LPM(red) sourced from mice treated with low dose zymosan 8 weeks prior (bottom). **(b)** Proportion of RM-LPM and Mo-LPM sourced from naïve mice (n=5) that are Ki67^{+}. To the right, proportion of RM^{Z10}-LPM and Mo^{Z10}-LPM sourced from mice treated 8 weeks prior with zymosan (n=8) that are Ki67^{+}. **p<0.001, students t test. Data shown as mean ± standard deviation. Each symbol represents an individual animal. Data were pooled from 2 independent experiments.

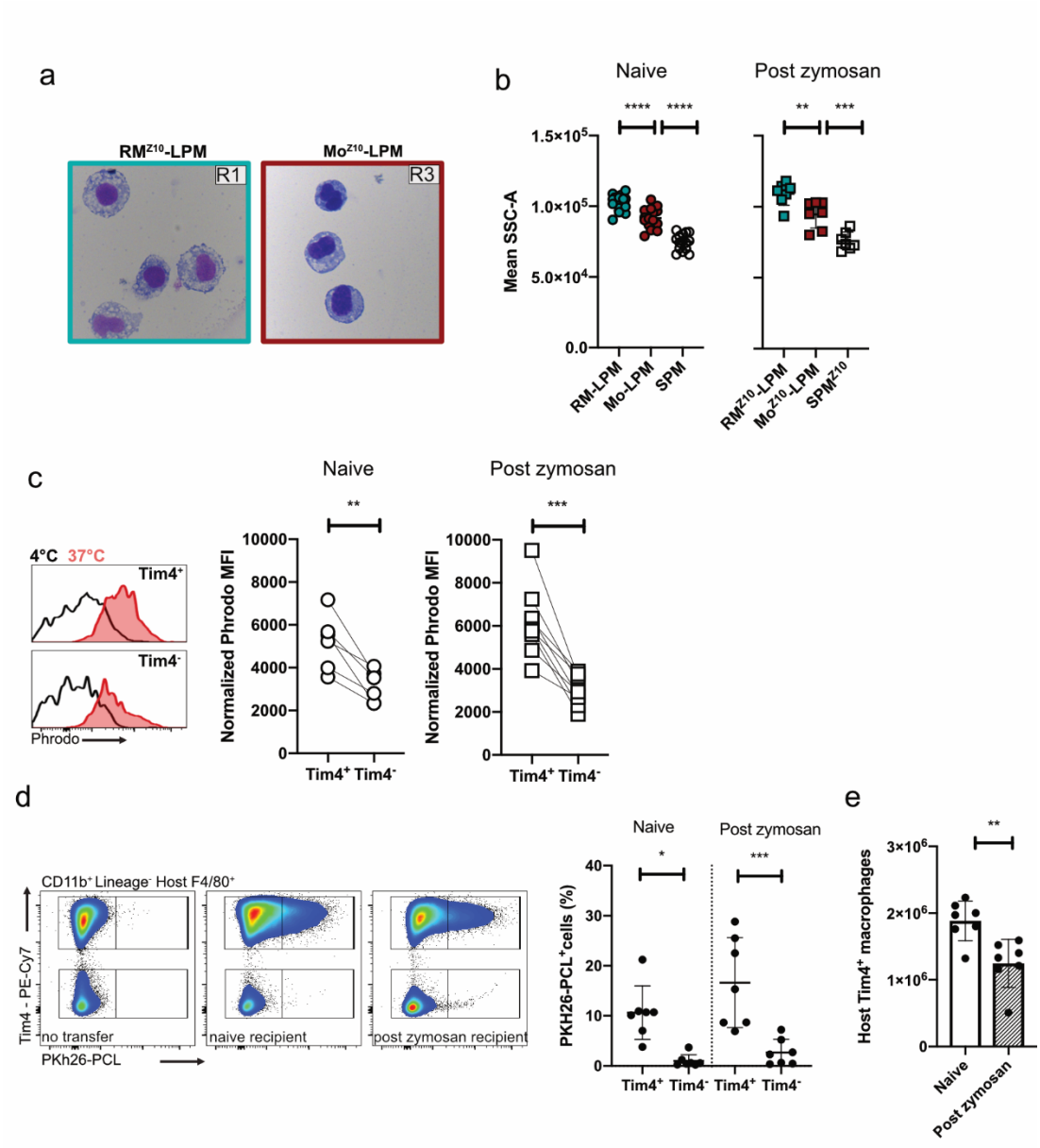

Figure 6.3 Monocyte-derived macrophages are less granular and phagocytic than embryonically-seeded macrophages.

(a) Morphological appearance of FACS purified RM^{Z10}-LPM and Mo^{Z10}-LPM sourced 8week after zymosan treatment. **(b)** Mean side-scatter of RM-LPM, Mo-LPM and SPM (n=5), sourced from naïve mice. To the right, mean side-scatter of RM^{Z10}-LPM, Mo^{Z10}-LPM and SPM^{Z10}(n=8) sourced from mice 8 weeks after zymosan treatment. **p<0.01, ***p<0.001 ****p<0.0001, one way ANOVA followed by Tukey's multiple comparisons test. **(c)** Phagocytosis of Phrodo *E. coli* particles by Tim4^{+} and Tim4^{-} LPM sourced from naïve mice (n=6) or mice treated with zymosan, 8 week prior (n=9). Data is presented as

normalized Phrodo MFI (Phrodo MFI 37°C- Phrodo MFI 4°C). **p<0.01, ***p<0.001, paired student's t test. **(d)** Proportion of F4/80^{+}Tim4$^{+/-}$ host macrophages that are PKH26-PCL labelled, 8 days after transfer of PKH26-PCL^{+} RMac^{Z10} into naïve recipient mice (n=7) or zymosan pre-treated recipient mice (n=7). *p<0.05***p<0.0001, one way ANOVA followed by Sidak multiple comparison test. **(e)** Number of F4/80^{+}Tim4$^{+\ host}$ macrophages, 8 days after receiving PKH26-PCL^{+} RMac^{Z10} (n=7). **p<0.01, student's t test. Data shown as mean ± standard deviation. Each symbol represents an individual animal. Data were pooled from 2 independent experiments.

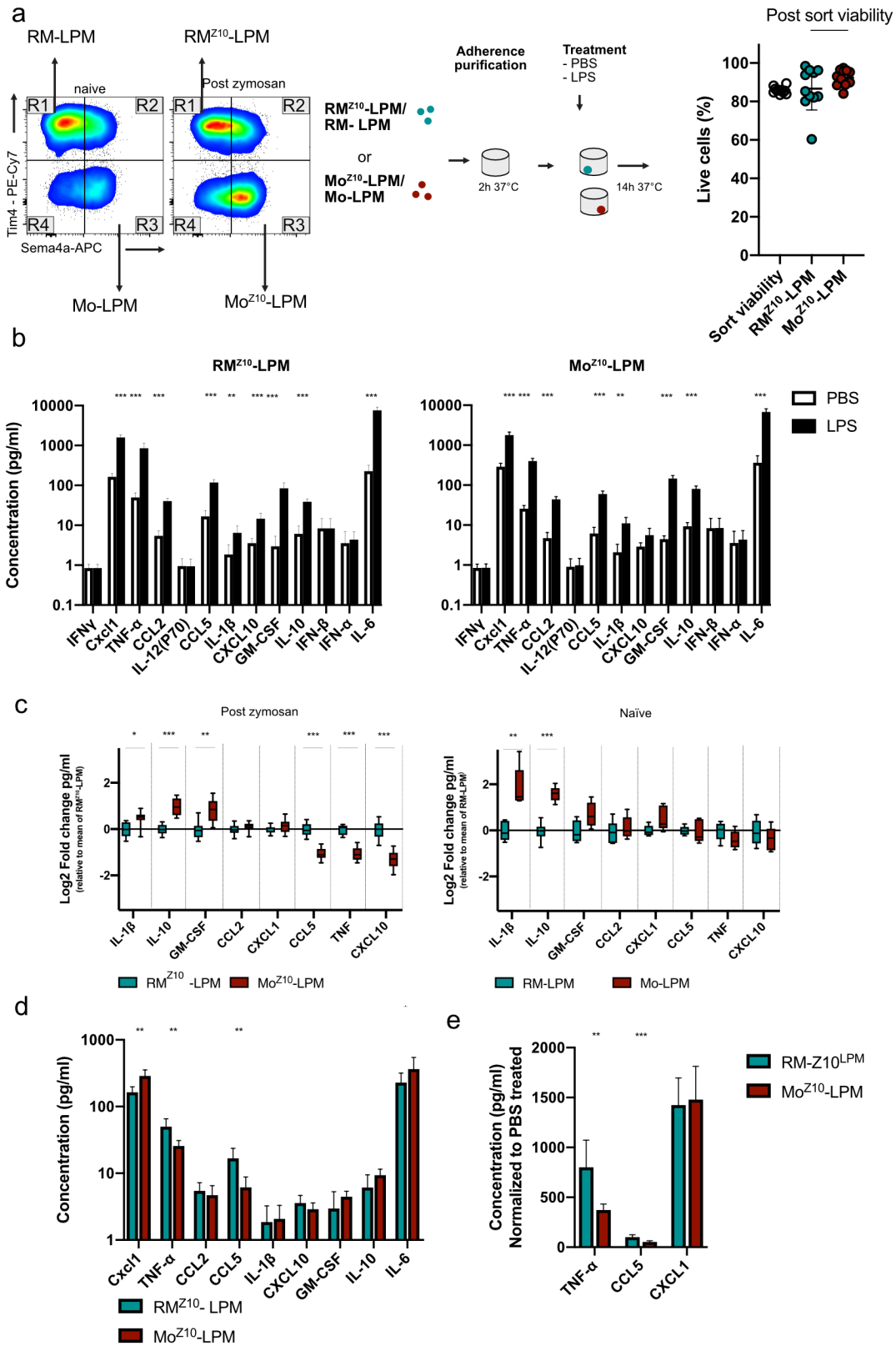
a
RM-LPM
RM^Z10-LPM
naive
Post zymosan
R1
R2
R3
R4
Tim4 - PE-Cy7
Sema4a-APC
Mo-LPM
Mo^Z10-LPM
RM^Z10-LPM/
RM- LPM
or
Mo^Z10-LPM/
Mo-LPM
Adherence
purification
Treatment
- PBS
- LPS
2h 37°C
14h 37°C
Post sort viability
Live cells (%)
Sort viability
RM^Z10-LPM
Mo^Z10-LPM
b
RM^Z10-LPM
Mo^Z10-LPM
PBS
LPS
Concentration (pg/ml)
IFNγ
Cxcl1
TNF-α
CCL2
IL-12(P70)
CCL5
IL-1β
CXCL10
GM-CSF
IL-10
IFN-β
IFN-α
IL-6
c
Post zymosan
Naïve
Log2 Fold change pg/ml
(relative to mean of RM^Z10-LPM)
(relative to mean of RM-LPM)
IL-1β
IL-10
GM-CSF
CCL2
CXCL1
CCL5
TNF
CXCL10
RM^Z10 -LPM
Mo^Z10-LPM
RM-LPM
Mo-LPM
d
Concentration (pg/ml)
Cxcl1
TNF-α
CCL2
CCL5
IL-1β
CXCL10
GM-CSF
IL-10
IL-6
RM^Z10- LPM
Mo^Z10-LPM
e
Concentration (pg/ml)
Normalized to PBS treated
TNF-α
CCL5
CXCL1
RM-Z10^LPM
Mo^Z10-LPM

Figure 6.4 Monocyte-derived macrophages are differentially responsive to LPS *in vitro.*

(a) Experimental outline for the purification and adherence of indicated macrophage subsets. To the right, post-sort viability of indicated macrophage subsets (n=8). **(b)** Assessed analytes in culture-supernatant of RM^{Z10}-LPM (left; n=8) and Mo^{Z10}-LPM (right; n=8), 14 hours after culture with PBS (white) or LPS (1ng/ml; black). **p<0.01 ***p<0.00, repeated student's t test followed by Holm-Sidak correction. Average theoretical lower and upper limits for: IFNγ (0.845-22802), CXCL1(1.805-27840), TNFα(2.835-63779.5), CCL2(3.51-20783), Il12(P70)(1.385-15563), CCL5(3.105-18512.5), Il1β(1.935-27838.5), CXCL10(2.35-16955), GM-CSF(2.285-31797), Il10(4.485-11829), IFNβ(6.665-31752), IFNα(2.32-15789.5), Il6(1.865-25500.5) **(c)** LPS-responsive analytes detected in culture-supernatant, 14 hours after culture of RM^{Z10}-LPM (n=8, teal) or Mo^{Z10}-LPM (n=8, red) with LPS (1ng/ml). Results are presented as log2 fold change relative to mean concentration detected in RM^{Z10}-LPM supernatant. Data are presented with a box-and-whiskers plot. To the right, LPS-responsive analytes detected in culture-supernatant, 14 hours after culture of RM-LPM (n=6, teal) or Mo-LPM (n=5, red) with LPS (1ng/ml). Results are presented as log2 fold change relative to mean concentration detected in RM-LPM supernatant. Data are presented with a box-and-whiskers plot.*p<0.05 **p<0.01***p<0.001, repeated student's t test followed by Holm-Sidak correction. **(d)** LPS-responsive analytes detected in culture-supernatant, 14 hours after culture of RM^{Z10}-LPM (n=8, teal) or Mo^{Z10}-LPM (n=8, red) with PBS (1ng/ml) **p<0.01 ***p<0.001, repeated student's t test followed by Holm-Sidak correction. **(e)** Supernatant levels of TNFα, CCL5, CXCL1, 14 hours after culture of RM^{Z10}-LPM (n=8, teal) or Mo^{Z10}-LPM (n=8, red) with LPS (1ng/ml), normalized to PBS-treated baseline levels. **p<0.01 ***p<0.001, repeated student's t test followed by Holm-Sidak correction. Data shown as mean ± standard deviation. Data were pooled from 2 independent experiments.

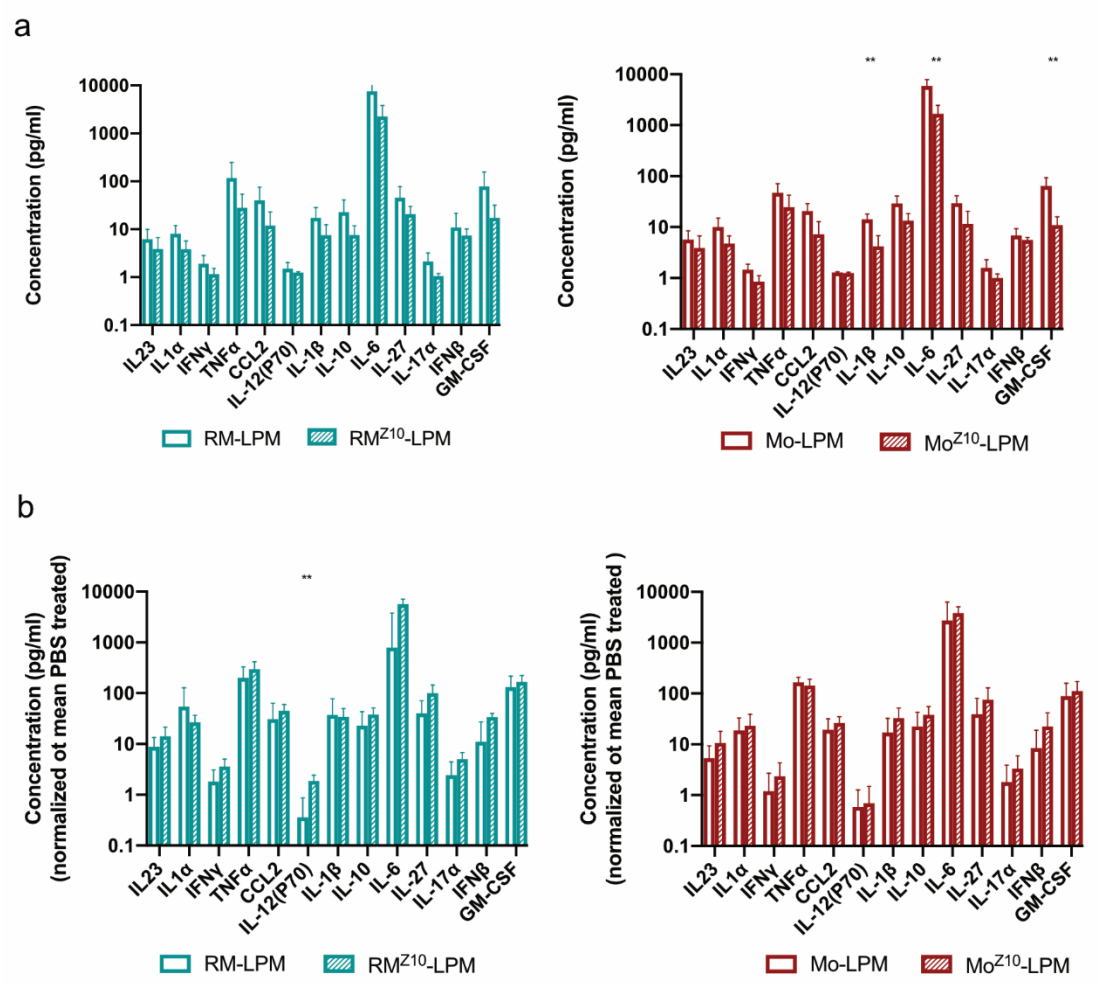

Figure 6.5 Zymosan-induced inflammation does not alter LPS-responsiveness of peritoneal macrophage subsets.

(a) Detected analytes in culture-supernatant of RM-LPM (n=6) or RM^{Z10}-LPM (n=6), 14 hours after culture with PBS. To the right, detected analytes in culture-supernatant of Mo-LPM (n=6) or Mo^{Z10}-LPM (n=6), 14 hours after culture with PBS. **p<0.01, repeated student's t test followed by Holm-Sidak correction. Average theoretical lower and upper limits for: Il23 (0.895-17752), Il1α(0.715-1204851), IFNγ(0.685-24636), TNFα(0.58- 90569.5),CCL2(0.63-95197.5), IL12(P70)(1.145-14185.5), Il1β(1.16-17233.5), Il10(0.8-31013.5), Il6(1.555-9623.5), Il27(1.215-17292), Il17a(0.73-27946.5), IFNβ(0.495-37763), GM-CSF(0.64-58259) **(b)** Detected analytes in culture-supernatant 14 hours after culture of RM-LPM (n=6) compared to RM^{Z10}-LPM (n=6) (left) and Mo-LPM (n=6) compared to Mo^{Z10}-LPM (n=6), with LPS (1ng/ml), normalized to mean PBS-treated baseline levels. **p<0.01, repeated student's t test

followed by Holm-Sidak correction. Data shown as mean ± standard deviation. Data were pooled from 2 independent experiments.

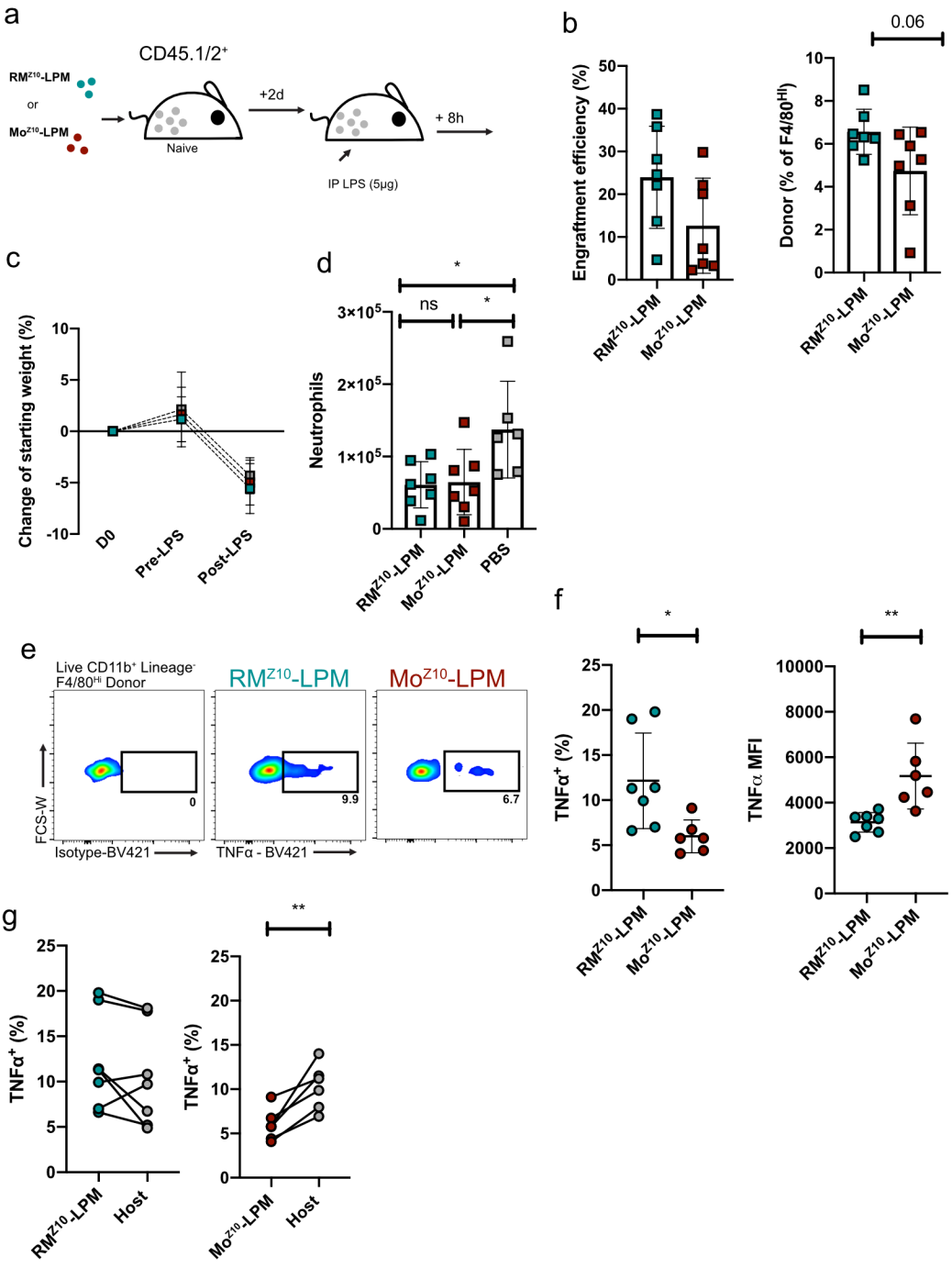

Figure 6.6 Monocyte-derived macrophages are differentially responsive to LPS *in vivo.*

(a) Experimental outline for the adoptive transfer of 250,000 RM^{Z10}-LPM or Mo^{Z10}-LPM (Gated as shown in 6.4a) or PBS into naïve recipient mice. Mice received a follow-up I.P injection with LPS (5µg) 2 days after cell transfer. **(b)** Engraftment efficiency of transferred RM^{Z10}-LPM and Mo^{Z10}-LPM. To the right,

proportion of F4/80^{Hi} MHCII^{Lo} macrophages that are of donor origin after indicated treatment. Statistical significance determined using student's t test. **(c)** Relative changes in body weight of treated mice, normalized to pre-experimental weight at D0. **(d)** Absolute number of Neutrophils present in the peritoneal cavity after PBS (n=6), RM^{Z10}-LPM (n=7) and Mo^{Z10}-LPM (n=7) transfer followed 2 days later by LPS-administration. *p<0.05 , one-way ANOVA followed by Tukey's multiple comparisons test. **(e)** Representative intracellular TNFα staining of RM^{Z10}-LPM and Mo^{Z10}-LPM, 8 hours following LPS administration. **(f)** Proportion of F4/80^{Hi} donor RM^{Z10}-LPM (n=7) and Mo^{Z10}-LPM (n=7) that express TNFα. To the right, normalized MFI of TNFα^{+} expression by RM^{Z10}-LPM (n=7) and TNFα^{+} Mo^{Z10}-LPM (n=7). *p<0.05 **p<0.01, student's t test. **(g)** Proportion of F4/80^{Hi} donor RM^{Z10}-LPM (n=7) and F4/80^{Hi} Mo^{Z10}-LPM (n=7) that express TNFα and the proportion of F4/80^{Hi} host macrophages that express TNFα in the same cavity. **p<0.01, paired student's t test. Data shown as mean ± standard deviation. Each symbol represents an individual animal. Data were pooled from 2 independent experiments.

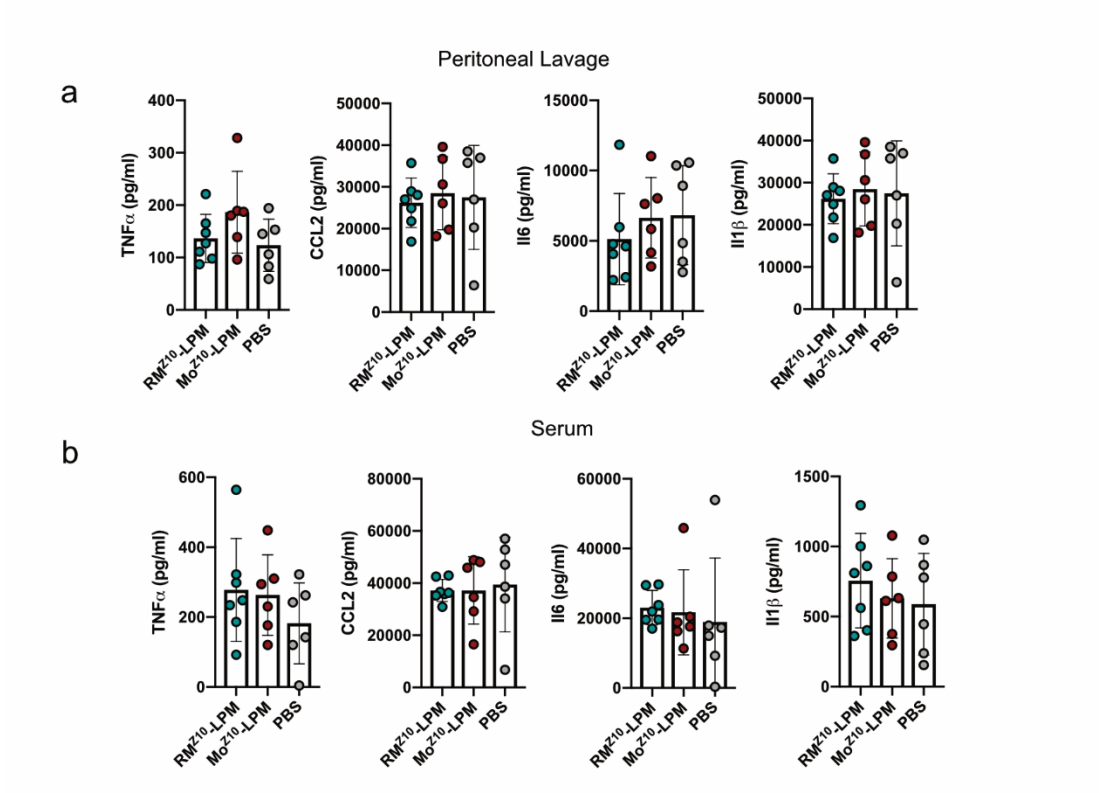

Figure 6.7 Transferred cells do not affect the systemic response to LPS. **(a)** Detected levels of TNfα, CCL2, Il6 and Il1β measured in the peritoneal lavage, 8 hours following LPS treatment of indicated groups (from the same experiment presented in Figure 6.6). **(b)** Detected levels of TNfα, CCL2,Il6 Il1β measured in the serum, 8 hours following LPS treatment of indicated groups. Theoretical detection limit for: TNfα (10-2500pg/ml), CCL2 (160-2500pg/ml), Il6 (40-2500pg/ml) and Il1β (20-2500pg/ml). Samples were collected by me and the assay was carried out by Dr. Georgia Perona Wright and Ms. Holly Webster. Data shown as mean ± standard deviation. Each symbol represents an individual animal. Data were pooled from 2 independent experiments.

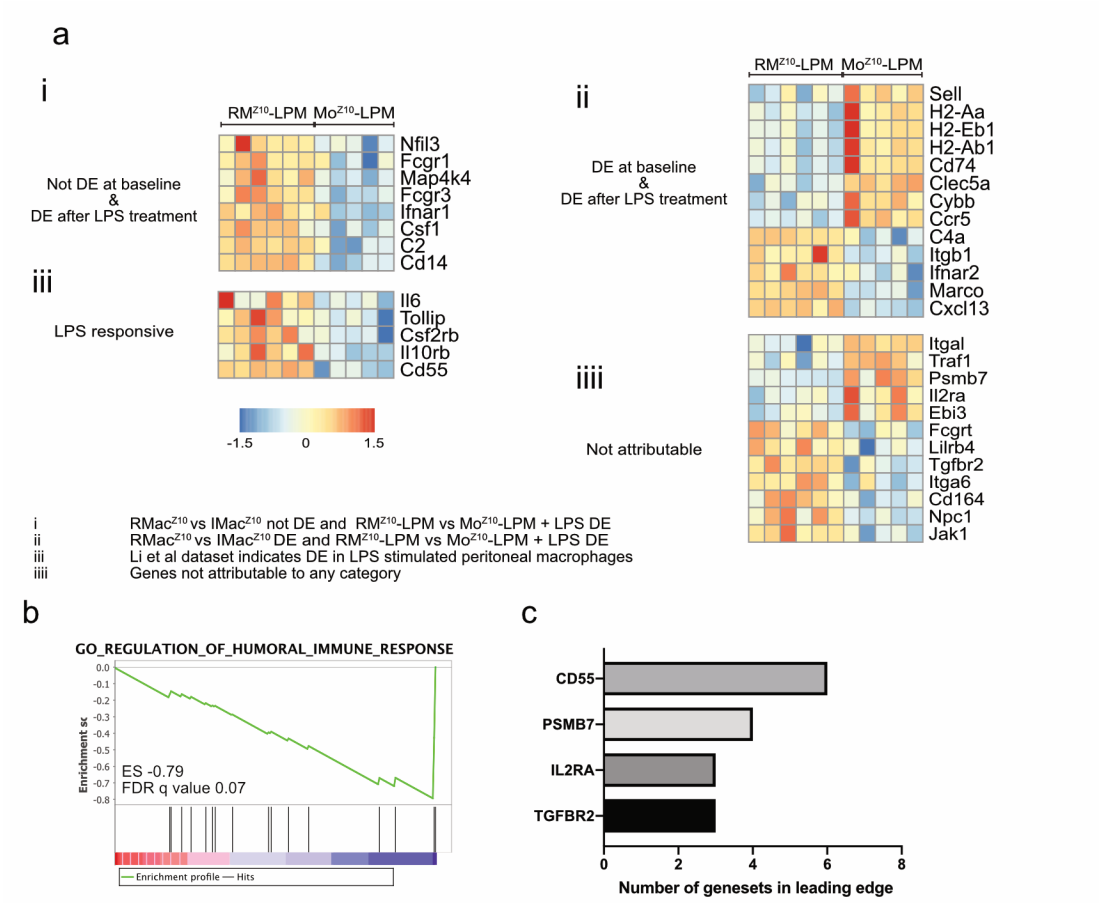

Figure 6.8 Monocyte-derived macrophages exhibit dampened transcriptional responsive to LPS.

(a) Expression of mRNA transcripts that are differentially expressed between RM^{Z10}-LPM and Mo^{Z10}-LPM, 8 hours following LPS treatment (from the same experiment presented in Figure 6.6). Data shown in the heatmaps has been split into (i) Genes not differentially expressed between RMac^{Z10} and IMac^{Z10} in prior analysis (Chapter 5), (ii) Genes known to be driven by LPS-stimulation on peritoneal macrophages *in vivo*[177], *(iii)* Genes that are differentially expressed between RMac^{Z10} and IMac^{Z10} in prior analysis (Chapter 5) and (iiii) Genes of which expression cannot be attributed to LPS stimulation. Categories are summarized below the heatmaps. **(b)** GSEA analysis of ranked genes expressed by RM^{Z10}-LPM and Mo^{Z10}-LPM, 8 hours following LPS treatment for the humoral immune response GO term. **(c)** Leading edge analysis of GO terms that were enriched (nominal p value <0.05) to detect genes overrepresented across GO terms that are more likely to be of biological importance.

Chapter 7

Assessing the survival and phenotype of inflammatory macrophages following severe peritonitis.

7.1 Introduction

Up to this point the main focus of my project was on the long-term survival, phenotype and functional profile inflammatory macrophages after mild peritonitis. Critically, following mild peritonitis a distinct population of macrophages with a resident F4/80^{hi} MHCII^{lo} phenotype persist through the inflammatory event (**Figure 3.1 & 3.6**)[144] whereas after higher doses of zymosan, these cells are largely lost (**Figure 3.1**)[64,87,111,120,139]. Recent work has indicated that formation of clots is the main mechanism responsible for macrophage disappearance after zymosan induced peritonitis[103]. Whether macrophages sequestered in clots undergo apoptosis or can be released from the clots and repopulate the cavity is unclear. In addition to the larger degree of disappearance of resident-like macrophages, the inflammatory microenvironment after high dose zymosan treatment is very different from that after low dose zymosan treatment. For example, after treatment with a high dose of zymosan (1000μg), the peritoneal cavity lavage fluid contains high levels of CCL5, a chemokine which is largely absent after injection of low dose zymosan (10μg)[122,188]. Moreover, injection of higher doses of zymosan (100μg/1000μg) leads to infiltration of the cavity by significantly higher numbers of neutrophils and monocytes compared to low dose zymosan (10μg) treatment[122,139]. Consequently, the macrophage compartment as a whole appears to be considerably expanded following the more severe inflammation induced by higher doses of zymosan[122,139].

As more severe peritonitis seemingly leads to almost complete loss of resident macrophages, this could allow inflammatory macrophages to adopt a more resident-like identity', somewhat similar to inflammatory macrophages transferred into clodronate-depleted recipients. Hence, I postulated that the long-term fate of inflammatory macrophages is likely dictated by the severity of the inflammatory event.

To investigate whether the severity of peritoneal inflammation indeed dictated inflammatory macrophage fate I aimed to ascertain if:

- Severe sterile peritonitis induced by high-dose zymosan leads to the complete loss of embryonically-seeded resident macrophages.
- Inflammatory macrophages infiltrating during severe peritonitis persist long-term and if they adopt a more complete resident phenotype than inflammatory macrophages after mild peritonitis.
- If severe inflammation alters the peritoneal macrophage niche, and consequently alters the fate and phenotype of the macrophages that inhabit the cavity.

7.2 Severe peritonitis leads to an influx of monocytes and neutrophils.

Numerous publications have described the macrophage compartment after zymosan peritonitis but few publications have directly compared the macrophage compartment after mild and severe peritonitis. Generally, it has been assumed that during severe peritonitis resident macrophages are almost completely lost. However, studies that investigate this phenomenon are not definitive, as they utilized a dye-labelling methodology or markers, such as, F4/80 and CD11B[122,162]. These studies did indicate that peritoneal inflammation led to an expansion of myeloid compartment, largely due to the influx of high numbers of monocytes that give rise to inflammatory macrophages[122,139,162].

To investigate if I was able to replicate the expansion of the peritoneal myeloid compartment following injection of high-dose of zymosan, and if the peritoneal myeloid-compartment contracts after resolution of inflammation, I carried out a time-course experiment to investigate the dynamics of macrophages numbers after low-dose (10μg) and high-dose (1000μg) zymosan treatment. To confirm that high-dose zymosan induced more severe peritonitis I enumerated the number of neutrophils at these timepoints. Similar to my earlier findings, by day 3 following low-dose zymosan treatment, the absolute

number of myeloid cells in the cavity had increased. During the succeeding 8 days the number of myeloid cells contracted back to pre-inflammation levels **(Figure 7.1a)**. After high-dose zymosan treatment, by day 3, the myeloid compartment was strikingly enlarged and, similar to low dose zymosan, contracted considerably in the succeeding 8 days. Following high dose zymosan treatment, the overall size of the myeloid compartment seemingly remained somewhat enlarged **(Figure 7.1a)**. Moreover, after high-dose zymosan treatment higher numbers of neutrophils where present by day 3 than after low-dose zymosan treatment, indicative of more severe inflammation. The number of neutrophils contracted considerably over the succeeding 8 days **(Figure 7.1b)**.

After high-dose zymosan treatment there appeared to be a complete loss of F4/80^{Hi} MHCII^{Lo} resident macrophages. This loss corresponded with a complete loss of Tim4^{+} macrophages by day 3 **(Figure 7.1c)**. By day 11, a clear population of Tim4^{+} macrophages had reappeared, despite the apparent absence of macrophages with a resident F4/80^{Hi} MHCII^{Lo} phenotype **(Figure 7.1c)**. This population seemingly expanded considerably during the succeeding weeks as by week 8 the population of Tim4^{+} macrophages was considerably larger (**Figure 7.1c)**.

As Tim4 is largely restricted to embryonic resident macrophages after mild peritonitis (**Figure 5.7b**), I set out to ascertain whether this reappearing Tim4^{+} fraction indeed consisted of repopulating embryonically-seeded resident macrophages. To investigate this, tissue-protected partial bone marrow chimeric mice were generated by my supervisor Dr. Steve Jenkins and Dr. Calum Bain. By day 17 after high-dose zymosan treatment, the chimerism of the entire myeloid compartment was equivalent to that of circulating monocytes **(Figure 7.2a,b)**, indicating that the entire compartment had been reconstituted by monocytes. After low-dose zymosan treatment there was a moderate increase in chimerism of the myeloid compartment by day 17, consistent with inflammatory macrophage integration shown in my adoptive

transfer studies, but this did not reach statistical significance. This lack of statistical significance was largely because the study was underpowered to detect smaller changes in chimerism. In addition, one datapoint in the low-dose treatment group had very low chimerism likely because of incomplete injection of zymosan **(Figure 7.2b, square datapoint)**.

Moreover, those Tim4^{+} macrophages present after high-dose zymosan were, contrary to Tim4^{+} macrophages found in naïve mice or after low-dose zymosan treatment almost exclusively of monocyte origin as indicated by a high degree of chimerism (**Figure 7.2c**). Hence, severe zymosan-induced peritoneal inflammations leads to complete loss of embryonically-seeded resident macrophages. Signals present shortly after severe peritoneal inflammation allow rapid acquisition of Tim4 by inflammatory monocyte-derived macrophages.

Note, during these experiments tissue-protected bone marrow chimeric mice were injected with the indicated dose of zymosan after 8 (**Figure 7.2b,c** datapoints in circles) or 26 weeks (**Figure 7.2b,c** datapoints in squares). The reason for this discrepancy was that COVID19 lockdown rules forced me to postpone zymosan treatment during the second iteration of the experiment.

7.3 Inflammatory macrophages persist after severe peritonitis and adopt a unique phenotype.

Having established that after high dose zymosan the entire macrophage compartment was replaced by monocyte-derived macrophages I set out to investigate if, similar to my earlier findings in mild peritonitis, inflammatory macrophages recruited during the acute inflammatory response persisted after severe peritonitis. To investigate this, 200,000 dye-negative F4/80^{Int} inflammatory macrophages were purified 3 days after injection of high-dose zymosan (IMac^{Z1000}) and adoptively transferred into equivalent severely inflamed recipients **(Figure 7.3a)**. In order to compare their phenotype and

survival with my earlier experimental findings, I adoptively transferred $RMac^{Z10}$ and $IMac^{Z10}$ purified 3 days after low-dose zymosan treatment into equivalent mildly inflamed recipients **(Figure 4.8a)**.

By 8 weeks post transfer all three donor populations had persisted but $IMac^{Z1000}$ had engrafted significantly poorer than $IMac^{Z10}$ or $RMac^{Z10}$ **(Figure 7.3b)**. Moreover, surviving $IMac^{Z1000}$ had universally adopted an $F4/80^{Hi}$ $MHCII^{Hi}$ phenotype, unlike either donor population after low-dose zymosan treatment **(Figure 7.3c)**. Importantly, $IMac^{Z1000}$ adopted a more resident-like identity as they expressed equivalent levels of GATA6 as $RMac^{Z10}$ **(Figure 7.3d)**. Since resident macrophages were completely lost after high dose zymosan **(Figure 7.2b,c)** the acquisition of high levels of GATA6 is likely due to lack of competition with resident macrophages in this setting. Using flow cytometry, I then investigated numerous markers that delineated $RMac^{Z10}$ and $IMac^{Z10}$ after mild peritonitis. This analysis revealed that $IMac^{Z1000}$ phenotype differed greatly from that of $IMac^{Z10}$ for almost every single marker assessed **(Figure 7.3e).** Notably, $IMac^{Z1000}$ expressed only low levels of CCR5 and Frβ ,both of which were identified as environment-dictated features of $IMAc^{Z10}$. Moreover, $IMac^{Z1000}$ also expressed strikingly higher levels of Tim4 than $IMac^{Z10}$ **(Figure 7.3e)**. This was surprising given that low expression of Tim4 by Mac^{Z10} was regulated independent of competition with resident macrophages, suggesting expression of this marker by $IMac^{Z1000}$ may instead arise due to alterations in the microenvironment **(Figure 7.3e)**. However, heightened Tim4 expression did not correspond to higher expression of other resident markers including VSIG4 and CXCL13, both largely absent on $IMac^{Z1000}$ **(Figure 7.3e)**.

Based on the combination of all these markers, the phenotype of $IMac^{Z1000}$ was indistinguishable from the phenotype of host macrophages in the same cavity **(Figure 7.4a,b)**. This contrasts with the situation following mild peritonitis as neither $RMac^{Z10}$ **(Figure 7.4a,c)** nor $IMac^{Z10}$ **(Figure 7.4a,d)** aligned perfectly with host macrophages, consistent with host cells containing

a mixture of both RMac^{Z10} and IMac^{Z10}. Consequently, by 8 weeks after high-dose zymosan host macrophages were, at the population level, phenotypically distinct from host macrophages after low-dose zymosan for every marker assessed **(Figure 7.4e)**. Moreover, the CD11b^{+} myeloid compartment remained somewhat enlarged by 8 weeks after severe peritonitis compared with the numbers found following mild peritonitis **(Figure 7.4f)**, as suggested by the time-course data previously **(Figure 7.1a)**. In addition, I found that the number of naïve CD62L^{+} T-cells[189,190] inhabiting in the cavity was significantly lower 8 weeks following high dose zymosan treatment, compared to mice treated with low dose zymosan (**Figure 7.4g**).

Combined these data indicate that severe peritoneal inflammation results in striking alterations to the peritoneal macrophage compartment by altering the origin, number and phenotype of phagocytes that inhabit the cavity.

7.4 Following severe peritonitis the peritoneal environment drives expression of MHCII and Tim4.

A surprising finding was that, during a period of inflammation that follows injection of high-dose zymosan, acquisition of Tim4 expression seemingly occurred independently of acquisition of a resident F4/80^{Hi} MHCII^{Lo} phenotype **(Figure 7.1c).** Even by 8 weeks after high-dose zymosan, when neutrophilic inflammation has seemingly resolved **(Figure 7.1b)**, IMac^{Z10} almost universally retained an MHCII^{Hi} phenotype whilst also largely acquiring expression of Tim4 **(Figure 7.3c,e)**. As F4/80 and MHCII were previously found to be rapidly responsive to retinoic acid and omentum factors respectively *in vitro,* I postulated that rapid acquisition of Tim4 in parallel with impaired F4/80 and heightened MHCII expression on infiltrating monocytes following severe inflammation arose from alterations in the cavity micro-environment.

To examine this, 400,000 RMac sourced from naïve mice were adoptively transferred into recipient mice treated with high-dose zymosan 3 days prior

(Figure 7.5a). By day 11, transferred RMac had acquired high levels of MHCII and had downregulated expression of F4/80 **(Figure 7.5b,c)**. On the basis of these markers, RMac appeared to be similar as monocyte-derived host macrophages **(Figure 7.5b)**. Moreover, transfer of $Tim4^{+}$ RMac inhibited acquisition of Tim4 by host cells as indicated by a drop in absolute numbers of $Tim4^{+}$ **(Figure 7.5d,left)**, but not $Tim4^{-}$ (**Figure 7.5d,right**) host macrophages. Hence, Tim4 expression appears to be driven by environmental cues after severe peritonitis and monocyte-derived macrophages are competitively disadvantaged from acquiring these cues compared to embryonically-seeded resident macrophages.

Combined, these data indicate that shortly after severe peritonitis the peritoneal microenvironment does not contain the factors, most likely retinoic-acid, required to maintain the $F4/80^{Hi}$ phenotype and contains factors that drive expression of MHCII and Tim4.

7.5 Sterile peritonitis leads to impaired B1 cell expansion.

One of the well-characterized functional markers seemingly not acquired by inflammatory macrophages irrespective of the severity of inflammation was CXCL13[97]. CXCL13 is a vital chemokine required for the homing of circulating B1 cells into peritoneal cavity. Genetic deletion of *Cxcl13* results in almost complete loss of peritoneal B1 cells[118] .Under homeostatic conditions the predominant source of CXCL13 is thought to be the resident peritoneal and omental macrophages[97,118], although recent work characterized a population of omental mesothelial cells that produce CXCL13[136]. Hence, I decided to investigate whether the number of B1 cells sequestered in the peritoneal cavity was altered following peritonitis and the resulting integration of CXCL13-deficient macrophages.

Indeed, the exaggerated loss of CXCL13-producing after severe peritonitis **(Figure 7.6a),** correlated with fewer peritoneal B1 cells **(Figure 7.6b)**. Previous

data in the lab had indicated that the number of peritoneal B1 cells increases with age. Hence, I postulated that the reduction of B1 cells 8 weeks after sterile peritonitis was due to an inability to sequester B1 cells in the cavity with time, rather than direct loss of B1 cells during the inflammatory event. To investigate this, I re-evaluated the time-course data and found that peritoneal B1 cells increased in number over an 8-week period in naïve mice but that this was marginally inhibited after mild peritonitis and completely abrogated after severe peritonitis **(Figure 7.6c)**.

An important function of peritoneal B1 cells is the production of natural antibodies, most notably against phosphorylcholine[118]. Recently, it was found that peritoneal B1 cells also produce natural antibodies against LPS-O127. Production of these antibodies is highly sex specific with higher levels of circulating antibodies in female mice compared to male mice[191].Hence, we investigated the levels of natural antibodies in the serum of mice 8 week after zymosan-induced peritonitis. The serum for these experiments was collected by me. The ELISA to detect natural antibodies to LPS-O127 and phosphorylcholine was carried out by Ms. Lucia Badiola Gomez and Dr. Steve Jenkins. This analysis indicated that 8 weeks after severe peritonitis the levels of serum IgG and serum IgM against LPS-O127 were unaltered **(Figure 7.6d)** but IgM against phosphorylcholine was increased after severe peritonitis and anti-phosphorylcholine IgG was detectable **(Figure 7.6d)**.

Combined, these data indicate that severe peritoneal inflammation has long-term systemic consequences by increasing levels of circulating natural antibodies against phosphorylcholine. This is likely resulting from altered levels of peritoneal CXCL13 and a failure to sequester B1 cells in the cavity.

7.6 Discussion

In this chapter I set out to investigate the survival and phenotype of inflammatory macrophages following severe peritonitis. Using tissue-protected

marrow chimeras I found that by 17 days after severe peritonitis the complete peritoneal macrophage compartment is replaced by monocyte-derived cells. Using the adoptive transfer approach, I found that at least some inflammatory macrophages present by day 3 of severe peritonitis survive long-term and adopt a phenotype unlike resident or inflammatory macrophages inhabiting the cavity after mild peritonitis at the same time. By week 8, IMac^{Z1000} adopted a more complete resident-like identity. Most notably, they expressed equivalent levels of GATA6 as established resident macrophages, and had completely downregulated CCR5 and FRβ, the latter of which is negatively regulated by GATA6[65]. However, despite adopting a more resident-like phenotype IMac^{Z1000} also retained strikingly high levels of MHCII. Phenotypically IMac^{Z1000} fully resembled the host macrophage compartment, indicating that, should monocytes recruited after day 3 also persist, the stage at which monocytes infiltrate the cavity after high-dose zymosan does not alter their phenotype. This is an important finding as the time of transfer that was chosen for these adoptive transfer experiments was not equivalent between low and high dose zymosan treated animals. Whereas by day 3 following low dose zymosan treatment inflammation is largely resolved, as indicated by resolution of neutrophilia, following high dose zymosan treatment there is still ongoing inflammation and neutrophilia is still present at this time. Consequently, the divergent engraftment efficiency of IMac^{Z10} and IMac^{Z1000} could simply be an effect of the stage of inflammation the donor populations were transferred at. Hence, although the phenotype of macrophages following high dose zymosan treatment appears unaltered by the stage at which monocyte infiltrate the cavity it is possible that the poorer engraftment efficiency of IMac^{Z1000} may be due to their transfer into more inflamed recipients. Additional adoptive transfer experiments to investigate whether the engraftment efficiency of IMac^{Z1000} carried out at a timepoint at which high dose zymosan-induce peritonitis is resolved (i.e. around day 11-17) could prove useful and would be more comparable to the engraftment efficiency calculated for IMac^{Z10} in the current experiments.

In these adoptive transfer experiments, I also found that persistent IMac^{Z1000} expressed significantly higher levels of Tim4 than IMac^{Z10}. This was surprising as I had previously identified that Tim4 expression was a cell-intrinsically driven feature, largely absent on IMac^{Z10} that is slowly acquired with time. Gain of Tim4, at least by part of the inflammatory macrophages, appeared to occur relatively shortly after severe peritonitis as tissue-protected chimeras indicated a monocyte origin of Tim4^{+} macrophages present at day 17**.** Moreover, transferred resident macrophages were unable to maintain their resident phenotype during this period and universally adopted an 'inflammatory like' F4/80^{Int}MHCII^{Hi} phenotype. My earlier findings indicated that MHCII expression was not acquired by resident macrophages *in vitro* after removing them from the cavity micro-environment, suggesting that the MHCII^{lo} phenotype of RMac does not depend on continual exposure to inhibitory signals. Hence, these data support the hypothesis that following high-dose zymosan treatment, the peritoneal micro-environment contains factors driving MHCII expression. Moreover, donor RMac retained Tim4 expression following transfer, and their presence inhibited acquisition of Tim4 by host macrophages. Combined these data suggest that severe peritonitis leads to changes in the peritoneal micro-environment that temporarily inhibit macrophages from acquiring a resident-like phenotype F4/80^{Hi} phenotype, but drive expression of Tim4 and MHCII.

Unlike after mild peritonitis the enlarged myeloid compartment remained somewhat expanded after severe peritonitis, indicating a long-term expansion of the peritoneal macrophage niche. Despite this expansion, the number of cells that produce the B1 cell chemoattractant CXCL13 was reduced considerably. Moreover, peritoneal B1 accumulation was abrogated after severe peritoneal inflammation, likely due to the inability of monocyte-derived macrophages produce CXCL13. Surprisingly, this loss of peritoneal B1 cells corresponded with increased levels of natural antibodies against phosphorylcholine. Although peritoneal B1 cells are thought to produce natural antibodies[191], production is much higher by B1 cells in the bone marrow and

the spleen[192]. Hence, a possible explanation for the increase in serum phosphorylcholine IgM in my experiments could be an inability to sequester B1 cells in the cavity and consequent accumulation of B1 cells in the spleen, a tissue more permissive of natural antibody production. Unfortunately, during my studies I did not investigate accumulation of B1 cells in other tissue-sites. To examine this hypothesis, the number of B1 cells in the spleen and bone marrow and their capacity to produce natural antibodies following severe peritoneal inflammation should be investigated.

The data presented in this chapter highlight that the degree of peritoneal inflammation is directly correlated with the degree of resident macrophage disappearance during acute inflammation and impacts the survival and phenotype of inflammatory macrophages. Moreover, after severe peritonitis the peritoneal niche does not effectively maintain a resident phenotype and drives aberrant MHCII expression. Whereas ineffective maintenance of the resident phenotype appears is a temporary phenomenon, aberrant MHCII expression is a long-term feature. Moreover, severe peritoneal inflammation leads to a long-term inability to sequester B1 cells in the peritoneal cavity and enhances levels of circulating natural antibodies against phosphorylcholine.

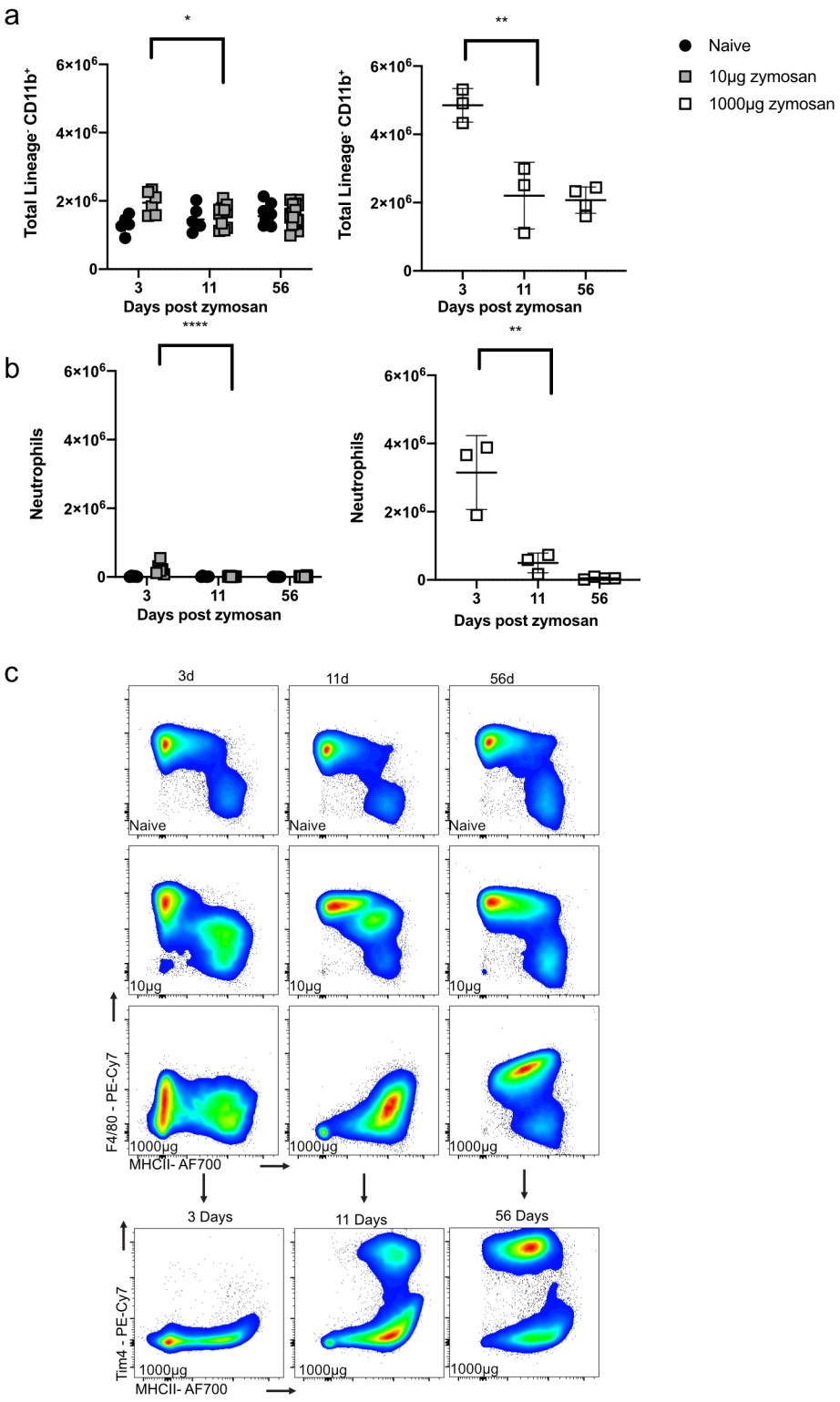

Figure 7.1 Macrophage and neutrophil dynamics after zymosan-induced peritonitis.

(a) Absolute number of $CD11b^+$ $Lineage^-$ myeloid cells at indicated timepoints in naïve mice (n= 5,6,10, for each time point respectively), mice treated with 10μg (n=6,11,20, for each time point respectively) or 1000μg (n=3,3,4, for each time point respectively) of zymosan. *p<0.05, **p<0.01. Statistical significance for naïve and 10μg zymosan treated mice was determined using two-way ANOVA followed by post hoc Tukey test. For 1000μg zymosan statistical significance was determined by one-way ANOVA followed by post hoc Tukey test. **(b)** Absolute number of neutrophils at indicated timepoints in naïve mice (n= 5,6,10), mice treated with 10μg zymosan (n=6,11,20) and mice treated with 1000μg zymosan (n=3,3,4) **p<0.01, ****p<0. Statistical significance for naïve and 10μg zymosan treated mice was determined using two-way ANOVA followed by post hoc Tukey test. For 1000μg zymosan treated mice, statistical significance was determined by one-way ANOVA followed by post hoc Tukey test. **(c)** Representative expression levels of F4/80,MHCII and Tim4 (bottom) by peritoneal $CD11B^+$ $Lineage^-$ myeloid cells at indicated timepoints in naïve or zymosan treated animals. Data shown as mean ± standard deviation. Each symbol represents an individual animal. Data for naïve and 10μg zymosan treated animals were pooled from 2 independent experiments.

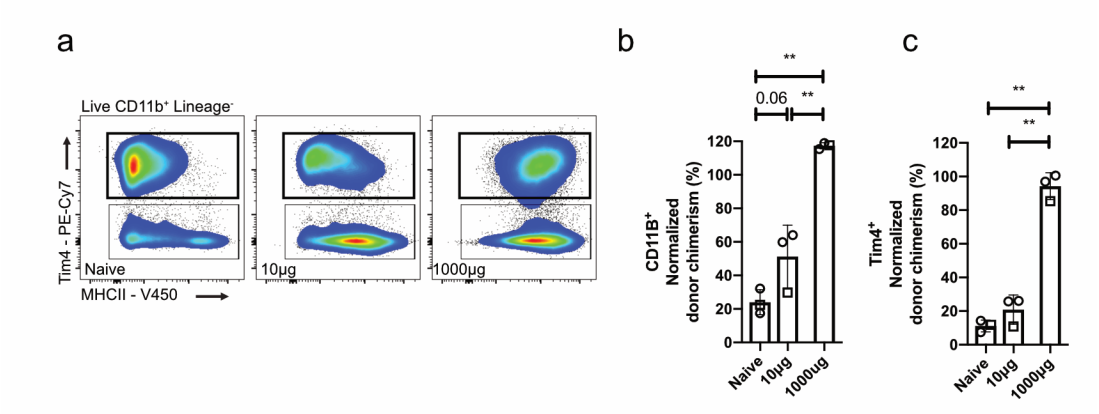

Figure 7.2 High dose zymosan leads to replacement of peritoneal macrophages by monocyte-derived macrophages.

(a) Representative Tim4 and MHCII expression by CD11B^{+}Lineage^{-} myeloid cells, 17 days after tissue-protected BM chimeric mice were injected with the indicated dose of zymosan. **(b)** Normalized donor chimerism of myeloid cells, 17 days after tissue-protected BM chimeric mice were injected with the indicated dose of zymosan. Chimerism was normalized to the chimerism detected in circulating Ly6C^{Hi} monocytes as described in the M&M. Tissue-protected BM chimeric mice were injected with zymosan 8 weeks after irradiation (circle) or 26 weeks after irradiation (square) **p<0.01 determined by one-way ANOVA and Tukey's multiple comparisons test **(c)** Normalized donor chimerism of Tim4^{+} macrophages, 17 days after tissue-protected BM chimeric mice were injected with the indicated dose of zymosan. Tissue-protected BM chimeric mice were injected with zymosan 8 weeks after irradiation (circle) or 26 weeks after irradiation (square) **p<0.01 determined by one-way ANOVA followed by Tukey's multiple comparisons test. Data shown as mean ± standard deviation. Each symbol represents an individual animal. Data were pooled from 2 independent experiments.

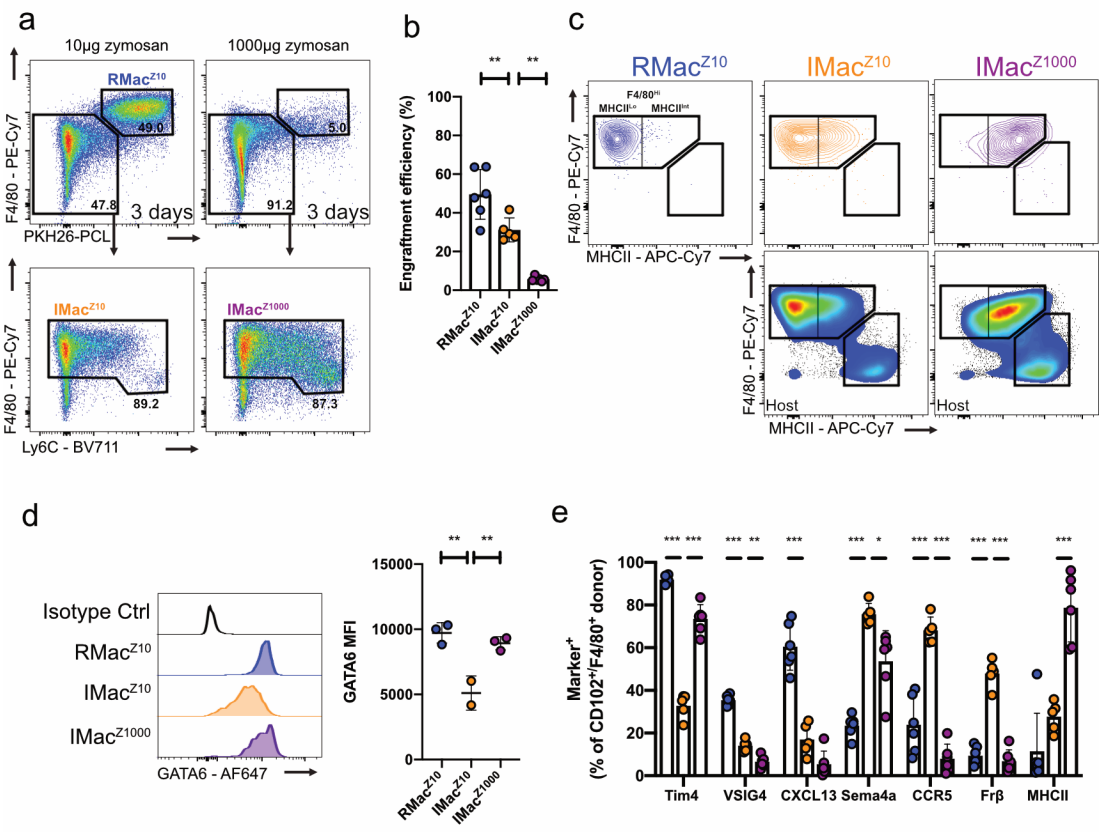

Figure 7.3 Inflammatory macrophages persist after severe peritonitis.

(a) Representative expression of of F4/80 and Ly6c in conjunction with PKH26-PCL dye labelling and gating strategy to identify RMac^{Z10}, IMac^{Z10} 3 days after low dose zymosan(10µg) treatment and IMac^{Z1000} 3 days after high dose zymosan (1000µg) treatment. **(b)** Engraftment efficiency of RMac^{Z10} (n=6), IMac^{Z10} (n=5), and IMac^{Z1000} (n=6), 8 weeks after transfer into mirroring inflamed recipient mice. **p<0.01, one-way ANOVA followed by Tukey's multiple comparisons test. Engraftment efficiency was calculated on the basis of absolute numbers as described in the M&M **(c)** Representative expression of F4/80 and MHCII on indicated donor (top) and host (bottom) macrophage populations, 8 weeks after indicated treatment. **(d)** GATA6 MFI on RMac^{Z10}, IMac^{Z10} and IMac^{Z1000} ,8 weeks following transfer into mirroring inflamed recipients (n=3,2,3 for each population respectively). **p<0.01, one-way ANOVA followed by Tukey's multiple comparisons test. **(e)** Proportion of donor CD102^{Hi}/F4/80^{Hi} RMac^{Z10} (blue), IMac^{Z10} (orange) or IMac^{Z1000} (purple), 8 weeks after transfer into mirroring inflamed recipient mice that express markers of interest (n=6,5,6 for each population respectively).*p<0.05

**p<0.01 ***p<0.001, one-way ANOVA followed by Dunnet's multiple comparisons test for each marker individually, followed by Bonferroni adjustment. Data shown as mean ± standard deviation. Each symbol represents an individual animal. Data were pooled from 3 independent experiments, except (d) which was pooled from 2 independent experiments.

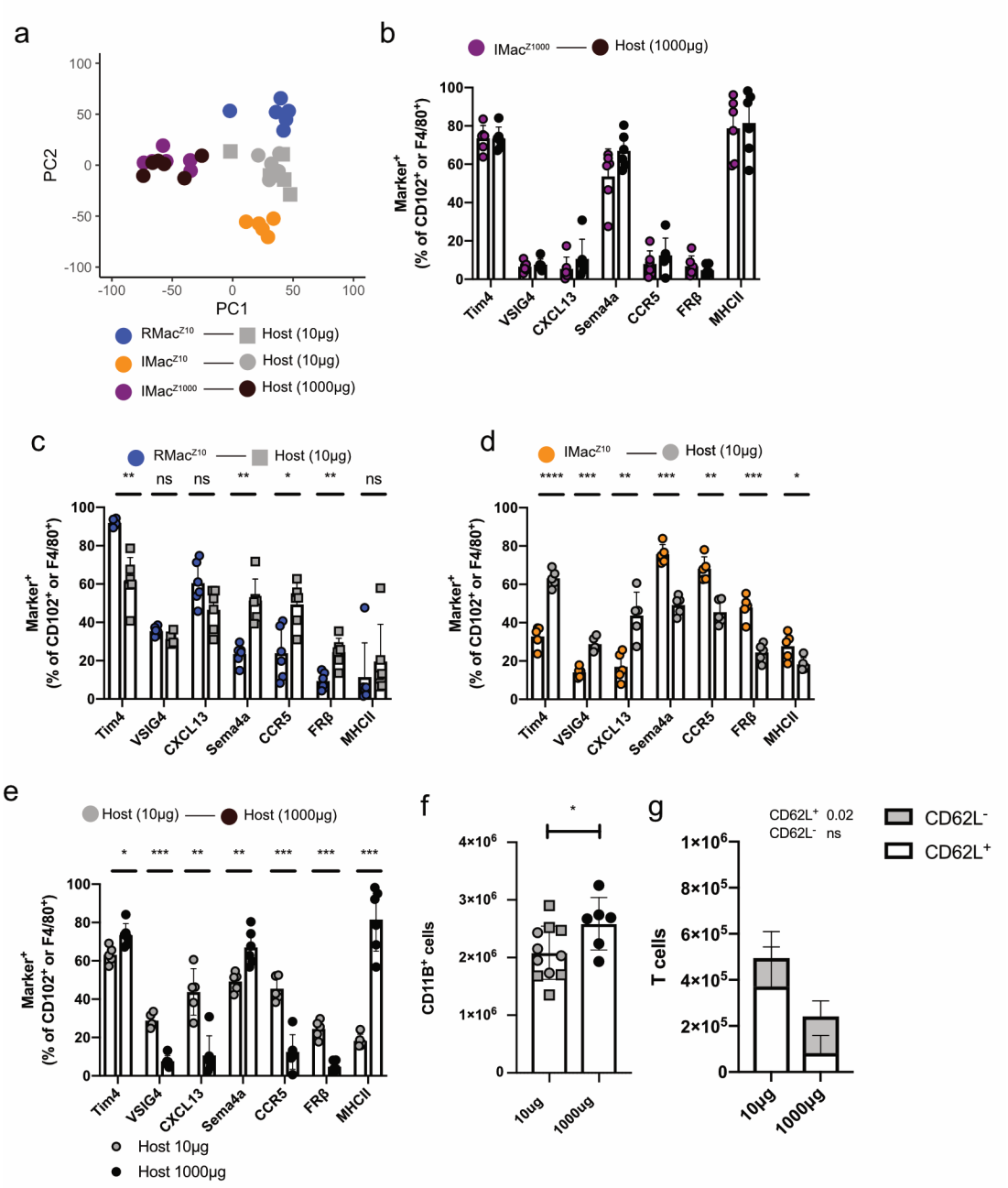

Figure 7.4 Persistent inflammatory macrophages after severe peritonitis are phenotypically unique.

(a) Principal component analysis of donor RMac^{Z10}, IMac^{Z10} and IMac^{Z1000} and F4/80^{Hi}/CD102^{Hi} host macrophages in the same mice. Principal components were calculated on based on the markers presented in Figure 6.3e. **(b)** Proportion of donor CD102^{Hi}/F4/80^{Hi} donor IMac^{Z1000}(n=6) and CD102^{Hi}/F4/80^{Hi} host macrophages in the same cavity that express markers

of interest 8 weeks after adoptive transfer. **(c)** Proportion of $CD102^{Hi}/F4/80^{Hi}$ donor $RMac^{Z10}$ (n=6) and $CD102^{Hi}/F4/80^{Hi}$ host macrophages in the same cavity that express markers of interest 8 weeks after adoptive transfer. *p<0.05 **p<0.01 ***p<0.001, repeated student's t test with Holm-Sidak correction. **(d)** Proportion of $CD102^{Hi}/F4/80^{Hi}$ donor $IMac^{Z10}$ (n=5) and $CD102^{Hi}/F4/80^{Hi}$ host macrophages that express markers of interest 8 weeks after adoptive transfer. *p<0.05 **p<0.01, repeated student's t test with Holm-Sidak correction. **(e)** Proportion of $CD102^{Hi}/F4/80^{Hi}$ host macrophages 8 weeks after treatment with low dose zymosan (n=6, grey) or high dose zymosan (n=6, black) that express markers of interest. *p<0.05 **p<0.01 ***p<0.001, repeated student's t test with Holm-Sidak correction. **(f)** Absolute number of $CD11B^{+}$ $lineage^{-}$ myeloid cells, 8 weeks after treatment with low dose zymosan (n=12) or high dose zymosan (n=6). *p<0.05, student's t test. **(g)** Absolute number of $CD62L^{+}/CD62L^{-}$ T cells, 8 weeks after treatment with low dose zymosan (n=12) or high dose zymosan (n=6). Statistical significance determined using repeated t test with Holm-Sidak correction. Data shown as mean ± standard deviation. Each symbol represents an individual animal. Data were pooled from 3 independent experiments.

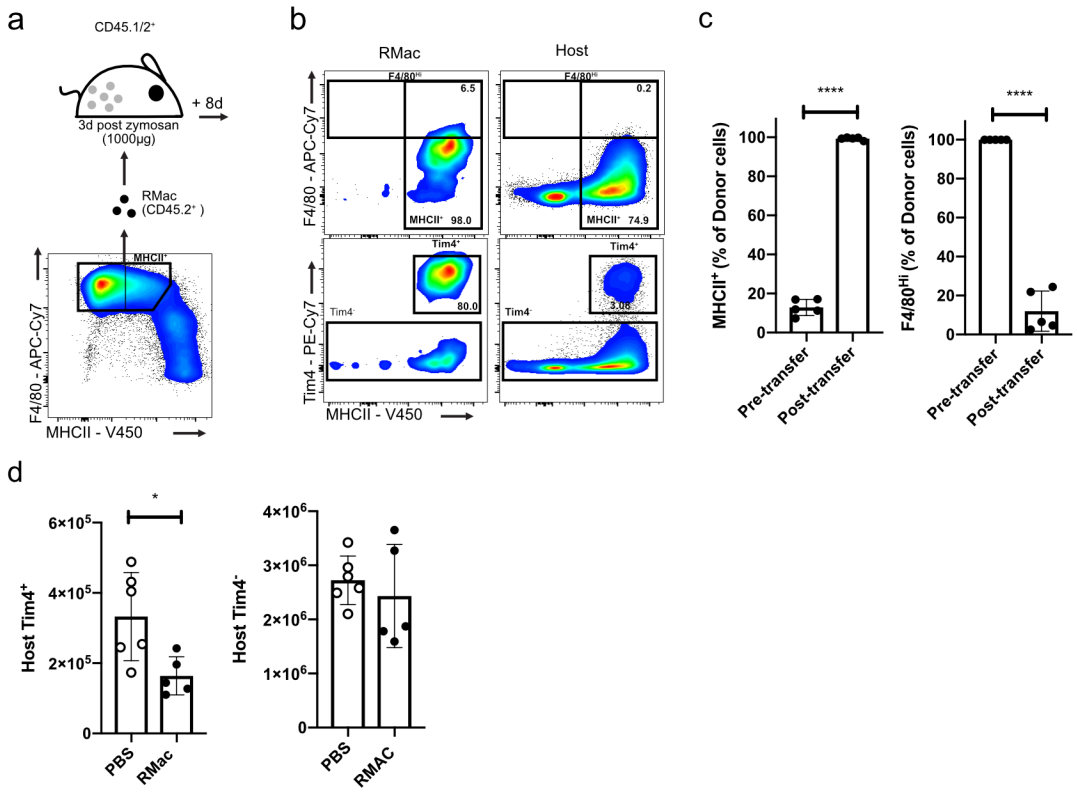

Figure 7.5 Following severe peritonitis the peritoneal microenvironment is altered.

(a) Experimental outline for the adoptive transfer of donor RMac (F4/80^{Hi} MHCII^{Lo}) into mice that were pre-treated with high dose zymosan 3 days prior. **(b)** Representative expression levels of of F4/80, MHCII and Tim4 by donor RMac (left) and host macrophages (right), 8 days following adoptive transfer. **(c)** Proportion of RMac (n=5) that express MHCII and F4/80, before transfer and 8 days following transfer into high dose zymosan treated recipient mice. Proportion of RMac that express F4/80 at the time of transfer is set to 100% as cells were sorted on this marker (see Figure 7.5a). ****p<0.0001, student's t test. **(d)** Absolute number of host macrophages that express Tim4 (left) or do not (right), 8 days after PBS treatment (n=6) or transfer of donor RMac (n=5). *p<0.05, student's t test. Data shown as mean ± standard deviation. Each

symbol represents an individual animal. Data were pooled from 2 independent experiments.

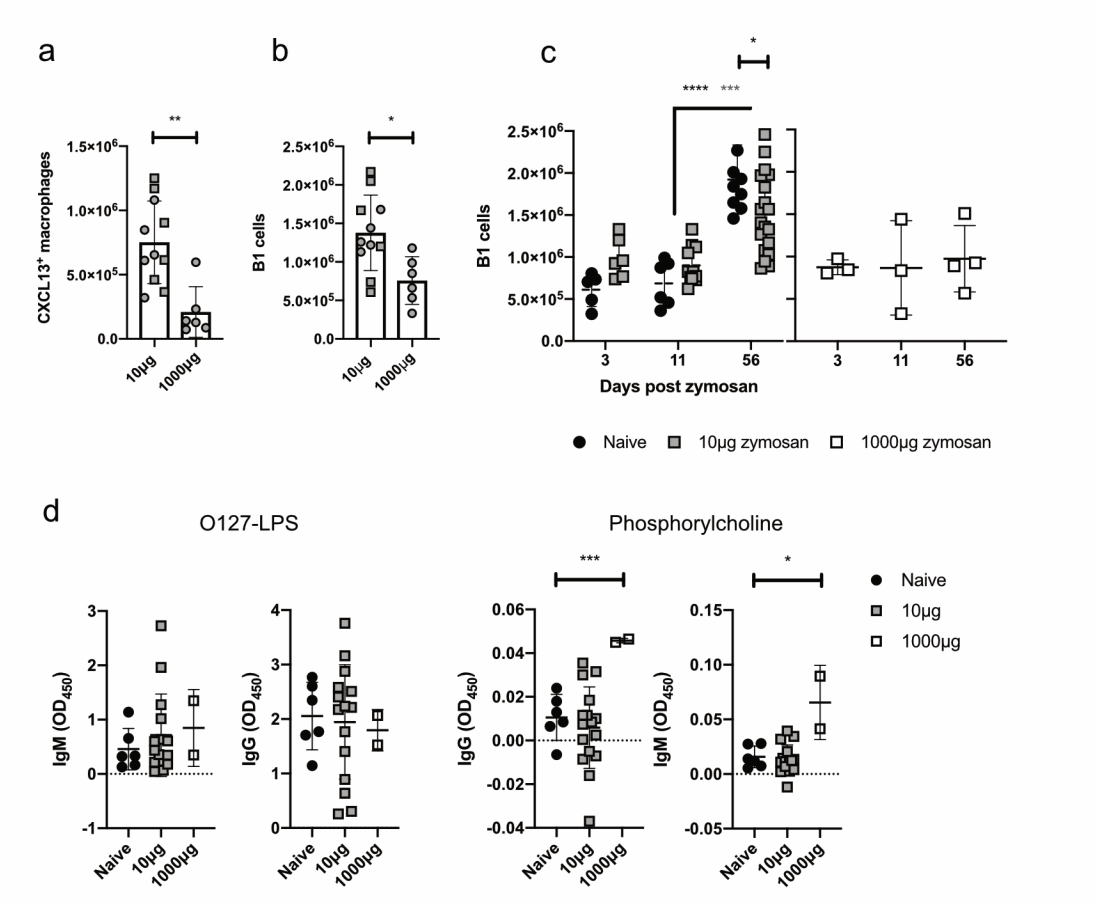

Figure 7.6 Severe peritonitis leads to impaired recruitment of B1 cells.

(a) Absolute number of host macrophages that express the B1 cell chemoattractant CXCL13, 8 weeks following treatment with 10μg of zymosan (n=11) or 1000μg zymosan (n=6). **p<0.01, student's t test. Data are derived from the adoptive transfer experiments presented in Figure 7.3. **(b)** Absolute number of host Lineage$^+$ CD11B$^+$ B1 cells, 8 weeks following treatment with 10μg of zymosan (n=11) or 1000μg zymosan (n=6). *p<0.05, student's t test. Data are derived from the adoptive transfer experiments presented in Figure 7.3. **(c)** Absolute number of peritoneal Lineage$^+$ CD11B$^+$ B1 cells present in the cavity at indicated timepoints in naïve mice (black; n= 5,6,10 for each time point respectively), mice treated with 10μg of zymosan (n=6,11,20 for each

time point respectively) and mice treated with 1000μg of zymosan (n=3,3,4 for each time point respectively) *p<0.05, ***p<0.001, ****p<0.0001, two-way ANOVA and post hoc Tukey test. **(d)** Levels of serum anti 0127-LPS or phosphorylcholine specific IgM and IgG detected using enzyme linked immunosorbent assay. Serum was sourced from naïve mice (n=6), mice treated with low dose zymosan treatment 8 weeks prior (n=16) and mice treated with high dose zymosan 8 weeks prior (n=2). *p<0.05 ***p<0.001, one way ANOVA and Dunnet's multiple comparisons test. Serum was collected by me but analysis was performed by Dr. Steve Jenkins and Ms. Lucia Badiola Gomez. Data shown as mean ± standard deviation. Each symbol represents an individual animal. Data for naïve and 10μg zymosan treated animals were pooled from 2 independent experiments.

Chapter 8

Discussion and perspective

8.1 Introduction

As described in the introduction the question of whether monocytes recruited into the inflamed peritoneal cavity persist long-term and integrate into the macrophage compartment has remained contentious. The same question has been asked in many tissues now, with numerous recent studies indicating that integration of monocytes into the macrophage compartment occurs following inflammation and that the presence of these cells can alter the long-term responsiveness of the tissue to further challenge. The degree to which inflammatory monocyte-derived cells integrate into the resident population appears to be, in part, dictated by the size and proliferative capacity of the remaining resident macrophage compartment. In the peritoneal cavity, seemingly contrasting results have been obtained suggesting resident macrophages repopulate by proliferation following zymosan induced peritonitis[87,144], thus limiting monocyte integration. Conversely, integration of monocytes into the macrophage compartment has been found following more severe thioglycolate-induced peritonitis, but the extent to which integration may occur is unclear[28,123,145]. Hence, in this project I set out to establish whether monocytes recruited into the inflamed cavity integrate into the peritoneal macrophage compartment and if so, whether these cells become transcriptionally and functionally equivalent to their bona-fide resident counterparts. Moreover, I set out to investigate whether this integration is impacted by the presence of a population of competing resident macrophages or the severity of the initial inflammatory insult.

8.2 A niche that determines peritoneal macrophage survival and proliferation

In chapter 3 it was found, using tissue-protected bone marrow chimeric mice, that the degree of resident-macrophage loss and replacement by monocyte-derived cells is dependent on the severity of the inflammatory insult. Following low-dose zymosan treatment (10μg), the macrophage compartment as a whole is temporarily expanded. When inflammation is resolved by day 3, as indicated by resolution of neutrophilia, resident and inflammatory

macrophages inhabit the cavity side by side. I used these well-defined populations for adoptive transfer studies throughout the thesis.

I first used this adoptive transfer methodology to investigate the short-term fate of inflammatory in chapter 4. Immediately following the resolution of inflammation the presence of a sizeable resident macrophage population with significant proliferation potential[42,146,147] failed to prevent survival of inflammatory macrophages during this period or, as shown in chapter 5, long-term. However, the presence of resident-macrophages did inhibit the proliferation of inflammatory macrophages as inflammatory macrophages expanded considerably following transfer into macrophage-deplete recipients. Surprisingly, transferred resident macrophages were unable to expand to a similar degree following transfer into macrophage-deplete recipient mice. These findings are similar to work by Cain et who found that LPM transferred into the cavity of macrophage-deplete CEBP$\beta^{-/-}$ recipient mice did not expand[60]. In contrast, monocytes are known to have the capacity to undergo high levels of proliferation and reconstitute an artificially-depleted macrophage compartment in the liver and lung[67,73]. A likely explanation for this observation is that monocyte-derived macrophages proliferate more rapidly than their resident-counterparts following transfer, similar to what occurs in the lung[67].

A slower rate of proliferation could be a general feature of mature resident macrophages. This would be consistent with earlier studies indicating that 6 weeks after transfer into alveolar macrophage-deficient CSF2Rb$^{-/-}$ mice, fetal-liver monocytes had expanded considerably more than transferred alveolar macrophages. By 1-year post-transfer, both populations had similar size, indicating that alveolar macrophages have the capacity to expand considerably, but do so at a slower pace than fetal-liver monocytes[67]. Although variable, the experiments where I transferred RMac^{Z10} or IMac^{Z10} info FIRE$^{-/-}$ mice, constitutively devoid of resident peritoneal macrophage[106], suggested more rapid expansion of IMac^{Z10} that RMac^{Z10} similar as following transfer into clodronate pre-treated recipients. To definitely establish whether RMac^{Z10}

ultimately have similar proliferative capacity to IMac^{Z10}, the transfer RMac^{Z10} or IMac^{Z10} into FIRE$^{-/-}$ mice should be repeated but expansion investigated at a later timepoint, similar to studies in the lung[67]. If both RMac^{Z10} and IMac^{Z10} prove capable of reconstituting the macrophage compartment, albeit at a different rate, the functional profile of each subset can be investigated in more detail as a cavity inhabited exclusively by one subset can then be generated using this experimental system.

Following adoptive transfer of IMac^{Z10} into naïve recipients, even in the presence of a completely intact macrophage compartment, IMac^{Z10} persisted. This finding was somewhat unexpected, as the naive cavity is inhabited by an intact macrophage compartment. Following transfer into naive recipients, RMac^{Z10} and IMac^{Z10} persisted equally well, suggesting that IMac^{Z10} have equivalent survival capacity as RMac^{Z10}. However, following transfer into inflamed recipients, IMac^{Z10} persisted marginally poorer, suggesting that following resolution IMac^{Z10} have lower survival capacity as RMac^{Z10}. As the period investigated corresponds with a contraction of the myeloid compartment, these observations support the notion that competitive pressure with both resident and other inflammatory macrophages limits but ultimately fails to prevent IMac^{Z10} survival, following peritoneal inflammation. These finding contrast with published work in the liver indicating that after partial depletion of Kupffer cells using Clec4f-DTR mice[38] or acetaminophen treatment[83], remaining Kupffer cells exhibit heightened proliferation to reconstitute the macrophage compartment thus limiting monocyte integration. This raises the question why the 'proliferative burst' exhibited by resident macrophages in the cavity in the first few days following zymosan treatment [144], fails to similarly prevent inflammatory macrophage survival.

The shared dependency of resident and inflammatory macrophages on CSF1 for their survival may underlie this discrepancy. During peritoneal inflammation, both resident and inflammatory macrophages rely on CSF1 for survival[87,193]. Moreover, the 'proliferative burst' of resident-macrophages is

mediated by CSF1 and not Il4[67,], another driver of resident-macrophage proliferation[146]. During early stages of thioglycolate-induced peritoneal inflammation levels of CSF1 are temporary increased, with high amounts transiently produced by macrophages and neutrophils[193]. However, after neutrophilia is resolved levels of CSF1 rapidly drop[193]. During resolution of zymosan-induced peritonitis, the levels of CSF1 in peritoneal fluid are equivalent to pre-inflammation levels[87]. However, the overall number of myeloid cells, including resident and inflammatory macrophages is increased, suggesting increased competition for CSF1. Following zymosan treatment, expression of CSF1r mRNA is equivalent between resident macrophages and inflammatory macrophages[64], which may explain why inflammatory macrophages are not outcompeted. In the liver both resident and inflammatory macrophages are also dependent on CSF1[73]. Unpublished data from our lab suggest that following CCL4-induced liver injury, monocytes infiltrate the liver that do not persist long-term. Importantly, these monocytes give rise to inflammatory macrophages that express lower levels of CSF1r than bona-fide Kupffer cells, as determined using a transgenic CSF1r-mApple reporter mouse line. Similarly, after acetaminophen treatment, inflammatory macrophages do not persist, an effect which can be ameliorated by exogenous CSF1 treatment[83]. Combined, these data would suggest that the impaired capacity of inflammatory macrophages to persist in the liver may be due to an inability to compete for CSF1 with incumbent Kupffer cells due to lower CSF1R expression. Conversely, the ability of inflammatory macrophages to effectively compete for CSF1, due to high levels of CSF1r, in the peritoneal cavity may underlie their capacity to persist long-term.

However, the fluidic nature of the peritoneal cavity may also affect the ability of inflammatory macrophages to persist. In the liver, there is a clear anatomically defined niche for which cells compete[73].In contrast, the peritoneal niche is largely a fluidic environment[103] with intermittent interaction with surrounding stromal niche cells[99]. Possibly, the fluidic nature of the peritoneal niche allows expansion of the macrophage compartment, even under

homeostatic conditions, as expansion only marginally impacts on the levels of niche factors, including CSF1, in the fluid that are available to individual macrophages. To test if levels of CSF1R directly impact on inflammatory macrophage survival, the transgenic FIRE$^{-/-}$ mice may prove useful. Loss of a single FIRE enhancer domain does not alter the peritoneal macrophage compartment[106]. My preliminary findings indicated that FIRE$^{+/-}$ mice recruit inflammatory macrophages similar to FIRE$^{+/+}$ mice following low-dose zymosan treatment. However, the level of CSF1R on both resident and inflammatory macrophages were noticeably lower in FIRE$^{+/-}$ mice than in FIRE$^{+/+}$ mice. Hence, adoptive transfer of resident/inflammatory macrophages sourced from (CSF1r^{Hi}) FIRE$^{+/+}$ mice into equivalently inflamed (CSF1r^{Int}) FIRE$^{+/-}$ recipients, could ascertain whether somewhat higher levels of CSF1r provide a survival advantage following zymosan-induced peritonitis.

8.3 The omentum as a short-term niche for inflammatory macrophage conversion

In vitro, studies indicated that inflammatory macrophages, sourced 11 days after low-dose zymosan treatment, upregulated F4/80 and downregulated MHCII in response to retinoic-acid and omentum factors respectively. As F4/80 is directly regulated by GATA6[63], these data support the notion that GATA6 can be upregulated by inflammatory macrophages in response to retinoic-acid. Importantly, in this *in vitro* assay, inflammatory macrophages were co-cultured with resident macrophages. As cells were co-cultured, these data suggest it is unlikely that resident macrophages secrete factors to actively inhibit the conversion of inflammatory macrophages. Instead, the impaired capacity to compete for retinoic-acid and omentum factors likely underlies the inability of inflammatory macrophages to adopt a resident phenotype. Published *in vitro* data indicates that a sizeable set of genes unique to peritoneal macrophages are regulated by retinoic-acid and/or

omentum factors[99] as co-culture with these factors was required for peritoneal macrophage to retain expression of these genes *in vitro*.

Consistent with a potential role for the omentum, *in vivo* adoptive transfer studies suggested that by day 8 post transfer both RMac^{Z10} and IMac^{Z10} migrated into the omentum of mice deplete of peritoneal and omental macrophages. Migration to the omentum has long been postulated to occur but to my knowledge this is the first evidence of peritoneal macrophage migration to the omentum that is not based on dye-labelling or inferred based on levels of chimerism in macrophage subsets in the cavity and the omentum[63,164]. Neither RMac^{Z10} nor IMac^{Z10} migrated into the omentum following transfer into inflamed or naïve recipient mice, both of which have an intact omental macrophage compartment. The importance of this migration is hard to asses as it is unclear if these cells persist in the omentum long-term. In the only long-term transfer into macrophage-deplete recipients experiments in which I investigated the omentum 8 weeks following transfer, neither one of the donor populations was detectable in the omentum, suggesting no long-term residency in the omentum. It should be noted, peritoneal macrophages that are transiently and weakly interacting with the omentum would likely not be detected in the omentum tissue-preparation, as the omentum was collected after repeated peritoneal washes. Hence, these findings support the notion that those donor IMac^{Z10} and RMac^{Z10} recovered from the omentum after 8 days, had either incorporated into the omental tissue or strongly adhered to the omentum.

A potential role of the omentum as a niche for peritoneal macrophages has been suggested[63]. Omentum factors affect expression of numerous peritoneal macrophage identity genes and some genes are thought to be driven by direct interaction between macrophages and the omentum[99]. In addition, the omentum is thought to be the predominant source of retinoic- acid in the cavity[63]. However, these studies have largely been carried out *in vitro* and are inconclusive concerning the role of the omentum *in vivo*. To investigate the potential role of the omentum *in vivo* is challenging. Omentectomy, the surgical

removal of the omentum, could be utilized to investigate the role of the omentum as a niche. However, this procedure causes a considerable degree of peritoneal inflammation (personal communication from Dr. Calum Bain), resolution of which will likely be altered by the absence of the omentum. To circumvent this issue, adoptive transfer of RMac^{Z10} or IMac^{Z10} into fully recovered omentectomized recipient mice might be an option. If transferred RMac^{Z10} lose their identity features, but IMac^{Z10} maintained their inflammatory gene-signature, this would be indicative of a role for the omentum in maintaining and establishing the peritoneal macrophage identity. However, it will not be possible to discriminate the effects of soluble factors secreted by the omentum from those that require direct interaction with the omentum. A starting point to investigate these temporal interactions could be previous work by a PhD student at the CIR, Simon Watson. He developed a methodology to externalize the omentum prior to peritoneal lavage. His studies indicated no changes in the overall number of peritoneal macrophages recovered, following lavage of the cavity with or without the omentum. However, absolute numbers retrieved are variable and he identified peritoneal macrophages solely on the basis of F4/80. Consequently, he could have missed out on small omentum-interacting subsets. To ascertain if temporal interactions with the omentum occur either under steady-state or inflamed conditions, his methodology could be used. In addition, the externalised omentum could be gently washed to collect cells loosely adhering to the omentum, although this may yield too few cells for analysis. In summary, the role of the omentum in shaping peritoneal macrophage identity remains unclear but should be investigated in more detail.

8.4 A niche that determines peritoneal macrophage identity.

In chapter 5 I elaborated on the early time-point findings and investigated the long-term survival of inflammatory macrophages. By 8 weeks following adoptive transfer into macrophage-deplete recipients, transferred resident macrophages did not appear to have expanded relative to the 8-day time-point. However, clodronate pre-treatment only temporarily depletes resident macrophages and leads to an influx of host monocytes that reconstitute the

niche in parallel to transferred cells. Although definitive conclusions cannot be drawn on these data it did appear that IMac^{Z10} seemingly did not proliferate between the 8 day and 8-week timepoints. If, RMac^{Z10} have lower proliferation capacity, the available niche space may be more rapidly colonized by host monocytes thus limiting expansion of RMac^{Z10}. Hence, these data suggest that mature RMac^{Z10} fail to undergo sufficient proliferation to prevent integration of monocytes into the macrophage compartment. Moreover, once monocytes have colonized the peritoneal cavity, mature resident-macrophages appear to be unable to recover occupied niche space. Studies by Rosas et al found that peritoneal macrophages devoid of GATA6 have heightened levels of baseline proliferation[64]. Hence, high expression of GATA6 by RMac^{Z10} relative to IMac^{Z10} at the time of transfer could underlie the impaired ability of the former to expand, following transfer into macrophage-deplete recipients.

Moreover, the short-term timepoint studies in chapter 4 indicated that, following transfer into similarly inflamed or naïve recipient mice, IMac^{Z10} failed to completely adopt a resident F4/80^{Hi} MHCII^{Lo} GATA6^{Hi} phenotype. This failure was still apparent even after 8 weeks, as shown in chapter 5. In contrast, following transfer into recipients deplete of macrophages, by 8 weeks IMac^{Z10} had completely adopted an F4/80^{Hi} MHCII^{Lo} GATA6^{Hi} phenotype. Combined with the *in vitro* data presented in chapter 4 indicating that inflammatory macrophages are retinoic acid responsive, these data suggest that the GATA6^{Int} phenotype of IMac^{Z10} is likely to exist, in part, due to competition with resident macrophages for retinoic-acid. Indeed, more complete acquisition of a GATA6^{hi} phenotype occurred following transfer of IMac^{Z10} into macrophage-deplete recipients, and by IMac^{Z1000} following transfer into severely inflamed recipients in which resident macrophages were absent, as presented in chapter 7.

Moreover, in chapter 5 it became apparent that the inability of transferred IMac^{Z10} to adopt a GATA6^{Hi} MHCII^{Lo} resident phenotype was indicative of an inability to undergo transcriptional conversion, as the mRNA profile of IMac^{Z10}

differed considerably from $RMac^{Z10}$ 8 weeks after transfer into inflamed recipient mice. A sizeable proportion of these gene differences are regulated by GATA6, of which, $IMac^{Z10}$ failed to acquire equivalent levels as $RMac^{Z10}$. However, following transfer into macrophage-deplete recipients, $IMac^{Z10}$ adopted a more complete resident macrophage mRNA profile and, importantly, equivalent levels of GATA6 and most GATA6-regulated genes. A number of genes that were differentially expressed between $RMac^{Z10}$ and $IMac^{Z10}$ are regulated by RXRα and/or RXRβ[98]. Signalling through these nuclear-receptors is mediated by retinoic-acid and regulates expression of GATA6 and numerous GATA6-regulated genes[98]. However, RXR-signalling also mediates expression of numerous GATA6-independent genes[98]. Indeed, the gene-profile of $IMac^{Z10}$ was enriched for genes downregulated on $RXRAB^{-/-}$ LPM.

Combined, these data indicate that the inability of inflammatory macrophages to effectively acquire retinoic-acid, hampers their conversion potential. These findings are consistent with published work, suggesting thioglycolate-induced inflammatory macrophages fail to adopt a resident $F4/80^{Hi}$ phenotype following transfer into mice deficient in vitamin-A and its active metabolite, retinoic acid[145].

However, over half of the genes that differentiated $IMac^{Z10}$ from $RMac^{Z10}$ are not regulated by retinoic-acid. The majority of these genes are environment-responsive as expression was altered following transfer into macrophage-deplete recipients. Some of these genes, including those encoding for the MHCII machinery, are likely regulated by omentum factors, as suggested by the *in vitro* studies described in chapter 4. However, these genes could be regulated by other peritoneal identity driving transcription factors, including CEBP/β[60] and BHLHE40[61,62]. These transcription factors may be regulated by unknown environmental cues. Indeed, expression of CEBP/β and BHLHE40 is lost by cultured peritoneal macrophages[9], suggesting that their expression relies on continual signals from the cavity micro-environment. Retinoic-acid

has been proposed to drive BHLHE40 in peritoneal macrophages *in vitro*[9] but this has been contrasted by other *in vitro* studies[99]. Loss of CEBP/β leads to almost complete loss of peritoneal macrophages[60]. However, the degree to which CEBP/β-deficiency alters the transcriptional profile of the few remaining peritoneal macrophage is unknown. In addition, little is known concerning the steady-state niche signals that could be driving expression of CEBP/β. However, CEBP/β has been studied extensively in the context of inflammation. LPS stimulation of macrophages induces expression of CEBP/β *in vitro* and *in vivo*[194-196]. Chromatin immunoprecipitation studies indicated that CEBP/β is constitutively present at the *Serpinb2* promoter and drives constitutive, low expression of *Serpinb2*, and upregulates levels of *Serpinb2* in response to LPS[197]. This CEBP/β- Serpinb2 interaction occurs in both resident-peritoneal macrophages and thioglycolate-elicited inflammatory macrophages[197]. This finding is likely to be of importance, since macrophage-specific loss of *Serpinb2* alters migratory capacity and transcriptional identity of peritoneal macrophages[156]. My Nanostring analysis suggested levels of CEBP/β were equivalent between $RMac^{Z10}$ and $IMac^{Z10}$ at week 8 and Serpinb2-regulated genes were not enriched in my dataset as assessed by GSEA analysis, unlike GATA6-regulated genes. As microbial products are thought to be present in the steady-state peritoneal cavity and affect development and identity of SPM[104] and potentially LPM[198], it is possible that low level of microbial LPS is required for constitutive expression of CEBP/β by peritoneal macrophages. However, the CEBP/β promoter also contains two CREB binding sites, loss of which abrogates LPS-mediated activation[199]. Prostaglandin E2 has been shown to activate CREB which proceed to bind CREB binding-sites in the CEBP/β promoter in bone-marrow derived macrophages[200]. Notably, prostaglandin E2 is produced in low-levels by steady-state by peritoneal macrophages[120], and it's production by peritoneal macrophages is highly responsive to IFNγ which, under steady-state conditions, is present in the peritoneal fluid in detectable levels[120]. Hence, CEBP/β signalling may be driven by autocrine signalling via peritoneal macrophage produced

prostaglandin E2, production of which is driven by peritoneal fluid IFNγ. Moreover, the bronchoalveolar fluid to which alveolar macrophages, that are also CEBP/β dependent, are exposed also contains quantifiable levels of prostaglandin that increase with age[201]. Loss of prostaglandin receptor E2 led to an increase in the number of alveolar macrophages and heightened proliferation[201], indicating that prostaglandin signalling is not required for alveolar macrophage survival, as would be expected if CEBP/β signalling relied solely on prostaglandin E2.

Hence, the environmental cues that drive the peritoneal macrophage identity, and how these may be altered following inflammation, remain unclear. However: IFNγ, Prostaglandin E2 and microbial products are possible signals that could be mediating CEBP/β-mediated gene expression, driving part of the peritoneal macrophage identity.

8.4.1 The influence of time and origin on peritoneal macrophage identity and functionality

As described in chapter 5, after 8 weeks of residence, a small set of genes remained differentially expressed between $RMac^{Z10}$ and $IMac^{Z10}$, irrespective of whether cells were transferred into inflamed or artificially-depleted recipients, thus supporting the idea that origin, in part, dictates macrophage identity. These features included proteins highly expressed by resident macrophages that are not acquired by $IMac^{Z10}$ (Tim4, VSIG4,CD209b), but gradually acquired with time. Other environment-independent features, are those more highly expressed by $IMac^{Z10}$ (CD62L), that are features of monocyte-derived cells that are retained, but gradually lost with time. By 22 weeks post-transfer, the engraftment efficiency of both $RMac^{Z10}$ and $IMac^{Z10}$ had dropped considerably, relative to earlier 8 week datasets, indicative of gradual loss of both populations. Hence, it remains unclear whether the lifespan of $IMac^{Z10}$ is sufficient to undergo complete conversion. This observation highlights the importance of the finding that the transcriptional

identity of IMac^{Z10} overlaps with that of a small population of monocyte-derived resident macrophages (Mo-LPM), present under steady-state conditions. Similar to IMac^{Z10}, the identity of Mo-LPM is, in part, an effect of lower GATA6 expression, supporting the notion that Mo-LPM are similarly less-able to compete for retinoic-acid with bona-fide resident macrophages. Hence, the developmental path that IMac^{Z10} traverse, following an inflammatory event, does not appear to differ from that of monocytes giving rise to resident macrophages under steady-state conditions. Consequently, the loss of IMac^{Z10} observed by week 22 is likely to result in replacement by 'new' monocyte-derived macrophages that similarly require a long time to acquire a resident-macrophage identity. Alternatively, these cells may, similar to IMac^{Z10}, not live long enough to undergo full conversion.

A key question that still remained was the functional implication of long-term inflammatory macrophage integration. Inflammatory macrophages failed to acquire expression of CD209b even after 22 weeks. Expression of CD209b by peritoneal macrophages is required for effective clearance of *S.Pneunomiae in vivo*[97]. Hence, the increases susceptibility mice that have received zymosan 21 days[120] or 8 weeks[111], prior to *S.Pneunomiae* infection may be due to loss of CD209b-expressing resident macrophages and presence of CD209b-deficient inflammatory macrophages. In addition, inflammatory macrophages failed to acquire expression of VSIG4 after 8 weeks but eventually acquired expression by 22 weeks. In the liver, VSIG4 has been identified as pattern recognition receptor required for Kupffer cells to clear circulating *S.aureus* and limit systemic dissemination[202]. Specifically, VSIG4 recognises lipoteichoic acid, which constitutes part of the cell wall of gram positive bacteria like *S. aureus*[202] but also *S. Pneunomiae*[203]. Hence, it is likely that CD209b/VSIG4-deficient inflammatory macrophages that inhabit the cavity following zymosan-induced peritonitis have impaired capacity to recognise and engulf gram-positive bacteria.

Combined, these data indicate that inflammatory macrophages persist long-term following zymosan-induced peritoneal inflammation, but that their inability to compete for niche factors inhibits conversion into bona-fide resident macrophages which has potentially functional implications. Part of their transcriptome is not responsive to environmental cues, and is cell-intrinsically regulated. Irrespective, with time inflammatory macrophages adopt a more resident-like phenotype by altering expression of both environment- and intrinsically-regulated features.

8.5 The functional effects of historic peritoneal inflammation

In chapter 6 I then set out to expand on the potential functional impact of inflammatory macrophage integration following peritoneal inflammation. Indeed, integration of monocytes into the peritoneal macrophage compartment after mild-peritonitis resulted in the presence of a sizeable population of functionally divergent cells. Using a combination of two markers Tim4 and Sema4a, I was able to identify persistent monocyte-derived inflammatory macrophages, and the corresponding population of monocyte-derived macrophages present under homeostatic conditions. Monocyte-derived macrophages exhibited higher baseline levels of proliferation than their resident counterparts, irrespective of whether they had differentiated under homeostatic or inflammatory conditions. Moreover, monocyte-derived LPM had lower granularity than their resident counterparts which correlated with impaired capacity to phagocytose Phrodo labelled *E.coli* particles, compared to RM-LPM. Following LPS stimulation both Mo-LPM populations had divergent cytokine/chemokine production from their resident counterparts. Whilst, Mo-LPM produced more Il1β the overall pattern of cytokine production of both Mo^{Z10}-LPM and Mo-LPM appeared to be less-inflammatory as indicated by lower production of TNFα and heightened secretion of Il10, than their resident counterparts. Consistent with these findings, a smaller proportion of Mo^{Z10}-LPM produced TNFα in response to LPS stimulation *in vivo*. Moreover, the transcriptional profile of Mo^{Z10}-LPM differed from that of RM^{Z10}-

LPM stimulated *in vivo* with LPS. The differential gene expression following *in vivo* LPS stimulation seemingly resulted from an inability of Mo^{Z10}-LPM to upregulate LPS-driven genes, to the same degree as RM^{Z10} -LPM.

Based on the data presented in this thesis a definitive conclusion regarding the *in vivo* effects of monocyte integration on subsequent inflammatory insults cannot be drawn. However, my findings support a model whereby having undergone a historic inflammatory event dampens the overall immune response and ability to limit dissemination of bacteria due to the presence of an enlarged population of less phagocytic and anti-inflammatory, monocyte-derived LPM.

However, zymosan-induced monocyte integration may have beneficial effects in other contexts. For example, peritoneal macrophages are key players in the development of ovarian cancer metastasis. Notably, $Tim4^+$ embryonically-seeded peritoneal macrophages that infiltrated the tumour enhanced growth whereas $Tim4^-$ monocyte-derived macrophages did not[204]. Moreover, using the clodronate-depletion methodology described in this thesis, the laboratory of Dr. Erin Greaves found that depletion of $Tim4^+$ peritoneal macrophages and consequent replacement by monocyte-derived $Tim4^-$ macrophages inhibited development of endometriosis. Hence, alterations to the macrophage compartment following peritoneal inflammation are likely a double-edged sword that has the potential to progress or inhibit the development of subsequent pathologies.

8.6 A severity-dependent state of altered homeostasis following peritoneal inflammation

In chapters 5 and 7 I had observed that one of the key features that was not acquired by transferred inflammatory macrophages, irrespective of the degree of inflammation was the B1 cell chemokine, CXCL13[118]. Peritoneal

B1 cells account for a sizeable proportion of the peritoneal exudate cells and are known to produce natural antibodies[118,192,205]. In addition, these cells have been shown to take over key phagocytic functions upon loss of resident peritoneal macrophages and have even been postulated to give rise to resident-macrophages[158,206]. Unpublished data from the lab indicate that during normal aging the number of B1 cells in the cavity increases. This expansion is thought to be due to homing of B1 cells from the blood into the cavity, a process mediated by CXCL13 produced by peritoneal cells[118]. The predominant source of CXCL13 in the peritoneal cavity are the resident macrophages[118] and omental stromal cells[136]. Importantly, CXCL13 is required for homing of B1 cells into the cavity but not for the survival of B1 cells that are already sequestered in the cavity[118]. Consistent with this, I found that loss of CXCL13-expressing macrophages, following zymosan induced peritonitis, did not result in a loss of B1 cells but rather an impaired ability to sequester B1-cells in the cavity with time.

Indeed, in chapter 8 it became apparent that, following high dose zymosan-treatment and the complete loss of CXCL13-expressing macrophages, the number of B1 cells remained stable rather than increasing with time, suggesting a failure to recruit further cells into the cavity. This failure to sequester B1 cells corresponded with increased levels of circulating natural antibodies against phosphorylcholine. A possible explanation for this result is that B1 cells in the peritoneal cavity produce very low levels of natural antibodies[118,192]. In contrast, B1 cells in the bone marrow and the spleen secrete higher levels of natural antibodies[118,192]. Hence, a failure to sequester B1 cells in the cavity may result in their accumulation in the spleen and bone marrow where they consequently produce higher antibody titters. This hypothesis is supported by the work of Broker et al, indicating that a failure to sequester B1 cells in the cavity, likely as a result of impaired CXCL13 production by peritoneal macrophages, led to accumulation of antibody producing B1 cells in the spleen[207].

Hence, these findings support the notion that local peritoneal inflammation can affect systemic immunity long-term. At present we don't have the tools to definitively attribute the failure to sequester B1 cells in the cavity to the failure of monocyte-derived-macrophages to produce CXCL13. A recent conference abstract by Wenxin Ma, describes a transgenic flox-STOP-flox-CXCL13 transgene mouse. A rescue experiment using this line crossed to a monocyte-specific CRE-driver line (e.g $MS4a3^{Cre}$)[123], driving CXCL13 on monocyte-derived macrophages, followed by high-dose zymosan treatment, could attribute the inability to sequester B1-cells in the cavity, to the inability of monocyte-derived macrophages to produce CXCL13.

Following high dose zymosan treatment, $IMac^{Z1000}$ retained high levels of MHCII until 8 weeks following the inflammatory event. Donor RMac upregulated MHCII, 8 days following transfer into high-dose zymosan treated recipient mice, suggesting the micro-environment is reprogrammed to drive MCHII expression. This effect could be regulated by cavity levels of IFNγ, a well-known regulator of MHCII expression[208] that has been found to increase following peritoneal inflammation[120]. Peritoneal NK cells have been proposed as a source of IFNγ[120], following zymosan treatment. However, in these studies the number of NK cells in the cavity dropped by 21 days following the inflammatory insult[120]. In my studies I found no indication of long-term alterations to the number of $CD11B^{Lo}$ $CD62L^{+}$ NK-cells in the cavity following high-dose zymosan treatment, compared to low-dose zymosan treatment. Another potential source of IFNγ could be activated T-cells[108,120]. The number of T-cells present in the cavity following high-dose zymosan treatment was decreased compared to mice treated with low-dose zymosan. This loss of T-cells was largely due to loss of $CD62L^{+}$ naïve T cells[98] whilst the population of activated $CD62L^{-}$ T-cells[98] cells was unaltered. Unfortunately, our panel lacked the markers required identify T-cell subsets. Unpublished findings from our laboratory indicate that approximately 60% of $Foxp3^{+}$ regulatory T-cells in the peritoneal cavity express CD62L. As I observed almost complete loss of $CD62L^{+}$ T cells, it is likely some regulatory T-cells are lost. This may be

important as absence of regulatory T-cells has been found to directly impact the transcriptional identity of LPM. Using an adoptive transfer methodology, it was revealed that WT-LPM transferred into regulatory T-cell deficient FOXP3-KO mice altered their transcriptome and MHCII expression. Conversely LPM sourced from FOXP3-KO mice rapidly downregulated MHCII following transfer into WT recipient mice[209]. Hence, changes to the peritoneal macrophage compartment following severe peritoneal inflammation may be, in part, knock-on effects of changes to other cell populations, such as T-cells and NK cells, that can alter the peritoneal-micro-environment.

8.7 Evidence for a peritoneal immune-cell niche.

These findings raise the question whether in addition to a fluidic biochemical niche and a surrounding stromal-cell niche, interactions between peritoneal macrophages and other peritoneal exudate cells play an important role in the programming of resident macrophages. The absence of regulatory T-cells seemingly alters the peritoneal micro-environment and as such these cells could be considered part of the peritoneal niche as this change in-turn affects peritoneal macrophage identity[209]. Peritoneal B1 cells, a population that is gravely affected by peritoneal inflammation due to their reliance on peritoneal macrophage derived CXCL13, may in-turn provide signals to peritoneal macrophages. Indeed, B1 cells have been shown to produce Il10 and modulate peritoneal macrophage polarization and phagocytic capacity *in vivo* and *in vitro*[210,211]. Moreover, residency in the peritoneal cavity uniquely protects resident B1 cells from CD20 antibody-mediated depletion but this effect is abrogated following thioglycolate induced-peritonitis and the corresponding loss of resident macrophages[212]. Finally, peritoneal B1 cells are largely absent in the peritoneal cavity of vitamin-A deficient mice. The active metabolite of vitamin-A, retinoic-acid drives expression of nuclear factor of activated T cells c1, a transcription factor required for B1 cell development and survival[213]. Hence, peritoneal macrophages and B1 cells both depend on retinoic-acid to drive key transcription factors. Taken together, these data are

suggesting a symbiotic relationship between peritoneal macrophages and peritoneal B1 cells that co-inhabit the fluidic peritoneal cavity.

One of the differentially expressed genes between $RMac^{Z10}$ and $IMac^{Z10}$ following transfer into mild inflamed recipients was CCL24, commonly known as Eotaxin 2. Under steady-state conditions both resident-LPM and SPM produce CCL24[214] and steady-state peritoneal lavage fluid contains a quantifiable amount of CCL24[215]. Under steady-state conditions eosinophil recruitment into the peritoneal cavity is uniquely dependent on G protein-coupled receptors, as pertussin toxin pre-treatment of eosinophils completely abrogated recruitment into the peritoneal cavity but not into the spleen and lung[216]. Moreover, recruitment of eosinophils into the peritoneal cavity occurs normally in $RAG^{-/-}$ mice but is partially reduced following clodronate treatment [216], indicating a potential role for peritoneal macrophages in eosinophil recruitment. Following *Ascaris suum* infection, a helminth infection model, peritoneal macrophages produce high levels of CCL24, driving expansion of peritoneal eosinophils. Conversely, eosinophils produce high levels of Il4 expanding resident macrophages. This effect required peritoneal macrophages and eosinophils to cluster closely together in a CCL24-dependent manner[215]. Similar interactions may be occurring under steady-state conditions and potentially more frequently following zymosan-induced peritonitis due to an influx of CCL24-expressing $IMac^{Z10}$. Moreover, $IMac^{Z10}$ exhibited heightened expression of numerous features associated with the M2 phenotype, driven by Il4, including *Retnla* (encoding for Relmα) and *Mrc1* (encoding for CD206)[217]. Although just speculation at this stage these findings could be indicative of increased exposure of $IMac^{Z10}$ to eosinophil derived Il4 as a result of increased CCL24-mediated proximity between the two cell-types.

Hence, future studies into the effects of inflammation on the peritoneal cavity should take full advantage of techniques such as single-cell RNA sequencing to investigate effects on all immune cells inhabiting the cavity. Indeed, using single-cell RNA sequencing Wang et al found that loss of *Beclin1* in peritoneal macrophages led to increased turnover of the peritoneal macrophage

compartment, but also affected various other immune cells in the cavity, including B1-cells and T-cells[108].

Combined, these data highlight that in a fluidic environment, such as the peritoneal cavity, different immune-cells are uniquely inhabiting the same fluidic niche. Consequently, the micro-environment is shaped by factors secreted by all cells inhabiting the fluidic niche. Hence, these various immune-cells are likely to affect the survival and identity of one-another. Consequently, changes to one cell population, for example through an inflammatory event, can lead to a domino effect which affects other cavity-resident cells that in-turn alters the micro-environment further.

8.8 The type of inflammatory stimuli likely dictates monocyte integration

Both the zymosan model of peritonitis and thioglycolate model of peritonitis are characterized by loss of resident-macrophages[123]. However, other models of peritoneal inflammation, most notably LPS injection, have generated contrasting results. Initial studies indicated a loss of resident-macrophages and a concurrent increase monocyte following LPS treatment[95]. In contrast, recent studies utilizing a novel transgenic monocyte fate-mapping mouse indicated no loss of resident-macrophages and no concurrent monocyte infiltration following LPS injection[123]. In the studies I carried out with LPS injection, no apparent loss of resident macrophages was detectable 8 hours following injection, but this this is likely because of the early time-point investigated, as disappearance in response to LPS is thought to occur later[132]. It is challenging to extrapolate between studies that have utilized LPS as model of peritoneal inflammation due to the use of different doses and, more importantly, different serotypes used. Recently published work from our lab indicated that following abdominal surgery, monocytes integrate into the macrophage compartment and concurrent with this, the number of B1 cells sequestered in the cavity following surgery is reduced[97]. Hence, my findings regarding the determinants of long-term integration of inflammatory

macrophages may not occur after LPS-induced peritonitis, but are likely to hold true following abdominal surgery.

8.9 Inflammation-driven integration of monocytes into the macrophage compartment likely occurs in humans

The human peritoneal cavity contains very similar populations of immune cells as the murine cavity[218]. Under steady-state conditions 2 populations of peritoneal macrophages that express CD14 and CD16 can be identified in the human cavity, both of which express GATA6[219]. Similarly, studies by Irvine et al. identified two subsets of peritoneal macrophages in the ascites fluid of liver cirrhosis patients. One populations had high capacity to phagocytose *E.coli in vitro* and expressed high levels of VSIG4 and Tim4. A second population that less effectively phagocytosed *E.coli in vitro* was characterized by low expression of VSIG4 and expressed Sema4a and CCR2[173]. GSEA analysis indicated that the gene signature of VSIG4$^+$ macrophages was enriched for genes regulated by GATA6, in murine peritoneal macrophage studies. In contrast, the transcriptional signature of Vsig4$^-$ human peritoneal macrophages overlaid with that of murine acute-stage thioglycolate-elicited inflammatory macrophages, suggesting these cells are likely inflammatory macrophages of monocyte origin. *Ex vivo* exposure of VSIG4$^+$ and VSIG$^-$ human macrophages to retinoic-acid induced upregulation of GATA6 and retinoic-acid receptor β by VSIG4$^-$ macrophages[173], suggesting that retinoic-acid is potentially driving GATA6 which could in turn drive human peritoneal macrophage identity. Finally, a macrophage disappearance reaction has been shown to occur in patients during spontaneous bacterial peritonitis, as indicated by a loss of resident CD206$^+$LPM[172]. Hence, key features of peritoneal inflammation such as loss of resident macrophages, an influx of macrophages likely of monocyte origin and a role for environmental retinoic-acid as a driver of GATA6 seemingly overlap between human and murine studies. Hence, it is likely that in humans inflammatory macrophages persist following resolution of inflammation. If so, it is likely that their phenotype is

dictated by a combination of environmental signals and cell-intrinsically regulated features, similar to what I have found to occur following murine peritonitis.

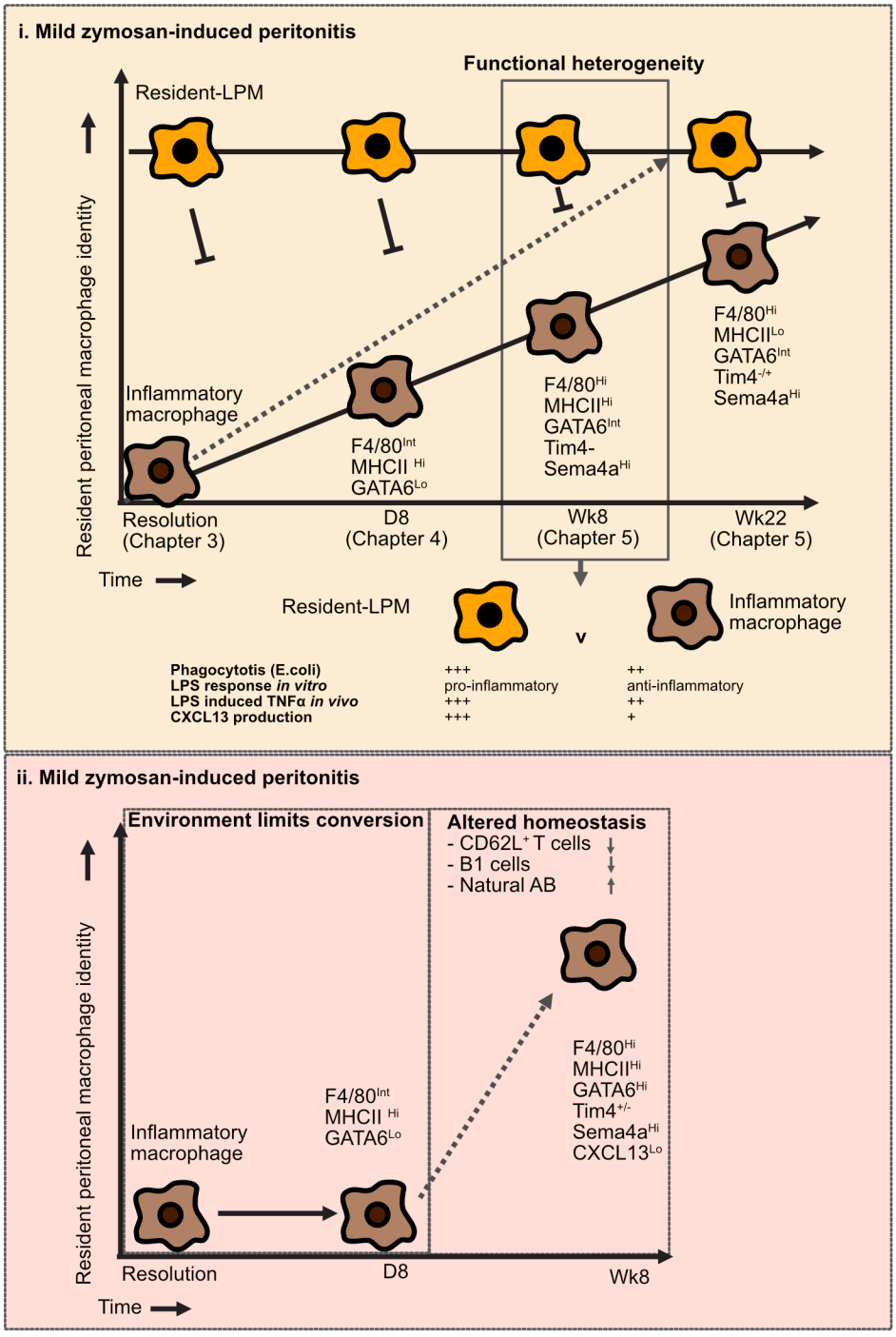

Figure 8.1 Long-term effects of zymosan-induced peritonitis

Overview of inflammatory macrophage dynamics following mild (i) or severe (ii) zymosan-induced peritonitis presented in this thesis. The x-axis denotes time following resolution of zymosan-induced peritonitis. The y-axis denotes the degree to which cells have the resident-LPM identity. During resolution of mild zymosan-induced peritonitis(i) phenotypically distinct resident-LPM and inflammatory macrophages inhabit the cavity. As time progresses inflammatory macrophages slowly adopt a more resident-like identity (black arrow) but this process is directly inhibited by competing resident-LPM and, in the absence of the resident-LPM, can occur more rapidly (dotted grey arrow). By 8 weeks the cavity contains a phenotypically distinct populations of persistent inflammatory macrophages that are less phagocytic and more immunoregulatory. Following severe zymosan-induced peritonitis (ii) resident-LPM are completely lost and the cavity is completely reconstituted by monocyte-derived inflammatory macrophages. Shortly following severe zymosan-induced peritonitis the cavity environment limits conversion of inflammatory macrophages to a resident-like identity but this is temporary phenomenon and by 8 weeks persistent inflammatory macrophages adopt a unique identity that is more resident-like than those inflammatory macrophages that persist following mild zymosan-induced peritonitis. Following severe zymosan-induced peritonitis an altered state of homeostasis is established during which the cavity is inhabited by phenotypically unique persistent inflammatory macrophages as well as lower numbers of B1 cells and CD62L^{+}T cells in the cavity, the former likely as a result of the ompaired capacity of persistent inflammatory macrophages produce CXCL13.

8.10 Conclusion

My PhD project has highlighted how different degrees of peritoneal inflammation alter the peritoneal macrophage compartment long-term. Monocytes that infiltrate the cavity during the early stages of inflammation persist long-term and competition for niche signals, time-of-residency and

alterations to the stromal and immune-cell niche underlie the ability of these monocytes to adopt a bona-fide resident LPM identity and, likely, functionality. These findings highlight the plasticity and environment-responsiveness of monocytes and macrophages in the peritoneal cavity and highlight how historic inflammation may alter progression of subsequent abdominal pathologies in which peritoneal macrophages are involved including endometriosis[114,115], ovarian cancer[204] and the development of peritoneal adhesions[116,117,220].

References

1 Soldati, T. & Cardenal-Munoz, E. A brief historical and evolutionary perspective on the origin of cellular microbiology research. *Cell Microbiol* **21**, e13083, doi:10.1111/cmi.13083 (2019).

2 Underhill, D. M., Gordon, S., Imhof, B. A., Nunez, G. & Bousso, P. Elie Metchnikoff (1845-1916): celebrating 100 years of cellular immunology and beyond. *Nat Rev Immunol* **16**, 651-656, doi:10.1038/nri.2016.89 (2016).

3 Gordon, S. Elie Metchnikoff, the Man and the Myth. *J Innate Immun* **8**, 223-227, doi:10.1159/000443331 (2016).

4 FURTH, R. V. *et al.* The mononuclear phagocyte system: a new classification of macrophages, monocytes, and their precursor cells. *Bull World Health Organ.*, 845–852. (1972).

5 Davies, L. C., Jenkins, S. J., Allen, J. E. & Taylor, P. R. Tissue-resident macrophages. *Nat Immunol* **14**, 986-995, doi:10.1038/ni.2705 (2013).

6 T'Jonck, W., Guilliams, M. & Bonnardel, J. Niche signals and transcription factors involved in tissue-resident macrophage development. *Cell Immunol* **330**, 43-53, doi:10.1016/j.cellimm.2018.02.005 (2018).

7 Lavin, Y. *et al.* Tissue-resident macrophage enhancer landscapes are shaped by the local microenvironment. *Cell* **159**, 1312-1326, doi:10.1016/j.cell.2014.11.018 (2014).

8 Gautier, E. L. *et al.* Gene-expression profiles and transcriptional regulatory pathways that underlie the identity and diversity of mouse tissue macrophages. *Nat Immunol* **13**, 1118-1128, doi:10.1038/ni.2419 (2012).

9 Gosselin, D. *et al.* Environment drives selection and function of enhancers controlling tissue-specific macrophage identities. *Cell* **159**, 1327-1340, doi:10.1016/j.cell.2014.11.023 (2014).

10 Varol, C., Mildner, A. & Jung, S. Macrophages: development and tissue specialization. *Annu Rev Immunol* **33**, 643-675, doi:10.1146/annurev-immunol-032414-112220 (2015).

11 Nimmerjahn, A., Kirchhoff, F. & Helmchen, F. Resting Microglial Cells Are Highly Dynamic Surveillants of Brain Parenchyma in Vivo. *Science* **308** (2005).

12 Wang, J. & Kubes, P. A Reservoir of Mature Cavity Macrophages that Can Rapidly Invade Visceral Organs to Affect Tissue Repair. *Cell* **165**, 668-678, doi:10.1016/j.cell.2016.03.009 (2016).

13 Rodero, M. P. *et al.* Immune surveillance of the lung by migrating tissue monocytes. *Elife* **4**, e07847, doi:10.7554/eLife.07847 (2015).

14 Gunter Weiss, U. E. S. Macrophage defense mechanisms against intracellular bacteria. *Immunological Reviews* **264**, 182-203 (2015).

15 Henson, P. M. & Hume, D. A. Apoptotic cell removal in development and tissue homeostasis. *Trends Immunol* **27**, 244-250, doi:10.1016/j.it.2006.03.005 (2006).

16 Gordon, S. Phagocytosis: An Immunobiologic Process. *Immunity* **44**, 463-475, doi:10.1016/j.immuni.2016.02.026 (2016).

17 Naeini, M. B., Bianconi, V., Pirro, M. & Sahebkar, A. The role of phosphatidylserine recognition receptors in multiple biological functions. *Cell Mol Biol Lett* **25**, 23, doi:10.1186/s11658-020-00214-z (2020).
18 A. Gonzalez, N. *et al.* Phagocytosis imprints heterogeneity in tissue-resident macrophages. *J Exp Med* **214**, 1281-1296, doi:10.1084/jem.20161375 (2017).
19 Yanagihashi, Y., Segawa, K., Maeda, R., Nabeshima, Y. I. & Nagata, S. Mouse macrophages show different requirements for phosphatidylserine receptor Tim4 in efferocytosis. *Proc Natl Acad Sci U S A* **114**, 8800-8805, doi:10.1073/pnas.1705365114 (2017).
20 Wong, K. *et al.* Phosphatidylserine receptor Tim-4 is essential for the maintenance of the homeostatic state of resident peritoneal macrophages. *Proc Natl Acad Sci U S A* **107**, 8712-8717, doi:10.1073/pnas.0910929107 (2010).
21 Roberts, A. W. *et al.* Tissue-Resident Macrophages Are Locally Programmed for Silent Clearance of Apoptotic Cells. *Immunity* **47**, 913-927 e916, doi:10.1016/j.immuni.2017.10.006 (2017).
22 Furth, R. V. Origin and Turnover of Monocytes and Macrophages. *Current Topics in Pathology* **79** (1989).
23 Hume, D. A., Irvine, K. M. & Pridans, C. The Mononuclear Phagocyte System: The Relationship between Monocytes and Macrophages. *Trends Immunol* **40**, 98-112, doi:10.1016/j.it.2018.11.007 (2019).
24 Ajami, B., Bennett, J. L., Krieger, C., Tetzlaff, W. & Rossi, F. M. Local self-renewal can sustain CNS microglia maintenance and function throughout adult life. *Nat Neurosci* **10**, 1538-1543, doi:10.1038/nn2014 (2007).
25 Merad, M. *et al.* Langerhans cells renew in the skin throughout life under steady-state conditions. *Nat Immunol* **3**, 1135-1141, doi:10.1038/ni852 (2002).
26 Kim, H., Kim, M., Im, S. K. & Fang, S. Mouse Cre-LoxP system: general principles to determine tissue-specific roles of target genes. *Lab Anim Res* **34**, 147-159, doi:10.5625/lar.2018.34.4.147 (2018).
27 Bouabe, H. & Okkenhaug, K. Gene targeting in mice: a review. *Methods Mol Biol* **1064**, 315-336, doi:10.1007/978-1-62703-601-6_23 (2013).
28 Yona, S. *et al.* Fate mapping reveals origins and dynamics of monocytes and tissue macrophages under homeostasis. *Immunity* **38**, 79-91, doi:10.1016/j.immuni.2012.12.001 (2013).
29 Schulz, C. *et al.* A Lineage of Myeloid Cells Independent of Myb and Hematopoietic Stem Cells. *Science* **336** (2012).
30 Hashimoto, D. *et al.* Tissue-resident macrophages self-maintain locally throughout adult life with minimal contribution from circulating monocytes. *Immunity* **38**, 792-804, doi:10.1016/j.immuni.2013.04.004 (2013).
31 Ginhoux, F. *et al.* Fate Mapping Analysis Reveals That Adult Microglia Derive from Primitive Macrophages. *Science* **330** (2010).

32 Bertrand, J. Y. *et al.* Three pathways to mature macrophages in the early mouse yolk sac. *Blood* **106**, 3004-3011, doi:10.1182/blood-2005-02-0461 (2005).
33 Ginhoux, F. & Guilliams, M. Tissue-Resident Macrophage Ontogeny and Homeostasis. *Immunity* **44**, 439-449, doi:10.1016/j.immuni.2016.02.024 (2016).
34 Hoeffel, G. *et al.* C-Myb(+) erythro-myeloid progenitor-derived fetal monocytes give rise to adult tissue-resident macrophages. *Immunity* **42**, 665-678, doi:10.1016/j.immuni.2015.03.011 (2015).
35 Hoeffel, G. *et al.* Adult Langerhans cells derive predominantly from embryonic fetal liver monocytes with a minor contribution of yolk sac-derived macrophages. *J Exp Med* **209**, 1167-1181, doi:10.1084/jem.20120340 (2012).
36 Gomez Perdiguero, E. *et al.* Tissue-resident macrophages originate from yolk-sac-derived erythro-myeloid progenitors. *Nature* **518**, 547-551, doi:10.1038/nature13989 (2015).
37 Sheng, J., Ruedl, C. & Karjalainen, K. Most Tissue-Resident Macrophages Except Microglia Are Derived from Fetal Hematopoietic Stem Cells. *Immunity* **43**, 382-393, doi:10.1016/j.immuni.2015.07.016 (2015).
38 Scott, C. L. *et al.* Bone marrow-derived monocytes give rise to self-renewing and fully differentiated Kupffer cells. *Nat Commun* **7**, 10321, doi:10.1038/ncomms10321 (2016).
39 Ginhoux, F. *et al.* Fate Mapping Analysis Reveals That Adult Microglia Derive from Primitive Macrophages. *Science* **330** (2010).
40 Bain, C. C. *et al.* Resident and pro-inflammatory macrophages in the colon represent alternative context-dependent fates of the same Ly6Chi monocyte precursors. *Mucosal Immunol* **6**, 498-510, doi:10.1038/mi.2012.89 (2013).
41 Epelman, S. *et al.* Embryonic and adult-derived resident cardiac macrophages are maintained through distinct mechanisms at steady state and during inflammation. *Immunity* **40**, 91-104, doi:10.1016/j.immuni.2013.11.019 (2014).
42 Bain, C. C. *et al.* Long-lived self-renewing bone marrow-derived macrophages displace embryo-derived cells to inhabit adult serous cavities. *Nat Commun* **7**, ncomms11852, doi:10.1038/ncomms11852 (2016).
43 Chakarov, S. *et al.* Two distinct interstitial macrophage populations coexist across tissues in specific subtissular niches. *Science* **363**, doi:10.1126/science.aau0964 (2019).
44 Shaw, T. N. *et al.* Tissue-resident macrophages in the intestine are long lived and defined by Tim-4 and CD4 expression. *J Exp Med* **215**, 1507-1518, doi:10.1084/jem.20180019 (2018).
45 Haniffa, M. *et al.* Differential rates of replacement of human dermal dendritic cells and macrophages during hematopoietic stem cell transplantation. *J Exp Med* **206**, 371-385, doi:10.1084/jem.20081633 (2009).

46 Amit, I., Winter, D. R. & Jung, S. The role of the local environment and epigenetics in shaping macrophage identity and their effect on tissue homeostasis. *Nat Immunol* **17**, 18-25, doi:10.1038/ni.3325 (2016).
47 REED, J. A. *et al.* Distinct changes in pulmonary surfactant homeostasis in common -chain- and GM-CSF-deficient mice. *Am J Physiol Lung Cell Mol Physiol* **278** (2000).
48 Suzuki, T. *et al.* Pulmonary macrophage transplantation therapy. *Nature* **514**, 450-454, doi:10.1038/nature13807 (2014).
49 Suzuki, T. *et al.* Familial pulmonary alveolar proteinosis caused by mutations in CSF2RA. *J Exp Med* **205**, 2703-2710, doi:10.1084/jem.20080990 (2008).
50 Theurl, I. *et al.* On-demand erythrocyte disposal and iron recycling requires transient macrophages in the liver. *Nat Med* **22**, 945-951, doi:10.1038/nm.4146 (2016).
51 Schafer, D. P. *et al.* Microglia sculpt postnatal neural circuits in an activity and complement-dependent manner. *Neuron* **74**, 691-705, doi:10.1016/j.neuron.2012.03.026 (2012).
52 Paolicelli, R. C. *et al.* Synaptic Pruning by Microglia Is Necessary for Normal Brain Development. *Science* **333** (2011).
53 Imperato, M. R., Cauchy, P., Obier, N. & Bonifer, C. The RUNX1-PU.1 axis in the control of hematopoiesis. *Int J Hematol* **101**, 319-329, doi:10.1007/s12185-015-1762-8 (2015).
54 DONG-ER ZHANG, C. J. H., HUI MINCHEN,AND DANIEL G. TENEN. The Macrophage Transcription Factor PU.1 Directs Tissue-Specific Expression of the Macrophage Colony-Stimulating Factor Receptor. *Mollecular and Cellular Biology* **14** (1993).
55 Athar Aziz, E. S., Sandrine Sarrazin, Michael H. Sieweke. MafB/c-Maf Deficiency Enables Self-Renewal of Differentiated Functional Macrophages. *Science* **326** (2009).
56 Scott, C. L. *et al.* The Transcription Factor ZEB2 Is Required to Maintain the Tissue-Specific Identities of Macrophages. *Immunity* **49**, 312-325 e315, doi:10.1016/j.immuni.2018.07.004 (2018).
57 Bleriot, C., Chakarov, S. & Ginhoux, F. Determinants of Resident Tissue Macrophage Identity and Function. *Immunity* **52**, 957-970, doi:10.1016/j.immuni.2020.05.014 (2020).
58 Kohyama, M. *et al.* Role for Spi-C in the development of red pulp macrophages and splenic iron homeostasis. *Nature* **457**, 318-321, doi:10.1038/nature07472 (2009).
59 Gonzalez, A. *et al.* The nuclear receptor LXRalpha controls the functional specialization of splenic macrophages. *Nat Immunol* **14**, 831-839, doi:10.1038/ni.2622 (2013).
60 Cain, D. W. *et al.* Identification of a tissue-specific, C/EBPbeta-dependent pathway of differentiation for murine peritoneal macrophages. *J Immunol* **191**, 4665-4675, doi:10.4049/jimmunol.1300581 (2013).

61 Rauschmeier, R. *et al.* Bhlhe40 and Bhlhe41 transcription factors regulate alveolar macrophage self-renewal and identity. *EMBO J* **38**, e101233, doi:10.15252/embj.2018101233 (2019).
62 Jarjour, N. N. *et al.* Bhlhe40 mediates tissue-specific control of macrophage proliferation in homeostasis and type 2 immunity. *Nat Immunol* **20**, 687-700, doi:10.1038/s41590-019-0382-5 (2019).
63 Okabe, Y. & Medzhitov, R. Tissue-specific signals control reversible program of localization and functional polarization of macrophages. *Cell* **157**, 832-844, doi:10.1016/j.cell.2014.04.016 (2014).
64 Rosas, M. *et al.* The Transcription Factor Gata6 Links Tissue Macrophage Phenotype and Proliferative Renewal. *Science* (2014).
65 Gautier, E. L. *et al.* Gata6 regulates aspartoacylase expression in resident peritoneal macrophages and controls their survival. *J Exp Med* **211**, 1525-1531, doi:10.1084/jem.20140570 (2014).
66 Schneider, C. *et al.* Induction of the nuclear receptor PPAR-gamma by the cytokine GM-CSF is critical for the differentiation of fetal monocytes into alveolar macrophages. *Nat Immunol* **15**, 1026-1037, doi:10.1038/ni.3005 (2014).
67 van de Laar, L. *et al.* Yolk Sac Macrophages, Fetal Liver, and Adult Monocytes Can Colonize an Empty Niche and Develop into Functional Tissue-Resident Macrophages. *Immunity* **44**, 755-768, doi:10.1016/j.immuni.2016.02.017 (2016).
68 Beattie, L. *et al.* Bone marrow-derived and resident liver macrophages display unique transcriptomic signatures but similar biological functions. *J Hepatol* **65**, 758-768, doi:10.1016/j.jhep.2016.05.037 (2016).
69 David, B. A. *et al.* Combination of Mass Cytometry and Imaging Analysis Reveals Origin, Location, and Functional Repopulation of Liver Myeloid Cells in Mice. *Gastroenterology* **151**, 1176-1191, doi:10.1053/j.gastro.2016.08.024 (2016).
70 Lund, H. *et al.* Competitive repopulation of an empty microglial niche yields functionally distinct subsets of microglia-like cells. *Nat Commun* **9**, 4845, doi:10.1038/s41467-018-07295-7 (2018).
71 Shemer, A. *et al.* Engrafted parenchymal brain macrophages differ from microglia in transcriptome, chromatin landscape and response to challenge. *Nat Commun* **9**, 5206, doi:10.1038/s41467-018-07548-5 (2018).
72 Guilliams, M. & Scott, C. L. Does niche competition determine the origin of tissue-resident macrophages? *Nat Rev Immunol* **17**, 451-460, doi:10.1038/nri.2017.42 (2017).
73 Bonnardel, J. *et al.* Stellate Cells, Hepatocytes, and Endothelial Cells Imprint the Kupffer Cell Identity on Monocytes Colonizing the Liver Macrophage Niche. *Immunity* **51**, 638-654 e639, doi:10.1016/j.immuni.2019.08.017 (2019).
74 Sakai, M. *et al.* Liver-Derived Signals Sequentially Reprogram Myeloid Enhancers to Initiate and Maintain Kupffer Cell Identity. *Immunity* **51**, 655-670 e658, doi:10.1016/j.immuni.2019.09.002 (2019).

75 Jenkins, S. J. & Hume, D. A. Homeostasis in the mononuclear phagocyte system. *Trends Immunol* **35**, 358-367, doi:10.1016/j.it.2014.06.006 (2014).
76 Lavin, Y., Mortha, A., Rahman, A. & Merad, M. Regulation of macrophage development and function in peripheral tissues. *Nat Rev Immunol* **15**, 731-744, doi:10.1038/nri3920 (2015).
77 MacDonald, K. P. *et al.* An antibody against the colony-stimulating factor 1 receptor depletes the resident subset of monocytes and tissue- and tumor-associated macrophages but does not inhibit inflammation. *Blood* **116**, 3955-3963, doi:10.1182/blood-2010-02-266296 (2010).
78 Dai, X.-M. *et al.* Targeted disruption of the mouse colony-stimulating factor 1 receptor gene results in osteopetrosis, mononuclear phagocyte deficiency, increased primitive progenitor cell frequencies, and reproductive defects. *Blood* **99** (2002).
79 Bellomo, A. *et al.* Reticular Fibroblasts Expressing the Transcription Factor WT1 Define a Stromal Niche that Maintains and Replenishes Splenic Red Pulp Macrophages. *Immunity* **53**, 127-142 e127, doi:10.1016/j.immuni.2020.06.008 (2020).
80 Ivanov, S. *et al.* Mesothelial cell CSF1 sustains peritoneal macrophage proliferation. *Eur J Immunol* **49**, 2012-2018, doi:10.1002/eji.201948164 (2019).
81 Zhou, X. *et al.* Circuit Design Features of a Stable Two-Cell System. *Cell* **172**, 744-757 e717, doi:10.1016/j.cell.2018.01.015 (2018).
82 Ramachandran, P. *et al.* Differential Ly-6C expression identifies the recruited macrophage phenotype, which orchestrates the regression of murine liver fibrosis. *Proc Natl Acad Sci U S A* **109**, E3186-3195, doi:10.1073/pnas.1119964109 (2012).
83 Zigmond, E. *et al.* Infiltrating monocyte-derived macrophages and resident kupffer cells display different ontogeny and functions in acute liver injury. *J Immunol* **193**, 344-353, doi:10.4049/jimmunol.1400574 (2014).
84 Lloyd, A. F. *et al.* Central nervous system regeneration is driven by microglia necroptosis and repopulation. *Nat Neurosci* **22**, 1046-1052, doi:10.1038/s41593-019-0418-z (2019).
85 Ajami, B., Bennett, J. L., Krieger, C., McNagny, K. M. & Rossi, F. M. Infiltrating monocytes trigger EAE progression, but do not contribute to the resident microglia pool. *Nat Neurosci* **14**, 1142-1149, doi:10.1038/nn.2887 (2011).
86 Gautier, E. L., Ivanov, S., Lesnik, P. & Randolph, G. J. Local apoptosis mediates clearance of macrophages from resolving inflammation in mice. *Blood* **122**, 2714-2722, doi:10.1182/blood-2013-01-478206 (2013).
87 Davies, L. C. *et al.* Distinct bone marrow-derived and tissue-resident macrophage lineages proliferate at key stages during inflammation. *Nat Commun* **4**, 1886, doi:10.1038/ncomms2877 (2013).
88 Amiya, T. *et al.* Bone marrow-derived macrophages distinct from tissue-resident macrophages play a pivotal role in Concanavalin A-induced murine liver injury via CCR9 axis. *Sci Rep* **6**, 35146, doi:10.1038/srep35146 (2016).

89 Ferrer, I. R. *et al.* A wave of monocytes is recruited to replenish the long-term Langerhans cell network after immune injury. *Sci Immunol* **4**, doi:10.1126/sciimmunol.aax8704 (2019).
90 Rua, R. *et al.* Infection drives meningeal engraftment by inflammatory monocytes that impairs CNS immunity. *Nat Immunol* **20**, 407-419, doi:10.1038/s41590-019-0344-y (2019).
91 Tran, S. *et al.* Impaired Kupffer Cell Self-Renewal Alters the Liver Response to Lipid Overload during Non-alcoholic Steatohepatitis. *Immunity*, doi:10.1016/j.immuni.2020.06.003 (2020).
92 Remmerie, A. *et al.* Osteopontin Expression Identifies a Subset of Recruited Macrophages Distinct from Kupffer Cells in the Fatty Liver. *Immunity* **53**, 641-657 e614, doi:10.1016/j.immuni.2020.08.004 (2020).
93 Misharin, A. V. *et al.* Monocyte-derived alveolar macrophages drive lung fibrosis and persist in the lung over the life span. *J Exp Med* **214**, 2387-2404, doi:10.1084/jem.20162152 (2017).
94 Aegerter, H. *et al.* Influenza-induced monocyte-derived alveolar macrophages confer prolonged antibacterial protection. *Nat Immunol* **21**, 145-157, doi:10.1038/s41590-019-0568-x (2020).
95 Ghosn, E. E. *et al.* Two physically, functionally, and developmentally distinct peritoneal macrophage subsets. *Proc Natl Acad Sci U S A* **107**, 2568-2573, doi:10.1073/pnas.0915000107 (2010).
96 Bain, C. C. & Jenkins, S. J. The biology of serous cavity macrophages. *Cell Immunol* **330**, 126-135, doi:10.1016/j.cellimm.2018.01.003 (2018).
97 Bain, C. C. *et al.* Rate of replenishment and microenvironment contribute to the sexually dimorphic phenotype and function of peritoneal macrophages. *Sci Immunol* **5** (2020).
98 Casanova-Acebes, M. *et al.* RXRs control serous macrophage neonatal expansion and identity and contribute to ovarian cancer progression. *Nat Commun* **11**, 1655, doi:10.1038/s41467-020-15371-0 (2020).
99 Buechler, M. B. *et al.* A Stromal Niche Defined by Expression of the Transcription Factor WT1 Mediates Programming and Homeostasis of Cavity-Resident Macrophages. *Immunity* **51**, 119-130 e115, doi:10.1016/j.immuni.2019.05.010 (2019).
100 Etzerodt, A. *et al.* Tissue-resident macrophages in omentum promote metastatic spread of ovarian cancer. *J Exp Med* **217**, doi:10.1084/jem.20191869 (2020).
101 Meza-Perez, S. & Randall, T. D. Immunological Functions of the Omentum. *Trends Immunol* **38**, 526-536, doi:10.1016/j.it.2017.03.002 (2017).
102 Zhu, H. *et al.* Macrophage differentiation and expression of macrophage colony-stimulating factor in murine milky spots and omentum after macrophage elimination. *Journal of Leukocyte Biology* **61** (1997).
103 Zhang, N. *et al.* Expression of factor V by resident macrophages boosts host defense in the peritoneal cavity. *J Exp Med* **216**, 1291-1300, doi:10.1084/jem.20182024 (2019).

104 Kim, K. W. *et al.* MHC II+ resident peritoneal and pleural macrophages rely on IRF4 for development from circulating monocytes. *J Exp Med* **213**, 1951-1959, doi:10.1084/jem.20160486 (2016).
105 Hawley, C. A. *et al.* Csf1r-mApple Transgene Expression and Ligand Binding In Vivo Reveal Dynamics of CSF1R Expression within the Mononuclear Phagocyte System. *J Immunol* **200**, 2209-2223, doi:10.4049/jimmunol.1701488 (2018).
106 Rojo, R. *et al.* Deletion of a Csf1r enhancer selectively impacts CSF1R expression and development of tissue macrophage populations. *Nat Commun* **10**, 3215, doi:10.1038/s41467-019-11053-8 (2019).
107 De Schepper, S. *et al.* Self-Maintaining Gut Macrophages Are Essential for Intestinal Homeostasis. *Cell* **175**, 400-415 e413, doi:10.1016/j.cell.2018.07.048 (2018).
108 Wang, Y.-T. *et al.* Select autophagy genes maintain quiescence of tissue-resident macrophages and increase susceptibility to Listeria monocytogenes. *Nature Microbiology* **5**, 272-281, doi:10.1038/s41564-019-0633-0 (2020).
109 Lantz, C., Radmanesh, B., Liu, E., Thorp, E. B. & Lin, J. Single-cell RNA sequencing uncovers heterogenous transcriptional signatures in macrophages during efferocytosis. *Sci Rep* **10**, 14333, doi:10.1038/s41598-020-70353-y (2020).
110 Miyanishi, M. *et al.* Identification of Tim4 as a phosphatidylserine receptor. *Nature* **450**, 435-439, doi:10.1038/nature06307 (2007).
111 Newson, J. *et al.* Resolution of acute inflammation bridges the gap between innate and adaptive immunity. *Blood* **124**, 1748-1764, doi:10.1182/blood-2014-03-562710 (2014).
112 Dahdah, A. *et al.* Mast cells aggravate sepsis by inhibiting peritoneal macrophage phagocytosis. *J Clin Invest* **124**, 4577-4589, doi:10.1172/JCI75212 (2014).
113 Deniset, J. F. *et al.* Gata6(+) Pericardial Cavity Macrophages Relocate to the Injured Heart and Prevent Cardiac Fibrosis. *Immunity* **51**, 131-140 e135, doi:10.1016/j.immuni.2019.06.010 (2019).
114 Hogg, C. *et al.* Macrophages inhibit and enhance endometriosis depending on their origin. *bioRxiv*, doi:10.1101/2020.04.30.070003 (2020).
115 Capobianco, A. & Rovere-Querini, P. Endometriosis, a disease of the macrophage. *Front Immunol* **4**, 9, doi:10.3389/fimmu.2013.00009 (2013).
116 Honjo, K. *et al.* Plasminogen activator inhibitor-1 regulates macrophage-dependent postoperative adhesion by enhancing EGF-HER1 signaling in mice. *FASEB J* **31**, 2625-2637, doi:10.1096/fj.201600871RR (2017).
117 Hoshino, A. *et al.* Inhibition of CCL1-CCR8 interaction prevents aggregation of macrophages and development of peritoneal adhesions. *J Immunol* **178**, 5296-5304, doi:10.4049/jimmunol.178.8.5296 (2007).
118 Ansel, K. M., Harris, R. B. S. & Cyster, J. G. CXCL13 Is Required for B1 Cell Homing,Natural Antibody Production,and Body Cavity Immunity. *Immunity* **Vol. 16**, 67–76 (2002).

119 Rittirsch, D., Hoesel, L. M. & Ward, P. A. The disconnect between animal models of sepsis and human sepsis. *J Leukoc Biol* **81**, 137-143, doi:10.1189/jlb.0806542 (2007).
120 Newson, J. *et al.* Inflammatory Resolution Triggers a Prolonged Phase of Immune Suppression through COX-1/mPGES-1-Derived Prostaglandin E2. *Cell Rep* **20**, 3162-3175, doi:10.1016/j.celrep.2017.08.098 (2017).
121 Thompson, A. *et al.* Dependence on Dectin-1 Varies With Multiple Candida Species. *Front Microbiol* **10**, 1800, doi:10.3389/fmicb.2019.01800 (2019).
122 Cash, J. L., White, G. E. & Greaves, D. R. in *Chemokines, Part B Methods in Enzymology* 379-396 (2009).
123 Liu, Z. *et al.* Fate Mapping via Ms4a3-Expression History Traces Monocyte-Derived Cells. *Cell* **178**, 1509-1525 e1519, doi:10.1016/j.cell.2019.08.009 (2019).
124 Taylor, P. R. *et al.* Dectin-1 is required for beta-glucan recognition and control of fungal infection. *Nat Immunol* **8**, 31-38, doi:10.1038/ni1408 (2007).
125 Teselkin, Y. O. *et al.* Combined Effect of TLR2 Ligands on ROS Production by Mouse Peritoneal Macrophages. *Bull Exp Biol Med* **166**, 26-30, doi:10.1007/s10517-018-4281-9 (2018).
126 Walachowski, S., Tabouret, G. & Foucras, G. Triggering Dectin-1-Pathway Alone Is Not Sufficient to Induce Cytokine Production by Murine Macrophages. *PLoS One* **11**, e0148464, doi:10.1371/journal.pone.0148464 (2016).
127 Goodridge, H. S. *et al.* Activation of the innate immune receptor Dectin-1 upon formation of a 'phagocytic synapse'. *Nature* **472**, 471-475, doi:10.1038/nature10071 (2011).
128 Takahashi, M., Galligan, C., Tessarollo, L. & Yoshimura, T. Monocyte chemoattractant protein-1 (MCP-1), not MCP-3, is the primary chemokine required for monocyte recruitment in mouse peritonitis induced with thioglycollate or zymosan A. *J Immunol* **183**, 3463-3471, doi:10.4049/jimmunol.0802812 (2009).
129 Boring, L. *et al.* Impaired monocyte migration and reduced type 1 (Th1) cytokine responses in C-C chemokine receptor 2 knockout mice. *J Clin Invest* **100**, 2552-2561, doi:10.1172/JCI119798 (1997).
130 Maureen N. Ajuebor, R. J. F., Robert Hannon, Mark Christie, Keith Bowers, Anne Verity, and Mauro Perretti. Endogenous monocyte chemoattractant protein-1 recruits monocytes in the zymosan peritonitis model. *Journal of Leukocyte Biology* **63** (1998).
131 Chen, W., Wang, J., Jia, L., Liu, J. & Tian, Y. Attenuation of the programmed cell death-1 pathway increases the M1 polarization of macrophages induced by zymosan. *Cell Death Dis* **7**, e2115, doi:10.1038/cddis.2016.33 (2016).
132 Ajuebor, M. N. *et al.* Role of Resident Peritoneal Macrophages and Mast Cells in Chemokine Production and Neutrophil Migration in Acute Inflammation: Evidence for an Inhibitory Loop Involving Endogenous IL-10. *Journal of Immunology* (1999).

133 Nieto-Patlan, A. *et al.* Recognition of Candida albicans by Dectin-1 induces mast cell activation. *Immunobiology* **220**, 1093-1100, doi:10.1016/j.imbio.2015.05.005 (2015).
134 Kolaczkowska, E., Koziol, A., Plytycz, B. & Arnold, B. Inflammatory macrophages, and not only neutrophils, die by apoptosis during acute peritonitis. *Immunobiology* **215**, 492-504, doi:10.1016/j.imbio.2009.07.001 (2010).
135 Wright, R. D. *et al.* Galectin-3-null mice display defective neutrophil clearance during acute inflammation. *J Leukoc Biol* **101**, 717-726, doi:10.1189/jlb.3A0116-026RR (2017).
136 Jackson-Jones, L. H. *et al.* Stromal Cells Covering Omental Fat-Associated Lymphoid Clusters Trigger Formation of Neutrophil Aggregates to Capture Peritoneal Contaminants. *Immunity* **52**, 700-715 e706, doi:10.1016/j.immuni.2020.03.011 (2020).
137 Hu, Y. *et al.* Depletion of activated macrophages with a folate receptor-beta-specific antibody improves symptoms in mouse models of rheumatoid arthritis. *Arthritis Res Ther* **21**, 143, doi:10.1186/s13075-019-1912-0 (2019).
138 Barth, M. W., Hendrzak, J. A., Melnicoff, M. J. & Morahan, P. S. Review of the macrophage disappearance reaction. *J Leukoc Biol* **57**, 361-367, doi:10.1002/jlb.57.3.361 (1995).
139 Liao, C. T. *et al.* IL-10 differentially controls the infiltration of inflammatory macrophages and antigen-presenting cells during inflammation. *Eur J Immunol* **46**, 2222-2232, doi:10.1002/eji.201646528 (2016).
140 Nguyen, H. H., Tran, B. T., Muller, W. & Jack, R. S. IL-10 acts as a developmental switch guiding monocyte differentiation to macrophages during a murine peritoneal infection. *J Immunol* **189**, 3112-3120, doi:10.4049/jimmunol.1200360 (2012).
141 Bellingan, G. J. *et al.* Adhesion molecule-dependent mechanisms regulate the rate of macrophage clearance during the resolution of peritoneal inflammation. *J Exp Med* **196**, 1515-1521, doi:10.1084/jem.20011794 (2002).
142 Cao, C., Lawrence, D. A., Strickland, D. K. & Zhang, L. A specific role of integrin Mac-1 in accelerated macrophage efflux to the lymphatics. *Blood* **106**, 3234-3241, doi:10.1182/blood-2005-03-1288 (2005).
143 Rosas, M., Thomas, B., Stacey, M., Gordon, S. & Taylor, P. R. The myeloid 7/4-antigen defines recently generated inflammatory macrophages and is synonymous with Ly-6B. *J Leukoc Biol* **88**, 169-180, doi:10.1189/jlb.0809548 (2010).
144 Davies, L. C. *et al.* A quantifiable proliferative burst of tissue macrophages restores homeostatic macrophage populations after acute inflammation. *Eur J Immunol* **41**, 2155-2164, doi:10.1002/eji.201141817 (2011).
145 Gundra, U. M. *et al.* Vitamin A mediates conversion of monocyte-derived macrophages into tissue-resident macrophages during alternative activation. *Nat Immunol* **18**, 642-653, doi:10.1038/ni.3734 (2017).

146 Jenkins, S. J. *et al.* IL-4 directly signals tissue-resident macrophages to proliferate beyond homeostatic levels controlled by CSF-1. *J Exp Med* **210**, 2477-2491, doi:10.1084/jem.20121999 (2013).
147 Jenkins, S. J. *et al.* Local Macrophage Proliferation, Rather than Recruitment from the Blood, Is a Signature of TH2 Inflammation. *Science* **332** (2011).
148 Bleriot, C. *et al.* Liver-resident macrophage necroptosis orchestrates type 1 microbicidal inflammation and type-2-mediated tissue repair during bacterial infection. *Immunity* **42**, 145-158, doi:10.1016/j.immuni.2014.12.020 (2015).
149 Weisser, S. B., van Rooijen, N. & Sly, L. M. Depletion and reconstitution of macrophages in mice. *J Vis Exp*, 4105, doi:10.3791/4105 (2012).
150 Guilliams, M., Thierry, G. R., Bonnardel, J. & Bajenoff, M. Establishment and Maintenance of the Macrophage Niche. *Immunity* **52**, 434-451, doi:10.1016/j.immuni.2020.02.015 (2020).
151 Netea, M. G., Latz, E., Mills, K. H. & O'Neill, L. A. Innate immune memory: a paradigm shift in understanding host defense. *Nat Immunol* **16**, 675-679, doi:10.1038/ni.3178 (2015).
152 Netea, M. G. *et al.* Trained immunity: A program of innate immune memory in health and disease. *Science* **352**, aaf1098, doi:10.1126/science.aaf1098 (2016).
153 Quintin, J. *et al.* Candida albicans infection affords protection against reinfection via functional reprogramming of monocytes. *Cell Host Microbe* **12**, 223-232, doi:10.1016/j.chom.2012.06.006 (2012).
154 Sarah Walachowski, G. T., Marion Fabre and Gilles Foucras. Molecular analysis of a short-term Model of β-glucans-Trained immunity highlights the accessory contribution of gM-csF in Priming Mouse Macrophages response. *Front Immunol* **8**, doi:10.3389/mmu.2017.01089 (2017).
155 Galatro, T. F. *et al.* Transcriptomic analysis of purified human cortical microglia reveals age-associated changes. *Nat Neurosci* **20**, 1162-1171, doi:10.1038/nn.4597 (2017).
156 Schroder, W. A. *et al.* SerpinB2 inhibits migration and promotes a resolution phase signature in large peritoneal macrophages. *Sci Rep* **9**, 12421, doi:10.1038/s41598-019-48741-w (2019).
157 Tsou, C. L. *et al.* Critical roles for CCR2 and MCP-3 in monocyte mobilization from bone marrow and recruitment to inflammatory sites. *J Clin Invest* **117**, 902-909, doi:10.1172/JCI29919 (2007).
158 Parra, D. *et al.* Pivotal advance: peritoneal cavity B-1 B cells have phagocytic and microbicidal capacities and present phagocytosed antigen to CD4+ T cells. *J Leukoc Biol* **91**, 525-536, doi:10.1189/jlb.0711372 (2012).
159 Rossi, V. A. a. E. Errors Related to Different Techniques of Intraperitoneal Injection in Mice. *APPLIED MICROBIOLOGY,*, 704-705 (1970).
160 in *Neglected Factors in Pharmacology and Neuroscience Research* Vol. 12 (ed V. Claassen) Ch. Intraperitoneal drug administration, 46-58 (Elsevier, 1994).

161 R Gaines Das & North, D. Implications of experimental technique for analysis and interpretation of data from animal experiments: outliers and increased variability resulting from failure of intraperitoneal injection procedures. *Laboratory Animals* **41**, 312-320 (2006).
162 Bystrom, J. *et al.* Resolution-phase macrophages possess a unique inflammatory phenotype that is controlled by cAMP. *Blood* **112**, 4117-4127, doi:10.1182/blood-2007-12-129767 (2008).
163 Luo, Y., Alvarez, M., Xia, L. & Casadevall, A. The outcome of phagocytic cell division with infectious cargo depends on single phagosome formation. *PLoS One* **3**, e3219, doi:10.1371/journal.pone.0003219 (2008).
164 J.F.A.M. Wijffels, R. J. B. M. H., J.J.E. Steenbergen, I.L. Eestermans and R.H.J. Beelen Milky spots in the mouse omentum may play an important role in the origin of peritoneal macrophages. *Res. Immunol*, 401-409 (1992).
165 Benezech, C. *et al.* Inflammation-induced formation of fat-associated lymphoid clusters. *Nat Immunol* **16**, 819-828, doi:10.1038/ni.3215 (2015).
166 Perez-Shibayama, C. *et al.* Fibroblastic reticular cells initiate immune responses in visceral adipose tissues and secure peritoneal immunity. *Sci Immunol* **3** (2018).
167 Wieser, F., Wu, J., Shen, Z., Taylor, R. N. & Sidell, N. Retinoic acid suppresses growth of lesions, inhibits peritoneal cytokine secretion, and promotes macrophage differentiation in an immunocompetent mouse model of endometriosis. *Fertil Steril* **97**, 1430-1437, doi:10.1016/j.fertnstert.2012.03.004 (2012).
168 A. K. Verma, H. M. R., B. G. Shapas, and R. K. Boutwell. Inhibition of la-O-Tetradecanoylphorbo MS-acetate-induced Ornithine Decarboxylase Activity in Mouse Epidermis by Vitamin A Analogs. *Cancer Research* **38**, 793-801 (1978).
169 Alsina-Sanchis, E. *et al.* Oil depletes resident peritoneal macrophages. *bioRxiv*, doi:10.1101/2020.07.15.203885 (2020).
170 Gorgani, N. N. *et al.* Complement receptor of the Ig superfamily enhances complement-mediated phagocytosis in a subpopulation of tissue resident macrophages. *J Immunol* **181**, 7902-7908, doi:10.4049/jimmunol.181.11.7902 (2008).
171 Lanoue, A. *et al.* SIGN-R1 contributes to protection against lethal pneumococcal infection in mice. *J Exp Med* **200**, 1383-1393, doi:10.1084/jem.20040795 (2004).
172 Stengel, S. *et al.* Peritoneal Level of CD206 Associates With Mortality and an Inflammatory Macrophage Phenotype in Patients With Decompensated Cirrhosis and Spontaneous Bacterial Peritonitis. *Gastroenterology* **158**, 1745-1761, doi:10.1053/j.gastro.2020.01.029 (2020).
173 Irvine, K. M. *et al.* CRIg-expressing peritoneal macrophages are associated with disease severity in patients with cirrhosis and ascites. *JCI Insight* **1**, e86914, doi:10.1172/jci.insight.86914 (2016).
174 WEI GUO FENG, Y. B. W., JIN SONG ZHANG, XING YU WANG, CHANG LIN LI, ZONG LIANG CHANG. cAMP elevators inhibit LPS-induced IL-12 p40

expression by inter- fering with phosphorylation of p38 MAPK in Murine Peritoneal Macrophages. *Cell Research* **12**, 331-337 (2002).
175 Oliveira, L. S. *et al.* A Defective TLR4 Signaling for IFN-b Expression Is Responsible for the Innately Lower Ability of BALB/c Macrophages to Produce NO in Response to LPS as Compared to C57BL/6. *PLoS One* **9**, doi:10.1371/journal.pone (2014).
176 Major, J., Fletcher, J. E. & Hamilton, T. A. IL-4 pretreatment selectively enhances cytokine and chemokine production in lipopolysaccharide-stimulated mouse peritoneal macrophages. *J Immunol* **168**, 2456-2463, doi:10.4049/jimmunol.168.5.2456 (2002).
177 Li, X. *et al.* Genomic and lipidomic analyses differentiate the compensatory roles of two COX isoforms during systemic inflammation in mice. *J Lipid Res* **59**, 102-112, doi:10.1194/jlr.M080028 (2018).
178 Takeuchi, O. *et al.* Cellular responses to bacterial cell wall components are mediated through MyD88-dependent signaling cascades. *International Immunology,* **12** (2000).
179 Ciesielska, A., Matyjek, M. & Kwiatkowska, K. TLR4 and CD14 trafficking and its influence on LPS-induced pro-inflammatory signaling. *Cell Mol Life Sci*, doi:10.1007/s00018-020-03656-y (2020).
180 Schmitz, F., Mages, J., Heit, A., Lang, R. & Wagner, H. Transcriptional activation induced in macrophages by Toll-like receptor (TLR) ligands: from expression profiling to a model of TLR signaling. *Eur J Immunol* **34**, 2863-2873, doi:10.1002/eji.200425228 (2004).
181 Dho, S. H., Lim, J. C. & Kim, L. K. Beyond the Role of CD55 as a Complement Component. *Immune Netw* **18**, e11, doi:10.4110/in.2018.18.e11 (2018).
182 Wendeln, A. C. *et al.* Innate immune memory in the brain shapes neurological disease hallmarks. *Nature* **556**, 332-338, doi:10.1038/s41586-018-0023-4 (2018).
183 Guilliams, M. & Svedberg, F. R. Does tissue imprinting restrict macrophage plasticity? *Nature Immunology* **22**, 118-127, doi:10.1038/s41590-020-00849-2 (2021).
184 Gerber, J. S. & Mosser, D. M. Reversing lipopolysaccharide toxicity by ligating the macrophage Fc gamma receptors. *J Immunol* **166**, 6861-6868, doi:10.4049/jimmunol.166.11.6861 (2001).
185 Rittirsch, D. *et al.* Cross-talk between TLR4 and FcgammaReceptorIII (CD16) pathways. *PLoS Pathog* **5**, e1000464, doi:10.1371/journal.ppat.1000464 (2009).
186 Delgoffe, G. M. *et al.* Stability and function of regulatory T cells is maintained by a neuropilin-1-semaphorin-4a axis. *Nature* **501**, 252-256, doi:10.1038/nature12428 (2013).
187 Min, C. *et al.* Tim-4 functions as a scavenger receptor for phagocytosis of exogenous particles. *Cell Death & Disease* **11**, 561, doi:10.1038/s41419-020-02773-7 (2020).
188 Aswad, M., Assi, S., Schif-Zuck, S. & Ariel, A. CCL5 Promotes Resolution-Phase Macrophage Reprogramming in Concert with the Atypical Chemokine

Receptor D6 and Apoptotic Polymorphonuclear Cells. *J Immunol* **199**, 1393-1404, doi:10.4049/jimmunol.1502542 (2017).
189 Composto, G. *et al.* Peritoneal T lymphocyte regulation by macrophages. *Immunobiology* **216**, 256-264, doi:10.1016/j.imbio.2010.04.002 (2011).
190 Takenaka, E., Van Vo, A., Yamashita-Kanemaru, Y., Shibuya, A. & Shibuya, K. Selective DNAM-1 expression on small peritoneal macrophages contributes to CD4(+) T cell costimulation. *Sci Rep* **8**, 15180, doi:10.1038/s41598-018-33437-4 (2018).
191 Zeng, Z. *et al.* Sex-hormone-driven innate antibodies protect females and infants against EPEC infection. *Nat Immunol* **19**, 1100-1111, doi:10.1038/s41590-018-0211-2 (2018).
192 Choi, Y. S., Dieter, J. A., Rothaeusler, K., Luo, Z. & Baumgarth, N. B-1 cells in the bone marrow are a significant source of natural IgM. *Eur J Immunol* **42**, 120-129, doi:10.1002/eji.201141890 (2012).
193 Tang, J. *et al.* Neutrophil and Macrophage Cell Surface Colony-Stimulating Factor 1 Shed by ADAM17 Drives Mouse Macrophage Proliferation in Acute and Chronic Inflammation. *Molecular and Cellular Biology* **38**, doi:10.1128/MCB (2018).
194 Nerlov, C. Transcriptional and translational control of C/EBPs: the case for "deep" genetics to understand physiological function. *Bioessays* **32**, 680-686, doi:10.1002/bies.201000004 (2010).
195 Bradley, M. N., Zhou, L. & Smale, S. T. C/EBPbeta regulation in lipopolysaccharide-stimulated macrophages. *Mol Cell Biol* **23**, 4841-4858, doi:10.1128/mcb.23.14.4841-4858.2003 (2003).
196 Albina, J. E. *et al.* Macrophage arginase regulation by CCAAT/enhancer-binding protein beta. *Shock* **23**, 168-172, doi:10.1097/01.shk.0000148054.74268.e2 (2005).
197 Udofa, E. A. *et al.* The transcription factor C/EBP-beta mediates constitutive and LPS-inducible transcription of murine SerpinB2. *PLoS One* **8**, e57855, doi:10.1371/journal.pone.0057855 (2013).
198 Yuan, X., Yang, B. H., Dong, Y., Yamamura, A. & Fu, W. CRIg, a tissue-resident macrophage specific immune checkpoint molecule, promotes immunological tolerance in NOD mice, via a dual role in effector and regulatory T cells. *Elife* **6**, doi:10.7554/eLife.29540 (2017).
199 Ruffell, D. *et al.* A CREB-C/EBP cascade induces M2 macrophage- specific gene expression and promotes muscle injury repair. *Proc Natl Acad Sci U S A* **106**, 17475–17480 (2009).
200 Na, Y. R., Jung, D., Yoon, B. R., Lee, W. W. & Seok, S. H. Endogenous prostaglandin E2 potentiates anti-inflammatory phenotype of macrophage through the CREB-C/EBP-beta cascade. *Eur J Immunol* **45**, 2661-2671, doi:10.1002/eji.201545471 (2015).
201 Penke, L. R. *et al.* PGE2 accounts for bidirectional changes in alveolar macrophage self-renewal with aging and smoking. *Life Sci Alliance* **3**, doi:10.26508/lsa.202000800 (2020).

202 Zeng, Z. *et al.* CRIg Functions as a Macrophage Pattern Recognition Receptor to Directly Bind and Capture Blood-Borne Gram-Positive Bacteria. *Cell Host Microbe* **20**, 99-106, doi:10.1016/j.chom.2016.06.002 (2016).
203 Han, S. H., Kim, J. H., Martin, M., Michalek, S. M. & Nahm, M. H. Pneumococcal lipoteichoic acid (LTA) is not as potent as staphylococcal LTA in stimulating Toll-like receptor 2. *Infect Immun* **71**, 5541-5548, doi:10.1128/iai.71.10.5541-5548.2003 (2003).
204 Xia, H. *et al.* Autophagic adaptation to oxidative stress alters peritoneal residential macrophage survival and ovarian cancer metastasis. *JCI Insight* **5**, doi:10.1172/jci.insight.141115 (2020).
205 Holodick, N. E., Vizconde, T., Hopkins, T. J. & Rothstein, T. L. Age-Related Decline in Natural IgM Function: Diversification and Selection of the B-1a Cell Pool with Age. *J Immunol* **196**, 4348-4357, doi:10.4049/jimmunol.1600073 (2016).
206 Popi, A. F., Osugui, L., Perez, K. R., Longo-Maugeri, I. M. & Mariano, M. Could a B-1 cell derived phagocyte "be one" of the peritoneal macrophages during LPS-driven inflammation? *PLoS One* **7**, e34570, doi:10.1371/journal.pone.0034570 (2012).
207 Katharina Bröker, J. F., Albert F. Magnusen, Rudolf A. Manz, Jörg Köhl and Christian M. Karsten. a novel role for c5a in B-1 cell homeostasis. *Front Immunol* **9**, doi:10.3389/mmu.2018.00258 (2018).
208 Viktor Steimle, C.-A. S., Annick Mottet, Barbara Lisowska-Grospierre, Bernard Mach. Regulationof MHC Class II Expressionby Interferon-γ Mediated by the Transactivator Gene CIITA. *Science* **265** (1994).
209 Skuljec, J. *et al.* Absence of Regulatory T Cells Causes Phenotypic and Functional Switch in Murine Peritoneal Macrophages. *Front Immunol* **9**, 2458, doi:10.3389/fimmu.2018.02458 (2018).
210 Pereira, A. *et al.* B-1 cell-mediated modulation of M1 macrophage profile ameliorates microbicidal functions and disrupt the evasion mechanisms of Encephalitozoon cuniculi. *PLoS Negl Trop Dis* **13**, e0007674, doi:10.1371/journal.pntd.0007674 (2019).
211 Thies, F. G. *et al.* Cross talk between peritoneal macrophages and B-1 cells in vitro. *PLoS One* **8**, e62805, doi:10.1371/journal.pone.0062805 (2013).
212 Hamaguchi, Y. *et al.* The peritoneal cavity provides a protective niche for B1 and conventional B lymphocytes during anti-CD20 immunotherapy in mice. *J Immunol* **174**, 4389-4399, doi:10.4049/jimmunol.174.7.4389 (2005).
213 Maruya, M. *et al.* Vitamin A-dependent transcriptional activation of the nuclear factor of activated T cells c1 (NFATc1) is critical for the development and survival of B1 cells. *Proc Natl Acad Sci U S A* **108**, 722-727, doi:10.1073/pnas.1014697108 (2011).
214 Accarias, S. *et al.* Single-cell analysis reveals new subset markers of murine peritoneal macrophages and highlights macrophage dynamics upon Staphylococcus aureus peritonitis. *Innate Immun* **22**, 382-392, doi:10.1177/1753425916651330 (2016).

215 Lee, S. H. *et al.* M2-like, dermal macrophages are maintained via IL-4/CCL24–mediated cooperative interaction with eosinophils in cutaneous leishmaniasis. *Sci Immunol* **5** (2020).
216 Ohnmacht, C., Pullner, A., van Rooijen, N. & Voehringer, D. Analysis of eosinophil turnover in vivo reveals their active recruitment to and prolonged survival in the peritoneal cavity. *J Immunol* **179**, 4766-4774, doi:10.4049/jimmunol.179.7.4766 (2007).
217 Orecchioni, M., Ghosheh, Y., Pramod, A. B. & Ley, K. Macrophage Polarization: Different Gene Signatures in M1(LPS+) vs. Classically and M2(LPS-) vs. Alternatively Activated Macrophages. *Front Immunol* **10**, 1084, doi:10.3389/fimmu.2019.01084 (2019).
218 Ruiz-Alcaraz, A. J. *et al.* Isolation of functional mature peritoneal macrophages from healthy humans. *Immunol Cell Biol* **98**, 114-126, doi:10.1111/imcb.12305 (2020).
219 Ruiz-Alcaraz, A. J. *et al.* Characterization of human peritoneal monocyte/macrophage subsets in homeostasis: Phenotype, GATA6, phagocytic/oxidative activities and cytokines expression. *Sci Rep* **8**, 12794, doi:10.1038/s41598-018-30787-x (2018).
220 Burnett, S. H. *et al.* Development of peritoneal adhesions in macrophage depleted mice. *J Surg Res* **131**, 296-301, doi:10.1016/j.jss.2005.08.026 (2006).